STUDY OF THERMAL NEUTRON CAPTURE GAMMA RAYS USING A LITHIUM-DRIFTED GERMANIUM SPECTROMETER

Victor John Orphan
Norman C. Rasmussen

MASSACHUSETTS INSTITUTE OF TECHNOLOGY
77 MASSACHUSETTS AVENUE
CAMBRIDGE, MASSACHUSETTS

Scientific Report No. 1
MITNE-80
Contract No. AF19(628)5551

Project 5620
Task 562003

January, 1967

Prepared for

AIR FORCE CAMBRIDGE RESEARCH LABORATORIES
OFFICE OF AEROSPACE RESEARCH
UNITED STATES AIR FORCE
BEDFORD, MASSACHUSETTS

AFCRL-67-0104

STUDY OF THERMAL NEUTRON CAPTURE GAMMA RAYS USING A LITHIUM-DRIFTED GERMANIUM SPECTROMETER

Victor John Orphan
Norman C. Rasmussen

Massachusetts Institute of Technology
77 Massachusetts Avenue
Cambridge, Massachusetts

SCIENTIFIC REPORT NO. 1
MITNE-80

Contract No. AF19(628)5551
Project No. 5620
Task No. 562003

January, 1967

Prepared for

Air Force Cambridge Research Laboratories
Office of Aerospace Research
United States Air Force
Bedford, Massachusetts

STUDY OF THERMAL NEUTRON CAPTURE GAMMA RAYS USING A LITHIUM-DRIFTED GERMANIUM SPECTROMETER

by

Victor John Orphan

Submitted to the Department of Nuclear Engineering on January 23, 1967 in partial fulfillment of the requirement for the degree of Doctor of Science.

ABSTRACT

A γ-ray spectrometer, using a 30 cc coaxial Ge(Li) detector, which can be operated as a pair spectrometer at high energies and in the Compton suppression mode at low energies, is described and shown to be an effective means of obtaining thermal neutron capture γ-ray spectra over nearly the entire capture gamma energy range. The energy resolution (fwhm) of the spectrometer is approximately 5 keV at 1 MeV and 7 keV at 7 MeV. Capture γ-ray energies may be determined to an accuracy of about 1 keV. The relatively high efficiency of this spectrometer allows the use of an external neutron beam facility, which simplifies sample changing. Use of a 4096-channel analyzer allows the complete capture spectrum of an element to be obtained in about one day.

The fabrication techniques used at this laboratory for making large coaxial Ge(Li) detectors are described. The performance of these detectors is illustrated at low and high energies by means of well known γ-ray spectra.

Capture γ-ray spectra along with tables of energies and intensities are given for beryllium, iron, scandium, germanium and zirconium. A large fraction of the capture γ-ray intensity is observed as resolved peaks for these elements (98% and over 200 γ rays in the case of iron). Proposed level diagrams are given for Fe^{57}, Fe^{55}, and Zr^{92}. Furthermore, binding energies, accurate to about 1 keV, are calculated for the product nuclei of the principal isotopes of the elements investigated.

TABLE OF CONTENTS

TABLE OF CONTENTS (Continued)

LIST OF FIGURES

LIST OF TABLES

ACKNOWLEDGEMENTS

Much of the work of this project would not have been possible without contributions from many people. The guidance, encouragement, and help of Prof. Norman C. Rasmussen, throughout the course of this research, is especially appreciated. His enthusiasm and interest in the project is, in large measure, responsible for its success. I wish to offer special thanks to Dr. Jerry A. Sovka for his tutoring in the fabrication of Ge(Li) detectors. Thanks are also offered to Prof. Franklyn M. Clikeman for acting as thesis reader and for his advice and constructive criticism of the thesis.

The assistance and cooperation of the Reactor Operations staff, the Lattice Project staff, the Reactor Machine Shop and Electronics Shop personnel, and the Radiation Protection Office staff, are most gratefully acknowledged. Also, thanks are offered to Mrs. B. R. Hites for her able assistance in the fabrication of detectors and for help with handling and processing of the experimental data. The assistance of Mr. John N. Hanson and Mr. Yosiyuti Hukai with some phases of the experimentation is greatly appreciated. I wish to thank also Miss Donna Dutton for the typing of this thesis.

Acknowledgement is made to the U.S. Air Force for providing the funds for this project, and for the research assistantship held during 1966. I wish to acknowledge two further sources of financial assistance, the General Electric Fellowship, 1965-66, and several U.S. Atomic Energy Commission Fellowships, 1962-65.

CHAPTER I

INTRODUCTION

The study of the prompt γ-rays emitted by a nucleus upon capturing a thermal neutron is of interest to workers in several fields. From capture gamma studies, the nuclear physicist derives basic knowledge about nuclear structure such as nuclear levels and their properties. The nuclear engineer desires radiative capture data for calculating gamma heating due to capture gammas in a nuclear reactor component or for accurately calculating the thickness of a neutron shield.

Several authors have considered prompt capture γ-ray activation analysis (I1, I2, G1, L1) as a technique complementary to normal activation analysis. Early attempts to develop prompt activation analysis were limited because an efficient gamma spectrometer with adequate energy resolution (especially for higher energy capture γ-rays)was not available. The development of lithium-drifted germanium gamma-ray detectors (E1) helped remove this limitation, and enhanced the possibility of performing useful prompt activation analysis for a number of elements. The desire to apply lithium-drifted germanium detectors to the development of prompt activation analysis was the principle motivation for the present work, which involves obtaining the characteristic capture gamma spectrum for various elements.

Several comprehensive review articles (M1, B1, B2, B3) have discussed the various experimental means used to study thermal neutron capture γ-rays. Compilations of thermal capture spectra have been published by several authors (B4, G2, G3). Table 1 summarizes the principle instruments used, their typical energy resolution, and their efficiency. The

TABLE 1

SUMMARY OF PERFORMANCE OF PRINCIPAL INSTRUMENTS USED TO STUDY CAPTURE γ RAYS

Instrument	Useful Energy Range	Typical Resolution	Efficiency	Reference
Magnetic Compton Spectrometer	.3 to 12 MeV	Low resolution spectrometer 2% High resolution spectrometer 0.6% at 1 MeV 0.3% for $E_\gamma > 2$ MeV	10^{-5} to 10^{-7} count per γ-quantum incident on spectrometer	G2 G4 M1
Magnetic Pair Spectrometer	3 to 12 MeV	1 to 2%	10^{-5} to 10^{-7} count per γ-quantum incident on spectrometer	B2 G2 M1
Diffraction Spectrometer	0.030 to 3 MeV	.1% at .1 MeV 1.0% " 1.0 MeV $\frac{\Delta E}{E}$ = E% (E in MeV)	10^{-5} to 10^{-7} count per γ-quantum incident on spectrometer	G2 K1 M1
Scintillation Spectrometer (NaI)	0.03 to 1 MeV 2 to 10 MeV (in a pair spectrometer)	20% at 0.1 MeV 6% at 1.0 MeV	10^{-1} count per γ quantum incident on spectrometer (at 1 MeV)	E1 G2
Lithium Drifted Germanium Spectrometer	0.03 to 12 MeV	1% at 0.1 MeV 0.2% at 1.0 MeV 0.08% at 8 MeV	10^{-2} count per γ quantum incident on spectrometer (at 1 MeV)	E1 M2 O1

magnetic and diffraction instruments have several disadvantages in common: (1) they have low efficiencies (10^{-5} to 10^{-7} counts per incident gamma quantum) which require that the capture source be placed near the reactor core (internal geometry), (2) each effectively covers only a portion of the energy range (0 - 1 2 MeV) in which capture gammas are usually found.

NaI(Tl) scintillation detectors have been used both directly and in a pair spectrometer to study capture γ rays. Although they overcome the above two disadvantages, their lack of resolution strongly restricts their usefulness for studying complex gamma spectra.

The development of lithium-drifted germanium [Ge(Li)] detectors has greatly improved the technique for measuring thermal capture gamma spectra. Ge(Li) detectors have comparable or better resolution than other high resolution spectrometers (with the exception of the diffraction spectrometer at energies less than several hundred keV), and at least several orders of magnitude greater efficiency. In addition, Ge(Li) detectors can cover practically the entire capture gamma energy range and make possible much faster data acquisition rates.

Several workers have reported using Ge(Li) detectors operated directly (i.e., without any coincidence gating) to study capture γ-ray spectra. In 1964, Wasson, et al (W1) reported use of a Ge(Li) detector and Pu-Be neutron sources to study the high energy γ rays resulting from thermal capture in Cl, V, Mn and Co. More recently, Namenson, et al (N1) have published high energy gamma spectra from neutron capture in the hafnium isotopes. They used a small 1 cc active volume planar detector and an internal target geometry. A group at McMaster University has recently studied (P1, H1, H2) some 15 odd-odd nuclei ranging from Cl^{36} to Tl^{204} using an external neutron beam arrangement and a 6 cc coaxial Ge(Li)

detector. Workers at Chalk River (B5, B6) have published capture gamma results for Cr^{50}, Cr^{52} and Cr^{53} obtained using a directly operated 26 cc Ge(Li) detector.

This report describes and presents results of a study of the gamma-ray spectra resulting from thermal neutron capture in natural elements. Chapter II discusses large volume coaxial Ge(Li) detectors. Fabrication techniques used in our laboratory are described and the performance characteristics of several large detectors are illustrated. Chapter III describes the experimental setup -- a Ge(Li) gamma spectrometer (O1), which can be used as a pair spectrometer at high energies and in the Compton suppression mode at low energies, and an external neutron beam capture gamma facility (O2). The analysis of the experimental spectral data to obtain capture gamma energies and intensities is considered in Chapter IV. Results for Be, Fe, Sc, Ge and Zr are presented and discussed in Chapter V.

CHAPTER II

LARGE VOLUME LITHIUM-DRIFTED GERMANIUM GAMMA-RAY DETECTORS

2.1 Introduction

The advent of lithium-drifted germanium (Ge(Li)) gamma-ray detectors, which yield about 10 times better resolution than NaI detectors, has provided the gamma spectroscopist with a new high resolution instrument. Tavendale, in 1963, reported the construction of Ge(Li) detectors of sufficiently large volumes (up to 4 cc active volume) to enable their use as practical gamma spectrometers (T1, E1). Shortly thereafter, workers at a number of other laboratories, including this one, successfully prepared Ge(Li) detectors (G5, G6, H3, S1).

Ge(Li) detectors have been constructed in two basic configurations -- planar and coaxial. Sketches of each type are shown in Fig. 1. The first Ge(Li) detectors were of the planar p-i-n configuration. The active volume (the depletion or i region in which radiation may be detected) of a planar detector, which is the product of the cross-sectional area of the Ge ingot and the depth of drift is limited by the size of available Ge ingots and the depth of drift capable of being achieved in a reasonable length of time. Typically, drift depths of about 1 cm can be obtained in about 4 to 6 weeks. To achieve a drift depth of 2 cm requires an unproportionately greater time (perhaps 4 to 8 months) and effort (several rediffusions would probably be necessary during the course of drift.) In 1965, Malm and Tavendale (M2) described a Ge(Li) detector with a coaxial configuration, which offered the possibility of obtaining a larger active volume for a given drift depth than with the planar configuration.

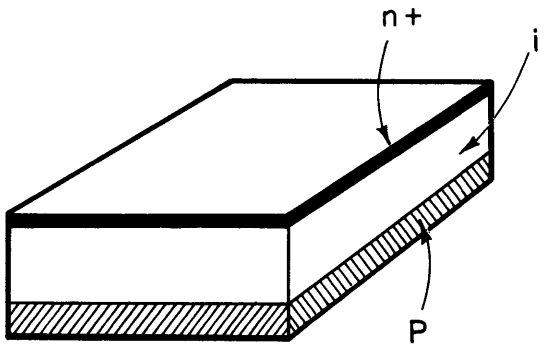

PLANAR DETECTOR

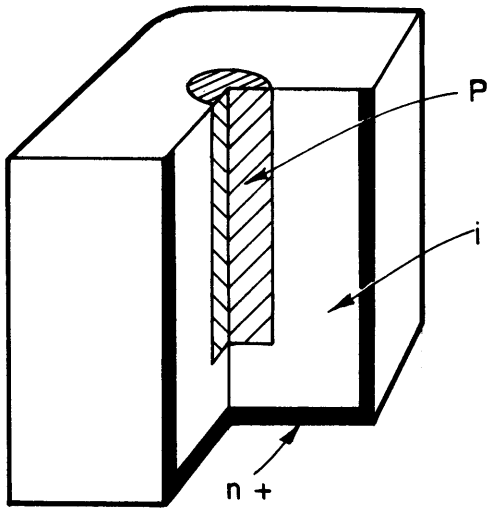

COAXIAL DETECTOR

FIGURE I SKETCHES OF THE PLANAR CONFIGURATION (LEFT) AND THE COAXIAL CONFIGURATION (RIGHT)

This section describes the fabrication techniques used in this laboratory to construct large volume coaxial Ge(Li) detectors. The fabrication techniques used for planar detectors have been described elsewhere (S1). A description of associated equipment is also given. The operating characteristics of several detectors are discussed and gamma spectra of standard radioactive sources are given to illustrate the performance of the detectors. In addition, the performance of large (> 10 cc) volume coaxial detectors is compared with that of smaller planar detectors.

2.2 Fabrication of Large Coaxial Ge(Li) Detectors

Many of the fabrication techniques developed for the preparation of planar Ge(Li) detectors were also used in the preparation of coaxial detectors. Since these techniques have been described in detail by Sovka (S1), the following will describe only those techniques which are not in common with both types of detectors.

2.2.1 Germanium

The germanium* used was p-type, gallium doped, zone-leveled refined and had dislocation densities of less than $3000/cm^2$ and minority carrier lifetimes of greater than 100 μ sec. Successful detectors have been produced using germanium with two different resistivity ranges: 5-12 ohm-cm and 30-45 ohm-cm. The germanium was obtained in ingots having a trapezoidal cross-sectional area, nominally 9 cm^2, and weighing approximately 120 gms per inch.

2.2.2 Preparation of Germanium for Diffusion of Lithium

The germanium ingots were cut into pieces, with lengths varying from

*Supplied by Sylvania Electric Products, Towanda, Pennsylvania.

about 1 cm to 10 cm depending on the detector volume desired, using a thin edge high-speed diamond saw. The germanium ingot was lapped smooth on all sides using water slurries of silicon carbide powders in the same fashion as for planar detectors (S1). Hand lapping of these larger pieces of germanium was laborious and time consuming; consequently, a commercial lapidary was bought and modified to run at a speed of several hundred rpm. Crystals were wet lapped on 8 in. diameter disks of silicon carbide paper. The final lapping step was done by hand. Most crystals were etched for 1 min. in 3:1 (HNO_3:HF) acid solution and rinsed with demineralized water prior to the diffusion of lithium. Whether or not this etching step was performed did not seem to affect the diffusion process.

2.2.3 Diffusion of Lithium to Form a p-n Diode

Three methods have been used to produce a lithium drifted n^+ contact on Ge(Li) detectors: (1) diffusion from a lithium-in-mineral oil suspension coated on the base material (S1), (2) diffusion following electrolytic deposition of lithium from a LiCl/KCl molten salt bath (F1), (3) diffusion following vacuum evaporation of lithium (T2).

The first coaxial detector (about 3 cc) was diffused using method (1). The lithium was suspended in toluene instead of mineral oil as the lithium-in-mineral oil suspension tended to run down the vertical sides of the crystal producing an uneven lithium coating. The toluene rapidly evaporated at room temperature leaving an even layer of lithium. Method (2), which proved to be most convenient for large crystals, was used for all succeeding detectors. Figure 2 shows schematically the apparatus used in applying the lithium from a salt bath. A 1:1 mixture of LiCl and KCl was heated to about 425°C in a graphite crucible. The KCl was added to lower the melting point of the salt bath to about 380°C. The germanium crystal, which is held by an

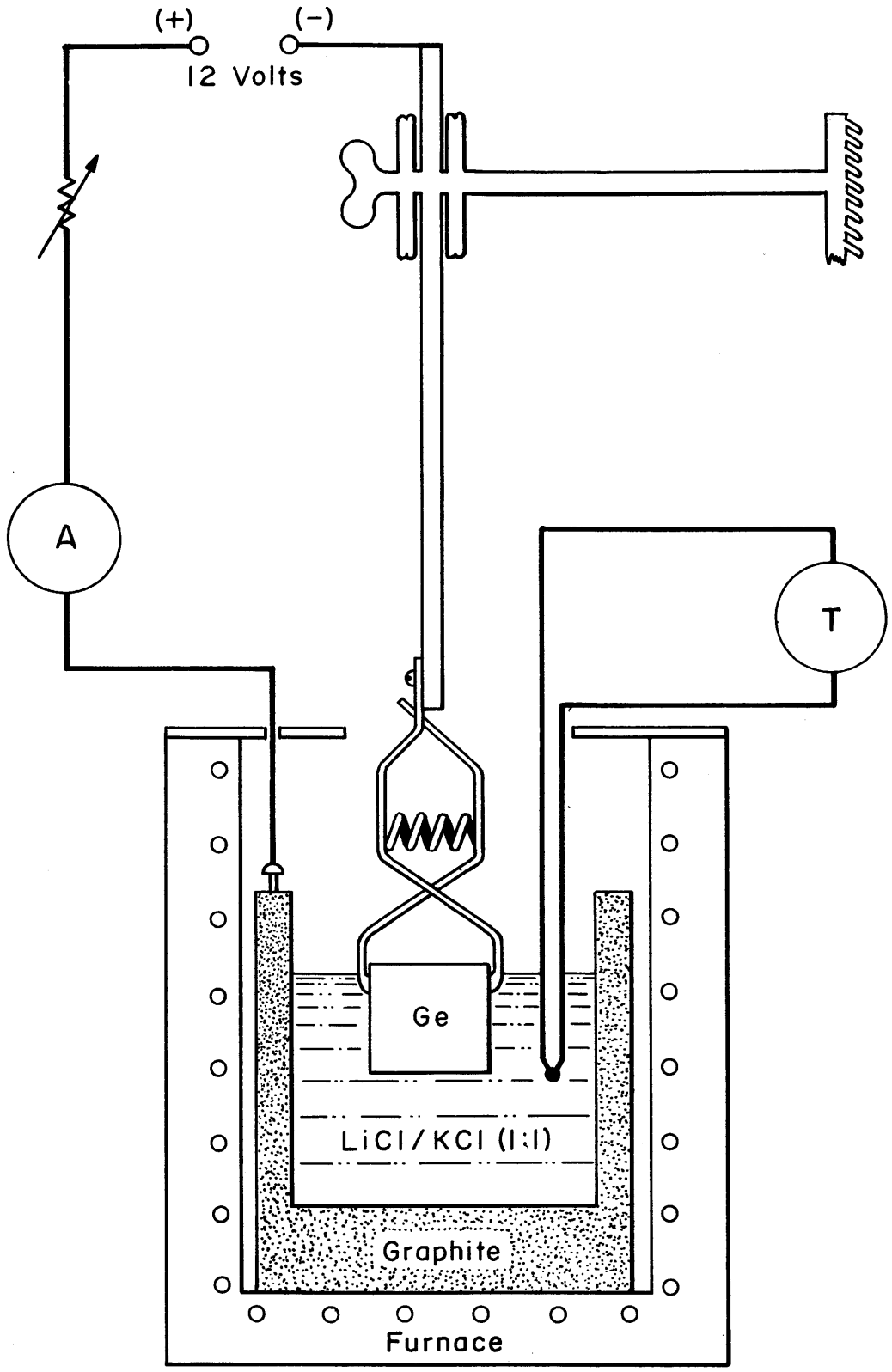

FIGURE 2 APPLICATION OF Li TO COAXIAL DETECTORS

iron clamp or in a nickel wire sling, was then lowered into the bath after preheating over the crucible for at least one hour (to avoid thermal fracture of the germanium).

The lithium was electroplated onto the germanium using a 12 volt d.c. current source. Currents of from 0.5 to 2.0 amps were used depending on the crystal size. It was found most convenient to allow lithium to diffuse on all sides of the crystal and then to lap off the n^+ layer on one end to form the "open end" of the detector. Typically, 15 min. to 30 min. diffusions produced uniform n^+ layers 1 mm to 2 mm thick. Following diffusion, the crystal was gradually cooled to room temperature in about 30 to 60 min. The depth of diffusion was revealed by etching the crystal in HNO_3:HF (2:1) solution for about 1 min. followed by a demineralized water rinse.

2.2.4 Drifting Procedure

Drifting of the lithium was carried out using the vapor-phase cooling method of Miller, et al (M3) in much the same manner as for the planar detectors (S1). Fluorocarbons* were used as the coolant. Prior to drifting, nickel contacts were applied using the electroless plating method (S1), the crystal was etched, first with CP-4 and then with HNO_3:HF (2:1) solution, and its diode resistance measured. Drifting was carried out in drift baths of the type shown in Fig. 3, using reverse d.c. bias voltages from 300 volts at initial stages down to 40 volts at final stages of drift. Current varied from about 0.1 amp to 3 amp and tended to increase (with a constant voltage) as the drift progressed. Up to 300 watts of joule heating in the crystal could be easily dissipated by the boiling fluorocarbon and transferred to the cooling water passing through the reflux condenser. The temperature

*FC-78 (BP = 52°C) from 3M, Inc.
Freon 115 (BP = 47°C) from Dupont.

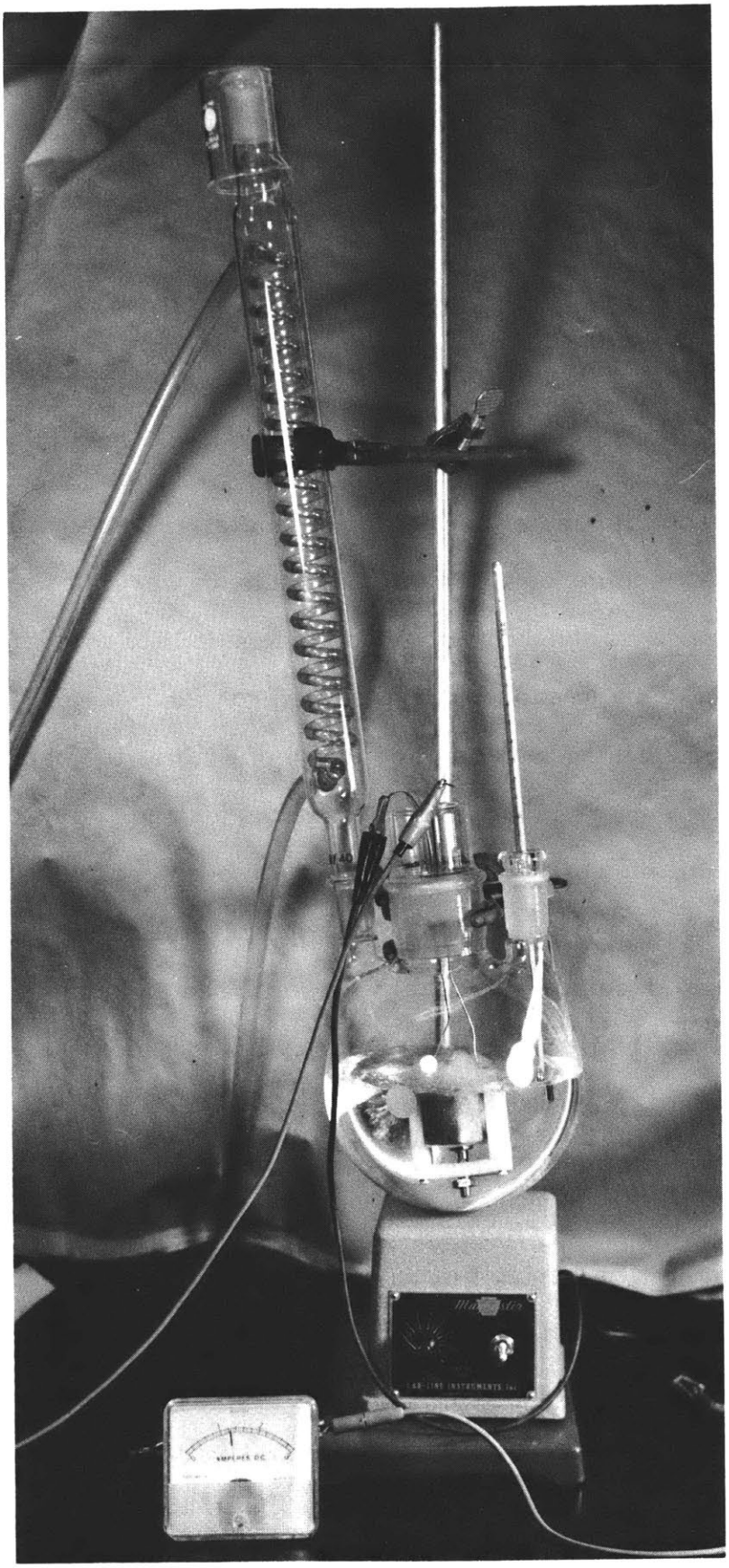

FIGURE 3 DRIFT BATH FOR LARGE COAXIAL Ge(Li) DETECTORS

of a large diode is about 10^{o} to 15^{o}C (T2, M4) warmer than the temperature of the boiling liquid (47^{o}C or 52^{o}C depending on the fluorocarbon used).

The depth of drift was checked periodically, about once a week, using a standard copper plating technique (S1). For the larger coaxial detectors, several drops of plating solution applied to the "open end" were sufficient to copper stain the p-type region when a bias of 2 to 10 volts was applied. In Fig. 4 a photograph of the "open end" of detector number 47, a 35 cc coaxial detector, shows the copper staining of the p-type core. The average depletion depth for this detector was approximately 12 mm with a maximum depth of 15 mm at one corner. The nickel contacts were masked with Apiezon black wax dissolved in trichloroethylene (S1) to protect them from the copper staining and a subsequent etching process.

The copper staining revealed the depth of drift at the open end, but gave no direct information on the drift progress at other points in the crystal. To establish whether drift depth at the open end was a reliable indicator of average drift depth throughout the crystal, a partially drifted crystal (which had developed a crack) was sectioned and copper stained to reveal the shape of the p-type core. The results are shown in Fig. 5. Note that the drift depth is fairly uniform.

The drift time varied greatly from crystal to crystal depending primarily on the initial reverse resistance of the diode. In the case of detector number 37, which had an initial reverse resistance of about 900 ohms, an average drift depth of about 8 mm was achieved in less than 170 hours of actual drift time. The first 4 mm of drift occurred in about 40 hours. Unfortunately, this fast rate of drift was not typical of drift rates of other diodes. An example of a more typical drift rate is afforded by detector number 45 which had an initial reverse resistance of about 80 ohms and which

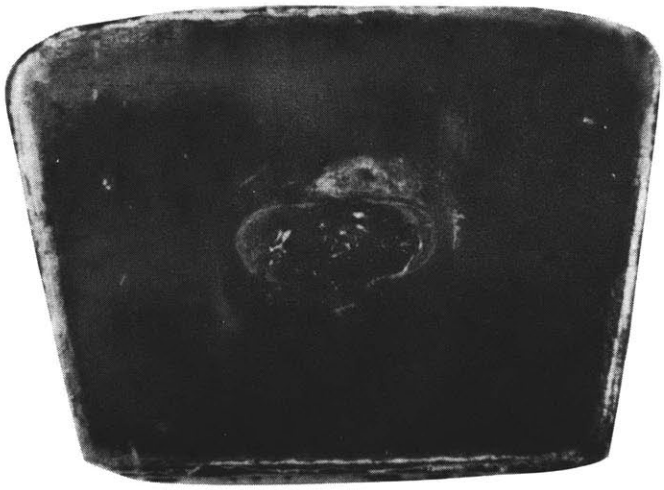

FIGURE 4 PHOTOGRAPH OF THE OPEN END OF A 35cc COAXIAL DETECTOR (NUMBER 47) SHOWING THE COPPER STAINING OF THE P-TYPE CORE.

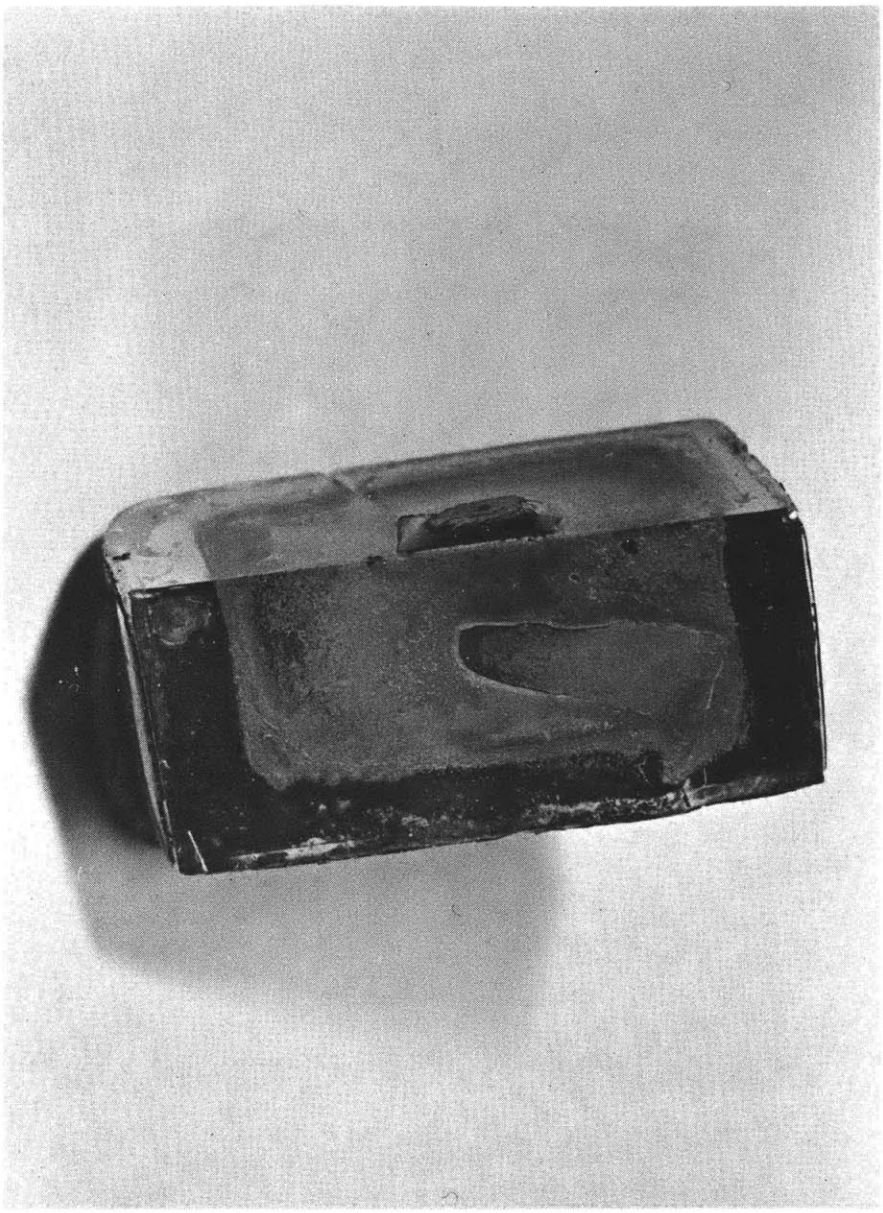

FIGURE 5 PHOTOGRAPH OF THE COPPER STAINING OF A SECTIONED SMALL COAXIAL DETECTOR SHOWING THE UNIFORMITY OF THE DEPLETION DEPTH.

drifted an average of 4 mm in about 300 hours. A rediffusion and a total drift time of about 1500 hours were required to achieve a final average drift depth of 9 mm. The unusually short drift time of detector number 37 can probably be explained by noting that prior to diffusing lithium, a small quantity of copper was diffused into the germanium (copper ions were accidentally introduced into the molten salt bath via dropping a copper wire into it). It is felt that the copper filled the precipitation sites in the germanium and thereby helped retard the precipitation of lithium. Hansen and Jarrett (H4) have reported diffusing copper in germanium to increase the time constant by which super-saturated lithium will precipitate. The success or failure of using copper to retard lithium precipitation depends strongly on the quantity of copper diffused. Too much copper, which is an interstitial impurity, can strain the germanium lattice and lead to cracking of the germanium. Since reasonable lithium precipitation time constants can be obtained in currently available germanium without first diffusing copper and since crystal cracking is a distinct danger associated with copper diffusion, this technique was not used for succeeding crystals.

It was not possible to drift most large coaxial detectors to completion (> 90% of total volume compensated) without reprocessing the diode at several stages of its drift. When, during the course of drifting, a diode either (1) deteriorated to the point when only 40 to 50 volts could be applied or (2) stopped drifting (usually indicated by a cessation of steadily decreasing diode resistance and verified by the copper staining technique), reprocessing was undertaken. In some cases, favorable diode characteristics could be restored by heating the crystal to approximately 400^{o}C -- redissolving the precipitated lithium in the n^{+} layer. Lapping about 0.5 mm off of all 5 n^{+} sides and rediffusing for about 10 min was most effective in re-

storing diode properties. Most diodes required only one or two reprocessing steps.

Following the "hot drift", the detectors were "clean up" drifted at a lower temperature (5°C to 20°C) at reverse biases of from 100 to 500 volts and currents of from 5 to 100 ma. This "clean up" procedure produced a "leveling" of the lithium ion distribution. If this were not done the lithium distribution would be tilted due to the effect, described by Mayer (M5), of the charge in transit across the device at elevated temperatures. Miller (M3) has pointed out that this effect should become very pronounced for extended drifts at high power levels. This probably accounts for the observation that large coaxial detectors required longer "clean up" drifts (as long as 4 or 5 days) than smaller planar detectors.

2.2.5 Cooling of Ge(Li) Detectors

In order to reduce the diode leakage current to an acceptable level ($< 10^{-9}$ amps) for use as a gamma-ray spectrometer, it is necessary to cool the detector to a temperature of less than 150°K (E1) and protect the sensitive surface. After the "clean up" drift, the detectors were given a standard etch treatment (S1) and were cooled in vacuo to 77°K in liquid nitrogen dewars, which have been described in detail elsewhere (K2, S1). In addition to these multi-purpose dewars, a special "snout" dewar, constructed for use in a pair spectrometer, was used. Figure 6 shows a photograph of the snout dewar. The Ge(Li) detector is mounted on a 1" dia. copper cold finger near the end of the snout in a manner which will be described in Chapter III. A Vacion pump (1 ℓ/sec capacity) was more than adequate for maintaining a vacuum of about 10^{-6} mm of Hg. One filling of the 2.5 liter capacity dewar lasts for about 70 hours. A Ge(Li) detector was maintained continuously at 77°K and under vacuum in the snout dewar

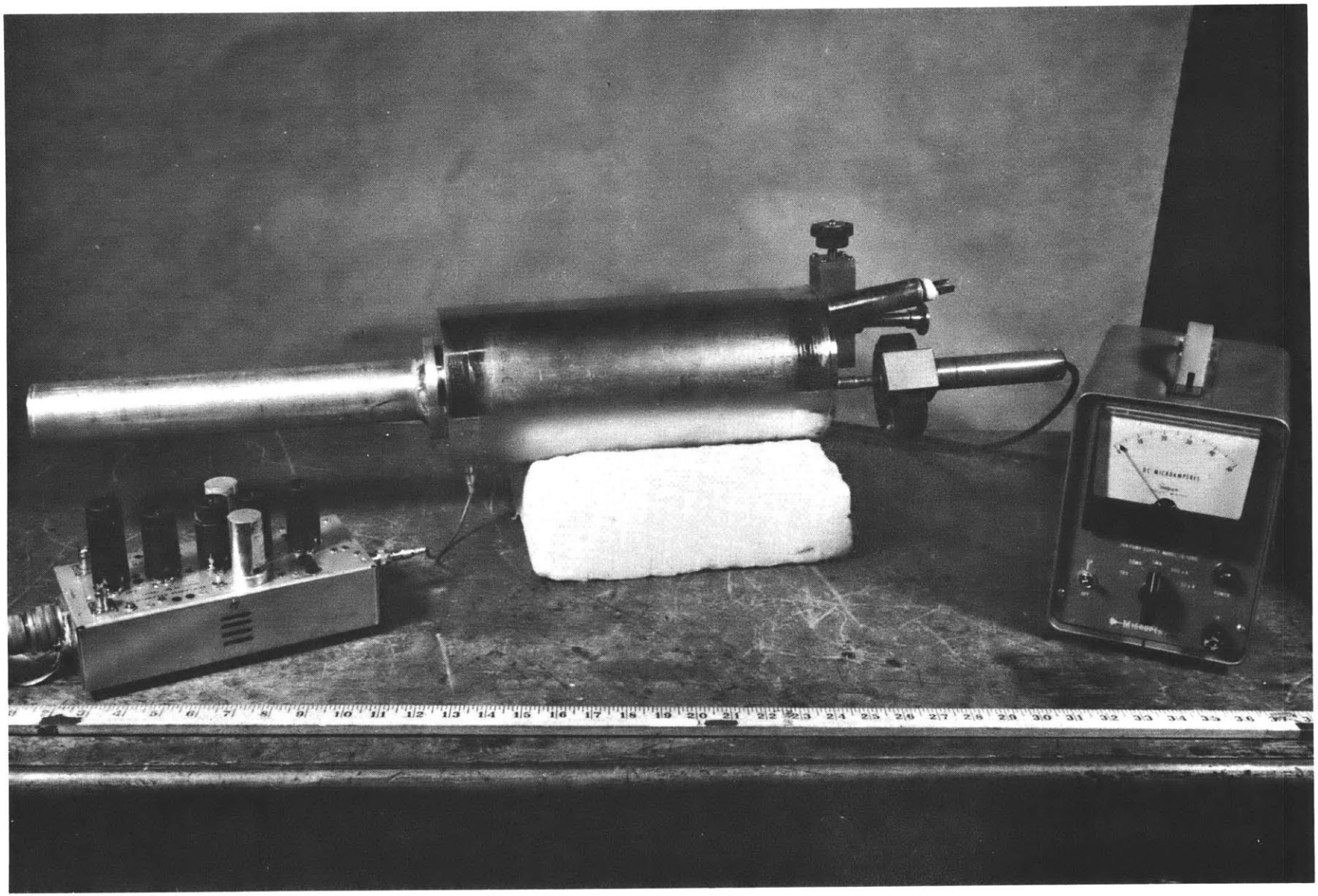

FIGURE 6 LIQUID NITROGEN "SNOUT" DEWAR

for nearly 9 months with no deterioration in detector performance.

2.2.6 Thermal Cycling to Improve V-I Characteristics

The most crucial, and perhaps least certain, step in the fabrication of a successful Ge(Li) detector is cooling of the diode to attain satisfactory reverse voltage vs leakage current characteristics. The reverse leakage current in a cooled Ge(Li) detector has two components: (1) bulk generated current and (2) surface generated current. The surface generate current may be reduced by proper preparation of the sensitive surfaces of the diode prior to cooling (A1).

A "final clean up" procedure, similar to one suggested by Tavendale (T3) was used in this laboratory to improve the V-I characteristics of coaxial Ge(Li) detectors. The detector was warmed up in vacuo in the liquid nitrogen dewar to a temperature of from -30°C to 0°C, with bias applied. Bias levels from 200 volts to 1500 volts with leakage currents of 1 to 10 ma were applied to the diode. After a period of several hours, the diode was re-cooled to 77°K with the bias applied and its V-I characteristics checked. The process was repeated until a satisfactory operating voltage was achieved.

Figure 7 shows the improvement of the V-I characteristic of detector number 37 (a 5cc coaxial detector) after each of two thermal cycles. Note the shift of the breakdown point to higher voltages which allows the detector to be operated at a higher bias level. A corresponding improvement in detector resolution, due to a decrease in charge carrier trapping at the higher voltage, was observed after each thermal cycle. Using this technique, the optimum operating bias has been increased from about 200 volts to over 600 volts for several large coaxial detectors.

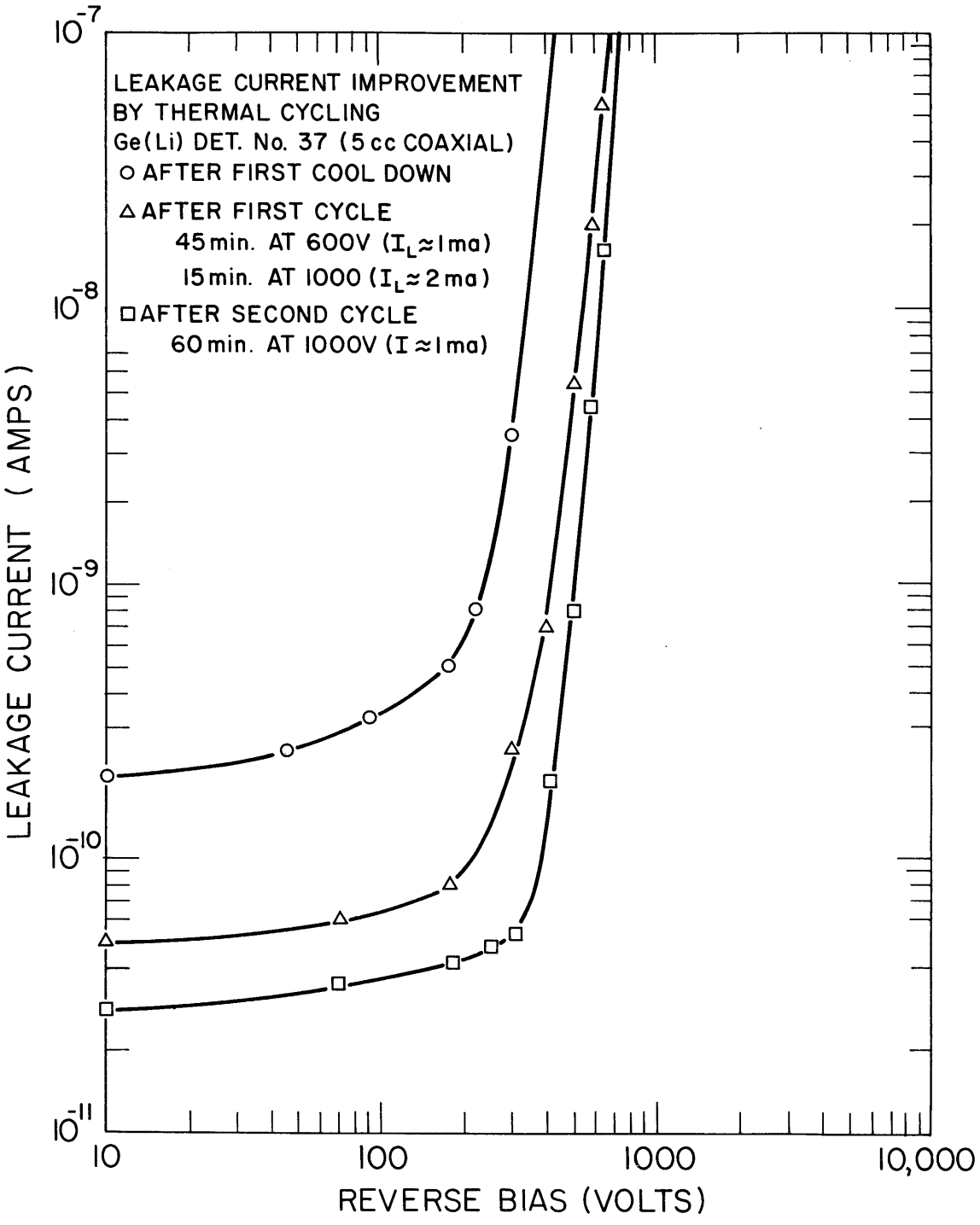

FIGURE 7 IMPROVEMENT OF V-I CHARACTERISTIC AT VARIOUS STAGES OF THERMAL CYCLING

TABLE 2

SUMMARY OF DETECTORS FABRICATED

Detector Designation	Date Started	Type d = average depletion depth for planar type	Active Volume (cm^3)	Current Use
29	2-19-65	planar, d = 5 mm	2	Given to Radiochemistry group
30	2-23-65	planar, d = 5 mm	2	retired
31	3-11-65	planar, d = 8 mm	1.2	Given to Radiochemistry group
32	3-31-65	planar, d = 8 mm	3	retired
33	7-12-65	planar, d = 3.5 mm	3	Given to Rockefeller Generator group
34	7-28-65	coaxial	3	retired
35	9-9-65	planar, d = 4 mm	3.2	Given to Radiochemistry group
37	10-15-65	coaxial	5	retired
43	11-23-65	coaxial	12	22.41 Laboratory
44	12-3-65	coaxial	17	Given to Rockefeller Generator group for $(n,n'\gamma)$ studies
45	12-21-65	coaxial	30	(n,γ) studies
46	1-18-65	coaxial	35	Given to Ray Cooper for Activation Analysis Studies
47	2-2-66	coaxial	35	Used to study feasibility of making large volume, low capacitance detectors
50	5-5-66	coaxial	35	Returned to drift bath unit to decrease p-core
54	7-27-66	coaxial	45	Stored in LN_2 dewar

2.2.7 Detectors Fabricated

Table 2 lists the Ge(Li) detectors fabricated in this laboratory during a period of about 18 months. Also listed is the active volume of each detector and its current use. Detectors in a "retired" status are those smaller detectors for which no liquid nitrogen dewar is currently available. They are stored at about - 20°C for possible later use. Restoration of the original performance of such detectors is not always possible. However, several detectors have been reclaimed. After over 4 months of storage, detector number 35 achieved its original performance (about 4 keV at 662 keV using an uncooled FET preamplifier.)

2.3 Performance of Large Coaxial Ge(Li) Detectors

2.3.1 General Characteristics of Large Coaxial Detectors

There are certain important differences between coaxial detectors and planar detectors. As can be seen in Fig. 1, the sensitive surface area (region of intersection of the p-i-n structure with the surface of the crystal) of a coaxial detector is smaller than that of a planar detector with the same active volume. More importantly, increasing the size of a planar detector increases its sensitive area; whereas, increasing the size of a coaxial detector does not. The relatively insensitive n^+ layer on 5 sides of a coaxial detector simplifies handling of these detectors. The extreme care required in the case of planar detectors to avoid contaminating any of the four sensitive sides is not necessary for coaxial detectors -- only the sensitive "open" end must be protected from contamination. In general, the reverse leakage currents for coaxial detectors (about 10^{-10} amps) are about 10 times lower than the leakage currents of planar detectors. This is probably a result of the smaller sensitive area of coaxial detectors. In

addition, experience indicates that attainment of high operating voltages is easier with the coaxial detectors. In this laboratory, planar detectors are operated in the range of 200 to 400 volts, while coaxial detectors are operated in the range of 600 to 800 volts.

Coaxial detectors appear to be able to withstand being warmed up repeatedly to room temperature better than planar detectors. Several planar detectors were "lost" after a warm up (i.e., they did not operate satisfactorily after re-cooling). All coaxial detectors have been warmed up at least once and none have been lost to date. Detector number 44 has been warmed up over ten times. In each case, an etch treatment and, in some cases, a cold clean up (for about one day) was sufficient to restore original performance.

2.3.2 Performance of Detectors in the Low Energy Range (0-3 MeV)

This section presents spectra of well-known energy calibration standards obtained with several different Ge(Li) detectors. The performance of a Ge(Li) detector depends to a great extent on the quality of the electronics used to process the signal from the detector. Since several different commercial preamplifiers were used, it is not appropriate to consider the following spectra as a strict measure of the quality of the performance of one detector vs another.

Figure 8 shows the gamma spectrum obtained from Co^{57}, which emits two gammas at 122.0 and 136.4 keV, using a 17 cc coaxial detector (number 44). The full-width at half-maximum (fwhm) is 3.4 keV for the 122-keV peak. Larger coaxial detectors also perform well in this energy range. Detector number 45 (a 30 cc coaxial detector) gave less than 4.0 keV (fwhm) on the 122-keV peak of Co^{57}. Coaxial detectors are relatively inefficient for detecting gammas in the X-ray region because of the thick (1 - 2 mm) n^+

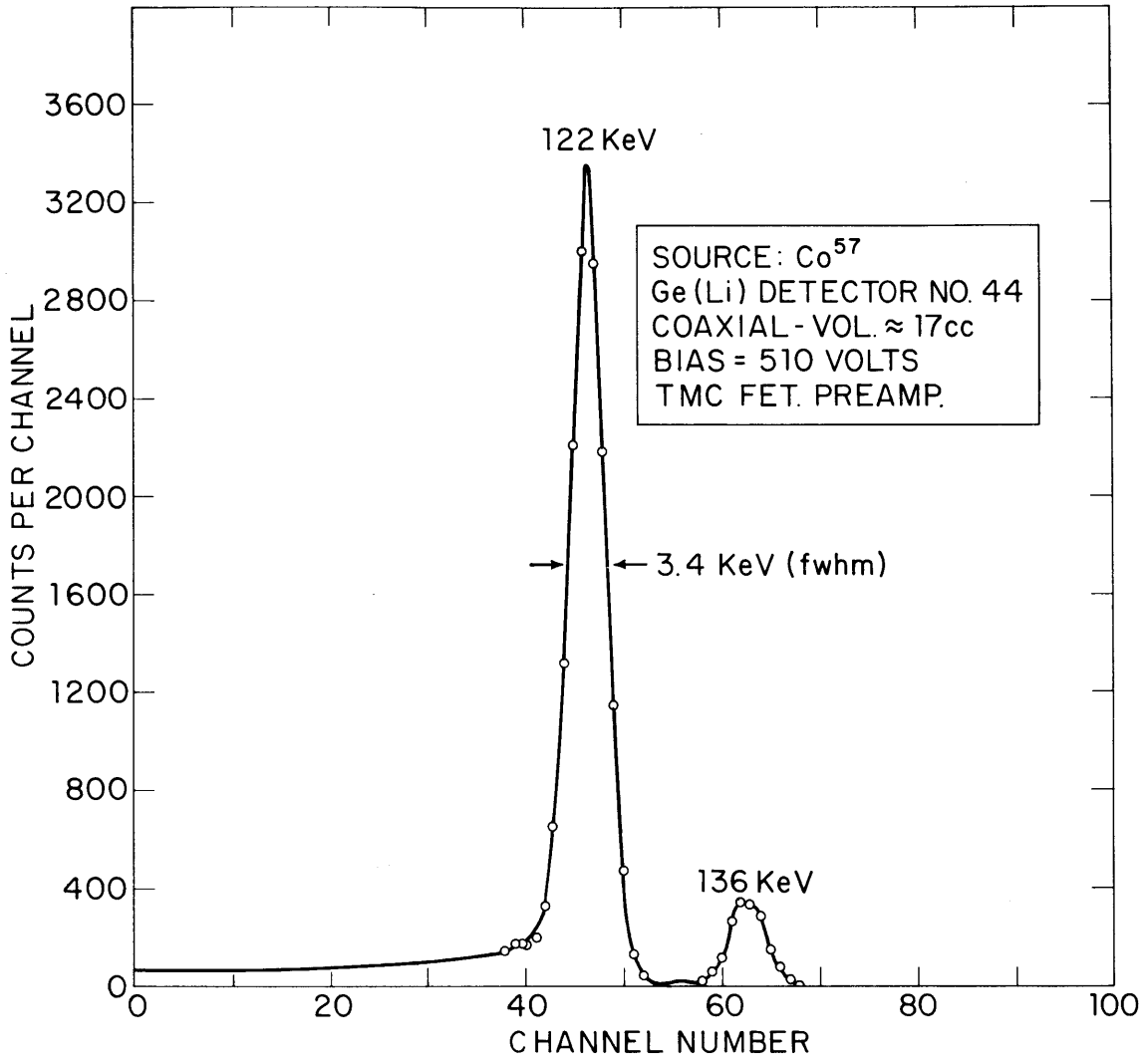

FIGURE 8 SPECTRUM OF Co^{57} OBTAINED WITH A LARGE COAXIAL Ge(Li) DETECTOR

dead layer which exists on 5 sides of the detector. This disadvantage may be overcome by orienting the detector so that the gamma rays enter through the "open" end. This has been done for detector number 44 and X-rays of about 40 keV have easily been detected (M6).

In order to compare the energy resolution of a coaxial with a planar detector, the Co^{57} spectrum measured with detector number 31 (a 1.2 cc planar detector) and comparable electronics is given in Fig. 9. The resolution is 2.16 keV (fwhm) for the 122 keV peak.

The spectrum of the 662 keV gamma of Cs^{137}, measured with a 30 cc coaxial detector (number 45) is shown in Fig. 10. The resolution is 4.7 keV (fwhm) and the peak to Compton ratio is about 8 to 1. Using a small planar detector (0.6 cc active volume), Sovka (S1) obtained for Cs^{137} comparable resolution (4.7 keV) using a vacuum tube-type preamplifier and a peak to Compton ratio of about 3 to 1. The improved peak to Compton ratio for this large coaxial detector results from an increase in the number of counts in the full energy peak due to multiple interactions. The same Cs^{137} spectrum measured with detector number 44 (a 17 cc coaxial) using a cooled Field-Effect Transistor (FET) preamplifier* is shown in Fig. 11. The resolution is 2.8 keV (fwhm) on the 662-keV γ ray and the peak to Compton ratio is about 12:1. This illustrates the degree of improvement in detector performance which can be accomplished through the use of higher quality low-noise electronics.

Figure 12 shows the spectrum of the 2614-keV gamma of ThC'' obtained with detector number 45 (a 30 cc coaxial detector). This spectrum illustrates the typical response of a large coaxial Ge(Li) detector to a monoenergetic medium-energy gamma. The photopeak (or full-energy peak), the single

---

*Designed and constructed by C. Takahata in this laboratory.

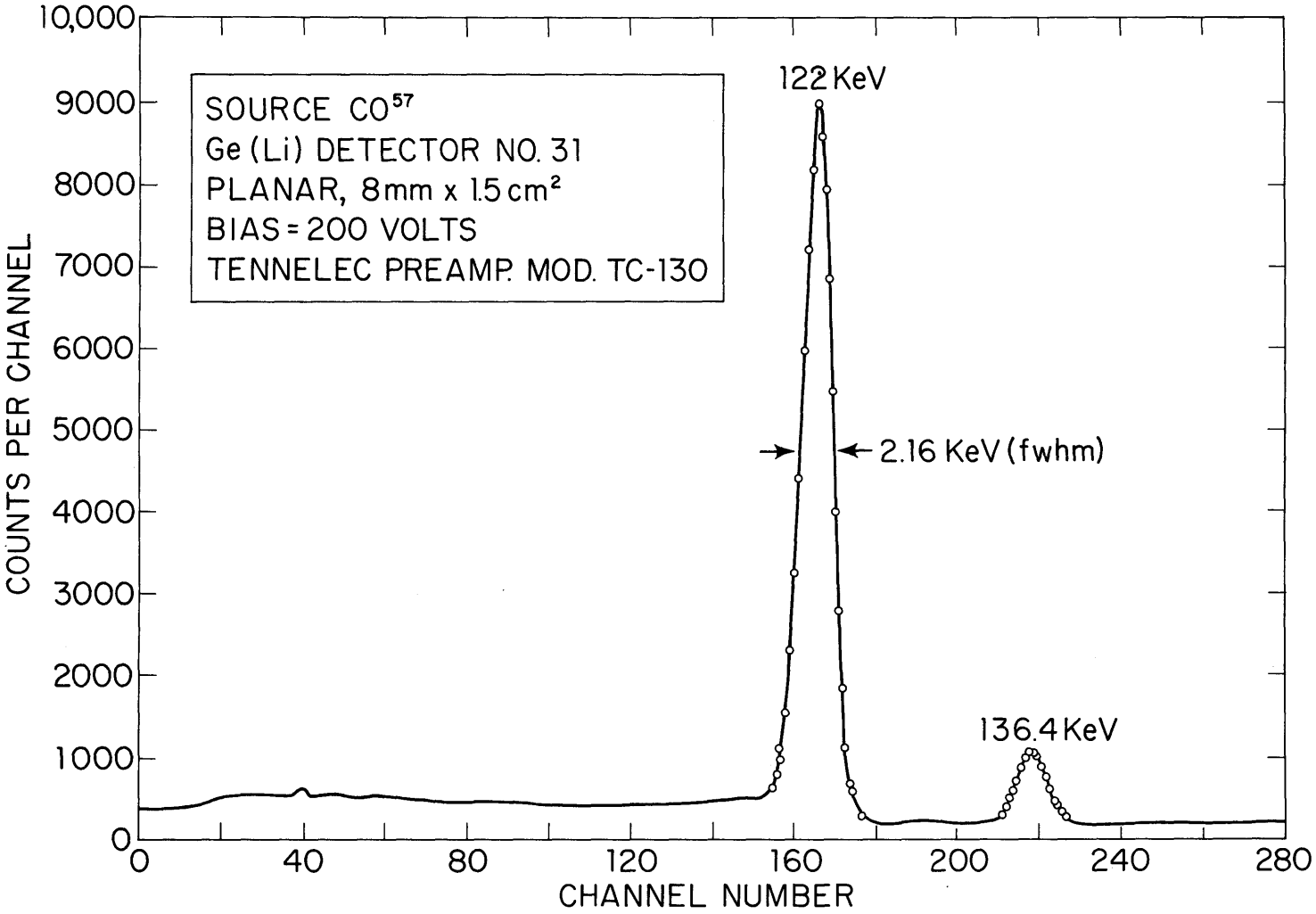

FIGURE 9 SPECTRUM OF Co^{57} OBTAINED WITH A SMALL PLANAR Ge(Li) DETECTOR

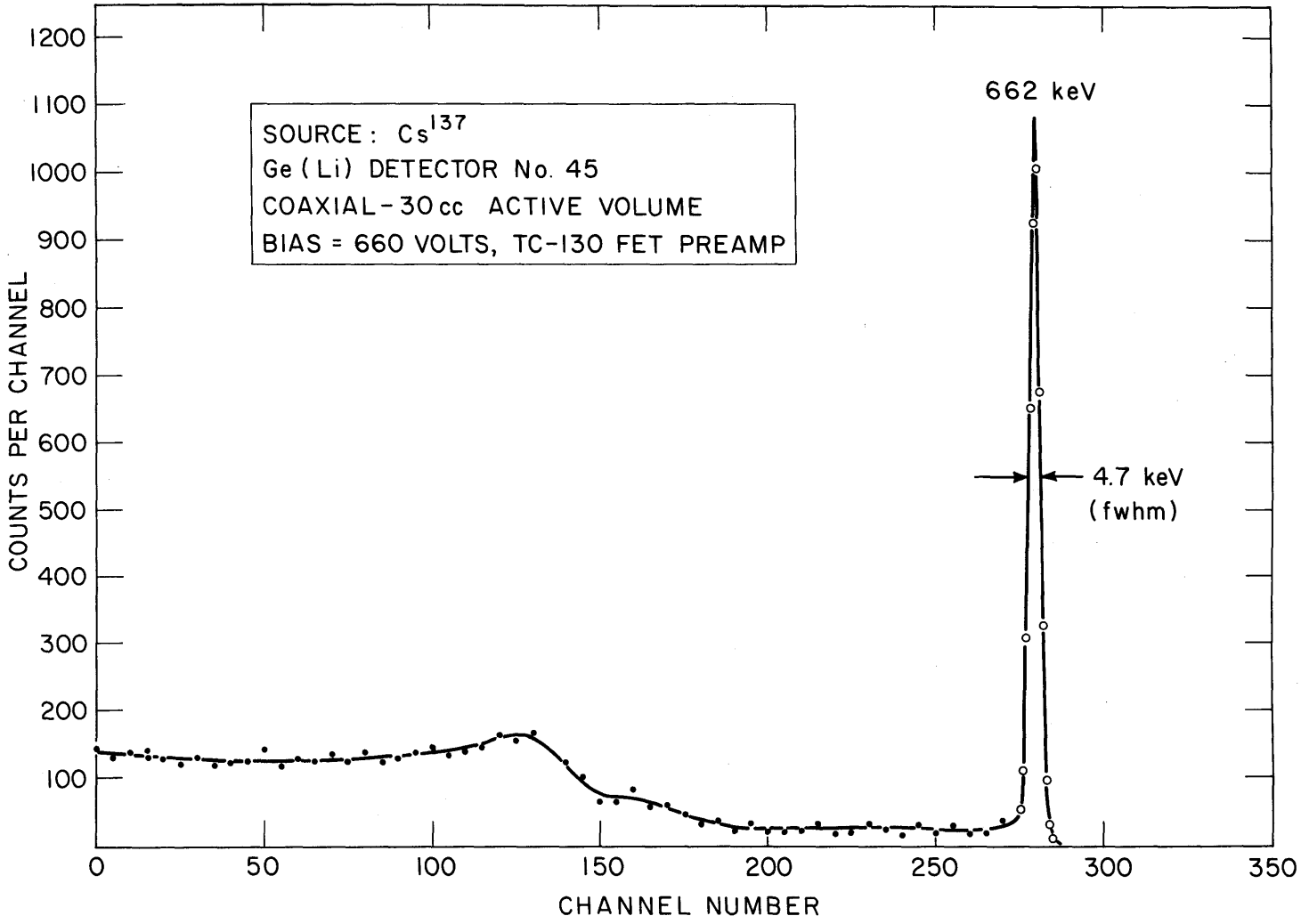

FIGURE 10 SPECTRUM OF Cs^{137} OBTAINED WITH A 30cc COAXIAL Ge(Li) DETECTOR AND AN UNCOOLED FET PREAMP

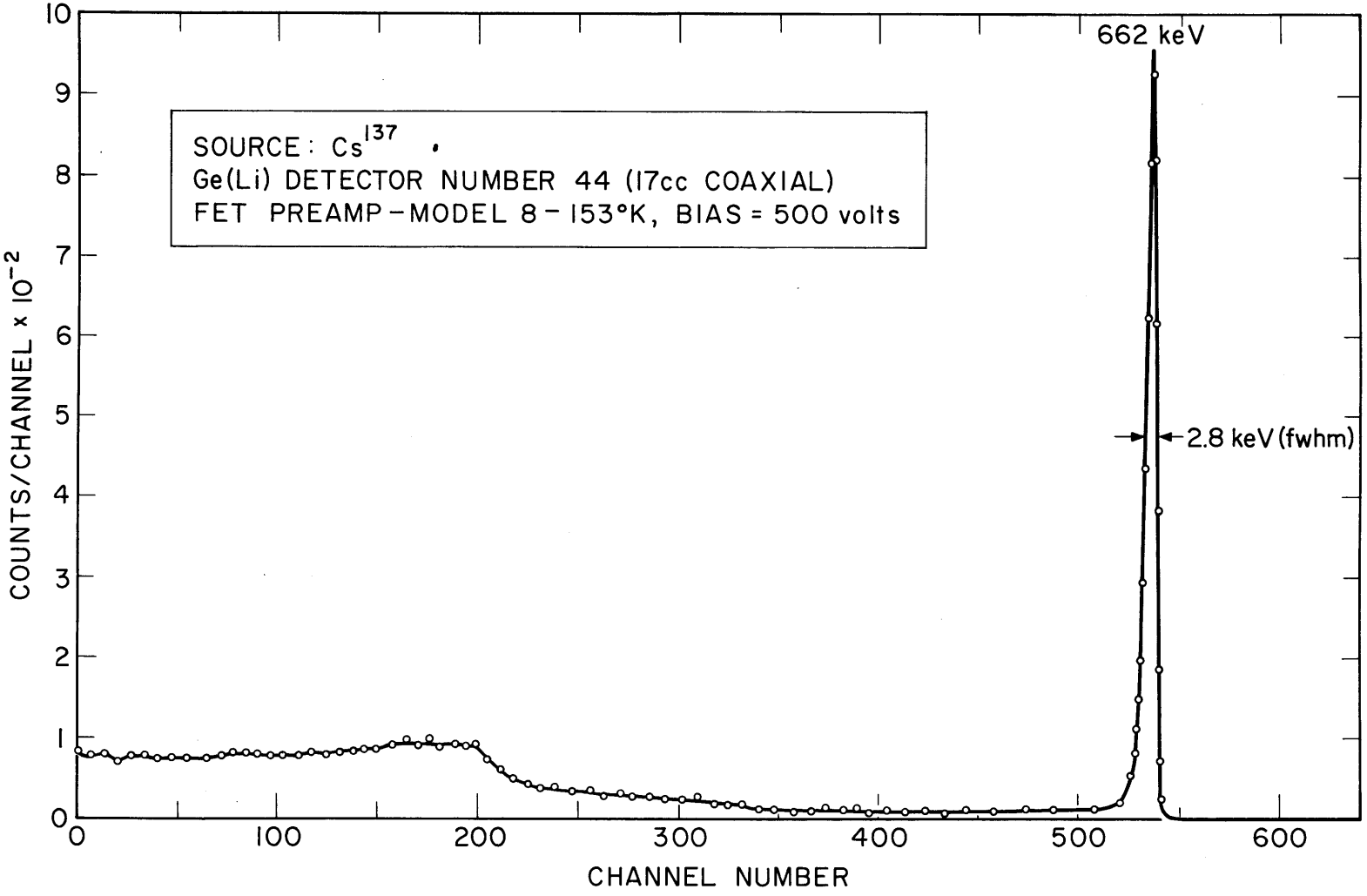

FIGURE 11 SPECTRUM OF Cs^{137} OBTAINED WITH A 17cc COAXIAL DETECTOR AND A COOLED FET PREAMP

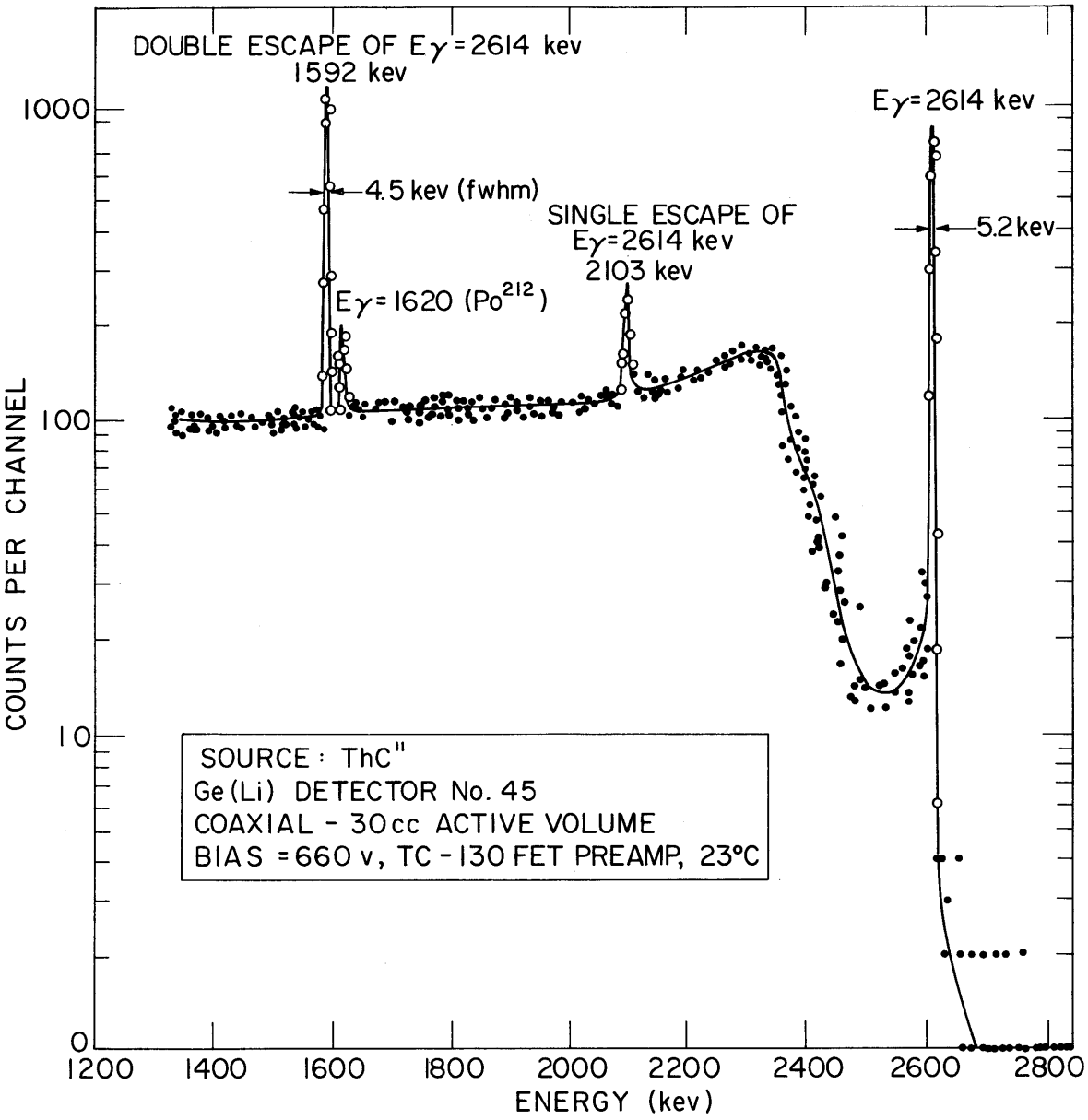

FIGURE 12 SPECTRUM OF 2614 kev γ-RAY OF ThC" OBTAINED WITH A 30cc Ge(Li) DETECTOR

escape pair peak, the double escape pair peak, and the Compton distribution are clearly evident for this 2614-keV gamma. The resolution of the full-energy peak (fep) is 5.2 keV (fwhm) and that of the double escape peak (dep) is 4.9 keV (fwhm). The peak to Compton ratio is nearly 6:1 using this large detector. Using the same small planar detector as for Cs^{137} Sovka (S1) obtained a resolution of about 8 keV (fwhm) and a peak to Compton ratio of about 0.8:1 for ThC''. The peak to Compton ratio increased by about a factor of 7 at 2614 keV compared to less than a factor of 3 increase in 662 keV.

2.3.3 Performance of Detectors in the High Energy Range (3-12 MeV)

The performance of detector number 45 (a 30 cc coaxial) at high energies is illustrated by the separation achieved on the well known 14-keV doublet at 7.646 MeV in the capture gamma spectrum of iron. Figure 13 shows this region of the iron capture gamma spectrum. The ratio of the peak to valley is about 5:1 for the double-escape peak (dep) of the doublet. Note that for this large detector, the full-energy peak (fep) and the single escape peak (sep) of the doublet are also observed. The intensities of these three peaks are approximately in the following ratio: dep:sep:fep = 21:3:1. The resolution at 7.646 MeV on the double escape peak is 6.8 keV (fwhm) using an uncooled FET preamplifier.

For comparison, Fig. 14 shows the double-escape peak of the same iron doublet as observed using detector no. 32 (a 3 cc planar detector). For this smaller detector, only the double-escape peak is observed. The resolution on the doublet at 7.646 MeV was 9.8 keV (fwhm) using a vacuum tube preamplifier. With better performance electronics, the energy resolution of the small detector would certainly have equaled and probably exceeded that of the larger detector.

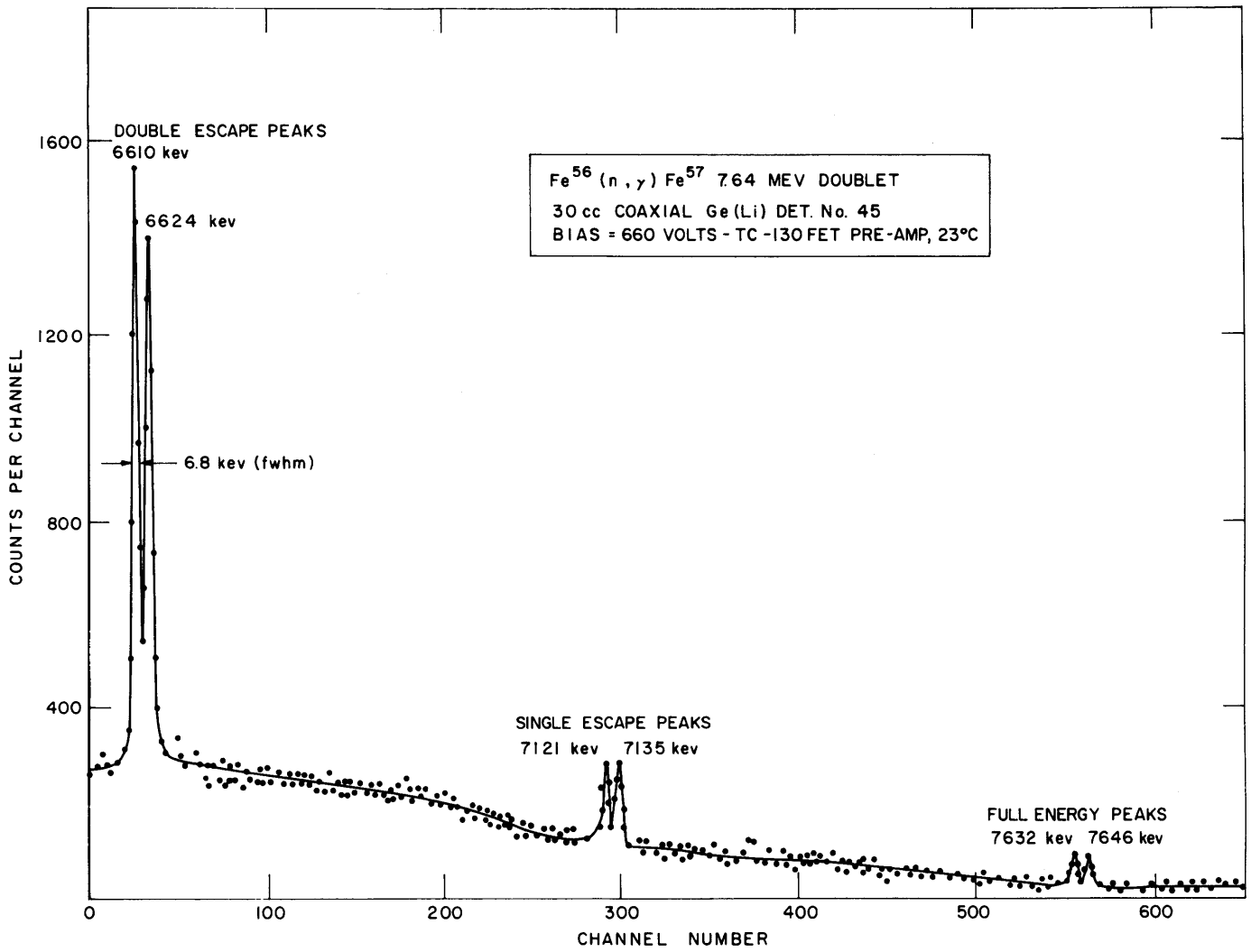

FIGURE 13 SPECTRUM OF 14-kev DOUBLET AT 7646 kev FROM Fe THERMAL CAPTURE OBTAINED WITH A 30cc Ge(Li) DETECTOR

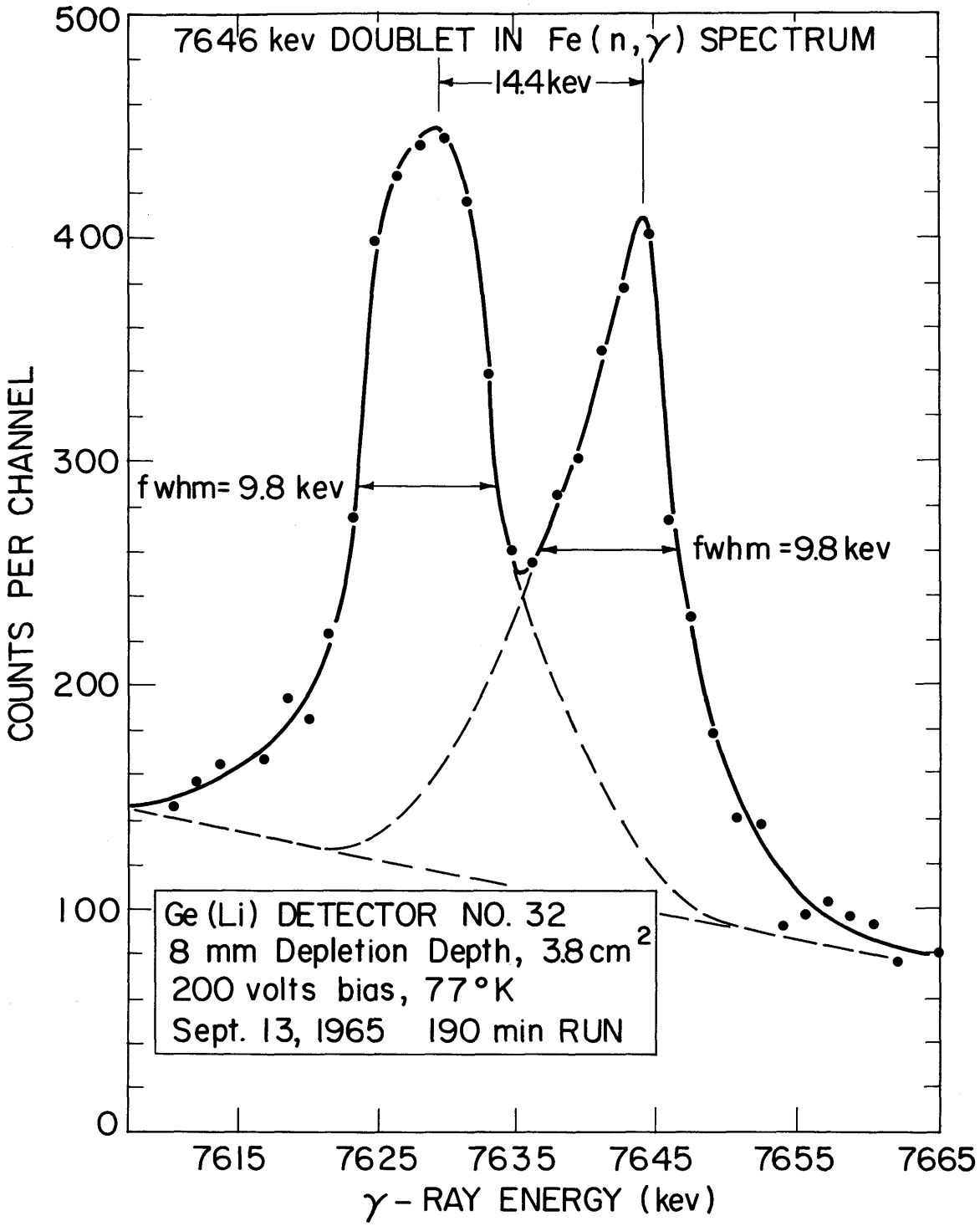

FIGURE 14 RESOLUTION OF 7646 KeV DOUBLET IN IRON SPECTRUM USING A SMALL PLANAR Ge(Li) DETECTOR

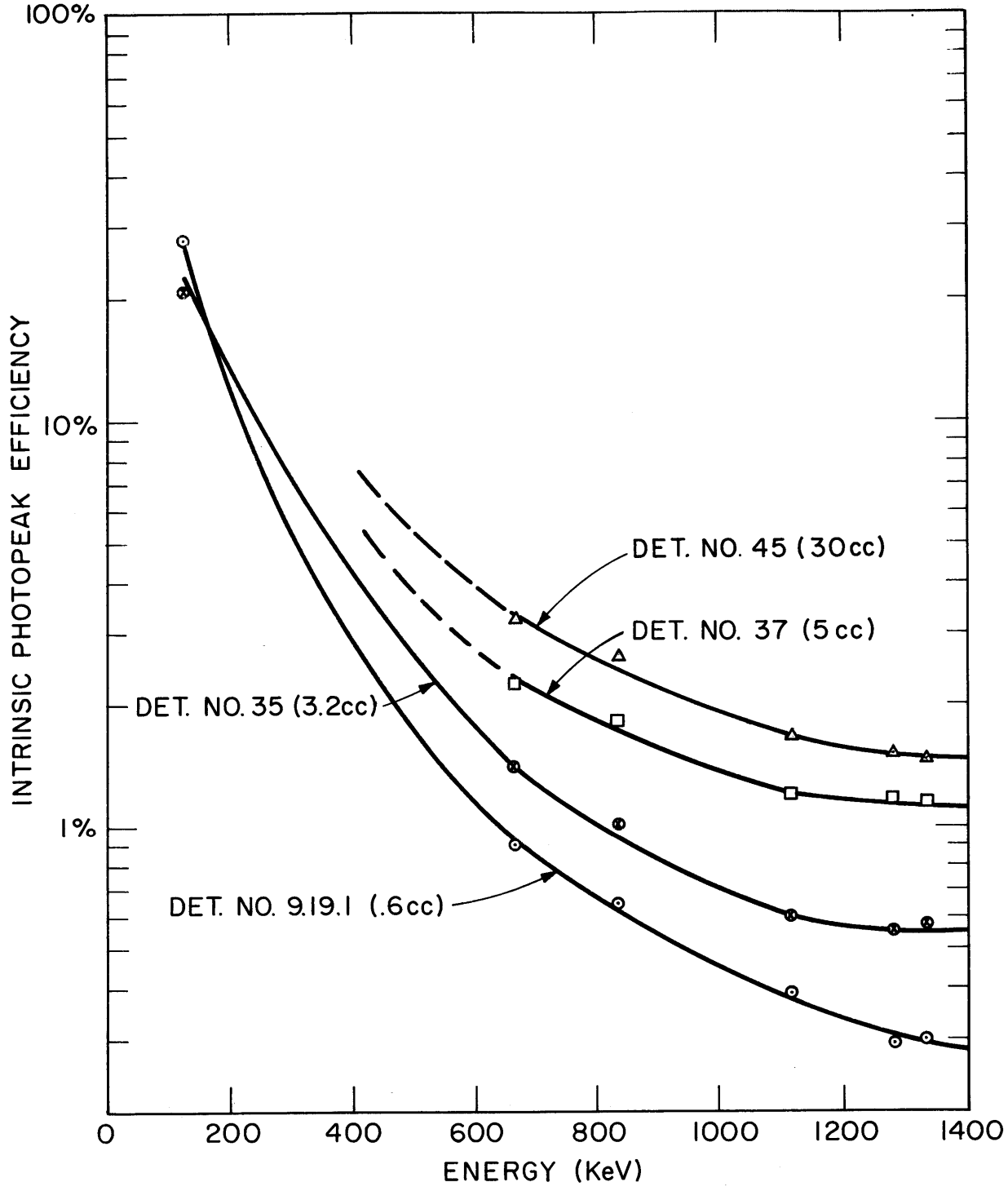

FIGURE 15 INTRINSIC PHOTOPEAK EFFICIENCY VS. ENERGY FOR 4 DIFFERENT SIZE Ge(Li) DETECTORS

2.3.4 Efficiency

The intrinsic photopeak efficiency increases with detector size because a greater percentage of multiple events are detected. This effect is illustrated in Fig. 15, which shows intrinsic photopeak efficiency curves for four different size detectors. The intrinsic photopeak efficiency of the 30 cc detector is approximately 7 times that of the 0.6 cc detector. The intrinsic photopeak efficiencies were measured using calibrated sources of Co^{57}, Cs^{137}, Mn^{54}, Na^{22} and Co^{60}. Detectors 9-19.1, 35 and 37 were oriented so that the maximum thickness of the active volume was in an uncollimated gamma-ray beam. In the case of detector 45, a 3/8" dia. collimated beam of gamma rays centered on the closed end of detector was used in order to facilitate calculation of the solid angle correction. Use of an uncollimated source would probably have yielded higher efficiencies.

2.3.5 Linearity

Ewan and Tavendale (E1) have verified the linearity of the response of a Ge(Li) detector from 60 keV to 2620 keV within 0.3% (the accuracy of their pulser calibration). Using detector 45 in a gamma spectrometer, the energies of capture gamma rays in the range of 0.1 to 11 MeV have been determined to an accuracy of about 1 keV -- using a method described in Chapter IV. The nonlinearity of the entire system, except for the detector, was accounted for in these energy determinations as described in Sec. 3.3. Hence, it may be concluded that within the accuracy of these measurements (0.1% at 1 MeV and 0.01% at 10 MeV), the Ge(Li) detector was linear over the energy range 0.1 to 11 MeV.

2.3.6 Energy Resolution

The energy resolution of a Ge(Li) detector and its associated low-

noise electronics is determined by the following factors:

(1) Noise associated with the reverse leakage current of the detector.

(2) Electronic noise contributed by the preamplifier and linear amplifier.

(3) Loss of resolution due to electronic instabilities (i.e., gain and zero shifting).

(4) Statistical fluctuations in the number of hole electron pairs produced in the detector.

The last factor represents the theoretical limit on the resolution which can be achieved using a Ge(Li) detector. The resolution contributed by this factor as measured by the full-width at half-maximum (fwhm) in a pulse height distribution is given by (H5):

$$\text{FWHM (keV)} = 2.355\sqrt{\epsilon F E}$$

where

E = the energy of the electron in keV,

ϵ = the average energy to create a hole-electron pair (2.94 eV in Ge)

F = the Fano factor (F2), which accounts for the fact that the statistical distribution is not a purely Poisson distribution.

Determination of the ultimate resolution obtainable from a Ge(Li) detector necessitates a measurement of the Fano factor. Measurements are made difficult by the requirement that factors (1) through (3) be eliminated or made negligible compared to the fwhm contributed by factor (4). Mann, et al (M7) have found that

$$F = 0.13 \pm 0.02 \text{ at } 122 \text{ and } 356 \text{ keV}$$

$$F \leqq 0.16 \pm 0.01 \text{ at } 1 \text{ MeV} \leqq E \leqq 10 \text{ MeV}$$

If the above equation is evaluated at 7.6 MeV, the fwhm is 4.5 keV. The fwhm observed using the 30 cc detector (number 45) was 6.8 keV, with an electronic noise contribution of 4.5 keV. The detector contributed resolution, 5.1 keV, is greater than the theoretical value due to contributions from

effects (1) and (3).

As illustrated in Figs. 8 and 9, the resolution of large coaxial detectors is, in general, not as good as that of planar detectors. The reason is that their greater detector capacitance (typically 30 to 100 pf vs 5 to 20 pf for planar detectors) causes an increase in the electronic noise contribution of the charge-sensitive preamplifier. Recent improvements (S2) in the design of preamplifiers (such as use of several paralleled FET's and cooled FET's) have decreased the effect of detector capacitance on electronic noise to the point where the resolution of large coaxial detectors is quite comparable to that of planar detectors.

CHAPTER III

EXPERIMENTAL EQUIPMENT

3.1 Introduction

As mentioned in Chapter I, directly operated Ge(Li) detectors have been and are being used to study complex gamma spectra such as those originating from thermal neutron capture. Even though Ge(Li) detectors offer comparable or better resolution and much higher efficiencies than other high resolution spectrometers, they suffer from two principal disadvantages, namely, inferior peak to background ratios compared to other high resolution spectrometers and a multiple spectral peak response for high energy gammas which greatly complicates the analysis of a complex spectrum.

Use of a Ge(Li) detector as the primary detector in a 3-crystal pair spectrometer helps remove the above two disadvantages for energies greater than about 2 MeV. Ewan and Tavendale (E1) have described a 3-crystal pair spectrometer which uses a small (< 3 cc) planar Ge(Li) detector and two 2" x 2" NaI crystals.

At low energies the ratio of the full-energy peak to Compton background may be improved by using a Compton suppression mantle. Kantelle and Suominen (K3) have described such a system which uses a large NaI annulus as a Compton suppression mantle for a small planar detector.

This chapter describes and discusses the performance of a Ge(Li) gamma-ray spectrometer which can be operated as a 3-crystal pair spectrometer at high energies and in the Compton suppression mode at low energies. The performance of the pair spectrometer is compared using three different size Ge(Li) detectors (a 3 cc planar, a 5 cc coaxial, and a 30 cc coaxial). The performance of the spectrometer in the Compton suppression mode is

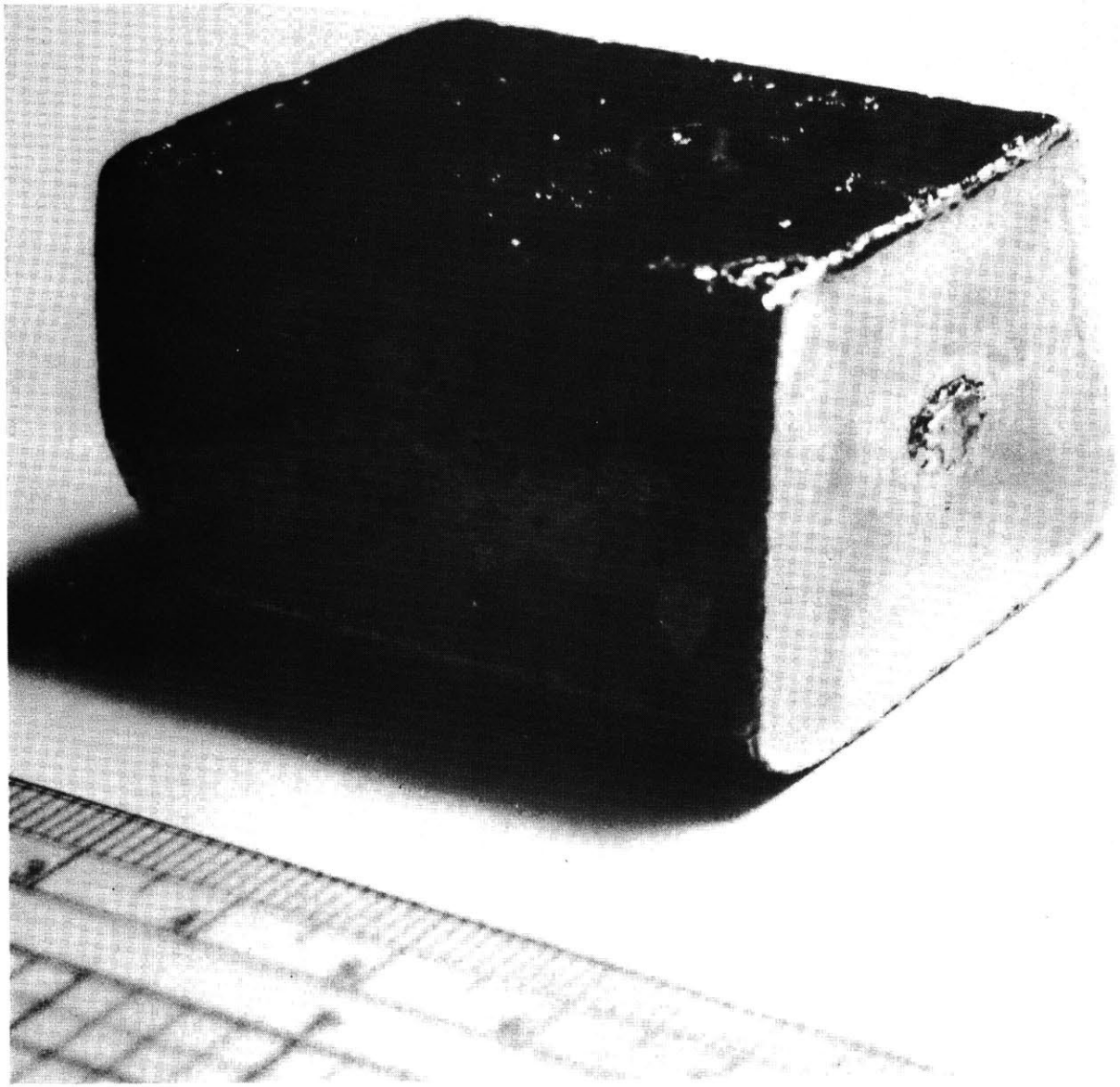

FIGURE 16 PHOTOGRAPH OF A 30 cc COAXIAL Ge(Li) DETECTOR (No. 45)

discussed for the two larger detectors. However, the performance using the 30 cc Ge(Li) detector is emphasized since this large detector was used to obtain the capture γ-ray data reported in this work. An external neutron beam facility is also described and its operating characteristics discussed.

3.2 Description

3.2.1 Detectors

Although detectors of smaller sizes were tried, the principal detector used in these studies had a sensitive volume of 30 cc (detector number 45 of Table 2). The detector is shown in Fig. 16. The optimum operating bias for this detector was 660 volts and the leakage current at this voltage was about 5×10^{-10} amps. The capacity under these conditions was approximately 70 pf.

The mounting of the 30 cc Ge(Li) detector on the copper cold finger of the snout dewar is shown in Fig. 17. The U-shaped detector mount was designed to minimize the absorption of 511 keV annihilation photons escaping from the Ge(Li) detector while maintaining adequate thermal contact with the detector. A teflon spacer, which had a 1" dia. hole so as to minimize gamma attenuation, was used to insure that the copper cold finger and Ge(Li) detector were centered inside the 2" dia. aluminum cover (shown removed in Fig. 17.) The "closed end" of the detector was oriented towards the γ-ray beam in order to assure maximum detection efficiency.

Figure 18 shows schematically the position of the Ge(Li) detector between two large (6" dia. x 3") NaI(Tl) detectors. Each NaI detector has a 1" radius semi-circular slot cut into its face so that the snout of the dewar containing the Ge(Li) detector will just fit into the 2" dia. hole formed when the NaI detectors are positioned face to face. A pair production interaction is shown taking place in the Ge(Li) detector. Annihilation of the position

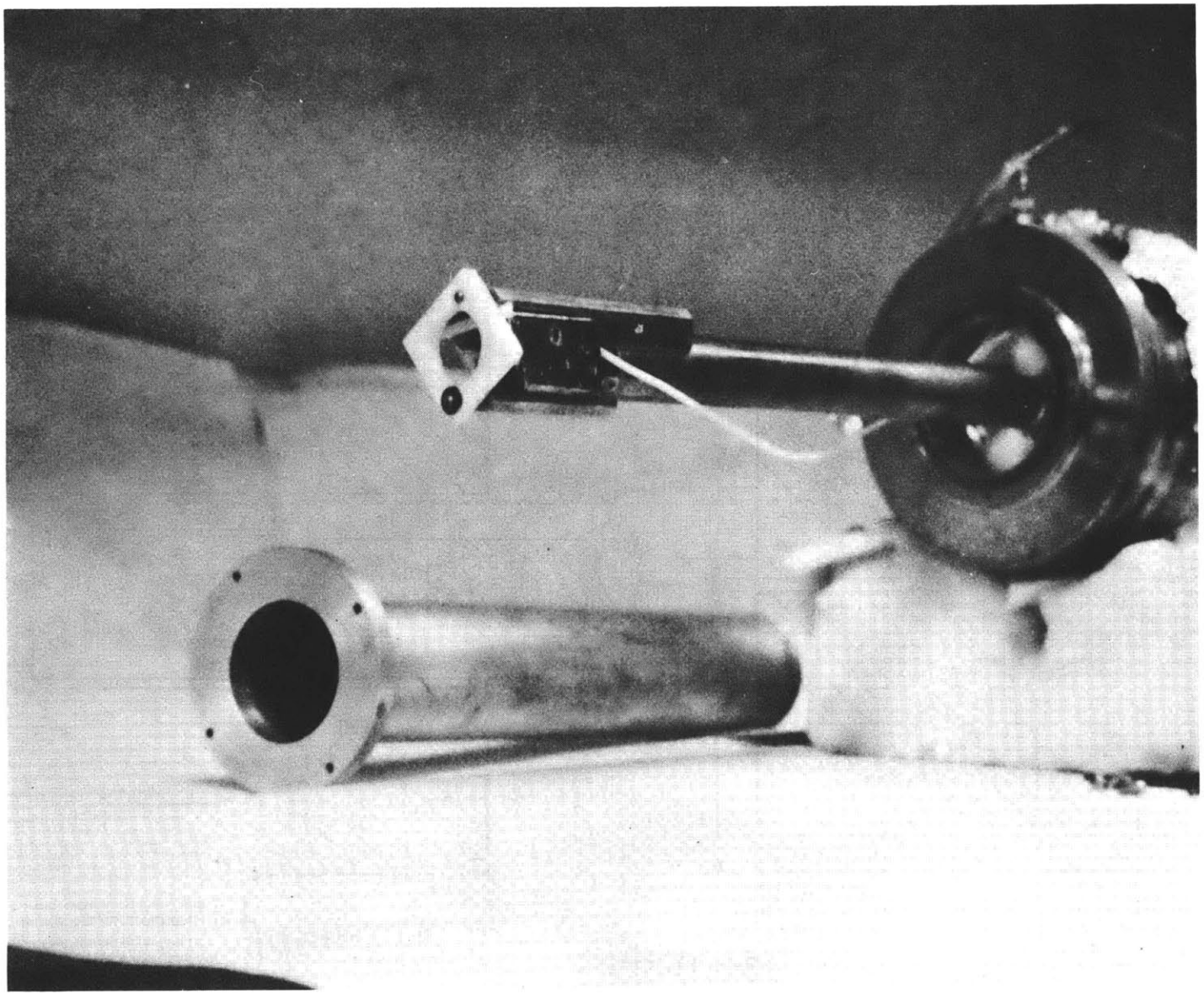

FIGURE 17 DISASSEMBLED "SNOUT" DEWAR SHOWING MOUNTING OF DETECTOR ON COPPER COLD FINGER

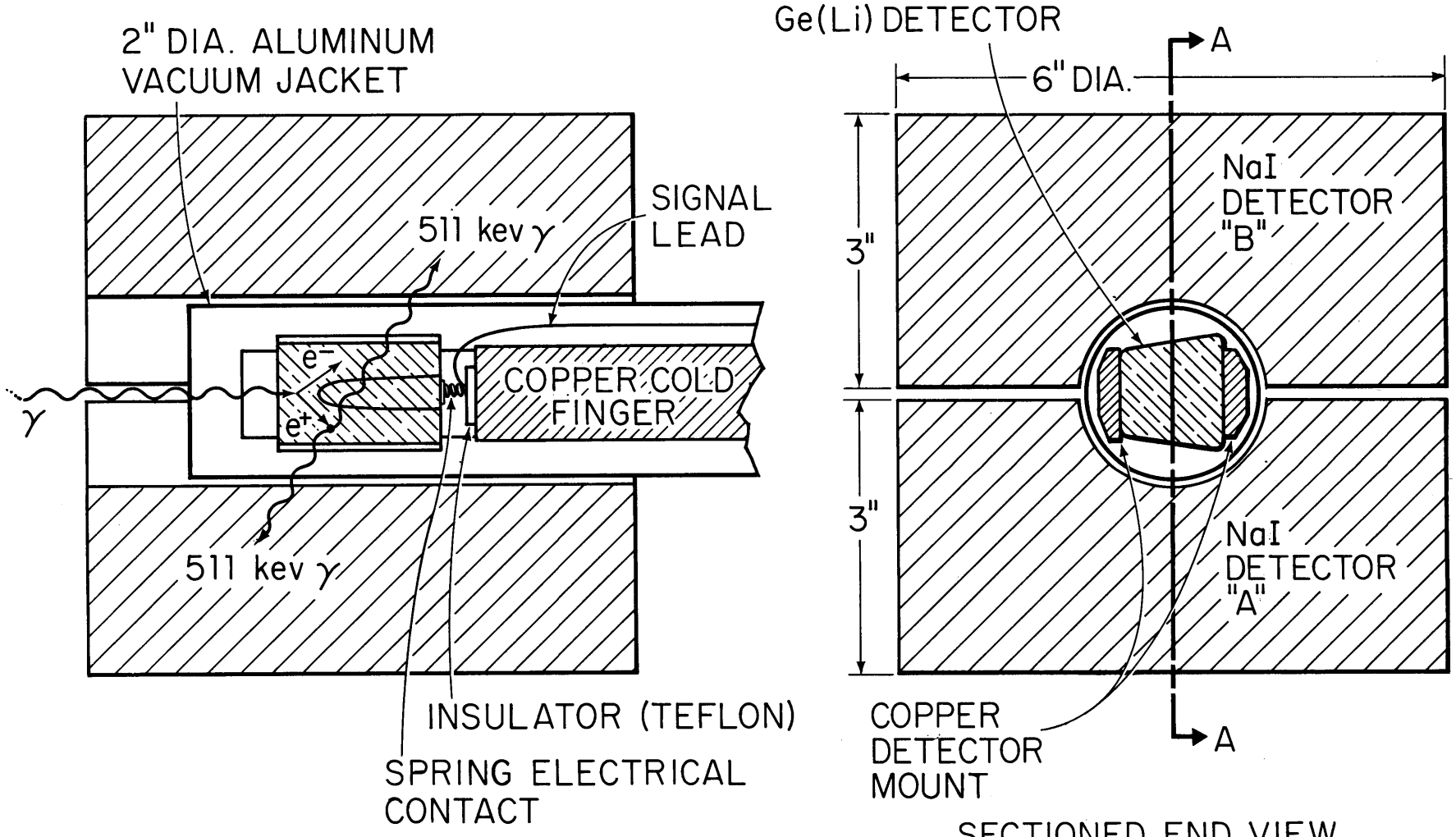

FIGURE 18 SCHEMATIC SHOWING THE ORIENTATION OF THE Ge (Li) DETECTOR BETWEEN THE TWO NaI CRYSTALS

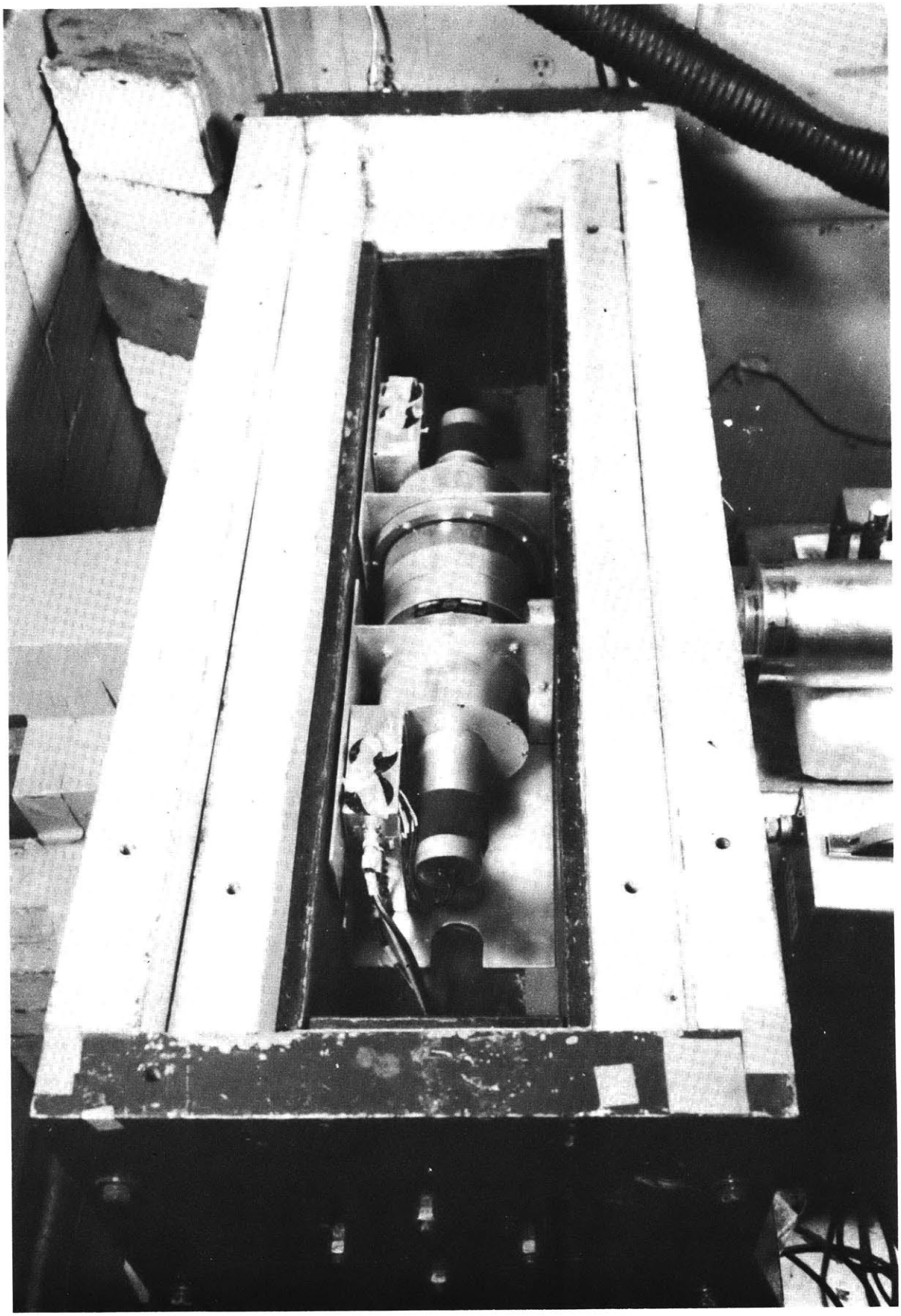

FIGURE 19 PHOTOGRAPH OF SPECTROMETER FROM ABOVE SHOWING THE POSITION OF THE 3 DETECTORS WITHIN THE SHIELD

produces two 511-keV gammas, 180^{o} apart, which are shown being absorbed by the NaI detectors. It is events of this type which are electronically selected for analysis in the pair spectrometer mode of operation.

A photograph, from above, of the Ge(Li) spectrometer is shown in Fig. 19. The coffin-like detector shield, which has 5" steel walls lined with 3/4" of lead, surrounds the detectors on all sides. The top of the shield has been removed in Fig. 19 to show the positions of the three detectors. As is shown, the body of the liquid nitrogen dewar remains outside of the detector shield, while the 2-in. diameter snout passes through a hole in the shield and positions the Ge(Li) detector between the two NaI detectors.

3.2.2 Associated Electronics

A block diagram of the triple coincidence electronics used for the pair spectrometer is shown in Fig. 20. Both single channel analyzer windows are set on the 511-keV peaks which result from the absorption of annihilation radiation in the NaI crystals. A cross-over pickoff is used in each NaI channel to generate a timing pulse whenever a pulse is within the 511-keV window. The signal from the Ge(Li) detector preamplifier is split into two branches -- one goes to the main amplifier to be pulse shaped for optimum energy resolution, and the other passes through a double delay line amplifier after which a cross-over pickoff generates a timing pulse. Each cross-over pickoff is equipped with a variable delay for adjusting the timing of the system.

When the two timing pulses from the NaI detectors and the timing pulse from the Ge(Li) detector are in triple coincidence ($2\tau = 75$ nsec) the multichannel analyzer is gated on, and the signal from the Ge(Li) detector is analyzed. This arrangement yields a spectrum in which only double-

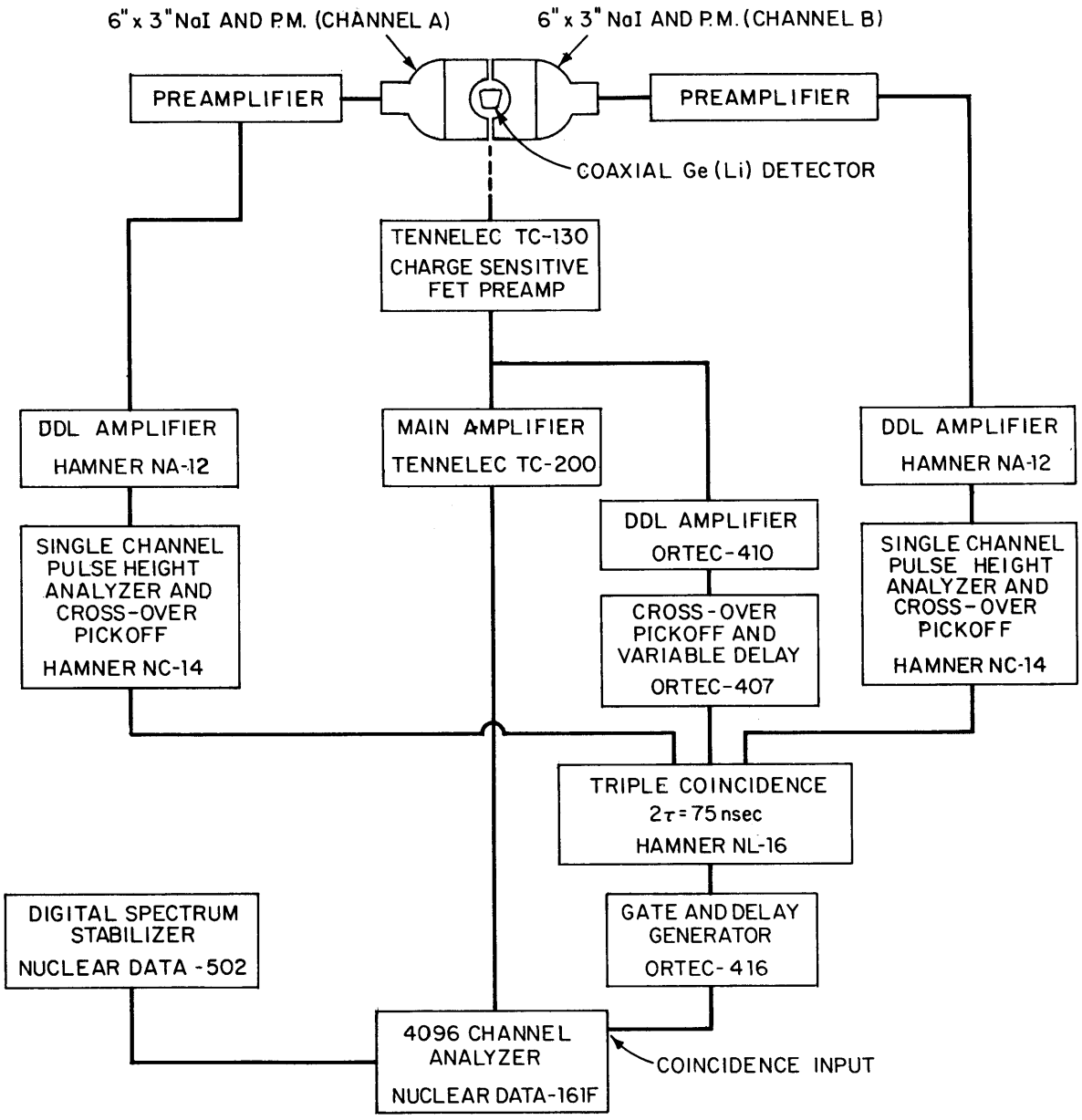

FIGURE 20 BLOCK DIAGRAM OF ELECTRONICS FOR OPERATION AS A PAIR SPECTROMETER

escape peaks appear -- full energy peaks, single escape peaks, and Compton background are rejected.

The 511-keV windows had a width equal to about three times the full-width at half maximum (fwhm) of the 511-keV peak, which was about 80 keV. On some runs it was observed that gain shifts in the NaI had caused the 511-keV peak to shift away from the center of the window. Such a shift would, of course, introduce an uncertainty in the spectrometer efficiency; consequently, the position of the 511-keV peak within the window was usually monitored before and after a run. If any significant drift had occurred the run was rejected.

The use of a 4096 channel Nuclear Data Analyzer (Model 161F) allowed the high energy capture spectrum (1.2 MeV to 9 MeV) of most elements to be obtained in a single run while still maintaining 6 or 7 channels per peak. Use of the digital stabilizer proved valuable in reducing resolution loss due to gain shifts during pair spectrometer runs, which were 12 to 24 hrs long.

Shown in Fig. 21 is a block diagram of the arrangement of the electronics for Compton suppression operation. Every signal from the NaI detectors is allowed to generate a timing pulse (integral mode of operation of the single channel pulse height analyzer). When a pulse from either NaI detector is in time coincidence with a pulse from the Ge(Li) detector, the multichannel analyzer is gated off and the signal from the Ge(Li) detector is not analyzed. This arrangement results in a reduction of the Compton background since all Compton events occuring in the Ge(Li) detector, in which the Compton scattered gamma is detected by either NaI, are rejected.

As pointed out in Section 2.3.6, the energy resolution achieved using a Ge(Li) detector depends primarily on the quality of the low-noise electronics used to process the signal from the detector. Several different commercial low-noise electronics systems were used. Vacuum-tube pre-

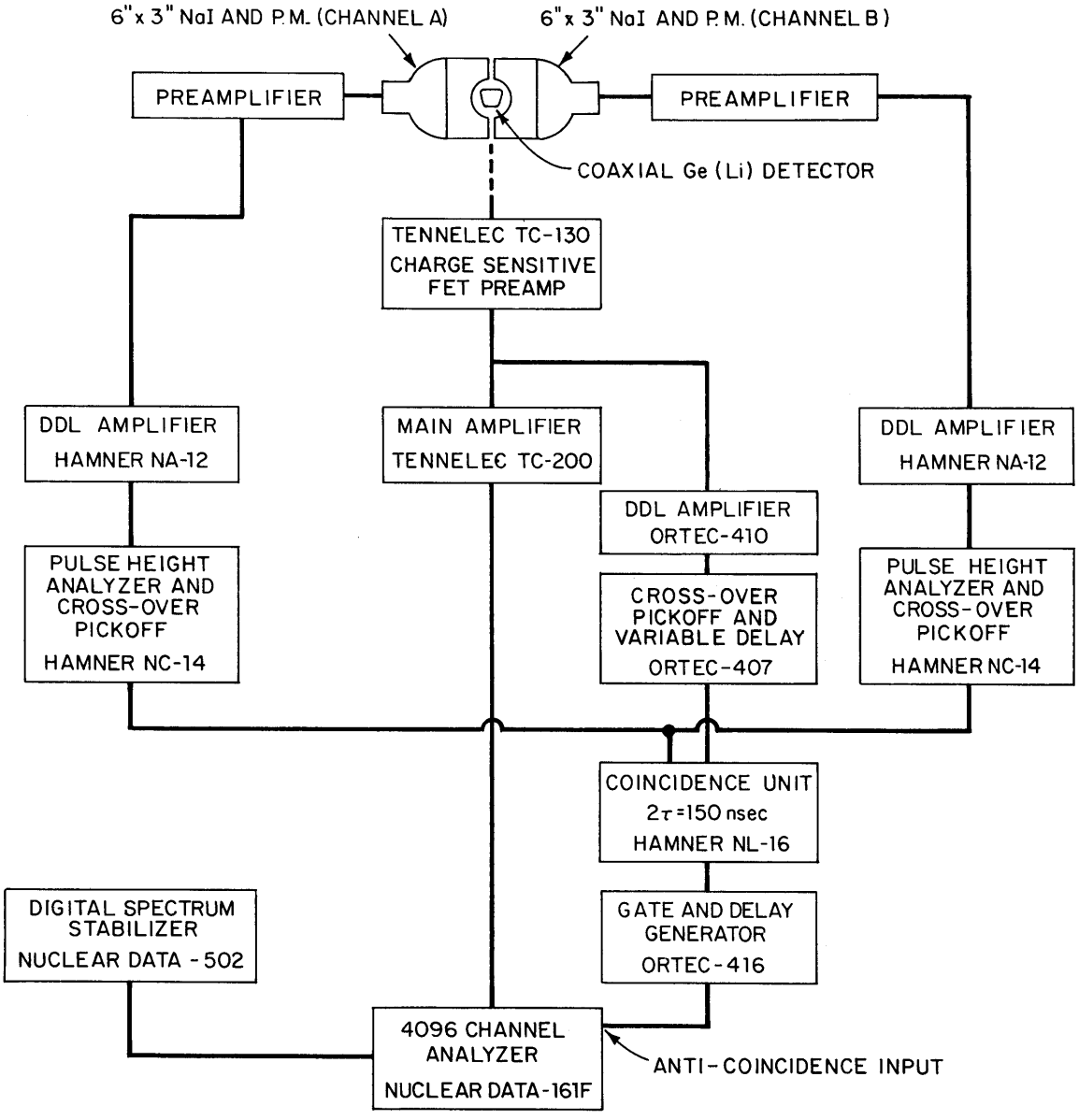

FIGURE 21 BLOCK DIAGRAM OF ELECTRONICS FOR OPERATION IN THE COMPTON SUPPRESSION MODE

amplifiers with pulse shaping (ORTEC-MODEL 103XL), and without pulse shaping (TENNELEC-MODEL 100C), were used in conjunction with several main amplifiers (ORTEC-MODEL 203, ORTEC-MODEL 410, and TENNELEC MODEL TC-200). Following the advent of high performance field-effect transistor (FET) preamplifiers, a commercial uncooled FET preamplifier (TENNELEC-MODEL TC-130) was incorporated into the system. This preamplifier, equipped with 4 paralleled FET's and optimized for about 70 pf detector capacitance, was used with the TC-200 main amplifier to obtain all final data. The electronic noise contribution, with the 30 cc detector, was about 4.5 keV (fwhm). The optimum pulse shaping was found to be single RC differentiation and single RC integration with equal time constants of 3.2 μ sec. With this pulse shaping, count rates in the Ge(Li) detector of up to 4000 counts/sec could be tolerated with little loss of resolution. The linearity of this system was checked in both modes of operation using a method described in Section 3.3.1.

3.2.3 External Neutron Beam Facility

An external neutron beam facility was constructed to provide a source of thermal neutron capture gamma-rays. A plan view of the external neutron beam facility, the gamma spectrometer, neutron and gamma collimation, and the orientation of these relative to the MIT Reactor is shown in Fig. 22. Port 9CH2, which extends into the graphite thermal column, was chosen instead of a core-oriented port, in order to reduce the number of core gammas seen by the spectrometer and to insure a highly thermal neutron flux.

The neutron collimation consists of the following: (1) a square hole, 30.5 cm on a side, from near the center of the graphite thermal column to the face of the reactor shielding, (2) a square collimator, 30.5 cm on a

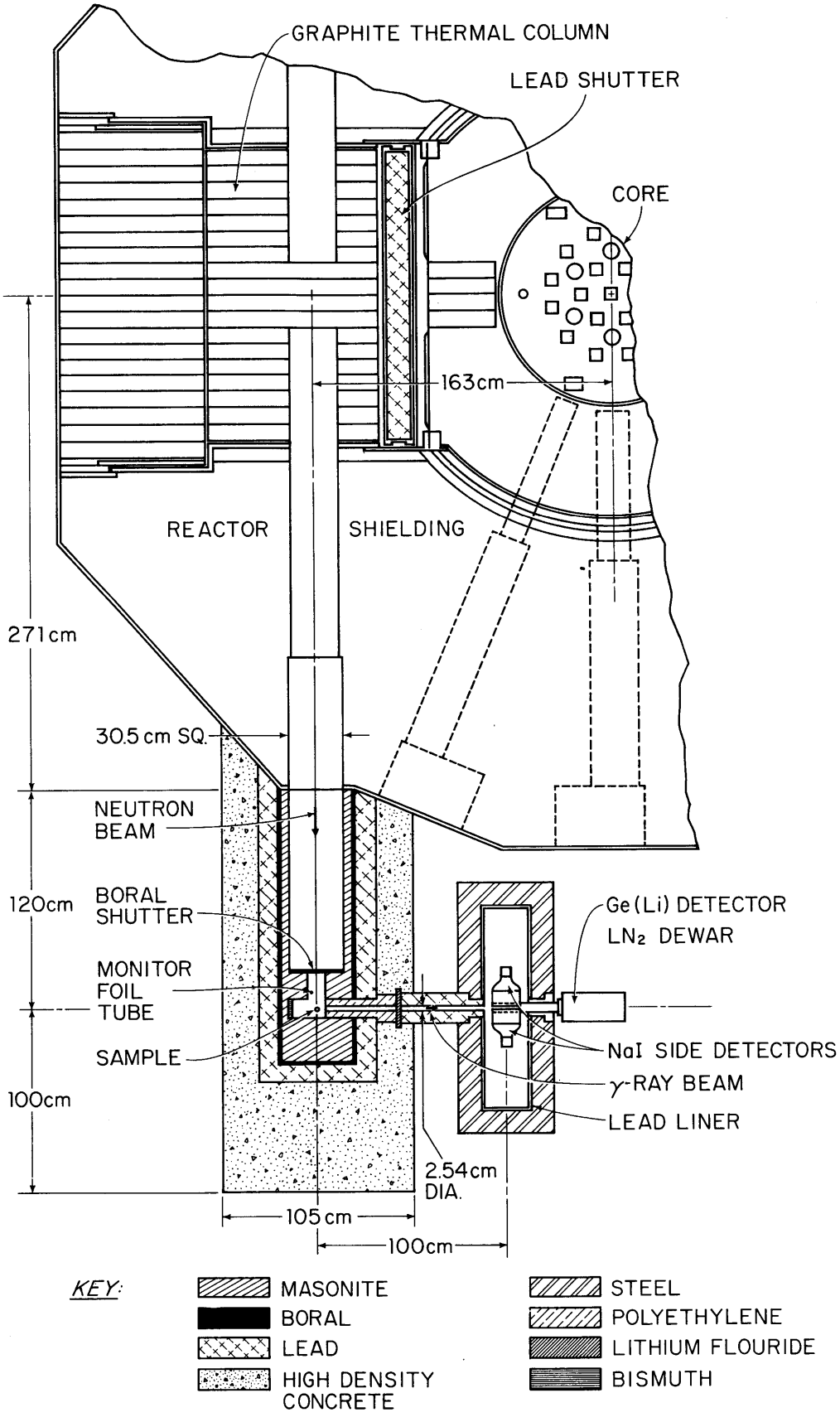

FIGURE 22 PLAN VIEW OF EXTERNAL NEUTRON BEAM FACILITY AND GAMMA SPECTROMETER

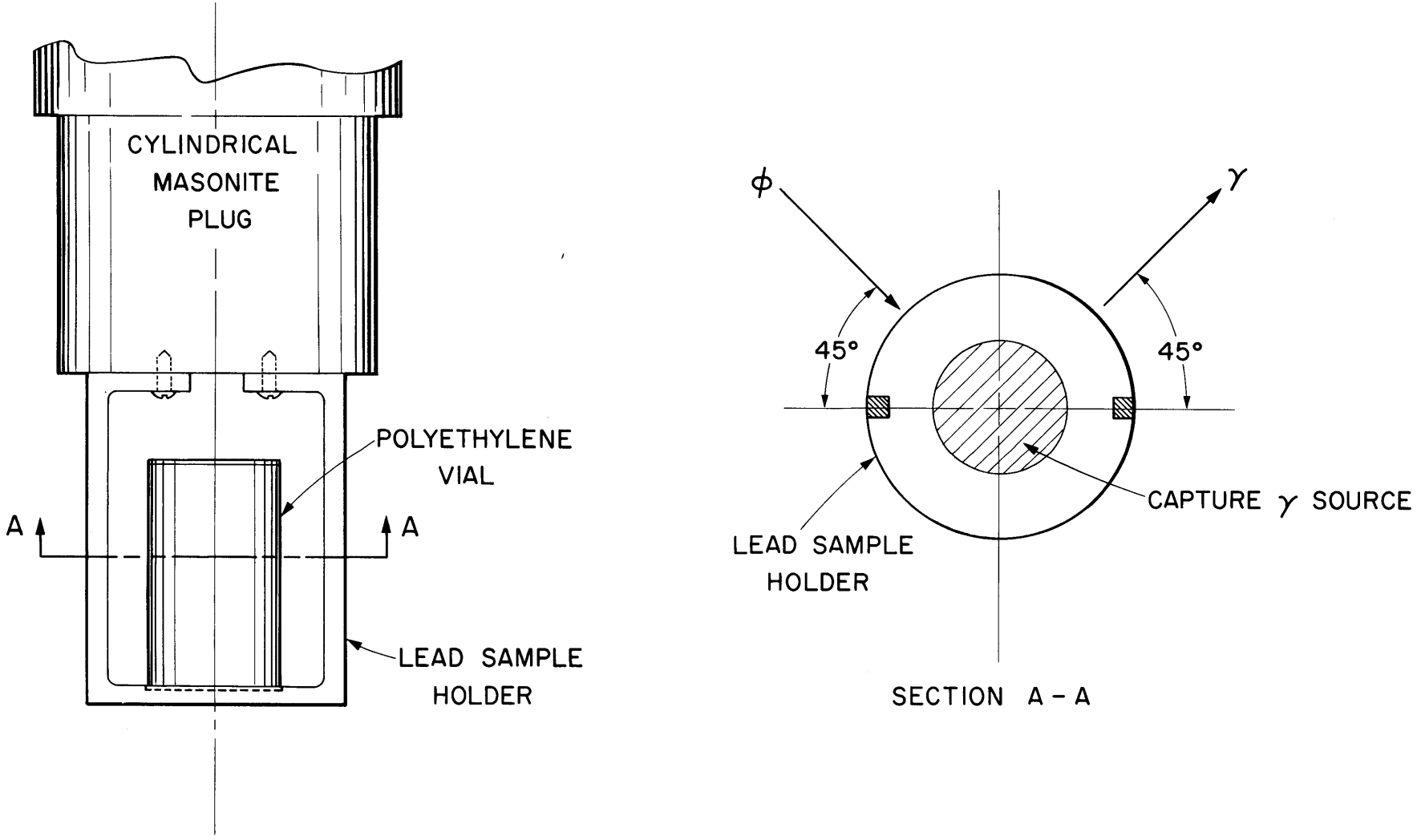

FIGURE 23 SKETCH OF SAMPLE HOLDER

side, with 2 in. thick masonite walls, which starts at the reactor shielding and is about 100 cm long, (3) a square collimator, 10 cm on a side, with masonite walls, about 25 cm long. A thermal neutron shutter made of 1/4 in. thick boral sheet is situated at the end of the larger square collimator, in order to facilitate sample changing with the reactor at power. A 3/8 in. O.D. steel tube is positioned about 8 cm in front of the sample position. A glass rod, to which a gold foil is attached, is inserted into the steel tube to monitor the flux during a run. The entire external beam facility is shielded on all sides by 1/4 in. boral sheet, 3 in. of lead, and a minimum of 8 in. of high density concrete in order to reduce radiation levels around the facility.

Samples are inserted through a vertical port directly over the sample position. The samples are held in a lead sample holder, which is fixed to a cylindrical masonite plug fashioned to fit into the sample port. Solid samples are shaped to fit into the lead sample holder, while powdered or liquid samples are placed in polyethylene vials of various sizes. Figure 23 shows a sketch of the lead sample holder attached to its cylindrical masonite plug. The largest size vial used, 3.2 cm in diameter and 5.3 cm high, is shown in the sample holder. A nylon sample holder was also used in obtaining preliminary data. However, use of the lead sample holder was preferable for two reasons: (1) it helped reduce the intensity of the 2.223-MeV γ ray originating from hydrogen capture in the nylon sample holder, (2) it provided an internal energy calibration γ ray at high energies without introducing additional background gammas.

The wall viewed by the gamma-ray collimator, which was made of masonite, produced intolerably strong hydrogen capture gamma background. Replacing this wall with graphite reduced the hydrogen background, but introduced a strong capture gamma background from carbon. Covering

the wall with a square piece, 10 cm on a side, of 2.5 cm thick bismuth, eliminated this carbon background problem. The bismuth introduced only two very weak lines in the background.

The gamma-ray collimator, which is perpendicular to the neutron beam and is positioned to view the sample, has two sections: (1) a 38 cm long polyethylene collimator with a 5.4 cm x 3.2 cm rectangular hole, and (2) a 45.2 cm long lead collimator with a 2.54 cm diameter hole. A 1.6 cm thick LiF sheet is placed directly in the beam between these two sections to reduce the thermal neutron flux on the detector. The lead section of the collimator shields the detector from unwanted gammas -- primarily from those originating from neutron capture in the irradiation facility shielding. In addition, the lead collimator shields the side NaI crystals from the direct gamma beam. Either of two 2.54 cm dia. x 15 cm long collimators, one of bismuth with a 0.95 cm dia. hole, and the other of lead with a 1.59 cm dia. hole, may be inserted into the lead collimator for those cases where a lower γ-ray intensity is desired. The distance from the sample to the Ge(Li) detector is approximately 100 cm.

A photograph of the assembled experimental apparatus is given in Fig. 24. Shown are the external neutron beam facility, the gamma spectrometer, and the associated electronics.

3.3 Operating Characteristics

3.3.1 Pair Spectrometer Using a Large 30 cc Detector

The performance of the Ge(Li) pair spectrometer using a standard radioactive source is illustrated in Fig. 25, which shows the spectrum of the 2.614-MeV γ ray of ThC'' measured directly (upper spectrum) and using the pair spectrometer (lower spectrum). A comparison of these two spectra reveals that use of the pair spectrometer eliminates the full energy peak and

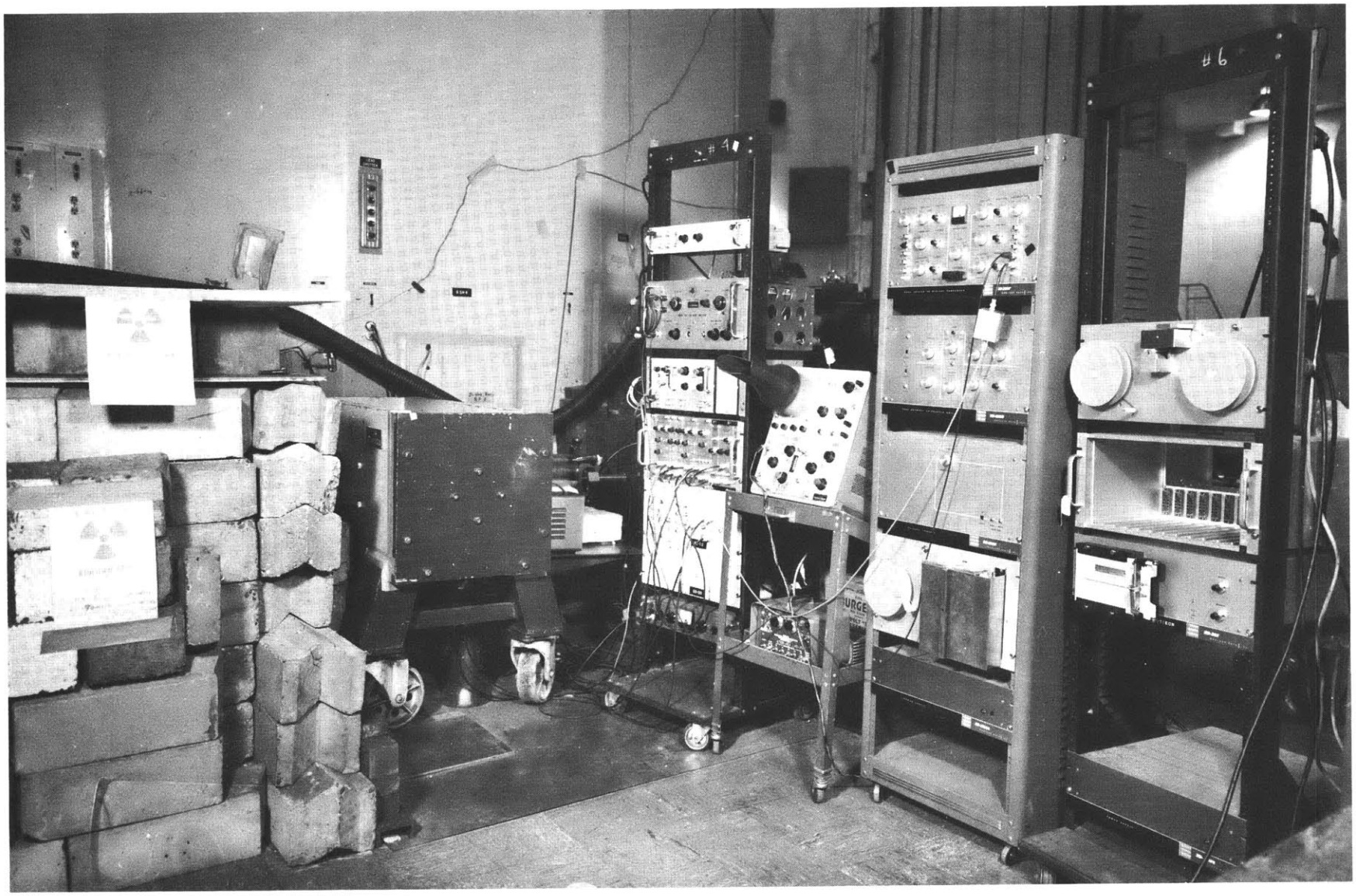

FIGURE 24 ASSEMBLED EXPERIMENTAL APPARATUS

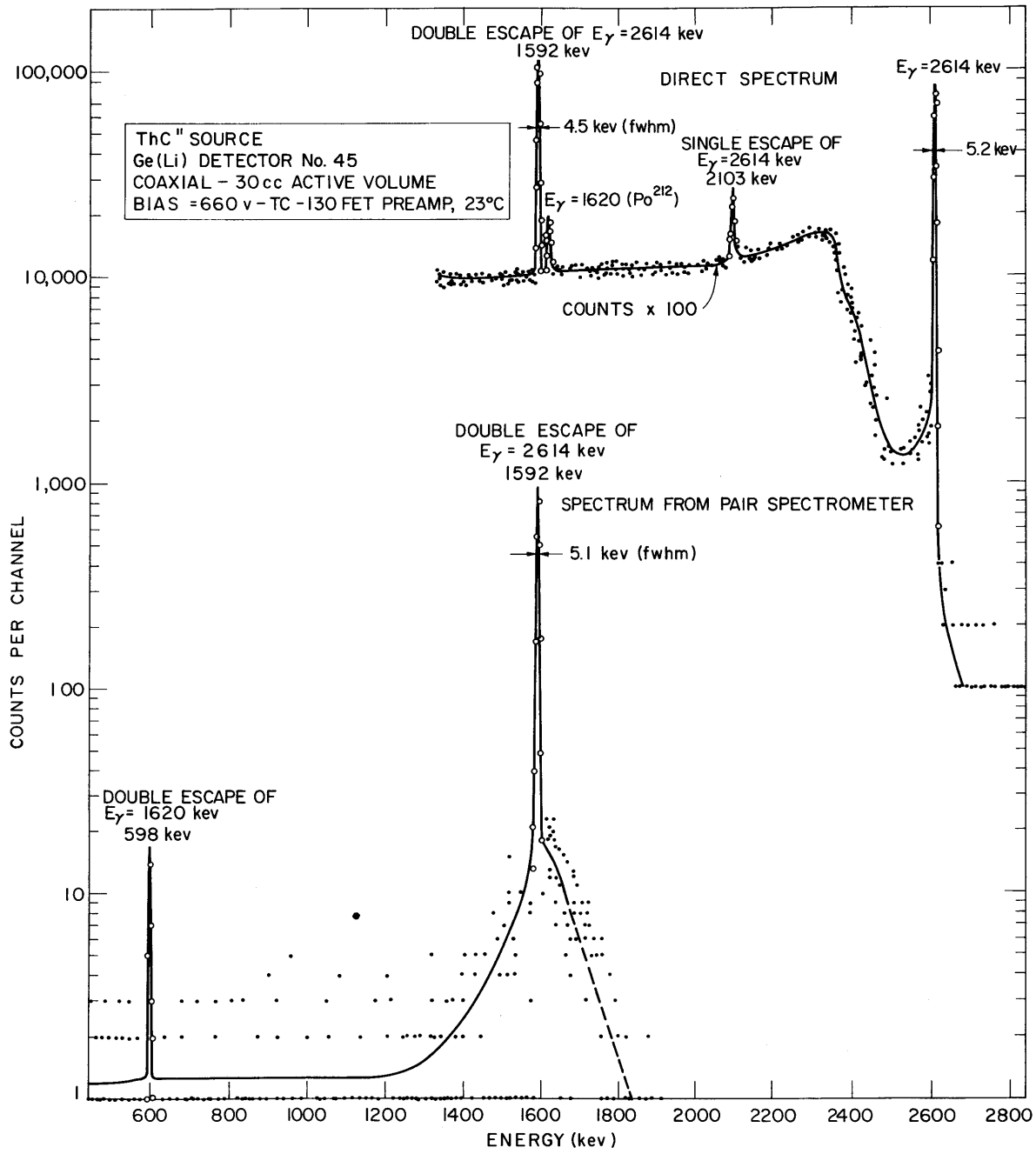

FIGURE 25 SPECTRUM FROM THE 2.614 MeV GAMMA FROM ThC" MEASURED DIRECTLY (UPPER SPECTRUM) AND USING THE PAIR SPECTROMETER (LOWER SPECTRUM) WITH THE 30 cc Ge(Li) DETECTOR

the single escape peak, and results in a considerable background reduction. The ratio of the double escape peak to the average background at energies less than that of the double escape peak, has been improved by about a factor of 70 (from about 10:1 to about 700:1). Of course, this peak to background enhancement is gained at a cost of detection efficiency. In this case, the loss of efficiency was less than a factor of 7. The double escape peak of the much weaker 1620-keV γ ray from Po^{212} is also visible in the pair spectrometer spectrum. The double escape of this weak gamma is not visible in the direct spectrum because of the large background from the high intensity gamma. This illustrates another advantage of the pair spectrometer mode of operation. Note also that the pair mode of operation does not significantly change the energy resolution of the system (approximately 5 keV (fwhm) at 2.614 MeV).

The value of using the pair spectrometer for studying complex gamma spectra is illustrated by a comparison of the titanium capture gamma spectrum obtained from the directly operated Ge(Li) detector with that obtained from the pair spectrometer. In Fig. 26, the direct titanium capture spectrum (upper two spectra) displays a large background which increases sharply with decreasing energy. However, the titanium spectrum obtained with the pair spectrometer has a smaller background which is quite uniform with energy. The contrast in the background shapes of the two spectra is striking even though the direct spectrum is plotted on a semi-logarithmic scale and the pair spectrum is plotted on a linear scale. The peak to background ratio is markedly improved by using a pair spectrometer. At 2.223 MeV the peak to background ratio improved from 0.86 to 18.9, a factor of about 22. At 6.760 MeV, the peak to background ratio improved from 4.85 to 29.6 -- more than a factor of 6. The pair spectrometer effectiveness for improving peak to background ratios increases with decreasing energy

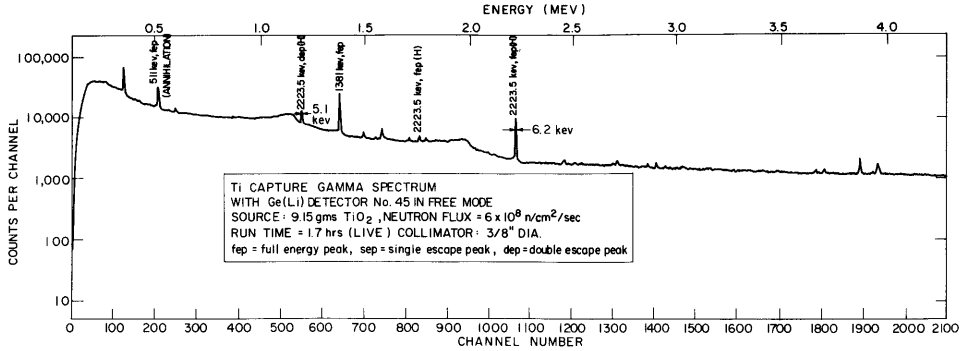

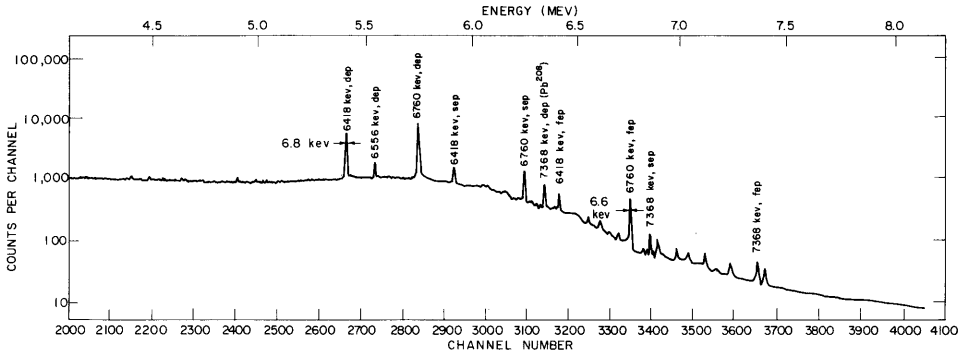

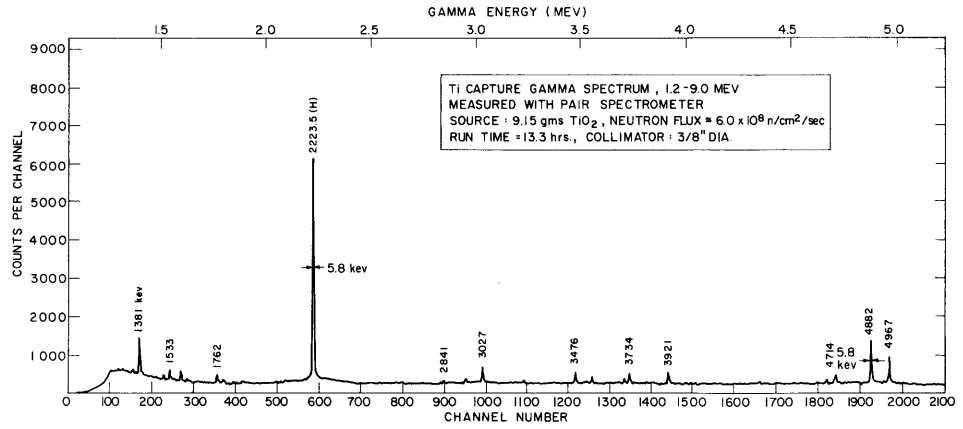

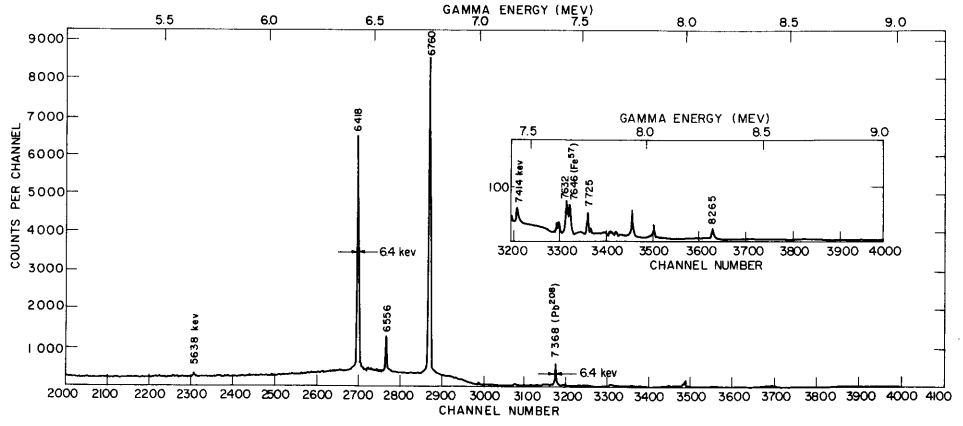

FIGURE 26 CAPTURE GAMMA SPECTRUM OF TITANIUM MEASURED DIRECTLY (UPPER TWO SPECTRA) AND USING THE PAIR SPECTROMETER (LOWER TWO SPECTRA)

since the Compton background, which is rejected by the pair spectrometer, increases with decreasing energy. The elimination of the full energy and single escape peaks reduces considerably the difficulty in analyzing these very complex spectra. The energy resolution of the pair spectrometer was typically 5 to 7 keV in this energy range.

Figure 27, which shows a portion of the zirconium capture gamma spectrum, illustrates the performance of the pair spectrometer in obtaining very complex γ-ray spectra originating from thermal neutron capture in low cross section elements. Natural Zr has $\sigma = 0.18$ b and has many weak intensity gammas. This and the other spectra were plotted using a digital computer as described in Section 4.1.

The pair spectrometer sensitivity is a function of the incident gamma energy. Figure 28 shows the absolute efficiency curve as a function of gamma energy for the pair spectrometer. This curve includes the effect of a 1.6 cm thick LiF sheet which is in the gamma beam. The data points represent experimentally determined values using various capture γ-rays, whose intensities are fairly well known (to about 10-30%), and several radioactive sources. The experimental efficiency points were determined using the 0.95 cm dia. collimator. The solid curve which agrees quite well with the experimental data was calculated using a simple model which assumes simple functions to describe the three principal contributions to the variation of efficiency with gamma energy: (1) gamma cross sections, (2) energetic electron losses, (3) and bremsstrahlung losses. The details of this efficiency calculation are given in Appendix A. The efficiency curve attains a maximum between 4 and 5 MeV. For the 30 cc Ge(Li) detector, the efficiency at 8 MeV is only a factor of about 2 less than at the maximum efficiency point. For smaller detectors (< 3 cc) this factor has been measured to be about 5 (E1). This increased efficiency is the principal

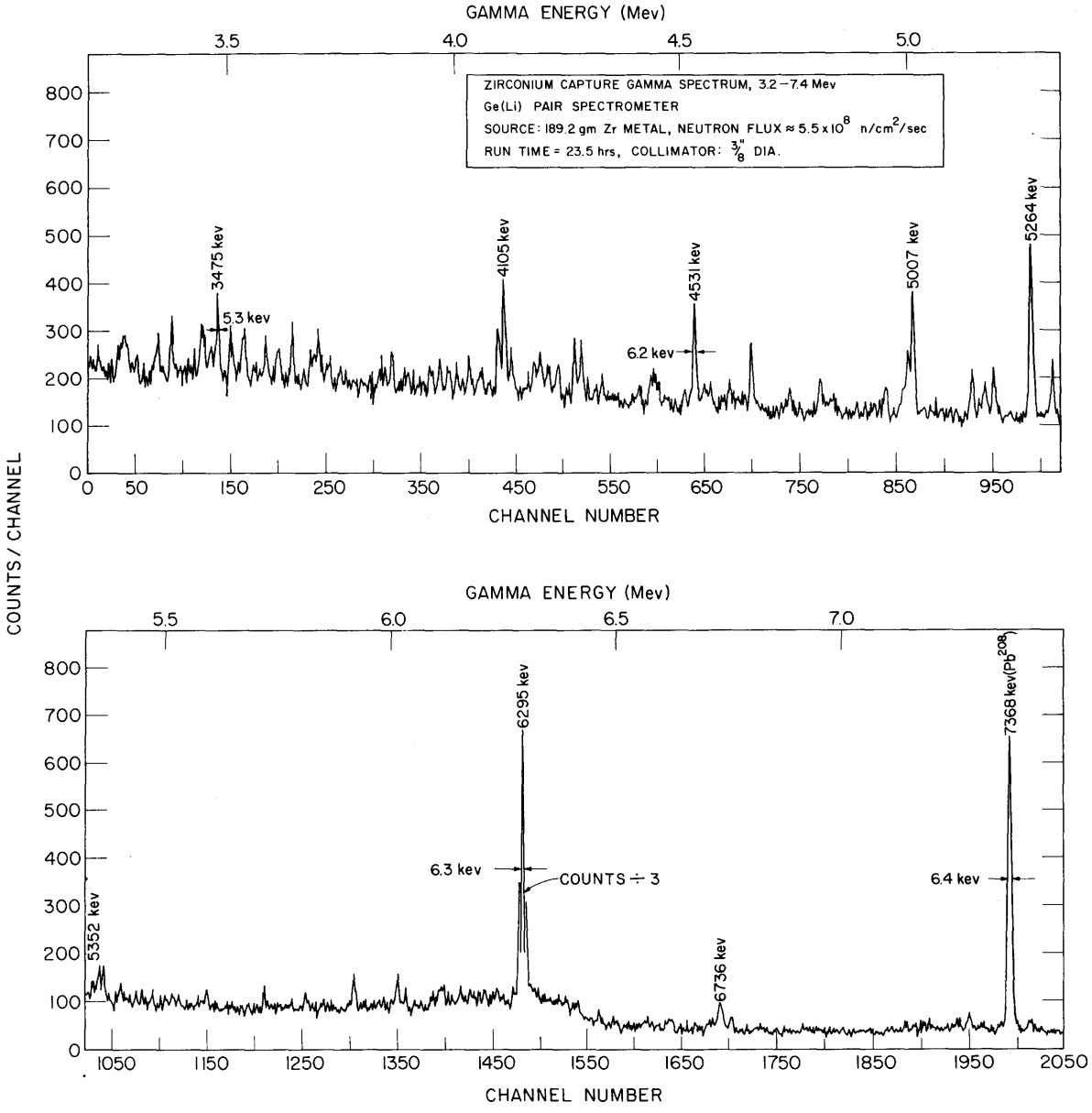

FIGURE 27 CAPTURE GAMMA SPECTRUM OF ZIRCONIUM BETWEEN 3.2 AND 7.4 MeV MEASURED WITH THE PAIR SPECTROMETER

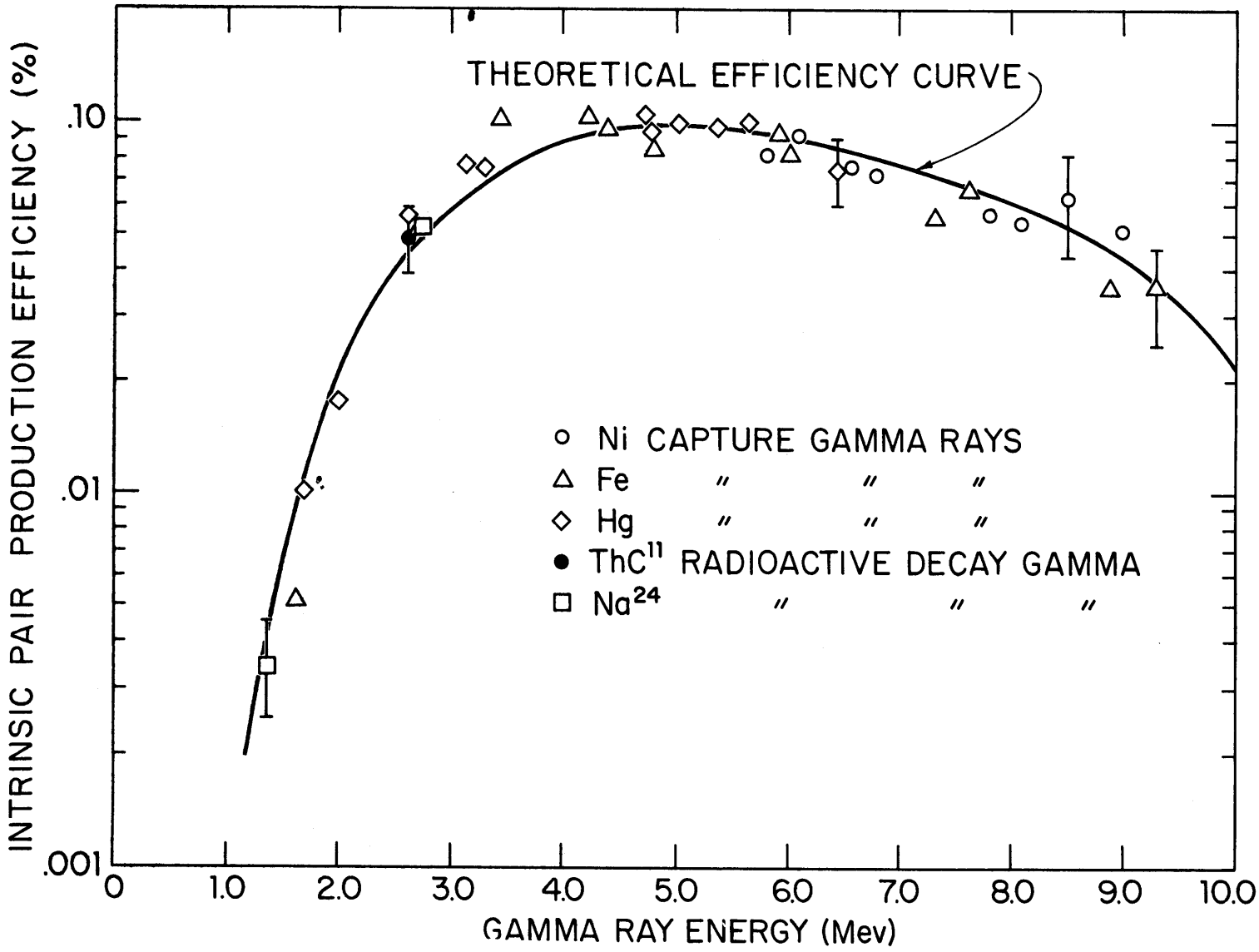

FIGURE 28 INTRINSIC EFFICIENCY AS A FUNCTION OF ENERGY FOR THE PAIR SPECTROMETER, DATA POINTS REPRESENT EXPERIMENTAL VALUES AND THE SOLID CURVE CALCULATED VALUES.

advantage of using large Ge(Li) detectors.

The linearity was checked using a method described by Health, et al. (H5). A high precision DC voltage standard* (0-10 volts output) with an absolute accuracy of 1 part in 10^4 was used in conjunction with a mercury relay pulser to perform the linearity check. Test pulses were inserted into the 4096 channel analyzer through the preamplifier with a uniform voltage spacing (corresponding to about 40 channels between pulser peaks). The analyzer was operated in the coincidence mode, with the test pulses being used to gate the analyzer, so that any nonlinearities in the linear gate would also be included in the linearity check. Figure 29 shows two linearity correction curves obtained nearly two months apart. The agreement between these curves illustrates the constancy of the system nonlinearity with time. The details of the linearity correction calculation are given in Section 4.2.3. The nonlinearity of the system was less than 0.1% over the upper 95% of the analyzer channel range.

3.3.2 Pair Spectrometer Using Two Smaller Ge(Li) Detectors

The performance of the pair spectrometer operated with a 3 cc planar detector (number 32) is illustrated in Fig. 30, which shows the direct spectrum and the pair spectrometer spectrum from ThC''. Figure 31 shows the performance of the pair spectrometer using a 5 cc coaxial detector (number 37). Figures 30 and 31, when compared with Fig. 25, show the general effects of varying the size of the primary detector. Table 3 lists the values of some parameters which indicate the performance of the pair spectrometer using the three different size Ge(Li) detectors.

---

*Model MV100, Electronic Development Corp., Boston, Massachusetts.

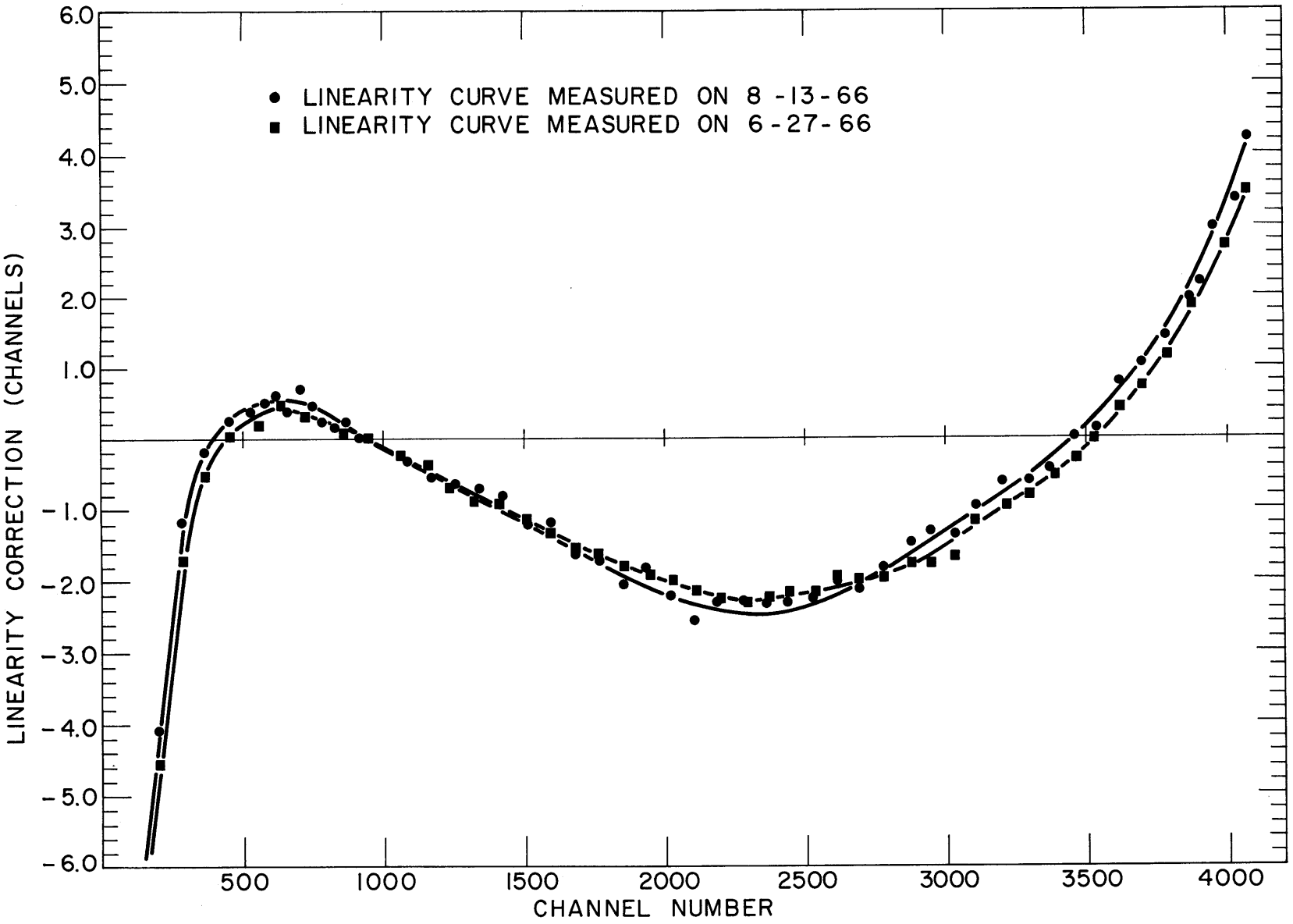

FIGURE 29 LINEARITY CORRECTION CURVES TAKEN NEARLY TWO MONTHS APART FOR THE PAIR SPECTROMETER.

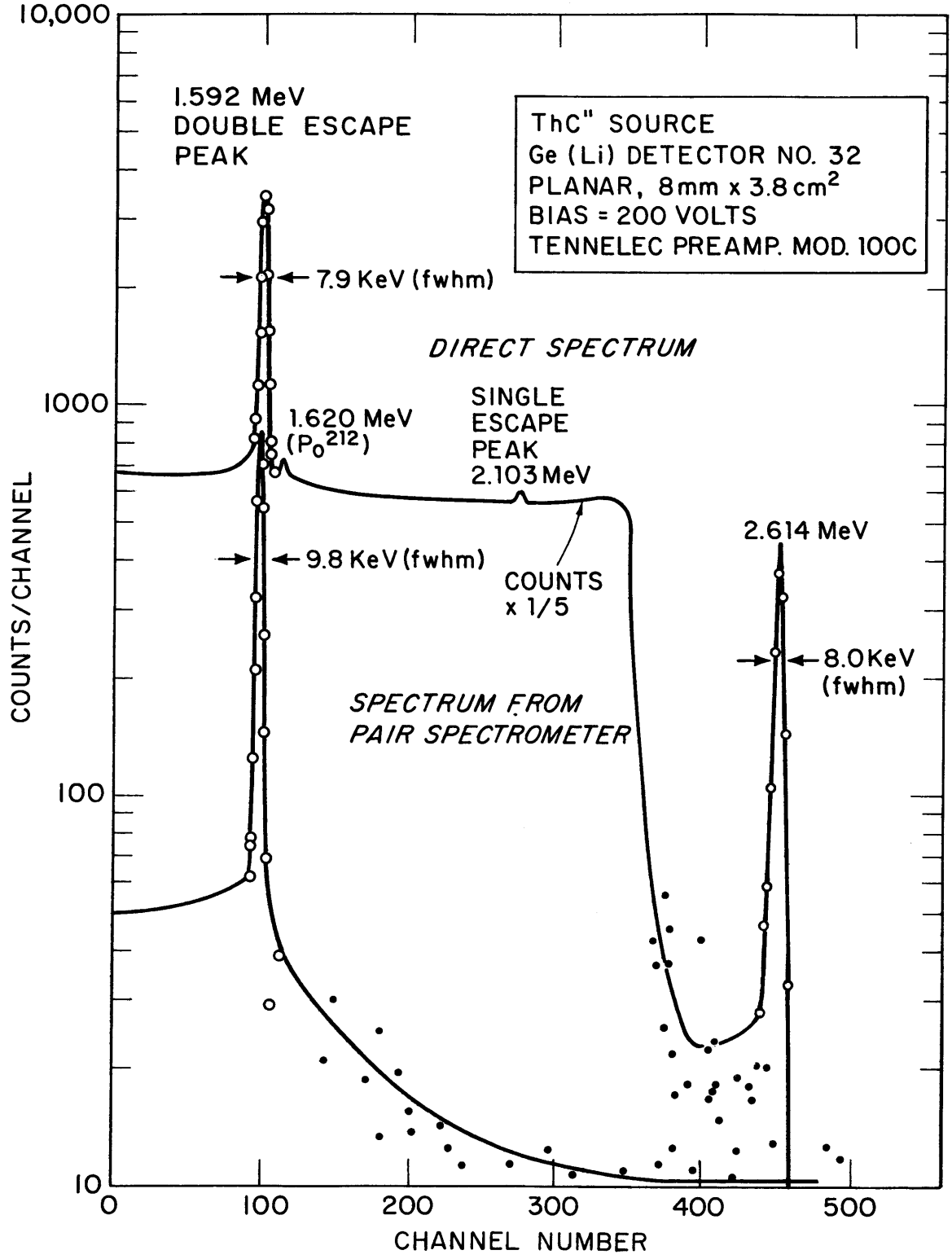

FIGURE 30 SPECTRUM FROM THE 2.614 MeV GAMMA FROM ThC" MEASURED DIRECTLY (UPPER SPECTRUM) AND USING THE PAIR SPECTROMETER (LOWER SPECTRUM) WITH THE 3cc PLANAR Ge(Li) DETECTOR.

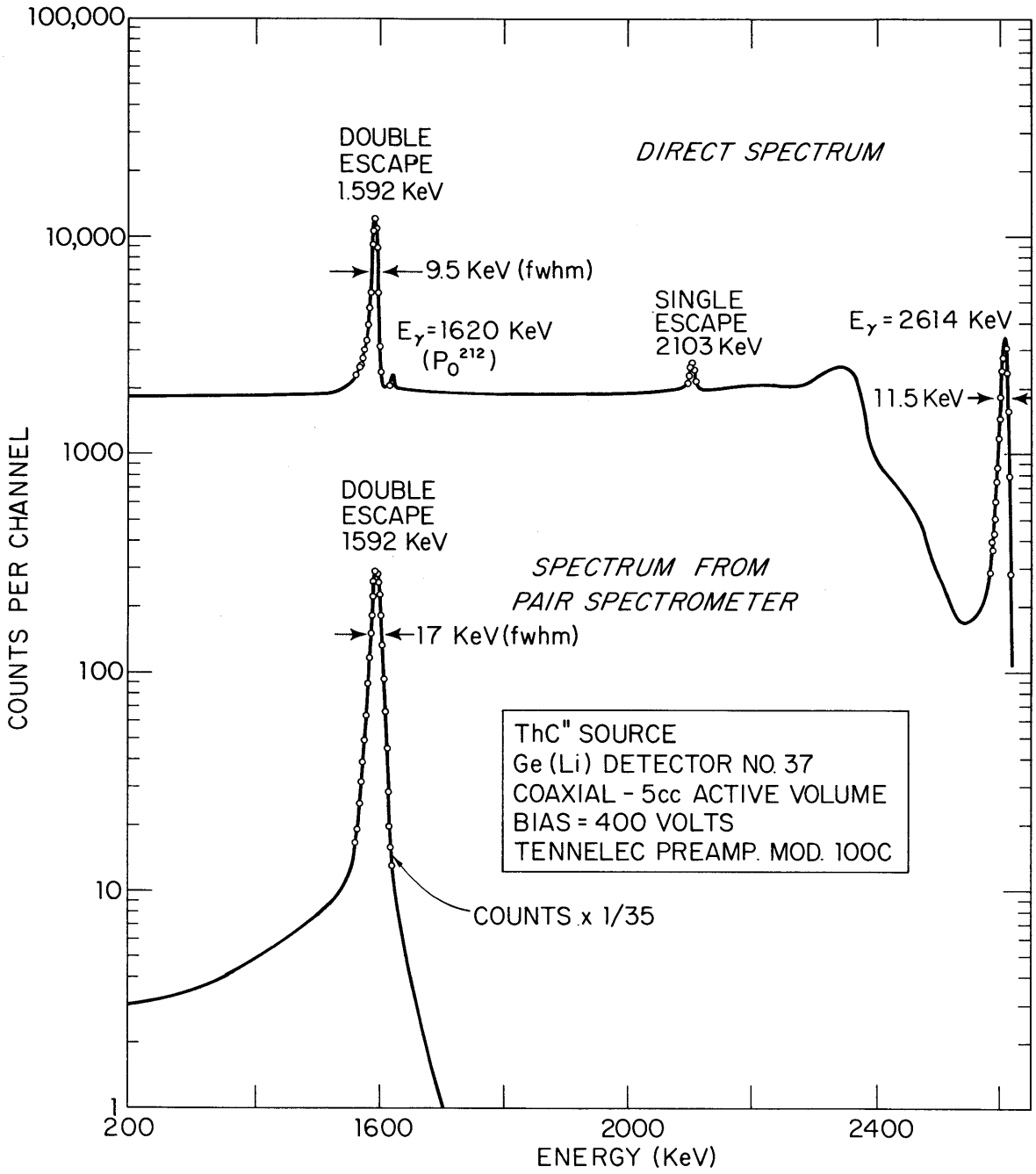

FIGURE 31 SPECTRUM FROM THE 2.614 MeV GAMMA FROM ThC" MEASURED DIRECTLY (UPPER SPECTRUM) AND USING THE PAIR SPECTROMETER (LOWER SPECTRUM) WITH THE 5cc COAXIAL Ge(Li) DETECTOR.

TABLE III

PERFORMANCE OF PAIR SPECTROMETER USING THREE DIFFERENT SIZE Ge(Li) DETECTORS

DETECTOR NUMBER	32	37	45
DETECTOR VOLUME (cc)	3	5	30
Peak/background ratio for 2.614 MeV double escape peak (direct spectrum)	6:1	6:1	10:1
Peak/background ratio for 2.614 MeV double escape peak (pair spectrometer)	25:1	100:1	700:1
Improvement in peak/background ratio realized by using pair spectrometer	4	17	70
$\frac{\text{Efficiency at 2.614 MeV (as pair spectrometer)}}{\text{Efficiency at 2.614 MeV (operated directly)}}$	0.04	0.06	0.14
Relative overall efficiency[4] at 7.64 MeV	1	13	52
Resolution at 2.614 MeV (operated directly) keV, fwhm	7.9 [1]	9.5 [1]	4.5 [2]
Resolution at 2.614 MeV (as pair spectrometer) keV, fwhm	9.8 [1]	17.0 [1,3]	5.1 [2]

1. Measured using a vacuum tube type preamplifier, Tennelec Mod. 100C.
2. Measured using an FET preamplifier, Tennelec TC-130.
3. Increased resolution due to gain shift during run of about 40 hours.
4. Measured with a 1" dia. collimator using the 14-keV doublet in the capture gamma spectrum of iron.

A strict comparison of pair spectrometer performance using different size Ge(Li) detectors is not possible since certain parts of the electronics (the low-noise electronics, for instance) were changed between experiments. With electronics comparable to that used for the 30 cc detector, the smaller detectors would probably have yielded comparable or better resolution than the large detector. Nevertheless, there is a significant improvement in the peak to background ratio and a large increase in overall efficiency, especially at high energies, with increasing detector size. Note that the overall pair spectrometer efficiency at 7.65 MeV was approximately 52 times as great with the 30 cc coaxial detector as with the 3 cc planar detector.

A comparison of capture gamma spectra obtained from the pair spectrometer using 3 different size detectors may be made by considering Fig. 32, 33, and 34, which show, respectively, the iron capture gamma spectrum obtained using a 3 cc planar, a 5 cc coaxial, and a 30 cc coaxial detector (numbers 32, 37 and 45). Note that the peaks in this spectra are double escape peaks and that 1.022 MeV must be added to their indicated energies to obtain gamma energies. A large improvement in the peak to background ratio with larger detectors is quite evident. At a gamma energy of 4.219 MeV, the peak to background ratio of the 5 cc detector was nearly 3 times that of the 3 cc detector and the 30 cc detector peak to background ratio was almost 9 times that of the 3 cc detector. At 7.64 MeV, the peak to background ratio of the 5 cc detector is about 1.4 times that of the 3 cc detector while that of the 30 cc detector is about 4 times greater. Note that the background becomes progressively more uniform with energy as the detector size increases. This reflects the fact that the pair efficiency of a small detector drops off much more sharply above 4 or 5 MeV because of energetic electron losses and bremsstrahlung losses. The sharp increase

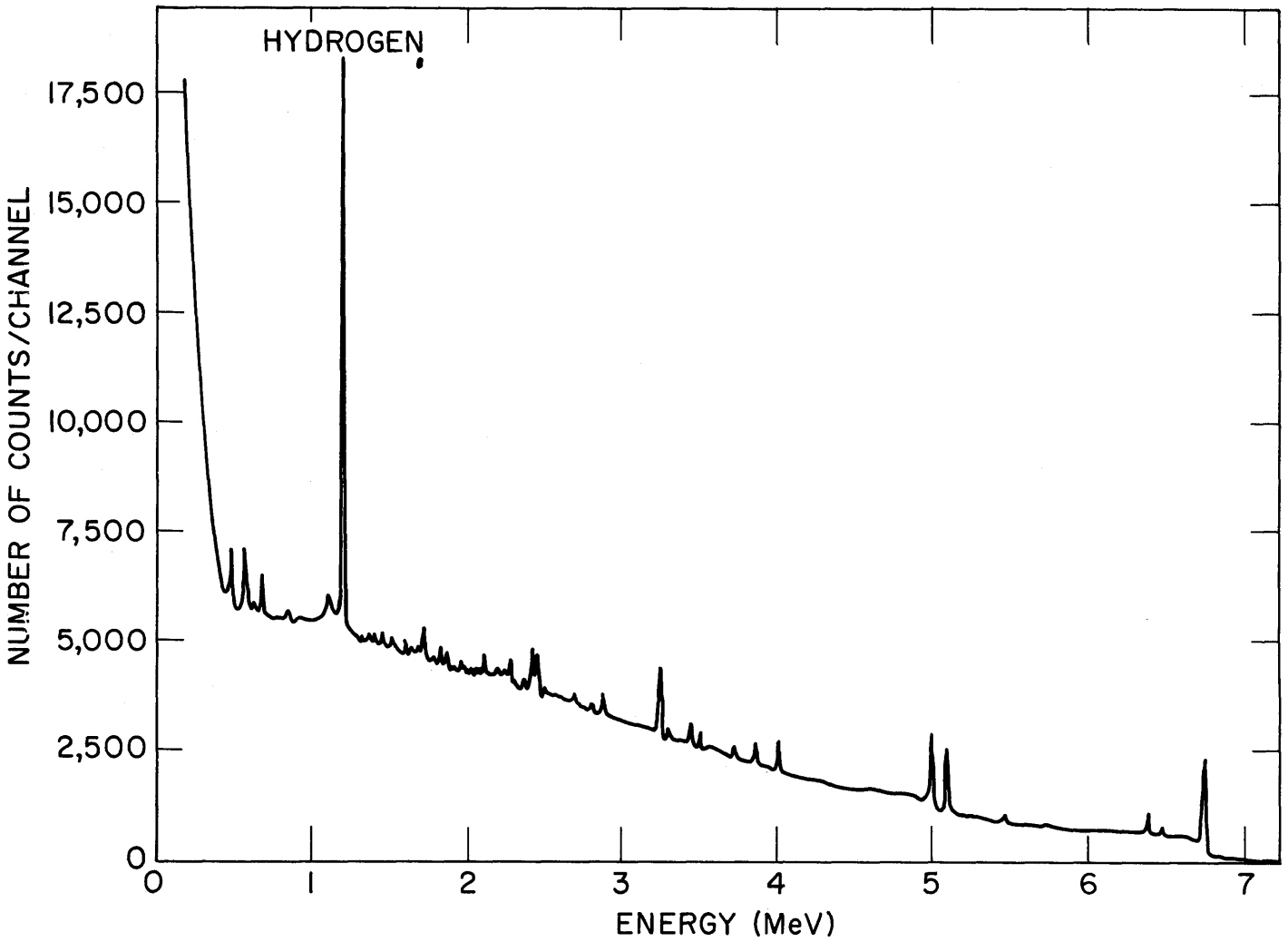

FIGURE 32 Fe CAPTURE γ-RAY SPECTRUM MEASURED WITH PAIR SPECTROMETER USING 3cc PLANAR Ge(Li) DETECTOR.

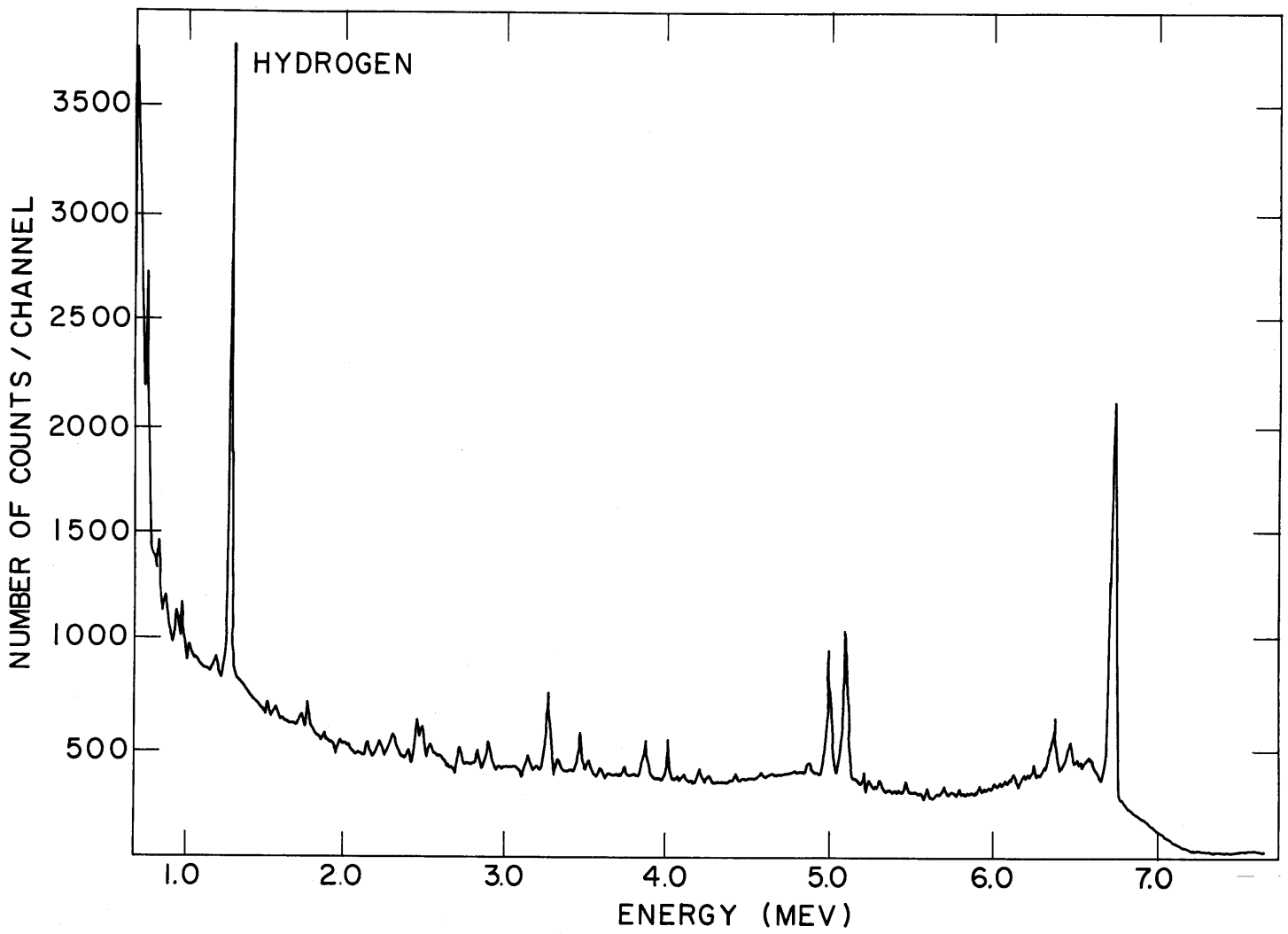

FIGURE 33 Fe CAPTURE γ-RAY SPECTRUM MEASURED WITH PAIR SPECTROMETER USING 5cc COAXIAL Ge(Li) DETECTOR.

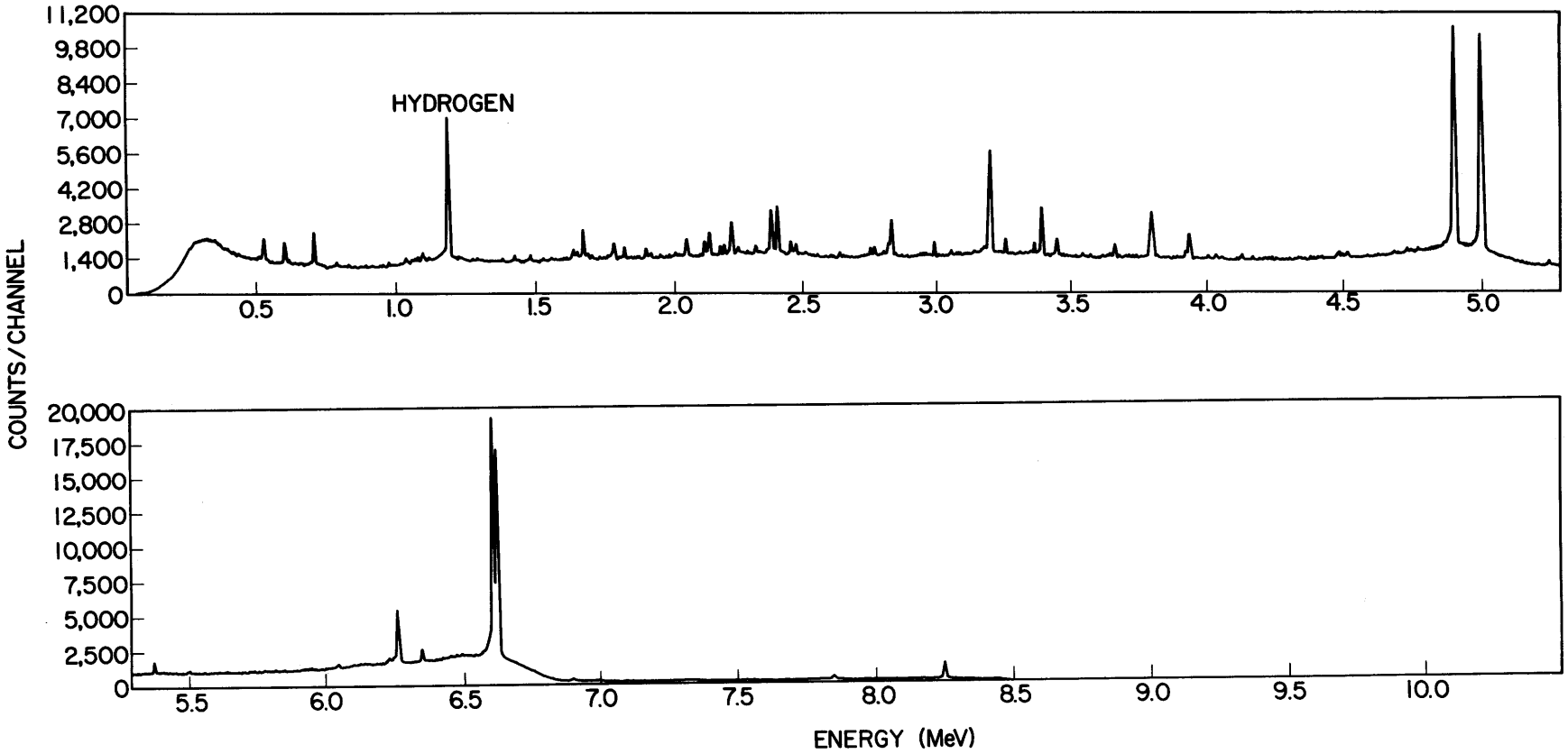

FIGURE 34 Fe CAPTURE γ-RAY SPECTRUM MEASURED WITH PAIR SPECTROMETER USING 30cc COAXIAL Ge (Li) DETECTOR.

in background at very low energies in the spectra from the two smaller detectors was unrelated to the detector size but was an indication that a refinement was needed in the coincidence electronics used to gate the analyzer. More precisely, the threshold of the cross-over pickoff used to generate the Ge(Li) timing pulse was low enough to trigger on electronic noise, thereby increasing the chance coincidence rate. As can be seen in Fig. 34, proper adjustment of the electronics eliminated nearly all effects of chance coincidences on the low energy background.

3.3.3 Compton Suppression Mode

Figures 35 and 36 show a comparison of the direct spectrum with the Compton suppression spectrum for a Na^{24} source using the 30 cc Ge(Li) detector. The average Compton background is seen to be reduced by a factor of about 2.2 at 2.754 MeV, while at the Compton edge the reduction is only by a factor of about 1.4. The reduced effectiveness in the region near the Compton edge is the result of large angle scattering events in which the scattered photon escapes in the direction of the collimator and passes through little or no NaI. Note also that, as expected, the single and double escape peaks are reduced. The effectiveness of the Compton suppression system increases with gamma energy since the ratio of the Compton to the photoelectric cross section also increases with gamma energy. At 1.369 MeV the average reduction of Compton background is a factor of 2, while at 662 keV, it is only 1.5. In this case, resolution on the 2.754-MeV photopeak is 3.9 keV (fwhm).

The absolute intrinsic photopeak efficiency of the Ge(Li) spectrometer using the 30 cc detector and operated in the Compton suppression mode was determined using calibrated radioactive sources; Co^{57}, Cs^{137}, Mn^{54}, Na^{22}, and Co^{60}. The sources were centered in the sample holder, about

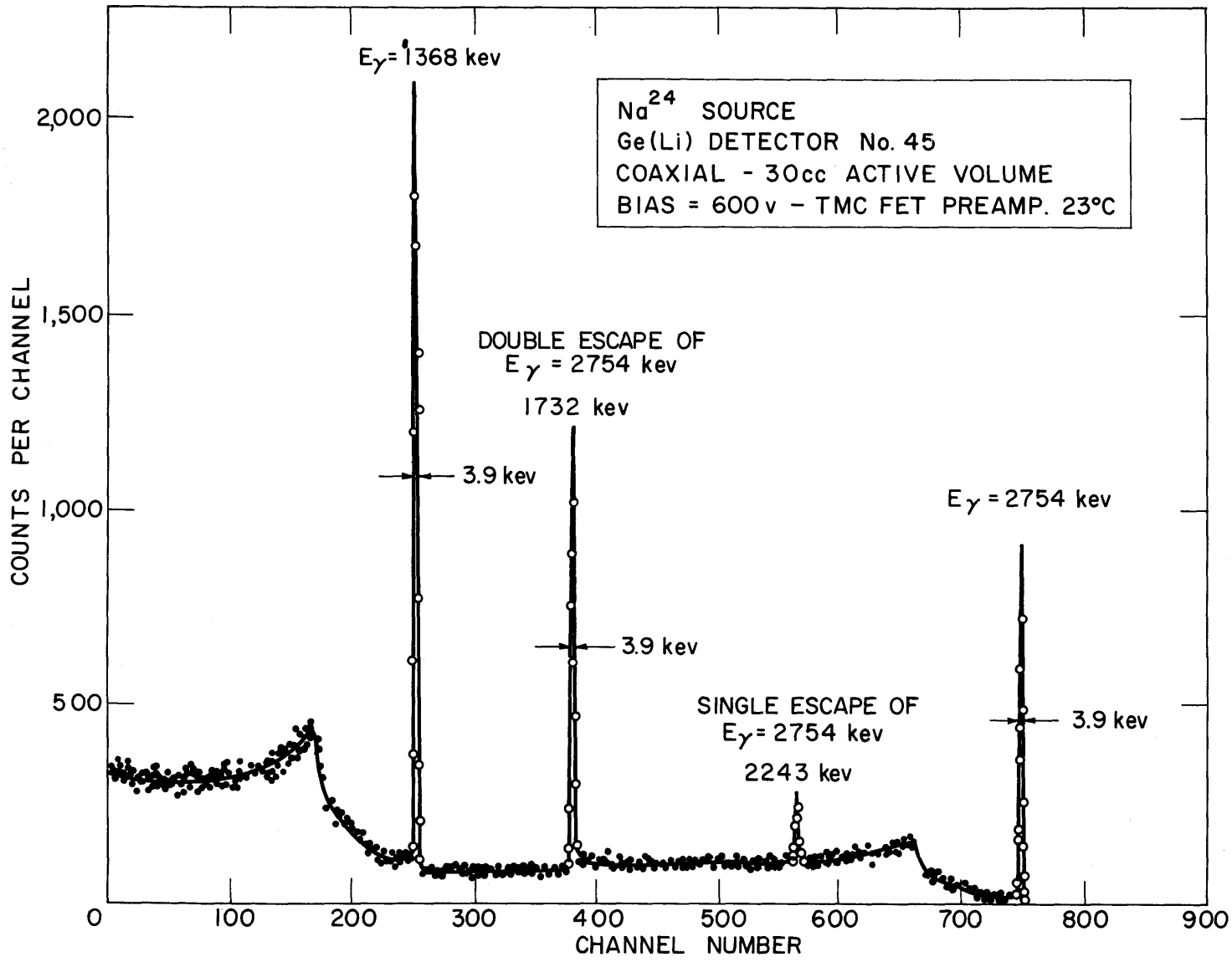

FIGURE 35 Na^{24} SPECTRUM MEASURED WITH 30cc Ge(Li) DETECTOR OPERATED DIRECTLY.

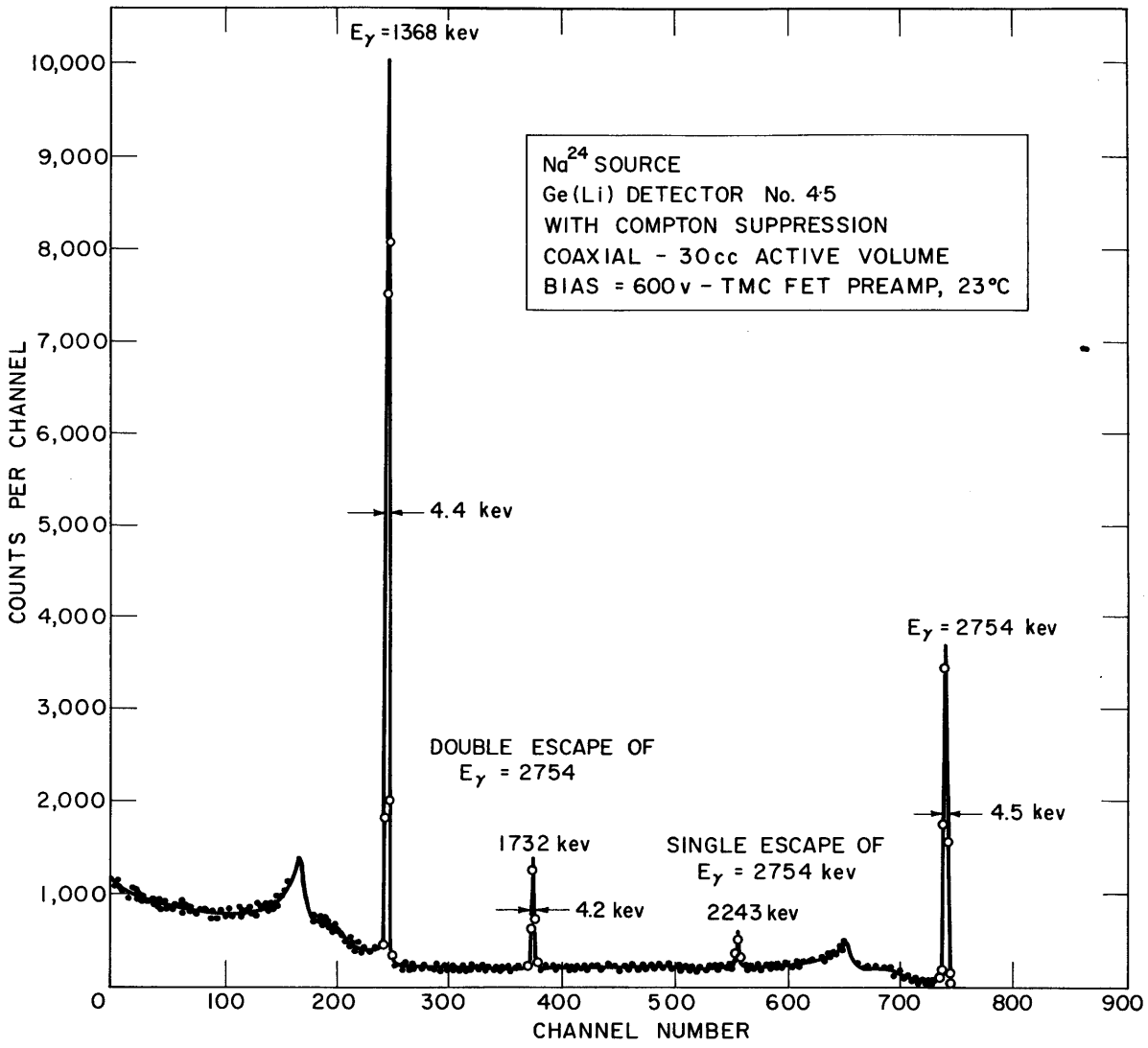

FIGURE 36 Na^{24} SPECTRUM MEASURED WITH 30 cc Ge(Li) DETECTOR OPERATED IN COMPTON SUPPRESSION MODE.

100 cm from the Ge(Li) detector, and were viewed through the 0.95-cm diameter collimator. A relative efficiency curve was determined using a Ra^{226} source. The efficiency curve is shown in Fig. 37. The relative efficiency curve has been normalized to the absolute curve at 1120 keV. Note that this efficiency curve includes the effect of the 1.6-cm thick LiF sheet and hence is lower than the efficiency curve plotted in Fig. 15 for detector number 45. Use of the Ge(Li) detector in the Compton suppression mode does not result in any measureable decrease in the photopeak efficiency of the directly operated detector.

The portion of the titanium capture gamma spectrum from about 150 keV to 2800 keV is shown in Fig. 38. This spectrum illustrates the operation of the Compton suppression system in the low energy range. The typical energy resolution is in the range of 4 to 6 keV. Energy resolutions are indicated on several of the stronger peaks in Fig. 38. The sensitivity of the Ge(Li) spectrometer decreases sharply below about 100 keV because of γ-ray absorption in the 1.6-cm thick LiF sheet in the γ beam. Hence, the spectrometer is, in general, effective only for capture γ rays with energies greater than 100 keV.

The linearity correction curve was determined for the Compton suppression mode of operation using the same procedure as for the pair spectrometer mode. Since only the first 2048 channels of the analyzer were used to record the Compton suppression spectra, the linearity correction curve was determined only for this region using a spacing between test pulses of about 20 channels. A linearity correction curve, similar to those shown in Fig. 29, was obtained. In the range from channel 300 to channel 2000 the maximum deviation from linearity was 1.3 channels.

A 5 cc coaxial detector (number 37) was also used in the Compton suppression mode. Figures 39 and 40 compare the performance at 1.28

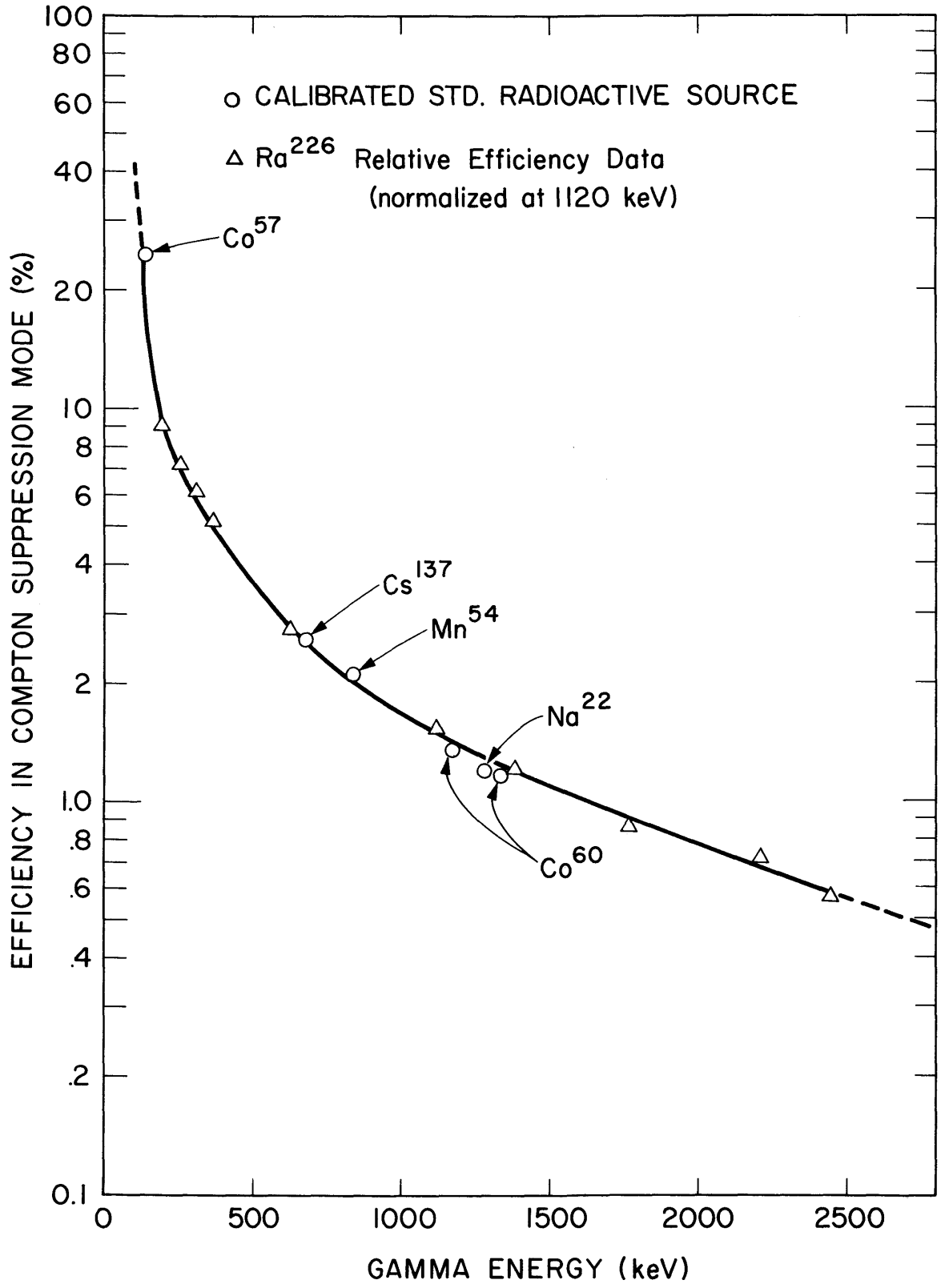

FIGURE 37 ABSOLUTE EFFICIENCY CURVE (INCLUDING EFFECT OF 1.6 cm THICK LiF ABSORBER) FOR 30 cc Ge(Li) DETECTOR OPERATED IN THE COMPTON SUPPRESSION MODE.

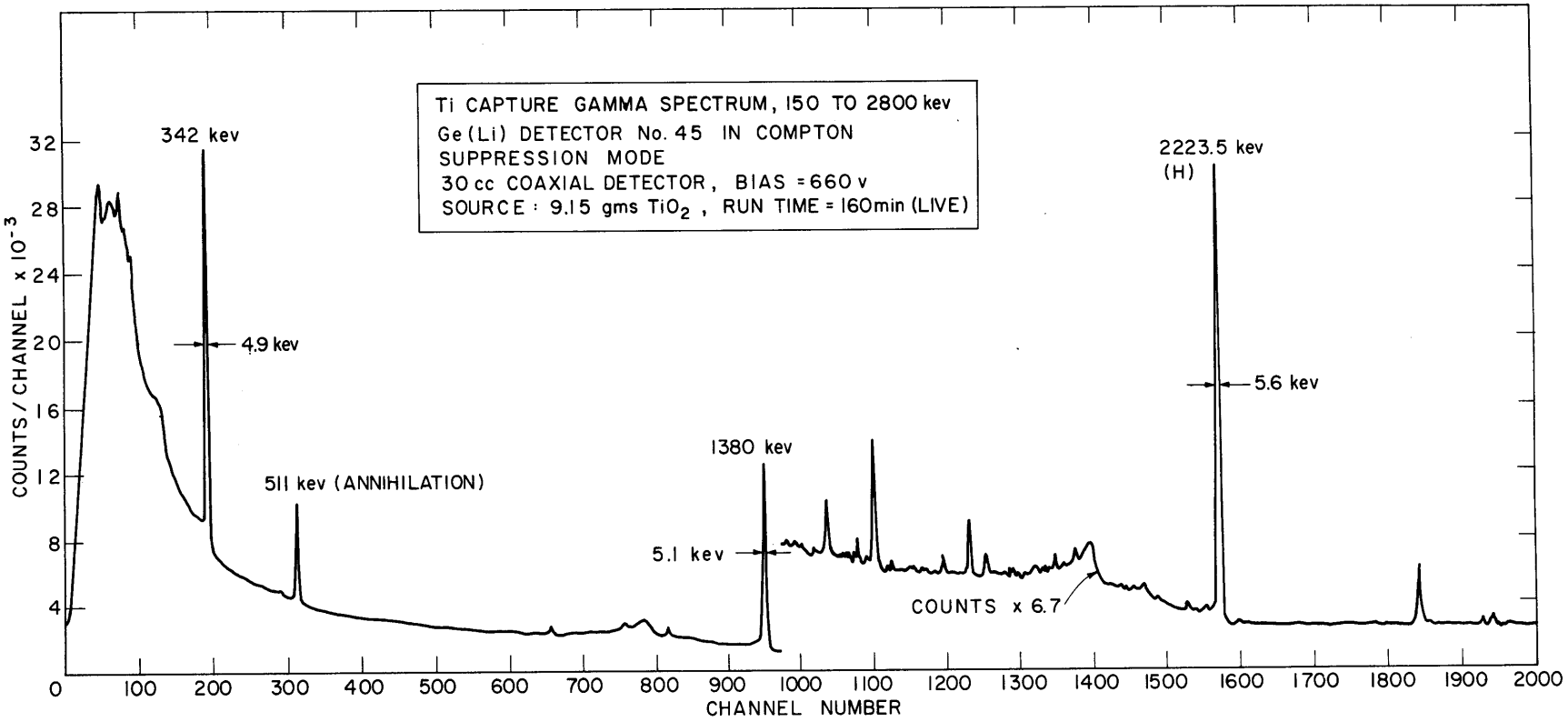

FIGURE 38 LOW ENERGY PORTION (150-2800 keV) OF Ti CAPTURE GAMMA SPECTRUM MEASURED WITH Ge(Li) SPECTROMETER IN COMPTON SUPPRESSION MODE.

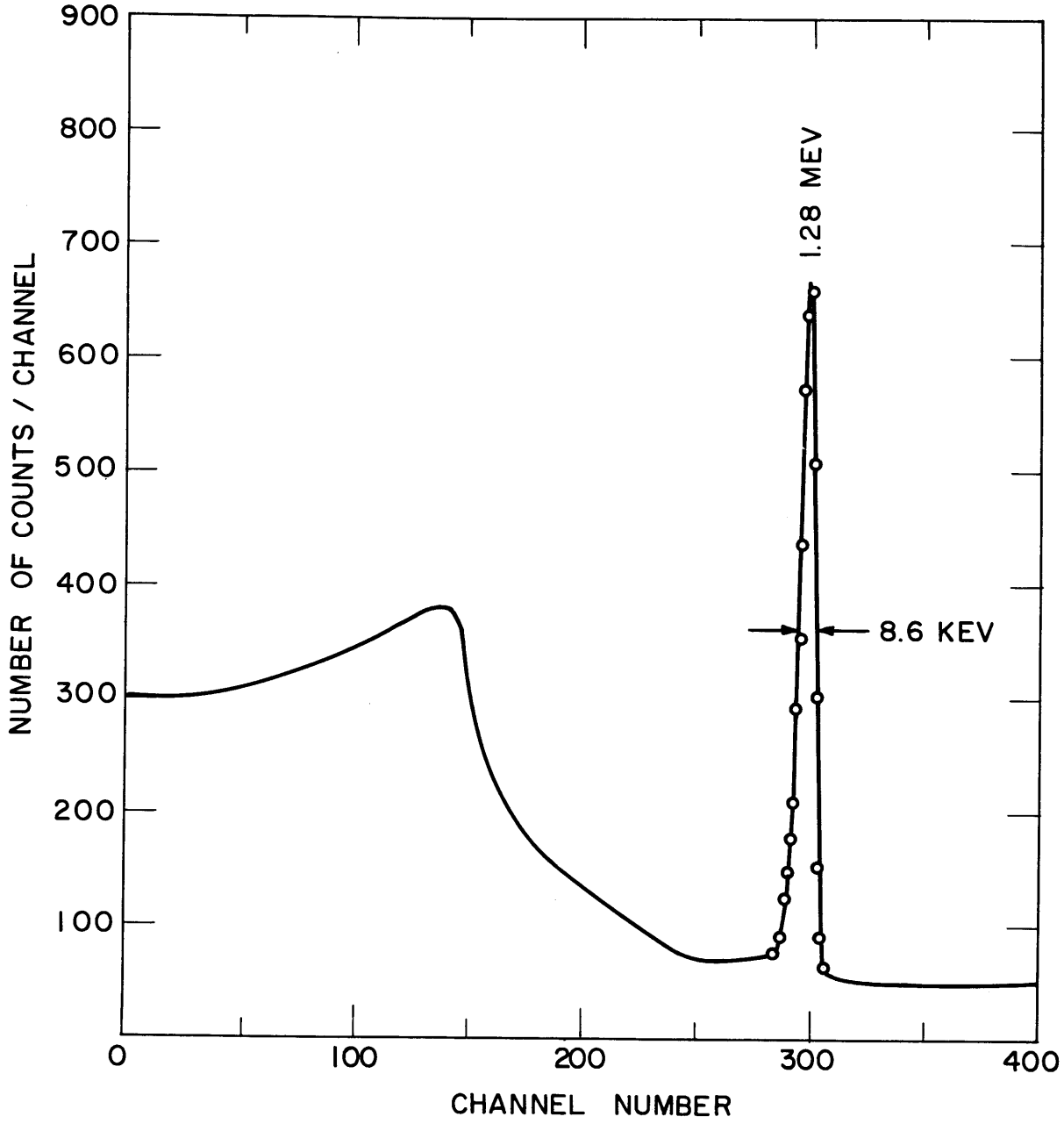

FIGURE 39 DIRECT SPECTRUM OF 1.28 MeV γ-RAY FROM Na^{22} MEASURED USING 5cc COAXIAL DETECTOR.

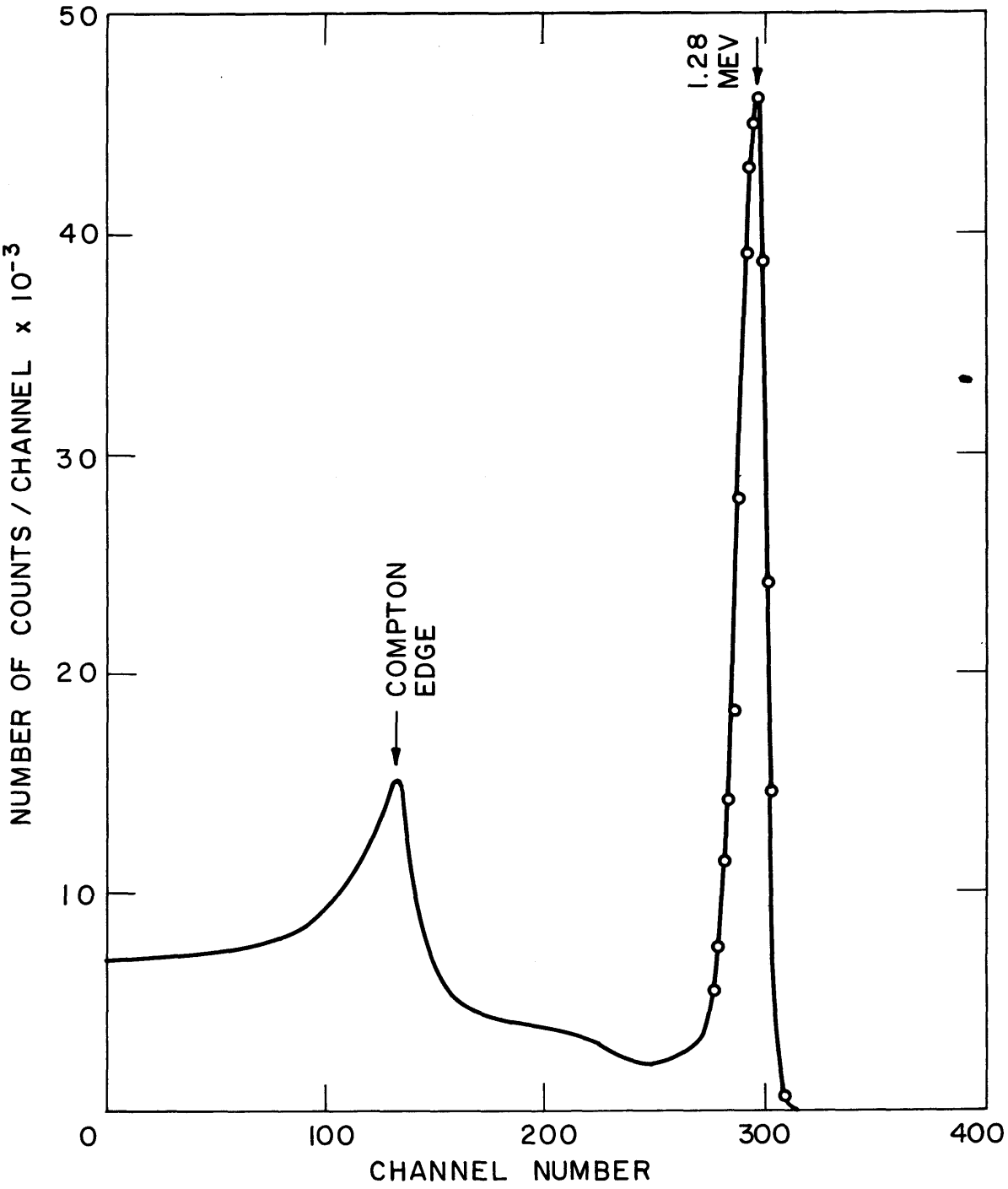

FIGURE 40 COMPTON SUPPRESSION SPECTRUM OF 1.28 MeV γ-RAY FROM Na^{22} MEASURED USING 5cc COAXIAL DETECTOR

MeV of this detector operated directly and in the Compton suppression mode respectively. The average Compton background has been reduced by about a factor of 3.0 and the Compton edge by about a factor of 2.

For purposes of comparison, Fig. 41 shows the spectrum of the 1.28-MeV γ ray from Na^{22} obtained using a 30 cc coaxial detector (number 45) operated in the Compton suppression mode. For this detector the average Compton background is reduced by a factor of about 2.3. The Compton edge is reduced by a factor of about 2. As one would expect, the improvement in the photopeak to Compton background ratio realized through the use of the Compton suppression system is somewhat greater for the smaller Ge(Li) detector. This is a result of the ability of the large detector to absorb more Compton scattered gammas. Nevertheless, because large Ge(Li) detectors have inherently greater photopeak to Compton ratios, it is more advantageous to use the large detector in the Compton suppression system. Comparing Figs. 40 and 41, one notes that the photopeak to average Compton background ratio is 10:1 for the 5 cc detector, and 25:1 for the 30 cc detector. The ratio of the photopeak to Compton edge is 3.6:1 for the 5 cc detector, and 10:1 for the 30 cc detector.

3.3.4 External Neutron Beam Facility

The uniformity of the neutron flux incident on a capture γ-ray source was checked using foil activation. Nine 1/8" dia., 5 mil thick, pure Au foils were attached to an empty polythylene vial (3.0 cm in diameter and 5.3 cm high) and were irradiated in the lead sample holder. Figure 42 shows the positioning of the foils on four sides of the polyethylene vial, and the orientation of the vial relative to the neutron beam during irradiation. The relative flux at each position was taken to be proportional to the count rate for the corresponding foil, as measured in a standard geometry GM tube setup.

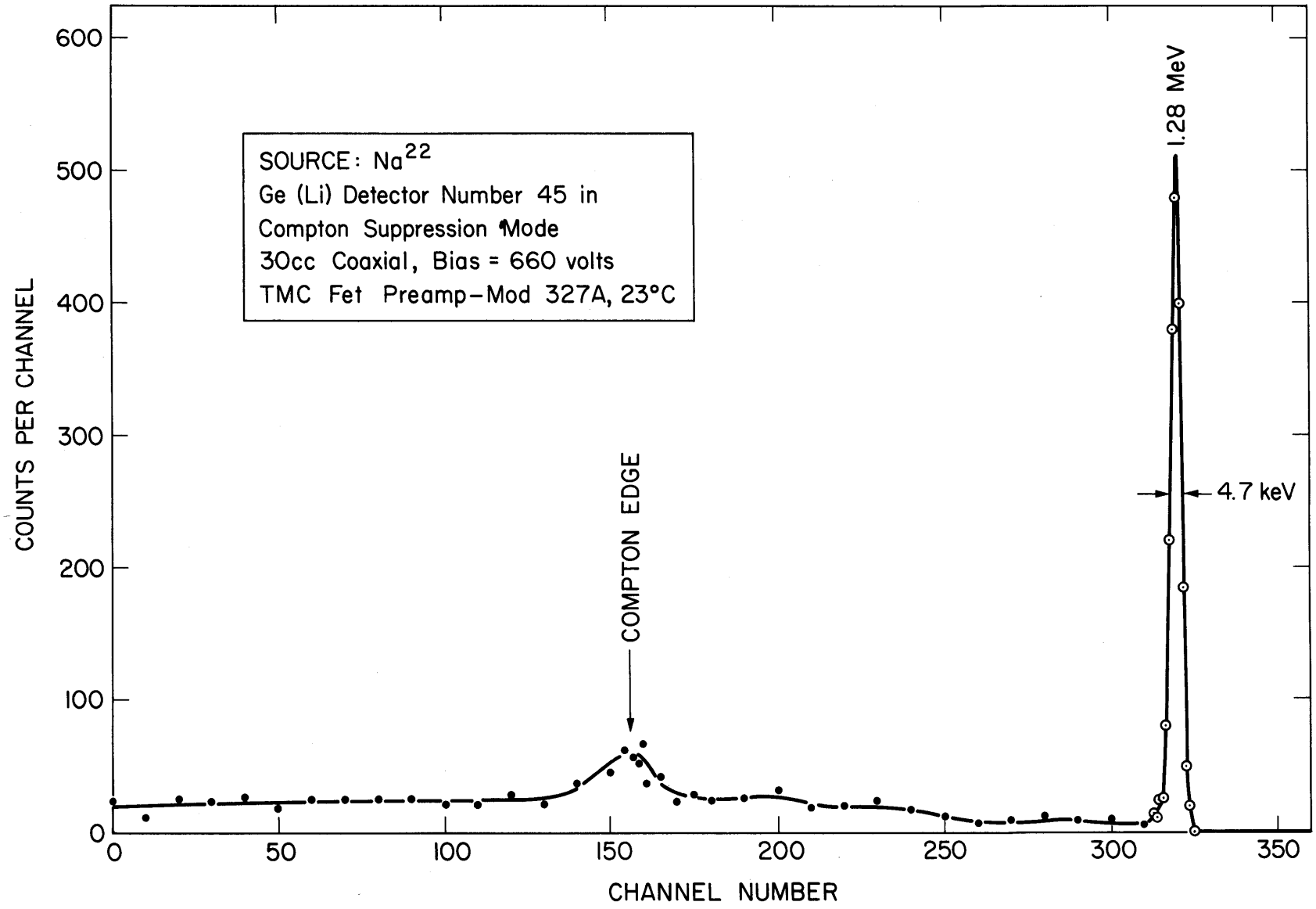

FIGURE 41 COMPTON SUPPRESSION SPECTRUM OF 1.28 MeV γ-RAY FROM Na^{22} MEASURED USING 30 CC COAXIAL DETECTOR

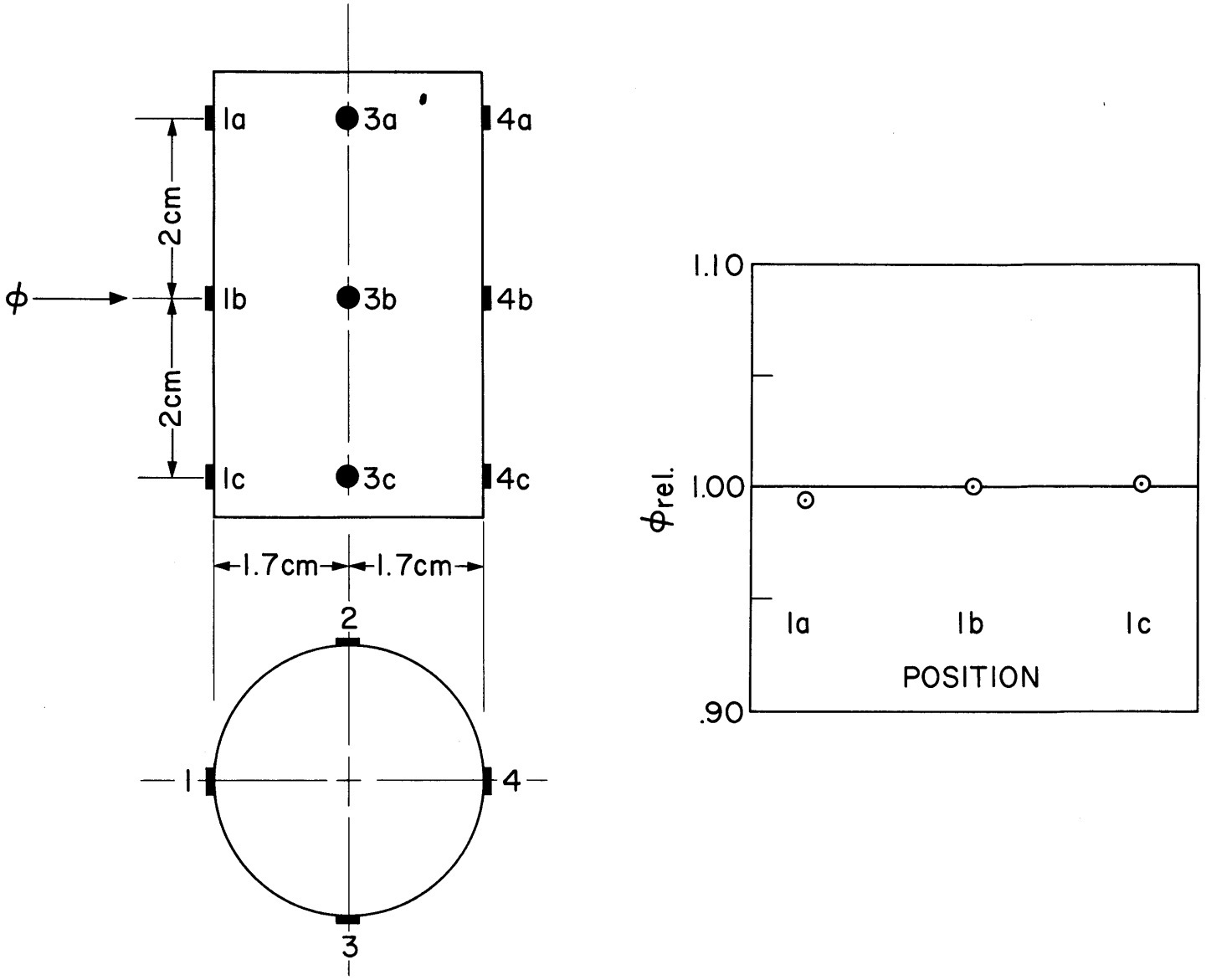

FIGURE 42 POSITIONING OF Au FOILS ON POLYETHYLENE VIAL FOR FLUX PLOT MEASUREMENT, FLUX PLOT FOR ONE GROUP OF FOILS

The usual corrections were made for differences in foil weights and decay times. A flux plot, shown in Fig. 42, for positions 1a, 1b, and 1c, reveals that the flux is quite uniform over the sample space. Flux plots for the other 3 groups of foils revealed a similar uniformity of flux. The average flux at positions 4a, 4b and 4c agrees with the average flux at positions 1a, 1b and 1c within 2%. The average flux at positions 2a, 2b and 2c and the average flux at positions 3a, 3b and 3c were about 10% lower than the average flux at positions 1a, 1b and 1c. This was probably a result of increased flux depression due to the orientation of these foils in the neutron beam (foil faces were parallel to the beam). These results confirmed earlier flux plots (H6) which also indicated flux uniformity over the sample space.

The amount of fast neutron flux contamination in the thermal neutron beam was investigated by measuring the Au cadmium ratio at the sample position. Using Au foils, the cadmium ratio was found to be approximately 2000. This highly thermal neutron beam greatly minimizes the possibility of observing resonance neutron capture γ rays in the thermal neutron capture spectra.

The absolute thermal flux was determined using two independent techniques. In the first method an Au foil was irradiated in the external neutron beam facility and its activity compared with an identical Au foil irradiated in a "known" neutron flux. The flux was determined in the usual way from the ratio of foil activities measured in a standard geometry GM tube setup. The second method involved the measurement of the absolute disintegration rate of a cobalt foil which had been irradiated in the external beam facility. A γ-γ coincident set up using two 3" x 3" NaI crystals, was used to determine the absolute disintegration rate of the Co^{60} formed. Knowing the number of atoms in the cobalt foil, the

activation cross section, and the length of time of the irradiation, it was possible to calculate the absolute thermal flux.

The second method gave a value for the thermal flux at the sample position of the external beam facility of

$$6.19 \times 10^{8} \ n/cm^{2}/sec$$

This value is accurate to about 5%. Most of the error arises from the determination of the absolute disintegration rate. The flux obtained using the first method agrees with this value within 5%. This is well within the 20% accuracy with which the "known" flux (inside the MITR rabbit facility) has been determined. The determination using the first method was carried out only as a check on the results of the second method.

Unfortunately, the flux in the external beam facility is not constant over long periods of time (order of days). To avoid having to perform an absolute flux determination for each capture γ-ray run, several Au foils were irradiated with the cobalt foil. Three foils were attached to a polyethylene vial in the following positions (as defined in Fig. 42): a pure Au foil (1/8" dia. x 5 mil) in position 1a, a Co foil (1/4" dia. x 5 mil) in position 1b and a 1% Au in Al foil (1/8" dia. x 3.5 mil) in position 1c. In addition, a dilute (1% Au in Al foil, 1/8" dia. x 3.5 mil) foil was irradiated in the foil monitor tube (see Section 3.2.3). This dilute Au foil was counted in a standard geometry GM tube setup and established as a standard. In later runs, it was possible to determine the flux by irradiating a similar dilute Au foil in the monitor tube and counting it in the same GM tube setup. The dilute Au foil was used for long pair spectrometer runs (12-30 hours) while the pure Au foil was used for short Compton suppression runs (about 3 hours). The use of two types of foils was necessary in order to satisfy the count-rate restrictions of the GM tube.

The flux in the external neutron beam facility may be reduced by

about a factor of 2 by closing the lead shutter (see Fig. 22) which exists between the graphite thermal column and the reactor core. This feature is quite useful as it allows for most elements the use of the same capture source and gamma collimation for both the pair spectrometer run and the Compton suppression run. The lead shutter is opened for the pair spectrometer and closed for the more sensitive Compton suppression mode of operation.

The effective fraction of the capture gamma source viewed by the gamma collimator was determined using a radioactive source. A 1 cc vial containing a solution of Co^{60} was positioned in the center of a large polyvial (3.2 -cm dia. x 5.3 cm high) which was placed in the sample holder and counted with the Ge(Li) detector through the 1" dia. collimator. The Co^{60} solution was then diluted to 40 cc, which just filled the large polyvial, and counted again. Assuming that all of the source was being viewed in the first counting, the fraction, f, of the large source being viewed was given by

$$f = \frac{N_2}{N_1}$$

where

N_1 = number of counts in Co^{60} peaks/unit time from 1 cc source,

N_2 = number of counts in Co^{60} peaks/unit time from 40 cc source (corrected for source self-absorption).

For the 1" dia. collimator f was found to be approximately 0.90.

The background spectrum observed in the Compton suppression mode is shown in Fig. 43. An empty large polyvial was positioned in the sample holder for this run, which used the 0.95-cm dia. collimator. About 12 prominent peaks have been identified. Their energies, relative intensities, and their origin are given in Table 4. The principal background gamma, from hydrogen capture, originates from the polyvial and the polyethylene

TABLE 4

PRINCIPAL BACKGROUND GAMMAS
(COMPTON SUPPRESSION)

Line Number	Energy (keV)	Relative Intensity*	Origin
1	138	1	Ge(?)
2	158	.6	Cu
3	175	2	Ge
4	198	3	Cu
5	239	.2	Cu(?)
6	249	.4	Ge(?)
7	253	2	Ge
8	511	16	annihilation
9	596	1	Ge
10	1201	8	H^2, double-escape
11	1712	4	H^2, single-escape
12	2223	100	H^2, full energy

* Normalized to 100 for hydrogen full energy peak

TABLE 5

PRINCIPAL BACKGROUND GAMMAS
(PAIR SPECTROMETER)

Line Number	Energy (keV)	Relative Intensity*	Origin**
1	1532	10	Fe^{57}
2	1616	5	Fe^{57}
3	2223	100	H^{2}
4	3684	.5	C^{13}
5	4053	.3	Bi^{210}
6	4102	.4	(?)
7	4172	.3	Bi^{210}
8	4219	.2	Fe^{57}
9	4946	.6	C^{13}
10	5067	.2	Cu^{64}
11	5270	.2	N^{15}
12	5919	.4	Fe^{57}
13	6018	.3	Fe^{57}
14	6115	.2	Ge
15	6316	.1	N^{15} (?)
16	6437	.2	(?)
17	6684	.1	(?)
18	6736	.8	Pb^{207}
19	6760	.4	Al^{28} (?)
20	7290	.4	Cu^{64}
21	7368	.8	Pb^{208}
22	7632	.5	Fe^{57}
23	7640	.4	Cu^{64}
24	7646	.5	Fe^{57}
25	7725	.5	Al^{28}
26	7915	.5	Cu^{64}

* Normalized to 100.0 for line 3.

** Emitting compound nucleus.

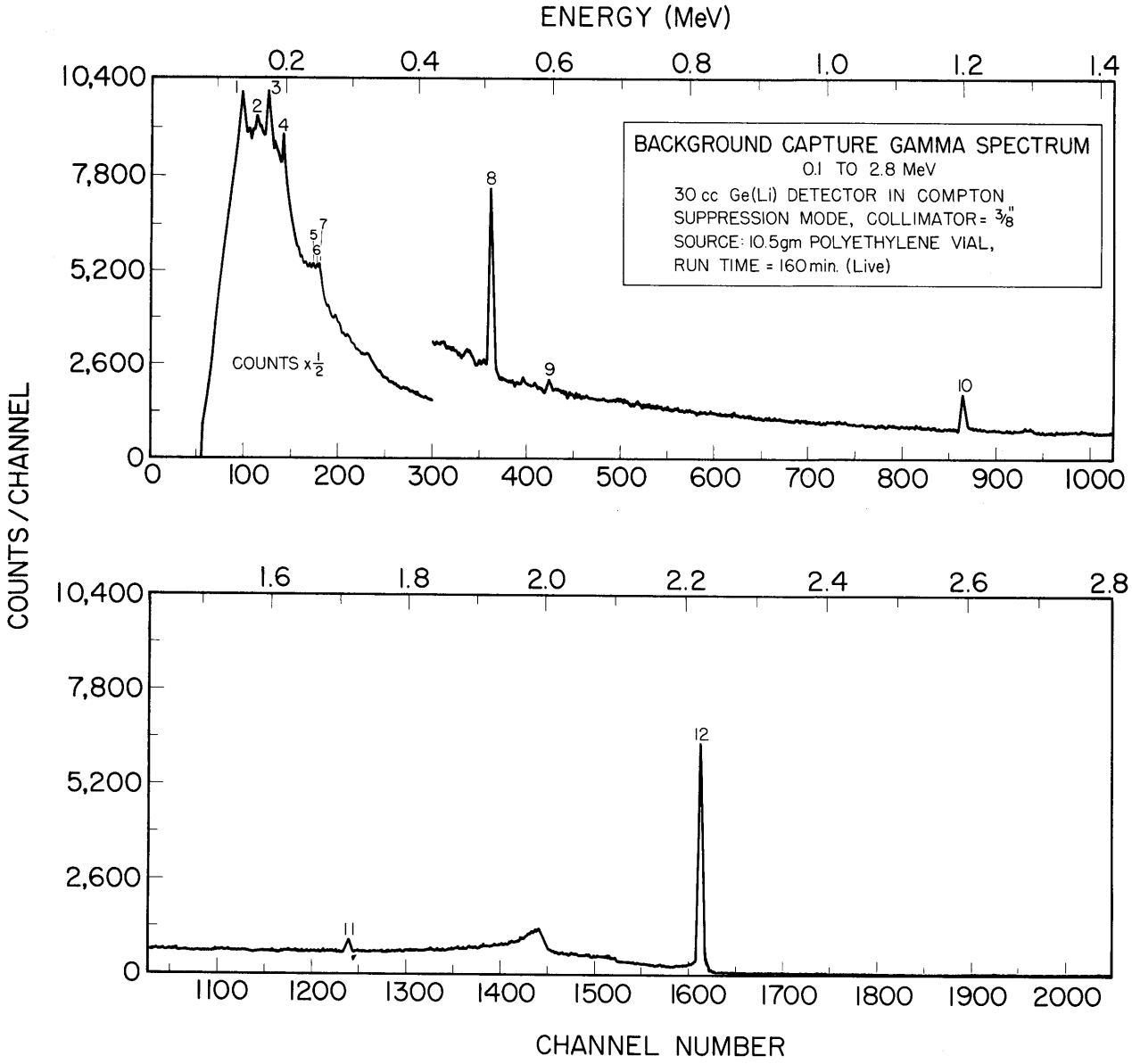

FIGURE 43 BACKGROUND SPECTRUM FOR COMPTON SUPPRESSION MODE OF OPERATION

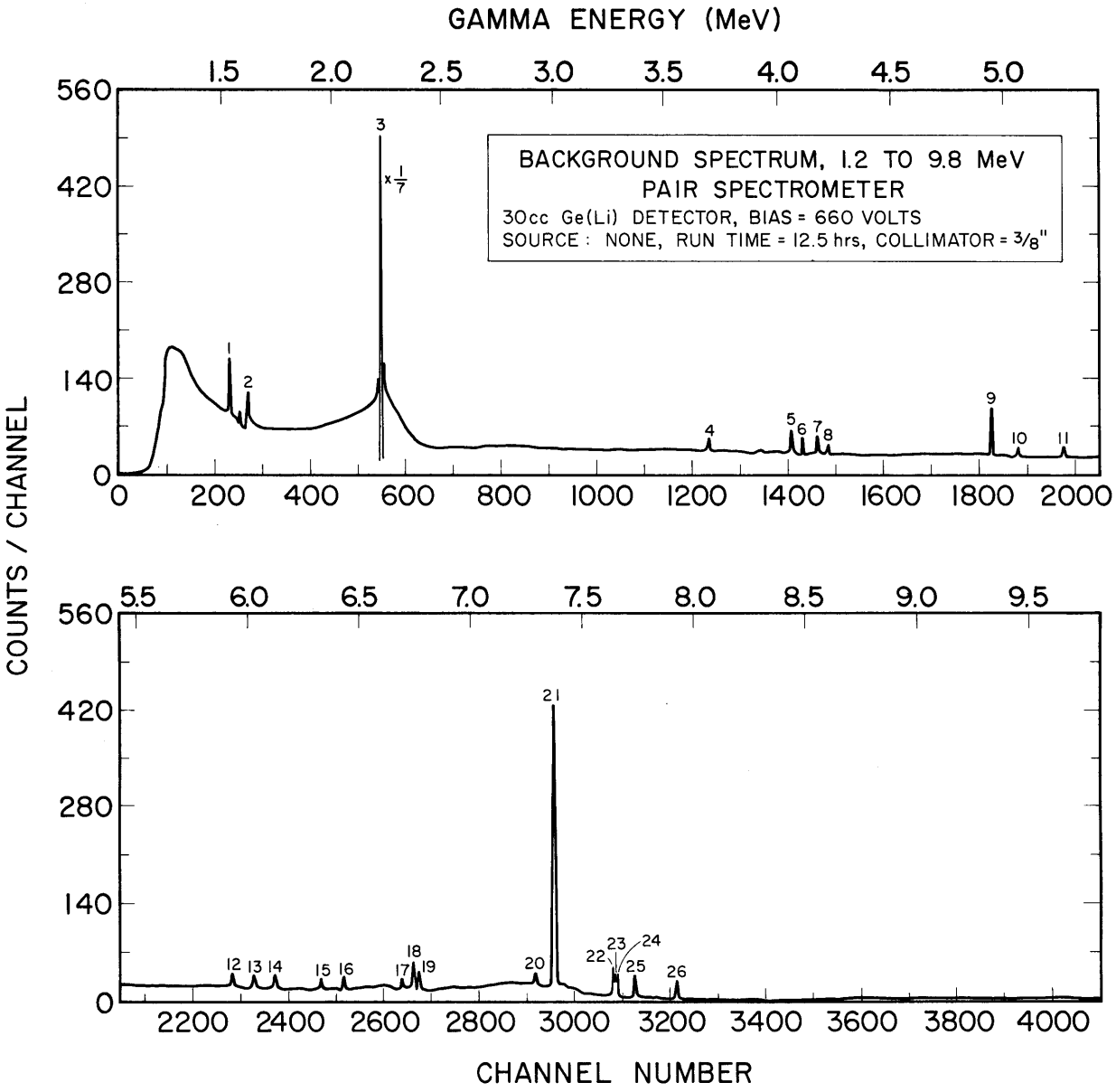

FIGURE 44 BACKGROUND SPECTRUM FOR PAIR SPECTROMETER

collimator. Although the hydrogen gamma contributes considerable background to the low energy capture spectra, its presence provides a convenient internal energy standard.

Figure 44 shows the background spectrum obtained in the pair spectrometer mode of operation. For this 12.5-hr run, the sample holder was empty, and the 0.95-cm dia. collimator was used. The background γ rays, their energies, relative intensities, and origin are given in Table 5. Capture in the detector shield accounts for the Fe γ rays, while capture in the Ge(Li) detector and dewar is responsible for the γ rays from Ge, Al and Cu. The principal background gammas, from hydrogen and lead, serve as internal energy calibration lines. The background contributes only a small fraction to a typical capture gamma spectra. For instance, this background contributes only about 3% of the total number of counts in the iron capture γ-ray spectrum.

CHAPTER 4

ANALYSIS OF EXPERIMENTAL DATA

4.1 Plotting of Spectra

A FORTRAN II computer program, PLOTS, was written to plot the spectra using an IBM-7094 digital computer and a Calcomp plotter.* The data from the 4096-channel analyzer was first recorded on punched paper tape, and subsequently transferred to IBM cards. These cards were then submitted with the PLOTS program, described in Appendix B, to obtain spectral plots. Several examples of such spectral plots have been presented earlier.

4.2 Gamma-Ray Energy Determination

4.2.1 Energy Standards

Internal energy calibration lines, which were present as background in all spectra, were used for both the high energy and low energy capture gamma determinations. In the Compton suppression spectra, the 511.0-keV annihilation peak and the full energy peak of the gamma from hydrogen capture were used as standards. The hydrogen capture gamma and the gamma from the $Pb^{207}(n,\gamma)Pb^{208}$ reaction were used as standards in the pair spectra. Table 6 lists the primary energy standards used in this work to determine these convenient secondary energy standards.

Two determinations of the hydrogen capture γ-ray energy were made using the 30 cc Ge(Li) detector operated directly. Using the double-escape peak and full energy peak of the 2.614-MeV γ ray from ThC'' as standards, the energy of the double escape peak of the γ ray from hydrogen capture

---

*MIT Computation Center facilities.

TABLE 6

PRIMARY ENERGY STANDARDS

Source	Energy (keV)	Reference
annihilation	511.006 ± .005	(a)
Na^{24}	1368.53 ± .04	(b)
ThC''	2614.47 ± .10	(b)
$Be^{9}(n,\gamma)Be^{10}$	6809.4 ± .4	(c)
$N^{14}(n,\gamma)N^{15}$	6322.00 ± .45	(c)
$Na^{23}(n,\gamma)Na^{24}$	6395.1 ± .4	(c)

(a) Electron rest mass from 1963 atomic constants.

(b) Murray, G., et al, Nucl. Physics, 63, (1965) 353.

(c) Greenwood, R. C., "Precise Measurements of Primary Capture Gamma-Ray Energies Using a 'Boot-Strap' Method," paper presented at ANL Slow Neutron Capture Conference, November 2-4, 1966.

was found to be 1201.3 ± .3 keV.* Using the difference between the double-escape and full energy peaks of the hydrogen γ ray to establish an energy scale and the 1.368-MeV γ ray from Na^{24} as a reference standard, the double escape peak of the hydrogen γ ray was found to be 1201.25 ± .3 KeV.* In both determinations, linearity correction curves, determined in the manner discussed in Section 3.3.1, were applied. The average of the above two values yields a value for the hydrogen capture γ-ray energy of

2223.3 ± .3 keV,*

*The errors quoted make an allowance for the errors in the standard.

This value is in good agreement with the value of 2223.18 ± .20 keV reported by Knowles (K4) and with the value of 2223.28 ± 0.15 keV reported by Prestwich (P2).

The energy of the capture γ ray from the $Pb^{207}(n,\gamma)Pb^{208}$ reaction was determined using the pair spectrometer. Three determinations were made, each one using two standards, the hydrogen γ ray and one of the capture γ ray standards listed in Table 6. Linearity corrections were made, using curves such as those shown in Fig. 29. The results of these determinations are listed in Table 7.

TABLE 7

VALUES OF THE ENERGY OF THE CAPTURE γ RAY FROM THE $Pb^{207}(n,\gamma)Pb^{208}$ REACTION

Run Number	Calibration Sources	Energy of γ ray from $Pb^{207}(n,\gamma)Pb^{208}$ (keV)
1	H and Be	7367.48 ± 1.0
2	H and N	7367.68 ± 1.0
3	H and Na	7368.02 ± 1.0

Mean = 7367.73 ± 1.0 keV

Note that the maximum difference between any two determinations is only about 0.5 keV.

4.2.2 Determination of Peak Center

A Gaussian function was fitted to the upper portion of each capture gamma spectral peak in order to establish the peak position and, hence, the energy. Let $F(x_i)$ be the number of counts per channel, x_i. In the region of a peak, $F(x_i)$ may be approximated by a continuous Gaussian function of x,

$$F(x_i) \approx e^{(ax^2 + bx + c)} \qquad (4-1)$$

where a, b and c are constants to be determined by a least squares fit.

This fitting procedure is simplified considerably if it is made to the natural logarithm of the experimental data, $f(x_i)$, since

$$f(x_i) \approx a x^2 + b x + c \equiv y(x) \qquad (4\text{-}2)$$

In general, a, b and c are determined by performing a least squares fit of this quadratic function (H7) to 5 points centered about a peak. Figure 45 shows the result of such a fit to a peak.

The peak center, x_c, is defined as that value of x corresponding to the maximum value of the fitted curve, i.e.,

$$x_c = -\frac{b}{2a} \qquad (4\text{-}3)$$

Using this method, the peak center of a well-defined peak may be determined to within about 0.1 channel. Once the background for a given peak has been ascertained (see Section 4.3.2), the fwhm of the peak may be determined in a straightforward manner from the fitted curve.

The "quality" of a particular fit is determined by calculating an estimate for the RMS deviation, E_{RMS}, between the true function and the observed function over the points considered (H7),

$$E_{RMS} \approx \sqrt{\frac{[R(x_i)]^2}{N - n}} \qquad (4\text{-}4)$$

where $R(x_i) = f(x_i) - y(x_i)$

N = number of points considered in fit - 1

n = order of polynomial fitted; n = 2, in this case.

Next, E_{RMS} is compared with an independent estimate of the RMS value of the observational errors. In this case, the observational (statisical) error in $F(x_i)$ may be taken to be $\sqrt{F(x_i)}$. The corresponding observational error in $f(x_i)$ is found to be approximated by

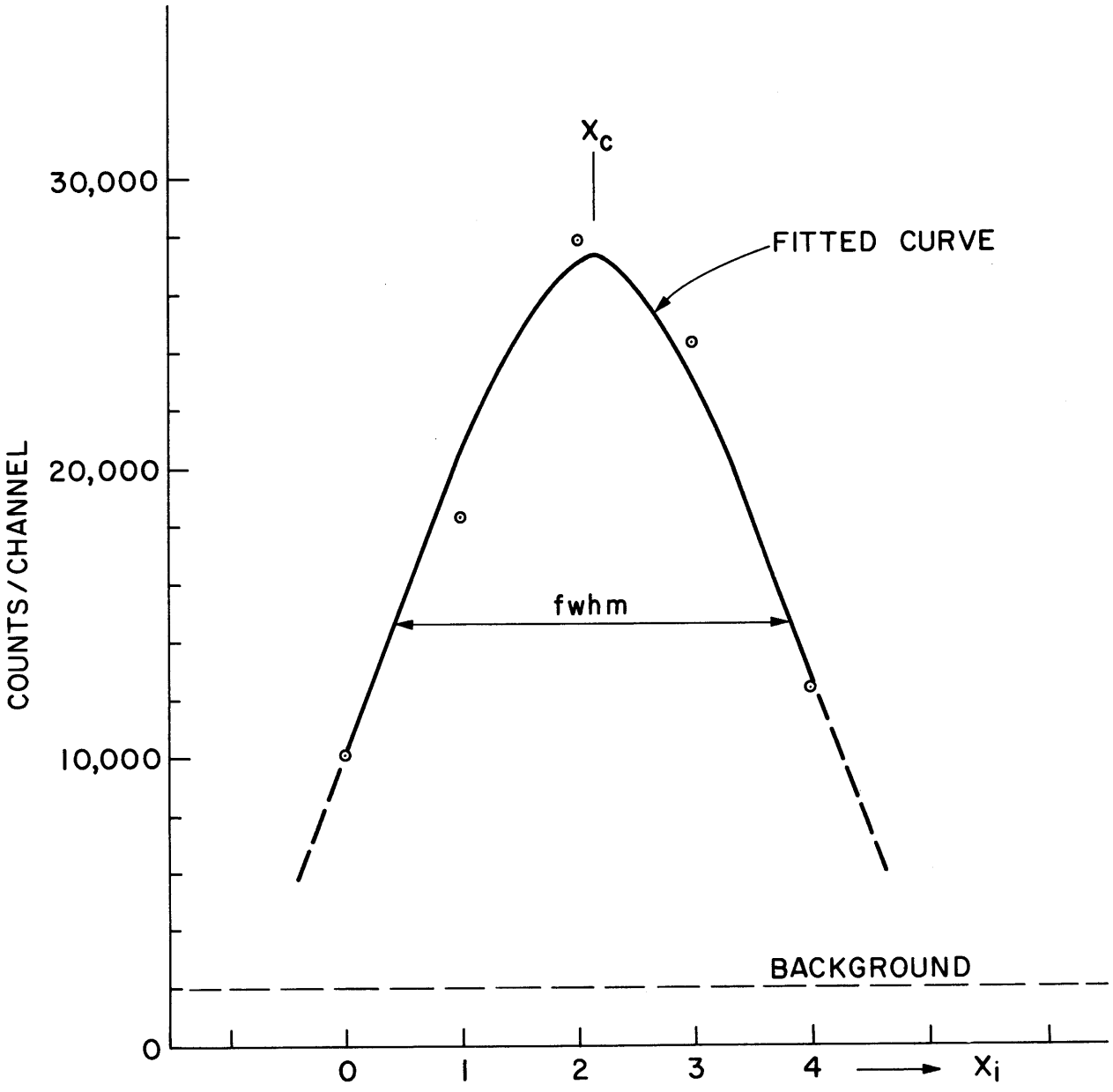

FIGURE 45 GAUSSIAN FIT TO UPPER PORTION OF SPECTRAL PEAK

$$\frac{1}{\sqrt{F(x_i)}}$$

if $\frac{1}{\sqrt{F(x_i)}} << 1$. Hence, the RMS value of the observational errors (arising from statistics) O_{RMS}, is given by

$$O_{RMS} = \sqrt{\frac{\sum_i \frac{1}{F(x_i)}}{N+1}} \quad . \tag{4-5}$$

The degree of agreement between this quantity and E_{RMS} is indicative of how "good" a fit was attained (i.e., it serves as a measure of the validity of the assumption that the true function is indeed a Gaussian over the points considered). For the peak fitting illustrated in Fig. 45, $E_{RMS} \approx 10\ O_{RMS}$, yet the fit appears quite reasonable. O_{RMS} is quite small for this peak because of the large number of counts in each channel (good statistics). Generally, the agreement between E_{RMS} and O_{RMS} was found to be much better than for the strong peak shown in Fig. 45. Indeed, analysis of over 30 peaks in a pair spectrum revealed that in all cases $E_{RMS} < 3\ O_{RMS}$, indicating that better 'quality' fits had been obtained than that shown in Fig. 45.

Despite the simplicity of the above method, it is capable of determining peak positions with more than adequate accuracy. In general, the error in the energy of a peak attributable to an error in peak position is much smaller than the error caused by other factors (for example, error in the linearity correction). A principal advantage of this method is that it does not involve a "trial and error" type of fitting procedure inherent in most complex spectral fitting techniques. Consequently, a fit and a measure of its "quality" is assured for every peak. The problem of non-convergence associated with "trial and error" procedures is avoided and the amount of

computer time required is reduced considerably.

A limitation of this simple method is its inability to sort out the peak positions of two peaks comprising a doublet. Since this method only fits to the upper portion of a peak, it may be used to find the peak centers of a partially resolved doublet by considering each peak separately. This was done for the well known 14.4-keV doublet in the iron capture gamma spectra with excellent results (the measured energy separation was 14.3 keV). Completely unresolved doublets are treated as a single peak -- their average peak center being determined. The fwhm of such a peak will be greater than for true singlets -- thus indicating a closely-spaced doublet.

4.2.3 Correction for System Non-linearity

Linearity correction curves such as those discussed in Sections 3.3.1 and 3.3.3 were used to correct all peak positions for the system non-linearity. The true peak center, TPC, is obtained from the observed peak center, PC, and the linearity correction factor, L(C), which is a function of channel number, C, by the following:

$$TPC = PC + L(PC). \qquad (4-6)$$

L(PC) is determined by second order interpolation on the appropriate linearity correction curve. This method has several possibilities for error. The voltage standard and mercury pulser used to obtain the linearity correction curve may themselves have a non-linearity. Furthermore, since a period of time elapses between the linearity correction curve determination and the actual run, gain and zero shifting may introduce error. Finally, this technique tacitly assumes that the Ge(Li) detector is linear. Fortunately, as will be discussed in Section 5.6, the accuracy of the resulting capture γ-ray energies may be checked. Such

checks reveal that any errors introduced by this linearity correction technique are smaller than approximately 0.5 channel (corresponds to about 1 keV in the pair mode of operation) over the middle 90% of the 4096 channel range. Near the ends of the channel range, where the linearity correction factor is greater, the linearity error may be somewhat larger.

4.2.4 Determination of Energies of Individual Peaks

Once the true peak centers of all peaks have been determined, two standard peaks (see Section 4.2.1) are used to establish an energy scale--assuming a linear relationship between energy and channel number. Having established an energy scale, all true peak centers are easily converted into equivalent energy values. A computer program has been written to perform all of the above mentioned steps in the energy determination. A listing and discussion of this program are given in Appendix C.

4.3 Intensity Determination

4.3.1 Summary of Methods Used to Determine Absolute Intensities

A variety of techniques have been employed to determine the absolute intensity of capture γ rays. If the nuclide under investigation has a radioactive product which saturates, then the capture γ-ray intensities may be found relative to the known absolute intensity of the radioactive decay γ ray. This method requires a knowledge of the relative detection efficiency of the spectrometer as a function of energy.

A second method involves the measurement of relative intensities (requires only a knowledge of the relative efficiency of the spectrometer); and the normalization of these to the binding energy of the product nucleus (for elements having several stable nuclides, an average binding energy computed from the binding energies of each product nucleus weighted by

its fractional contribution to the total capture cross section is used). The absolute intensities, I_γ, (in γ's/100 captures) are calculated from

$$\sum_{i=1}^{N} \frac{I_{\gamma i} E_{\gamma i}}{100} = B.E. \qquad (4\text{-}7)$$

where $I_{\gamma i}$ = intensity of i^{th} γ ray in γ's/100 captures,

$E_{\gamma i}$ = energy of i^{th} capture γ ray,

B.E. = binding energy,

N = number of capture γ rays emitted.

Unfortunately, this method requires that all of the γ rays emitted have been identified and that internal conversion is not significant.

A third method involves measuring the intensities relative to those of an element which has been mixed with the capture source and whose capture γ-ray intensities are well known. Alternately, one may mix with the source an element with a saturating radioactive product and measure γ-ray intensities relative to the γ ray of the radioactive product. This method requires a knowledge of the capture cross sections of both the element under investigation and the mixed element.

A final method and the principal one used in this present work involves the experimental determination of the total number of γ rays of a given energy emitted by the source and a calculation of the number of neutrons captured by the source. This direct approach has the disadvantage of requiring an absolute measurement, whereas the other methods all require only relative measurements. However, this method was chosen because: (1) it eliminated the need for using mixed sources, which usually results in an increase in the complexity of a spectrum, (2) it was convenient, allowing the study of many different elements at a rapid rate (about one element per day), (3) it yielded intensity values independ-

ent of any binding energy normalization, thus, a calculation of the fraction of the γ-ray intensity observed was possible -- providing a check on the intensity values (see Section 5.7), and (4) it was equally applicable in both the Compton suppression energy range and the pair spectrometer energy range.

4.3.2 Principal Method Used for Intensity Determination

The direct determination of the absolute intensity of capture γ rays by calculating the number of captures in the source and measuring the number of γ rays of a given energy emitted requires: (1) a knowledge of the neutron flux distribution (in space and energy), in the neighborhood of the target, and (2) a determination of the absolute efficiency of the detecting instrument.

It has been established in Section 3.3.4 that the neutron flux is quite uniform in the region of the capture source and that it is highly thermal. Also, a method for obtaining the absolute value of the flux, φ, has been outlined in Section 3.3.4. The total number of captures, C, occuring in the source during a run of time, τ, is given by

$$C = NV\sigma_c \varphi \tau \qquad (4\text{-}8)$$

where N = number of source atoms/unit volume,

V = total volume of source,

σ_c = capture cross section for 2200 m/sec neutrons.

This expression assumes that the source is à 1/v absorber and that it does not perturb the flux. For non-1/v absorbers, the effective capture cross section, $\hat{\sigma}_c$, as defined by Westcott (W2) may be used. Flux depression in the source may be estimated to an accuracy of about 5% using a simple method proposed by Nisle (N2). The flux depression is approximated by

$$1 - e^{-\Sigma_a x_{avg}} \qquad (4\text{-}9)$$

where $\Sigma_a = \sigma_a N$ = macroscopic absorption cross section of the source,

$x_{avg} = \frac{4V}{S}$ (the average distance through the source volume, V, for straight lines that cut the surface, S, in two, and only two, points.)

The effect of scattering inside the source on the flux depression has been neglected in this approximation. Proper consideration of this effect requires a complicated analysis and the use of a digital computer (P3). Consequently, an attempt has been made to minimize experimentally the magnitude of the flux depression so that any error in its calculation will not contribute significantly to the intensity determination. Because of the high thermal neutron flux ($\approx 6 \times 10^8$ n/cm^2/sec), capture sources of most elements may be chosen small enough so that the flux depression is either negligible or quite small. Flux depression in very high cross section materials may be decreased by mixing a small quantity of the material with graphite powder, thus reducing the Σ_a of the capture source.

The total number of capture gammas of energy, E_γ, emitted from the source during a run are determined from

$$\frac{A}{(\frac{\Omega}{4\pi})(\mathcal{F})(\eta)} \qquad (4\text{-}10)$$

where A = the area under the spectral peak corresponding to E_γ,

Ω = solid angle subtended by the detector,

(η) = efficiency of either the pair spectrometer or the Compton suppression spectrometer as given in Figs. 28 and 37.

$\mathcal{F}$ = a factor which accounts for all minor corrections, such as flux depression in the source, fraction of the source viewed, and source self absorption.

The solid angle subtended by the Ge(Li) detector may be expressed as

$$\Omega = \frac{\pi r^2}{d^2} \qquad (4\text{-}11)$$

where r = the diameter of the collimator,

d = the distance from the source to the detector since $\frac{d}{r} \gg 1$.

The pair spectrometer efficiency may vary slightly from run to run due to small changes in the alignment of the Ge(Li) detector with the γ-ray collimator and due to gain shifting of the 511-keV NaI peaks out of their windows. The efficiency of the pair spectrometer was checked periodically using a calibrated radioactive source. Any observed variation in efficiency was taken into account in the intensity determinations by means of the $\mathfrak{F}$ factor. Another means of determining small efficiency variations from run to run is afforded by the Pb capture γ-ray peak, present in every spectrum. The area under the Pb peak, normalized for flux and run time, serves as a direct measure of spectrometer efficiency if the Pb sample holder position is the same from run to run. This method has an advantage over the radioactive source method in that it measures the efficiency during the run, not at some later time.

The area under each peak is calculated as the sum of the total number of counts under the peak minus a background, which is assumed to vary linearly in the region of the peak. Figure 46 shows the peak area, A, and the background area, B, for an actual spectral peak. The upper boundary point, UC, and the lower boundary point, UL, must be chosen for each peak considered. For very large peaks the effect of statistical fluctuations in the region of UC and LC may be somewhat smoothed out by calculating the number of counts at UC and LC as the arithmetic mean of 3 designated points in each region.

The statistical error in the peak area may be expressed as,

$$\sqrt{N_{obs} + B}$$

Where $N_{obs} = A + B$

B = background.

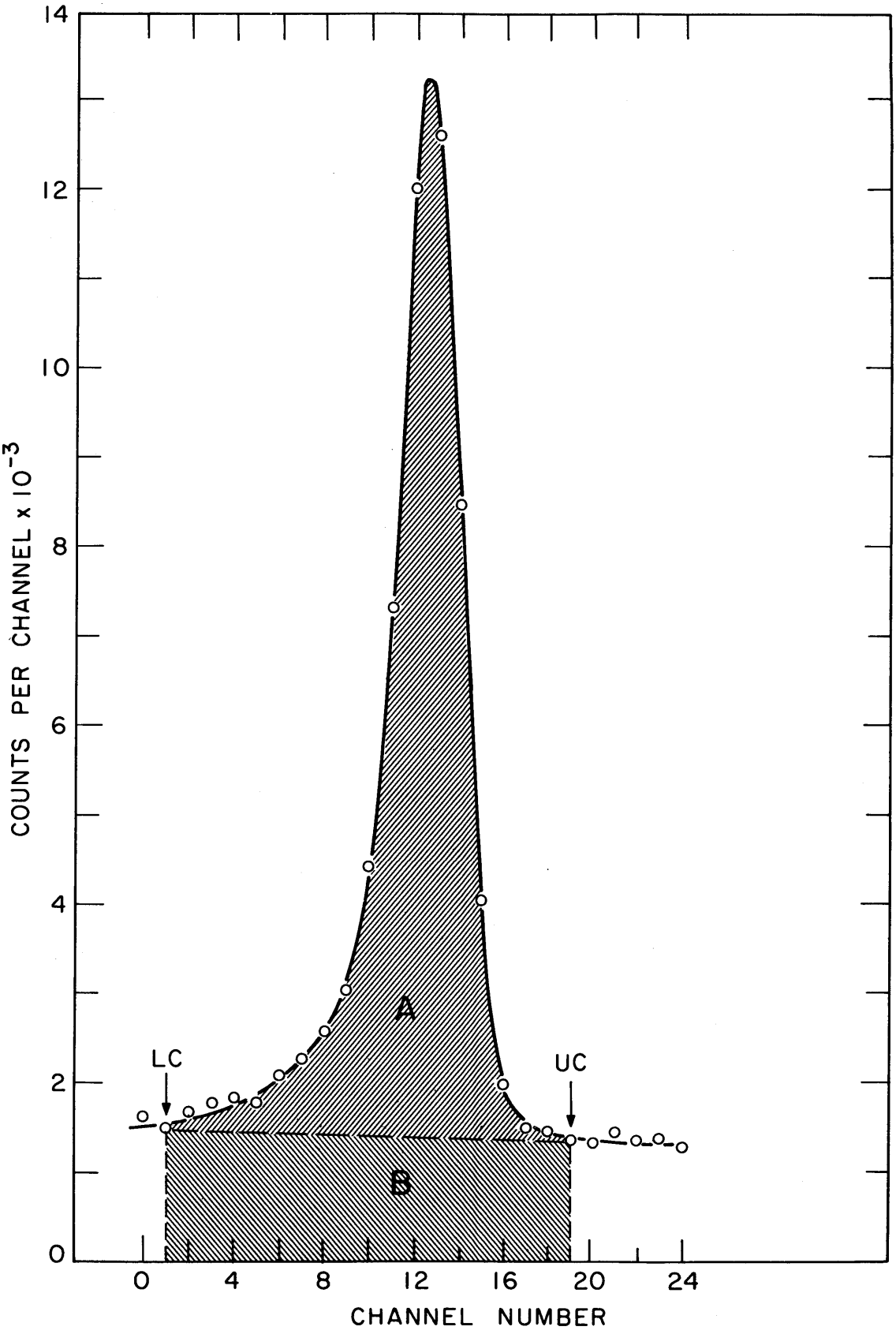

FIGURE 46 DETERMINATION OF AREA UNDER PEAK

Note that the error in the peak area is strongly a function of the magnitude of the background. The pair spectrometer, therefore, enables one to obtain peak areas with greater accuracy by significantly reducing this background.

In the case of multiple, partially resolved peaks (doublets, triplets, etc) the total area of the multiple peak is calculated as for a single peak. Then, if the peaks are sufficiently resolved to allow the fitting of a Gaussian function to their upper parts, this total area is apportioned to each constituent peak in proportion to its height. This method, though quite crude, gives reasonably accurate results. Use of this method on the 14-keV doublet in the iron capture γ-ray spectra gave relative intensities of 55.7% and 44.3% for the lower and higher energy components, respectively. These results are in good agreement with the values of (54 ± 4)% and (46 ± 4)% reported by Ewan (E1). Multiple peaks which are not sufficiently resolved to be treated by the above method are treated as singlets -- a note being made of their observed multiplicity.

A computer program has been written to perform all of the above steps in the intensity determination. The details of this program are given in Appendix C.

Results from this direct method of determining intensities have been compared with results from several of the other methods of determining intensities. As will be seen from the results for beryllium (Section 5.7), the intensities of this method agree within better than 2% with those obtained by normalizing the relative intensity values to the binding energy. Furthermore, the intensity of the 1779-keV γ ray emitted by the product of the $Al^{27}(n,\gamma)Al^{28}$ reaction was determined using this direct method and was found to be within 10% of its known intensity value, 1 γ ray/capture. Thus, intensity values based on the known intensity of this saturating

radioactive product would agree within 10% with values obtained by means of an absolute determination. Independent checks on the results of the intensity measurements, such as these, indicate that the direct method is capable of determining intensities of strong peaks to within 10 to 20%. Weak intensity peaks have a large statistical error which makes the intensity determination less accurate. Consequently, the intensity of weak peaks may be in error by factors of 2 or 3.

For γ rays observed in both the Compton suppression spectrum and the pair spectrum, the intensity values obtained from the former are more reliable. The efficiency of the pair spectrometer drops off sharply below about 2 MeV, consequently, statistics are poor in this region for all but very strong peaks.

4.4 Peak Selection

The principal disadvantage of the above method for extracting energies and intensities of γ rays in a complex spectrum is the requirement that peak positions be specified beforehand. In this work peaks were chosen by hand using rather arbitrary selection criteria (such as the peak height be at least 3 standard deviations above background and the peak width look reasonable). A rather conservative criterion was adopted; consequently, there are many marginal peaks which were not analyzed. Use of a more lenient criterion would increase the number of γ rays selected but would correspondingly increase the probability of selecting a statistical fluctuation as a peak.

No attempt was made in this preliminary data analysis to automate the peak selection process through the use of a computer. Work is in progress in our group (I3) on a spectrum analysis code which automatically selects peaks and which will allow more information to be extracted from a spectrum.

CHAPTER 5

RESULTS

5.1 Beryllium

Figures 47 and 48 show the thermal capture gamma spectra of beryllium obtained in the Compton suppression mode and the pair spectrometer mode, respectively. These and subsequent spectra were plotted from the multichannel analyzer data and contain no background subtraction. Numbered peaks result from capture in beryllium while all others are background peaks. Several of the more prominent background peaks have been identified. Note that a greater number of prominent background peaks are present in the beryllium spectrum (especially the Compton suppression spectrum) than in the background spectra given in Figs. 43 and 44. This is attributed to an increase in the number of thermal neutrons reaching the Ge(Li) detector and surrounding material due to the excellent neutron scattering properties of the beryllium sample.

Table 8 gives the energies and intensities of the six numbered peaks in the beryllium spectrum. These results are compared with the magnetic Compton spectrometer results of Motz (M8) and the Ge(Li) results of Greenwood (G7). The agreement of the energies and intensities of the present work with those of Motz is excellent. Since Greenwood's precise measurement of the 6809 keV beryllium γ ray was used as a primary energy standard, it is not surprising that the energies of the present work agree with Greenwood's energies within the accuracy of this energy determination, approximately 1 keV. No previously unreported beryllium capture γ rays were discovered; however, the intensity of the 853 keV lines, not reported by Motz (M8), was measured.

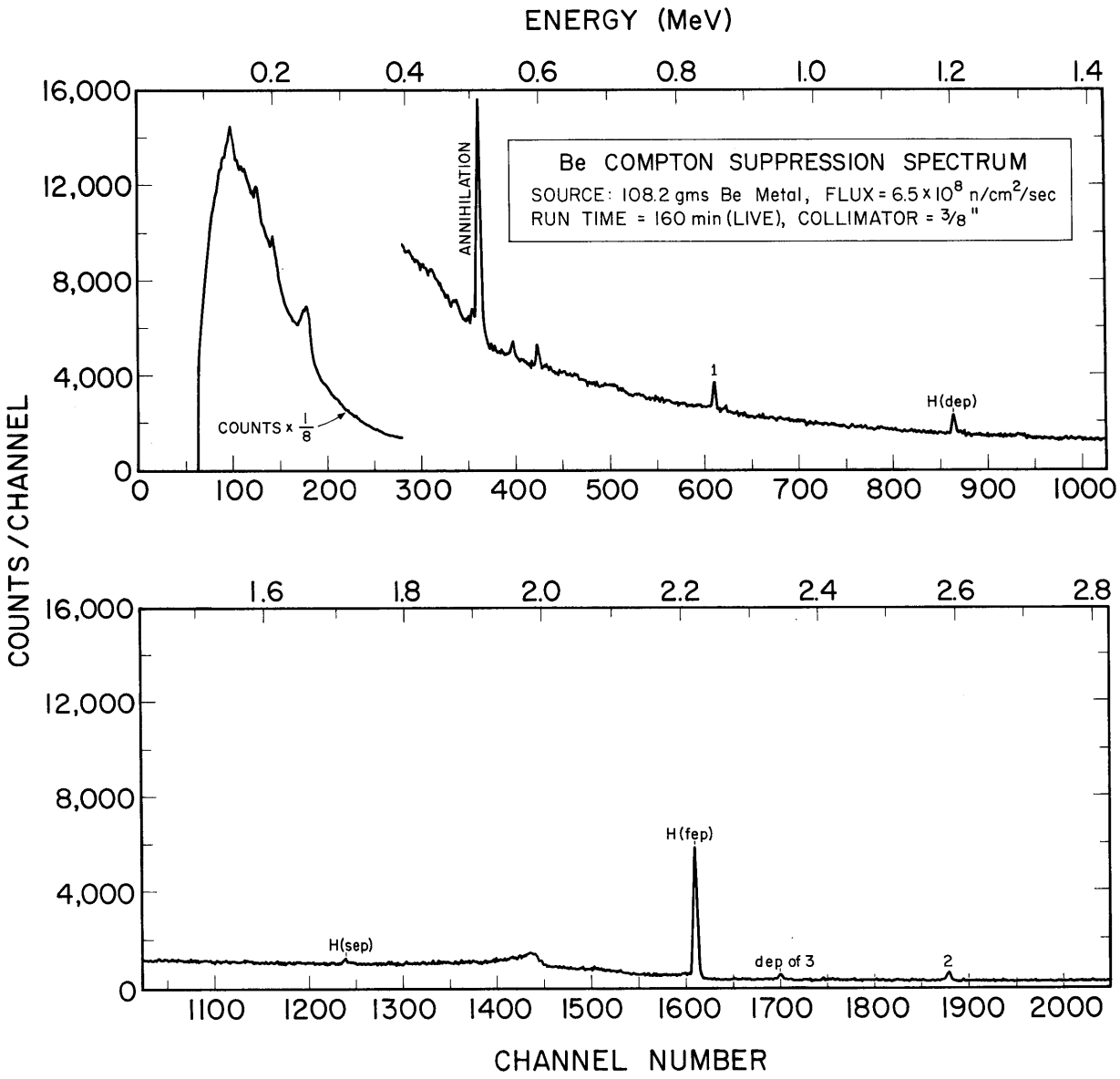

FIGURE 47 BERYLLIUM COMPTON SUPPRESSION SPECTRUM

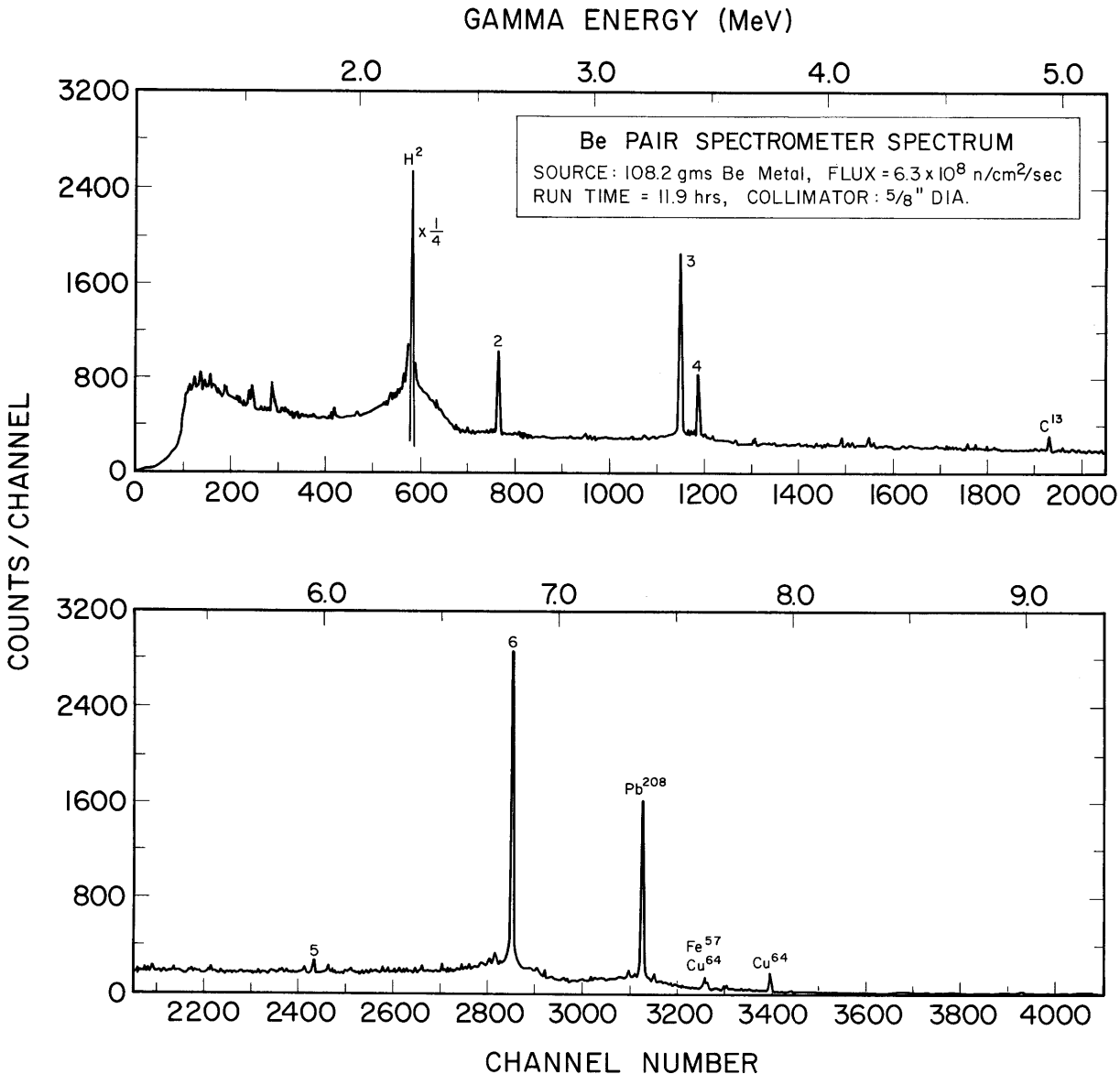

FIGURE 48 BERYLLIUM PAIR SPECTROMETER SPECTRUM

TABLE 8

ENERGIES AND INTENSITIES OF BERYLLIUM CAPTURE γ RAYS

Line	Present Work E (keV)	Present Work I (no./100 capts)	Notes	Motz (M8) E (keV)	Motz (M8) I (no./100 capts)	Greenwood (G7) E (keV)
1	853.3[a]	24[b]	CS[c]	855	--	853.5 ± .3
2	2590.0	25	CS & PS[d]	2590	28	2589.9 ± .25
3	3367.0	35	PS	3365	37	3367.4 ± .2
4	3443.5	13	PS	3442	11	3443.3 ± .2
5	5958.0	1.2	PS	5956	1.4	--
6	6809.4	61	PS	6807	62	6809.4 ± .4[e]

(a) Accuracy of energies is about 1 keV.

(b) Intensities of strong peaks accurate to about 10-20%.

(c) Compton suppression data.

(d) Pair spectrometer data.

(e) Obtained by summing two cascade γ rays.

The level scheme for Be^{10}, as proposed by Motz (M8), is shown in Fig. 49. The transition energies and intensities shown are from the present work. Note that each transition energy is equal to the corresponding γ-ray energy plus a small recoil energy correction. As will be explained in Section 5.7, this simple level diagram can be used to check the accuracy of the intensity values. The fraction of the total emitted γ-ray intensity that is observed, obtained as the ratio of the left hand side of Eq. (4-7) to the right hand side, is 0.98.

An average value for the binding energy of Be^{10} may be obtained from

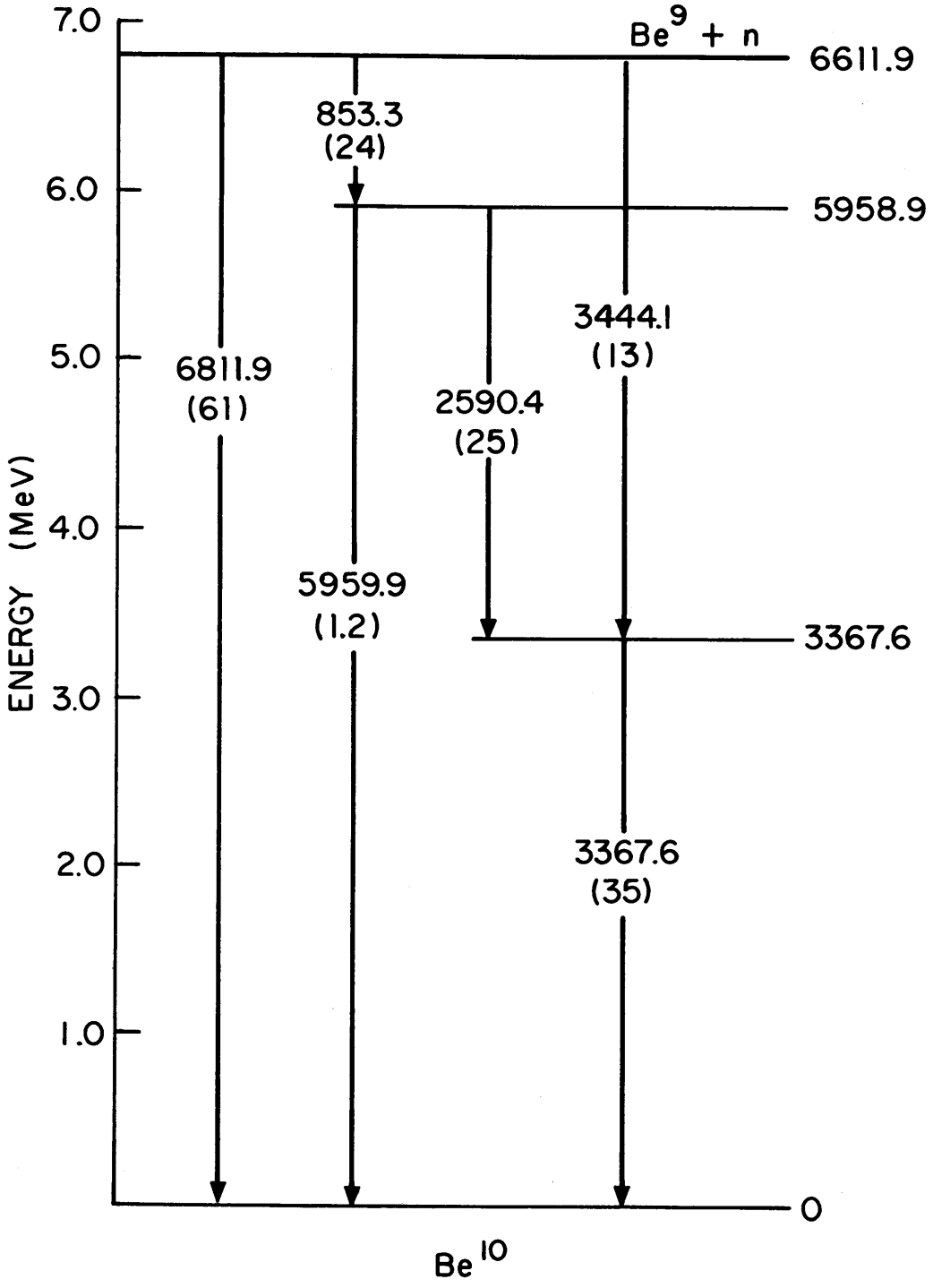

FIGURE 49 LEVEL DIAGRAM FOR Be^{10}

TABLE 9

Be^{10} CASCADE SUMS

Cascade	γ_1 (keV)	γ_2 (keV)	γ_3 (keV)	$\gamma_1+\gamma_2+\gamma_3$ (keV)
1	6811.9*	--	--	6811.9
2	5959.9	853.3	--	6813.2
3	3444.1	3367.6	--	6811.7
4	3367.6	2590.4	853.3	6811.3
			Mean =	6812.0
			Standard deviation of an individual cascade =	0.82 keV

*All energies corrected for recoil.

different cascade sums, as shown in Table 9. Using the 4 indicated cascades a binding energy of

$$6812.0 \pm 1.0 \text{ keV}$$

is obtained, which is in excellent agreement with Greenwood's value of 6811.9 $\pm$ 0.4 keV (G7).

5.2 Iron

A 28.35 gm iron metal source, 99.9% pure, was used to obtain the Compton suppression spectrum shown in Fig. 50. This metal source was used instead of a powdered source, which must be contained in a polyvial, in order to reduce the hydrogen capture gamma background. Figure 51 shows the pair spectrometer spectrum obtained using a 93.49 gm iron powdered source, 99.9% pure. The extra hydrogen capture background resulting from the use of a polyvial was quite reasonable in the pair spectrum

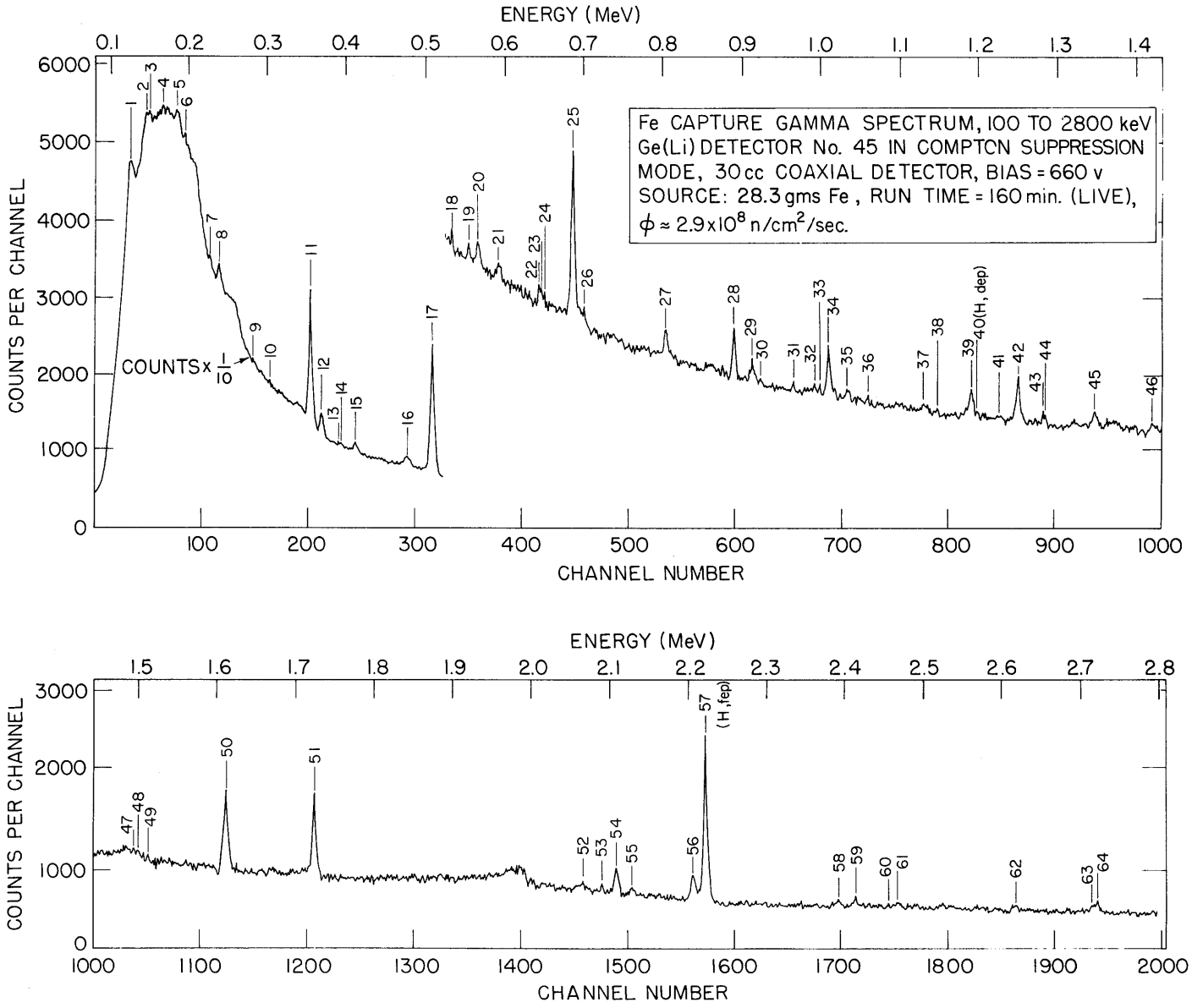

FIGURE 50 IRON COMPTON SUPPRESSION SPECTRUM

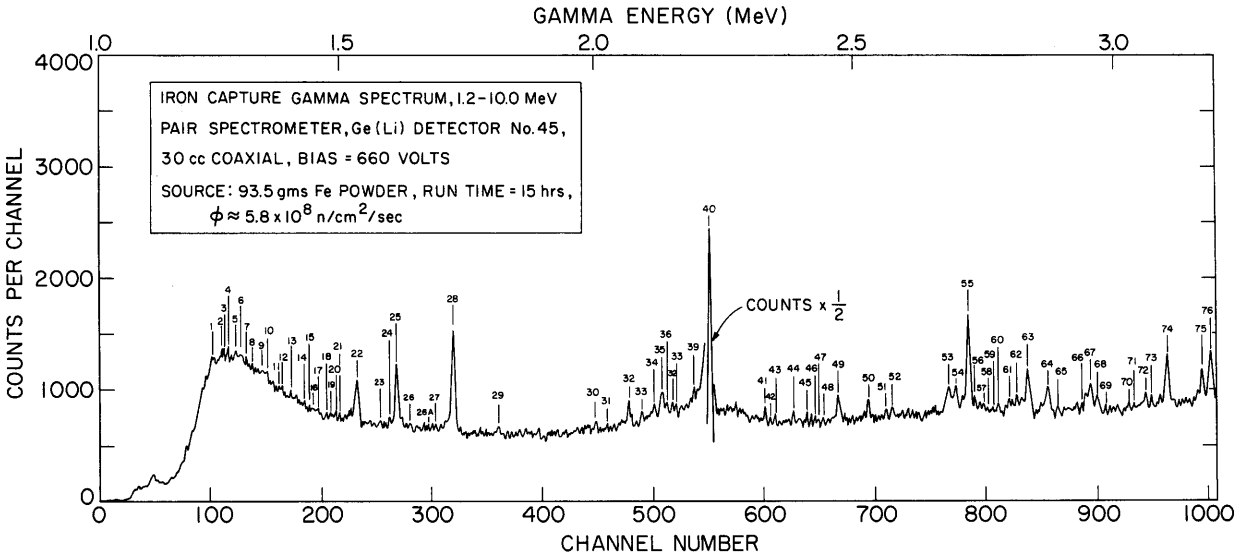
GAMMA ENERGY (MeV)
1.0
1.5
2.0
2.5
3.0
IRON CAPTURE GAMMA SPECTRUM, 1.2-10.0 MeV
PAIR SPECTROMETER, Ge(Li) DETECTOR No. 45,
30 cc COAXIAL, BIAS = 660 VOLTS
SOURCE: 93.5 gms Fe POWDER, RUN TIME = 15 hrs,
$\phi \approx 5.8 \times 10^8$ n/cm^2/sec
COUNTS x 1/2
COUNTS PER CHANNEL
CHANNEL NUMBER

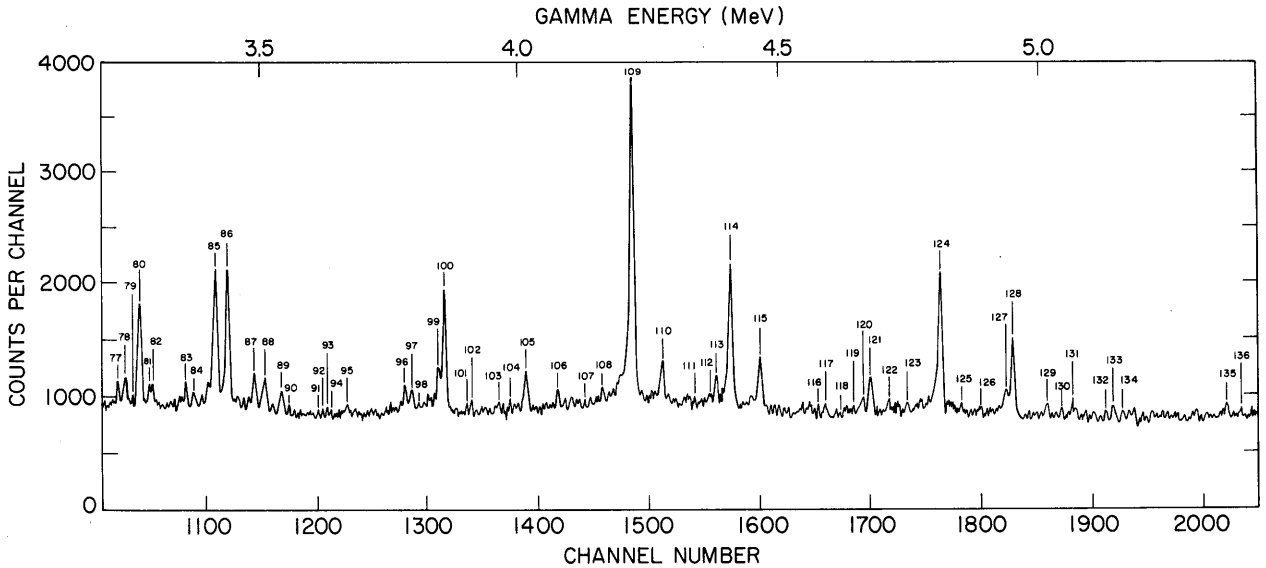
GAMMA ENERGY (MeV)
3.5
4.0
4.5
5.0
COUNTS PER CHANNEL
CHANNEL NUMBER

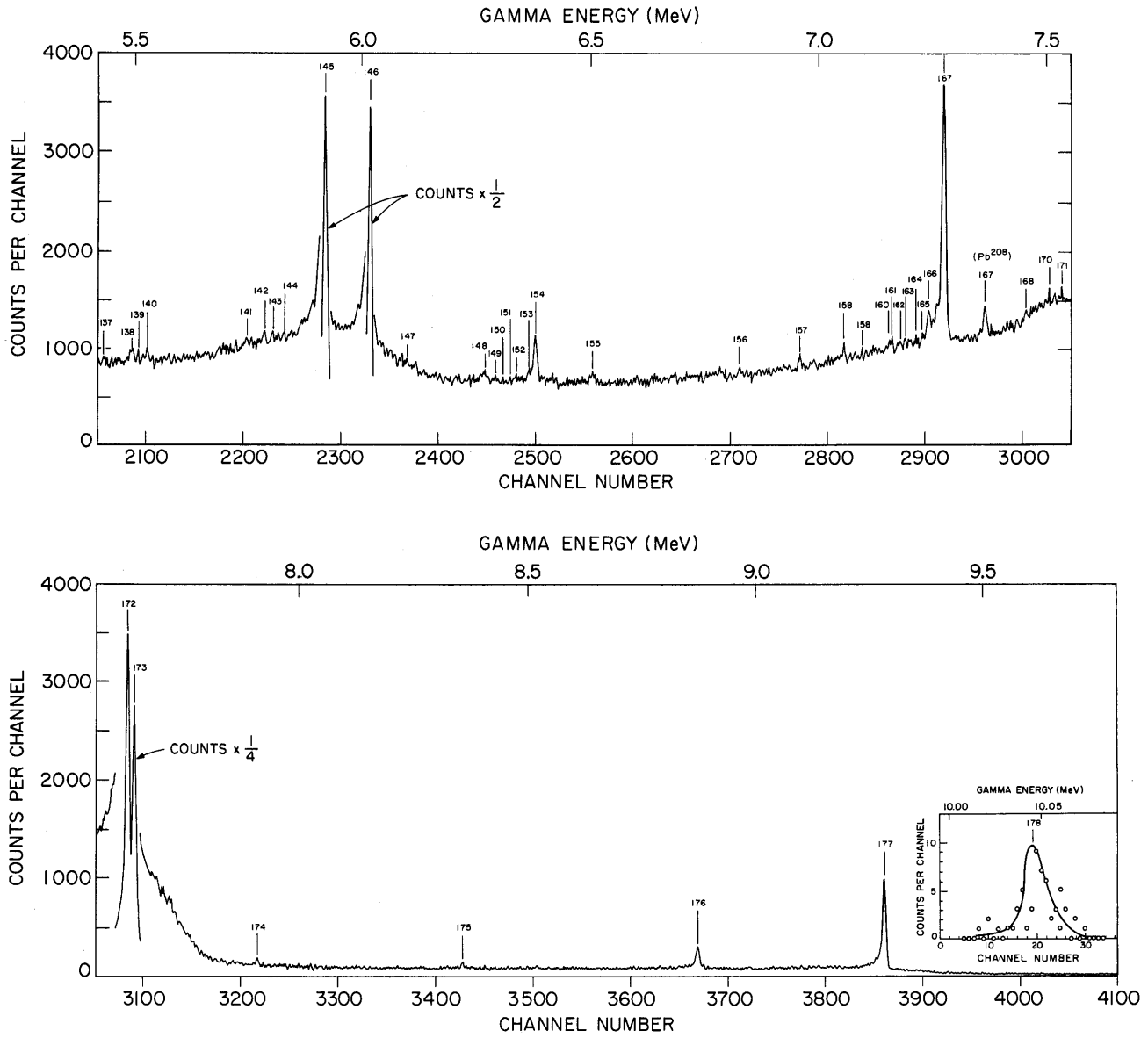

FIGURE 51 IRON PAIR SPECTROMETER SPECTRUM

and did not tend to obscure iron capture γ-ray peaks as in the Compton suppression spectrum.

The energies and intensities of the numbered peaks in Figs. 50 and 51 have been determined using the method described in Chapter 4. As noted there, the peak selection process is carried out with a rather arbitrary criterion, consequently, many marginal peaks have not been numbered. Table 10 gives the energies and intensities obtained from the Compton suppression spectrum. These results are compared with two sets of earlier energy values obtained using NaI (G1, F3). The improved resolution of the Ge(Li) spectrometer allows about 4 times as many peaks to be observed. The energies and intensities obtained from the pair spectrum are given in Table 11 and are compared with the values obtained by Groshev (G4) using a high resolution magnetic Compton spectrometer. Note that a small percentage of the numbered peaks in both spectra are background peaks -- these are so designated in Tables 10 and 11 with the letter "B". Some numbered peaks, which were judged to be marginal, have a "Q" designation in the remarks column of the tables. The agreement of the energies and intensities of this work with those of earlier work is seen to be quite good. Approximately 225 iron capture gammas have been identified in this work compared to 60 reported by Groshev (G4).

A proposed level diagram for Fe^{57}, containing some 90 observed capture γ-ray transitions, is given in Fig. 52. All energies shown have been corrected for recoil and are in keV. The intensity of each transition, in number of γ rays emitted per 100 captures in Fe^{57}, is shown in parentheses. To the right of the level diagram are listed 34 level energies determined from the (n,γ) data. The corresponding levels, obtained from (d,p) and (p,p') studies (S3) are listed to the right of the (n,γ) values. The

TABLE 10

ENERGIES AND INTENSITIES OF GAMMA RAYS IN IRON COMPTON SUPPRESSION SPECTRUM

	THIS WORK			GREENWOOD(G1)	FIEBIGER(F3)
LINE	E (KEV)	I (NO./100 CAPTS)	NOTES	E (KEV)	E (KEV)
1	121.2(X)	4.0302(Y)		122	118
2	135.8	.7559			
3	139.2	.2631	B		
4	154.7	.3465	B		
				169	
5	172.9	.8695	B		
6	184.2	.2437			
7	216.6	.2196			
8	228.5	1.3076		232	226
				286	
9	276.2	.1499	B		
10	311.1	.1129	Q		
11	352.1	11.9564		355	353
12	366.5	1.8074			
13	389.7	.3678			
14	392.5	.3700			
15	409.4	.8552		415	
16	478.3	1.3971			
17	511.0	17.7446	B	512	514
18	536.1	.1531			
19	558.3	.1787			
20	569.8	.3044			
21	597.1	.2981	B		
22	649.6	.2599			
23	652.3	.2152			
24	656.4	.2411			
25	691.7	4.8049		690	698
26	706.4	.1902			
27	809.9	.4324			812
28	898.0	1.3692		900	916
29	918.0	.4810	D		
30	932.2	.2192			
31	973.3	.2067			
32	1001.5	.2438			
33	1006.9	.0791	Q		
34	1019.1	1.8777		1025	1028
35	1042.4	.4280			
36	1068.3	.2840			
37	1139.1	.4315	D		
38	1157.5	.4065			
39	1201.9	1.2149	B		
40	1208.6	.1942	Q		
41	1237.1	.5555			
42	1261.3	2.2367		1265	1274
43	1293.5	.4066			

CONTINUATION OF TABLE 10

LINE	THIS WORK E (KEV)	THIS WORK I (NO./100 CAPTS)	NOTES	GREENWOOD(G1) E (KEV)	FIEBIGER(F3) E (KEV)
44	1295.3	.6273			
45	1357.9	1.0541			
46	1431.4	.3606			
47	1495.4	.2736			
48	1500.9	.2499			
49	1514.0	.3138			
50	1613.0	6.0845			1628
51	1724.9	6.3083			1722
52	2066.8	.3616			
53	2090.9	.3399			
54	2109.0	1.7611			
55	2122.3	.2752	Q		
56	2206.7	2.7086			
57	2223.3	17.3773	B		
58	2392.3	.4464			
59	2414.8	.2216	Q		
60	2457.7	.2989	Q		
61	2467.4	1.0905			
62	2614.2	1.2170			
63	2715.2	.6191			
64	2722.5	1.0201			

(X) ACCURACY OF ENERGIES IS ABOUT 1 KEV
(Y) ONLY TWO SIGNIFICANT FIGURES, INTENSITIES OF STRONG PEAKS ACCURATE TO ABOUT 20 PERCENT

NOTES
B --- BACKGROUND GAMMA RAY
D --- PARTIALLY RESOLVED DOUBLET PEAK
Q --- MARGINAL PEAK

TABLE 11

ENERGIES AND INTENSITIES FOR GAMMA RAYS IN IRON PAIR SPECTROMETER SPECTRUM

	THIS WORK			GROSHEV (G4)	
LINE	E (KEV)	I (NO./100 CAPTS.)	NOTES	E (KEV)	I (NO./100 CAPTS)
1	1244.1(X)	2.7958(Y)			
2	1261.8	1.0045			
3	1266.1	1.0401		1264(5)(Z)	4.0
4	1272.5	2.7824			
5	1287.1	.2747			
6	1295.9	4.0528			
7	1309.1	.7700			
8	1319.3	1.2352			
9	1340.3	.8124			
10	1351.5	2.8046			
11	1380.7	.2873			
12	1385.1	.2845			
13	1398.8	.5787			
14	1426.0	.3230	Q		
15	1434.9	.3376	Q		
16	1440.3	.8191			
17	1451.5	.4743			
18	1471.2	.5740			
19	1478.0	.2738	Q		
20	1493.6	.7024			
21	1498.2	.4544			
22	1532.3	3.9160			
23	1579.2	.6604			
24	1600.9	.5730			
25	1612.7	6.7063		1613(4)	10.0
26	1637.7	.3596			
27	1690.2	.3811			
28	1724.9	5.9328		1727(4)	11.0
29	1811.6	.2797			
30	2001.9	.5040			
31	2024.7	.1517	Q		
32	2060.3	.6239		2070(6)	0.7
33	2091.4	.3556			
34	2115.1	.4113			
35	2132.2	.7382		2138(5)	0.8
36	2140.8	.3681			
37	2151.5	.3673			
38	2157.2	.3689			
39	2192.4	.1950			
40	2223.3	13.4464	B,H-2		
41	2328.9	.2768			
42	2339.2	.1287			
43	2349.6	.1701			
44	2384.7	.2476			
45	2410.3	.2186			
46	2419.1	.1290			
47	2425.5	.1084			
48	2441.9	.0962			

CONTINUATION OF TABLE 11

LINE	THIS WORK E (KEV)	THIS WORK I (NO./100 CAPTS.)	NOTES	GROSHEV (G4) E (KEV)	GROSHEV (G4) I (NO./100 CAPTS)
49	2470.0	.4492		2476(6)	0.5
50	2527.6	.3330		2535(6)	0.6
51	2560.4	.1849			
52	2574.1	.2489			
53	2683.1	.3278		2683(6)	0.5
54	2696.9	.3752		2698(6)	0.5
55	2721.6	1.1221		2720(6)	2.1
56	2733.5	.1160			
57	2750.2	.0597	Q		
58	2756.6	.0416	Q		
59	2769.3	.0557	Q		
60	2777.9	.1663			
61	2799.4	.1349	Q		
62	2814.2	.0988			
63	2834.2	.5762		2836(5)	0.8
64	2873.8	.3470		2880(6)	0.5
65	2893.2	.1391			
66	2939.1	.0582	Q		
67	2955.7	.4460		2955	0.7GR
68	2968.6	.1735			
69	2985.1	.0926	Q		
70	3029.5	.1070			
71	3036.6	.0680	Q		
72	3061.1	.0756			
73	3071.9	.0298		3068(6)	0.5
74	3103.6	.6125		3109(6)	0.7
75	3168.0	.3262		3172(6)	0.6
76	3186.3	.5240		3192(5)	1.0
77	3226.2	.1737		3228(6)	0.5
78	3240.2	.1855		3242(6)	0.4
79	3256.4	.0686			
80	3267.5	1.0673		3272(5)	1.7
81	3288.2	.2951			
82	3294.7	.1200		3296(6)	0.5
				3325(6)	0.1
83	3356.5	.1746		3360	0.5GR
84	3371.6	.1706			
85	3413.9	1.6106		3416(6)	2.5
86	3437.2	1.4631		3440(5)	2.2
87	3486.1	.2525		3489(7)	0.6
88	3508.5	.2779		3504(7)	0.3
89	3540.3	.2007			
90	3553.6	.0473			
91	3610.1	.0500			
92	3619.1	.0415			
93	3627.6	.0430			
94	3636.1	.0542			
95	3665.9	.0606		3665(6)	0.2
96	3777.9	.2418		3778(6)	0.3

CONTINUATION OF TABLE 11

LINE	THIS WORK E (KEV)	THIS WORK I (NO./100 CAPTS.)	NOTES	GROSHEV (G4) E (KEV)	GROSHEV (G4) I (NO./100 CAPTS)
97	3792.8	.1827		3792(6)	0.3
98	3806.9	.0255	Q		
99	3843.5	.3782			
100	3854.9	1.1395		3855	1.2GR
101	3898.4	.0503			
102	3905.3	.0906			
103	3960.0	.0571			
104	3981.5	.0631			
105	4012.1	.3349		4014(6)	0.4
106	4073.1	.1394			
107	4129.7	.0601	Q		
108	4159.3	.1189			
109	4218.3	3.2445		4217(6)	3.3
110	4274.7	.3608		4274(6)	0.4
111	4337.3	.0560	Q		
112	4371.0	.0780	Q		
113	4379.4	.1557			
114	4406.2	1.2325		4405(6)	1.4
115	4462.1	.4257		4462(6)	0.5
116	4575.3	.0750			
117	4588.1	.0354			
118	4609.9	.0406	Q		
119	4630.2	.0841			
120	4661.6	.1040		4662(7)	0.1
121	4675.4	.2770		4680(7)	0.3
122	4709.7	.0489			
123	4762.8	.0403			
124	4809.8	1.4370		4810(5)	1.9
125	4850.1	.0491			
126	4888.2	.0832		4885(7)	0.1
127	4934.7	.2555			
128	4949.0	.7284		4950(5)	0.8
129	5015.2	.1125		5013(8)	0.2
130	5043.2	.0858		5046(8)	0.2
131	5064.1	.0639			
132	5127.2	.0760			
133	5140.6	.0968			
134	5177.9	.1188			
135	5358.0	.1152			
136	5388.0	.0873			
137	5431.9	.0926			
138	5495.1	.1842		5499(6)	0.2
139	5515.4	.1064			
140	5527.3	.0869			
141	5746.0	.1371		5750(6)	0.2
142	5786.6	.1027		5787(6)	0.2
143	5799.2	.0657			
144	5845.2	.0660			

CONTINUATION OF TABLE 11

LINE	THIS WORK E (KEV)	THIS WORK I (NO./100 CAPTS.)	NOTES	GROSHEV (G4) E (KEV)	GROSHEV (G4) I (NO./100 CAPTS)
145	5920.0	6.7986		5920(5)	8.3
146	6018.2	8.1489		6018(5)	8.5
147	6097.3	.0538	Q		
148	6269.3	.0491		6269(8)	0.1
149	6292.5	.0850		6295(8)	0.1
150	6307.8	.0297			
151	6324.4	.0438			
152	6342.3	.0367			
153	6365.8	.1127			
154	6380.2	.5817		6379(7)	0.6
155	6504.7	.1879		6504(8)	0.1
156	6826.2	.1111		6831(8)	0.07
157	6961.6	.1602			
158	7058.3	.2528			
159	7096.0	.0199	Q		
160	7159.4	.1048			
161	7163.6	.1367			
162	7182.5	.1705			
163	7193.0	.1024	Q		
164	7219.1	.1519			
165	7231.2	.1478	Q		
166	7244.8	.4536			
167	7278.3	4.7956		7277(6)	5.3
168	7367.7	.3571	B,PB-208		
169	7458.8	.1287			
170	7507.9	.0873			
171	7537.7	.0440			
172	7630.8	26.6221		7629(4)	21.5
173	7645.1	21.1157		7643(4)	21.5
174	7914.7	.0939	B,CU-64		
175	8366.9	.0877		8368(6)	0.3
176	8884.9	.4799		8882(6)	0.5
177	9297.6	3.2943		9298(5)	3.3
178	10046.0	.1100	*	10038(8)	0.03

(X) ACCURACY OF ENERGIES IS ABOUT 1 KEV, UNLESS NOTED OTHERWISE
(Y) ONLY TWO SIGNIFICANT FIGURES, INTENSITIES OF STRONG PEAKS ACCURATE TO ABOUT 20 PERCENT
(Z) NUMBERS IN PARENTHESES INDICATE ERROR IN LAST DIGIT

NOTES
B --- BACKGROUND GAMMA RAY
Q --- MARGINAL PEAK
* --- OBSERVED IN A SEPARATE, LOWER GAIN RUN --ENERGY ACCURATE TO ABOUT 3 KEV

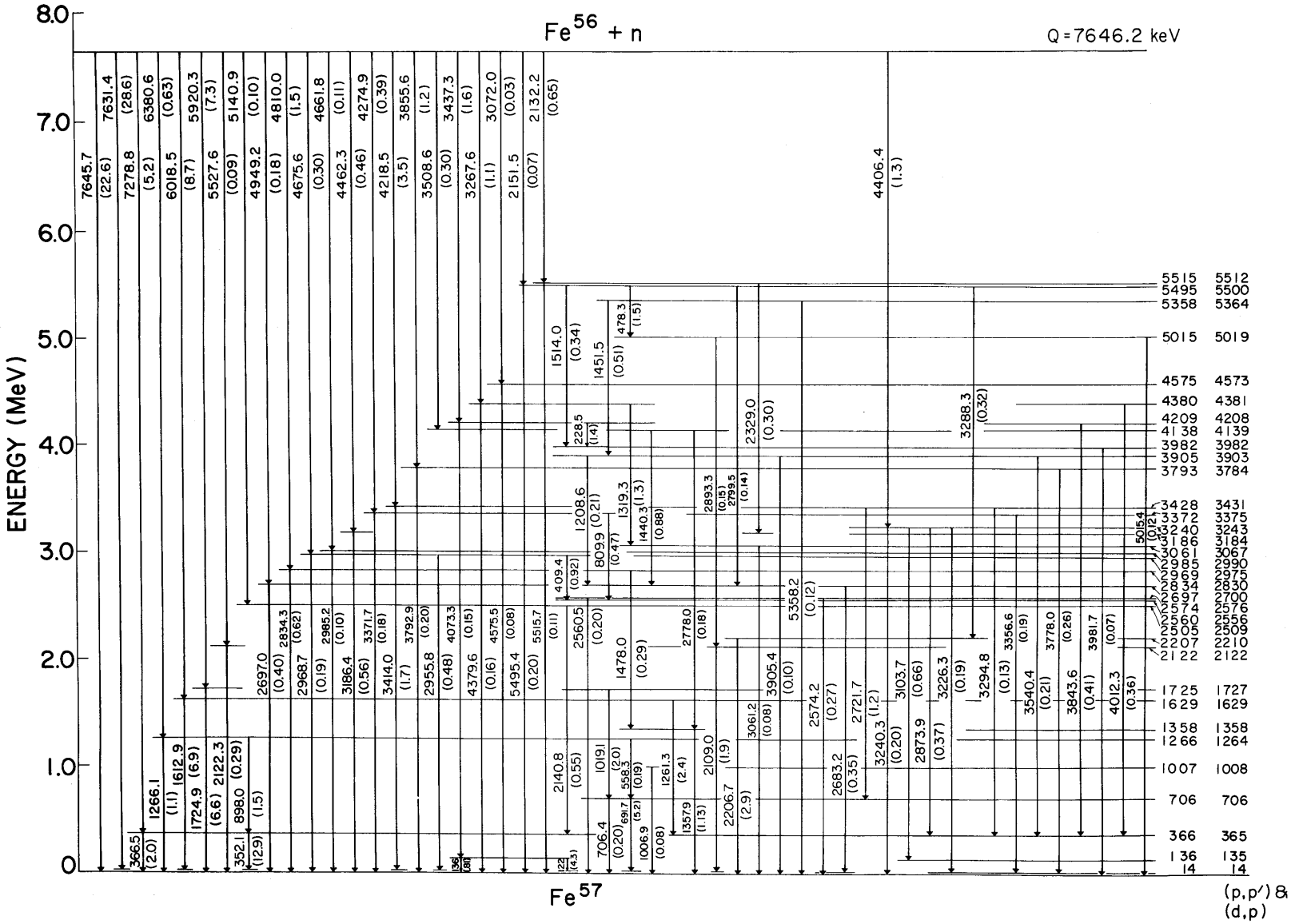

FIGURE 52 PROPOSED LEVEL DIAGRAM FOR Fe^{57}

agreement between these two sets of level energies is quite good -- considering the uncertainity of the (d,p) and (p,p') data, 5 to 10 keV. This level diagram is in good agreement with one proposed by Groshev (G4), in which some 42 capture γ-ray transitions were included.

The level diagram was constructed by applying the Ritz combination principle to the Fe capture γ-ray energies. In order to establish a level, only those energy combinations $a + b = c + d$ were kept for which $/a + b - c - d/$ was smaller than the combined estimated error of the transitions. A computer program, CASFND, described in Appendix D, was written to scan the energies and pick out all one-and two-step transitions within a pre-set tolerance between any two specified levels. Generally, the tolerance was set at $\pm$ 1.5 keV. Only those levels in agreement with (d,p) and (p,p') results were included in Fig. 52. If additional levels were assumed, many more of the capture γ rays could be included in the level scheme. The completeness of the level diagram was checked by determining the number of γ quanta passing through several different horizontal sections of the diagram. For sections at 1, 3, 5 and 7 MeV, this number was found to be 93, 87, 88 and 87, respectively per 100 neutron captures in Fe^{57}. This means that most of the γ-ray intensity of Fe^{57} transitions (about 90%) has been included in the level scheme.

A proposed level scheme for Fe^{55} is shown in Fig. 53. Since Fe^{54} contributes only 5% to the capture cross section of natural iron, only the strongest transitions in Fe^{55} are visible in the capture spectra. Following the same procedure as for Fe^{57}, 18 γ rays were fitted into the level scheme of Fe^{55}. The intensities are in number of γ rays per 100 captures in Fe^{55}. The 11 energy levels show good agreement with those obtained from (d,p) studies (S3). Furthermore, the level scheme is in fairly good agreement with one proposed by Groshev (G4), which included 6 transitions. The

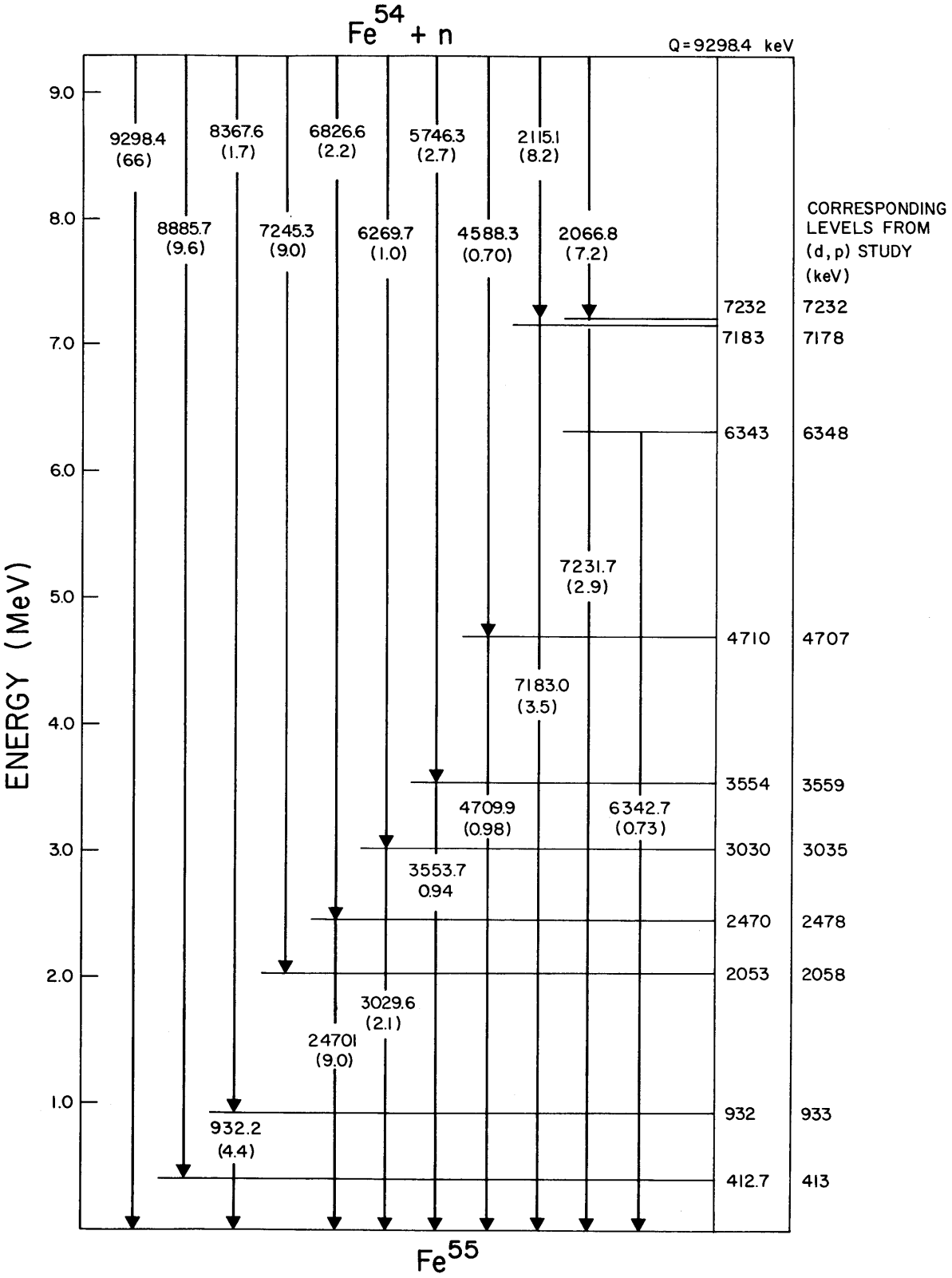

FIGURE 53 PROPOSED LEVEL DIAGRAM FOR Fe^{55}

TABLE 12

SOME CASCADES FROM THE CAPTURING STATE TO THE GROUND STATE OF Fe^{57}

Cascade	γ_1(keV)	γ_2(keV)	$\gamma_1 + \gamma_2$ (keV)
1	7645.7	--	7645.7
2	7278.8	366.5	7645.3
3	5920.3	1724.9	7645.3
4	6380.6	1266.1	7646.7
5	4949.2	2697.0	7646.2
6	4406.4	3240.3	7646.7
7	4379.6	3267.6	7647.2
8	4274.9	3371.7	7646.6
		Mean =	7646.21 keV

Standard deviation of an individual cascade sum = 0.83 keV

transition to the 932 keV level in Fe^{55}, which must be an M2 transition, has a low probability according to the Weisskopf estimate (E2). However, because of the excellent agreement of the energies, transitions to and from the 932 keV level were included in the level scheme.

The binding energy of Fe^{55} and Fe^{57} may be obtained as the average of the sums of cascades from the capturing state to the ground state. Table 12 lists 8 cascades used to obtain an average value for the binding energy of Fe^{57} of

$$7646.2 \pm 1.0 \text{ keV}$$

which is in good agreement with a recent determination (J1) of 7646.5 ± 1.0 keV. Note that the standard deviation of an individual cascade sum is

0.83 keV. Seven cascades, listed in Table 13, gave a binding energy of

$$9298.4 \pm 1.0 \text{ keV}$$

for Fe^{55}, which agrees quite well with the value of 9298 $\pm$ 5 keV obtained by Groshev (G4). In this case the standard deviation of an individual cascade was 0.96 keV.

The fraction of the capture γ-ray intensity observed was found to be 0.98. A computer program, CHKBE, described in Appendix D, was written to perform this calculation.

TABLE 13

SOME CASCADES FROM THE CAPTURING STATE TO THE GROUND STATE OF Fe^{55}

Cascade	γ_1 (keV)	γ_2 (keV)	$\gamma_1 + \gamma_2$ (keV)
1	9298.4	--	9298.4
2	8367.6	932.2	9299.8
3	7231.7	2066.8	9298.5
4	7183.0	2115.1	9298.1
5	6826.6	2470.1	9296.7
6	6269.7	3029.6	9299.3
7	4709.9	4588.3	9298.2

Mean = 9298.43 keV

Standard deviation of an individual cascade sum = 0.96 keV

5.3 Scandium

A 1.517 gm sample of Sc_2O_3 powder (99.9% pure) was used to obtain both the Compton suppression spectrum given in Fig. 54 and the Pair spectrometer spectrum given in Fig. 55. The capture γ-ray source was

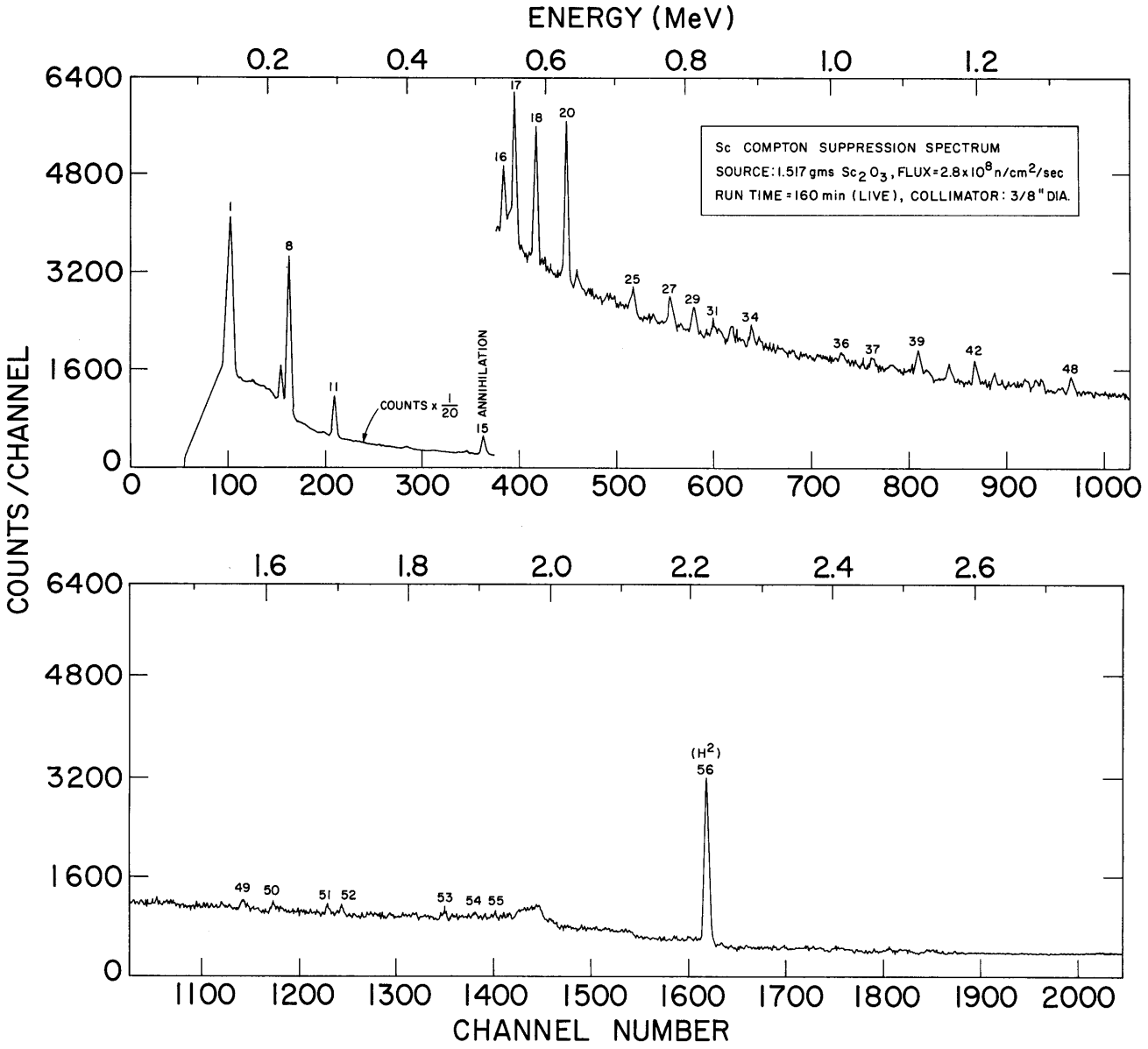

FIGURE 54 SCANDIUM COMPTON SUPPRESSION SPECTRUM

contained in a 1.8 cm^3 polyvial. Scandium, even though of low Z and monoisotopic, has quite a complex capture γ-ray spectrum. It is interesting to note the appearance of a slight hump in the scandium pair spectrometer spectrum in the region between about 3 and 6 MeV. This hump results from many closely spaced γ rays which are only partially resolved. The fact that this hump has almost been eliminated in this spectrum is an indication that a large percentage of the capture γ-ray intensity emitted has been resolved. The fraction of the capture γ-ray intensity observed was found to be 0.76.

The energies and intensities of the γ-rays observed in the Compton suppression spectrum are listed in Table 14. Line numbers in the table correspond to a numbering of peaks in Fig. 54. However, note that only the numbers of the more prominent peaks have been included in Fig. 54. For comparison, the scandium low energy capture γ ray data obtained using a bent crystal spectrometer is also listed in Table 14. The superior resolution and sensitivity of the bent crystal spectrometer below about 1 MeV allows the separation of several closely spaced doublets and a greater number of weak intensity lines to be observed. The lower limit on the intensity of an observable line using the Ge(Li) spectrometer is seen to be about 0.4 γ rays per 100 captures. The agreement between energies and intensities for the stronger lines observed by both instruments is within the limits of error of the two determinations.

Table 15 lists the scandium high energy capture γ-ray energies and intensities obtained from the pair spectrometer spectrum shown in Fig. 55. Previous high energy capture γ-ray data obtained by Groshev, using a magnetic Compton spectrometer, and by Bartholomew, using a magnetic pair spectrometer, are also listed. The higher resolution of the Ge(Li) pair spectrometer allows over 200 high energy capture γ rays to be

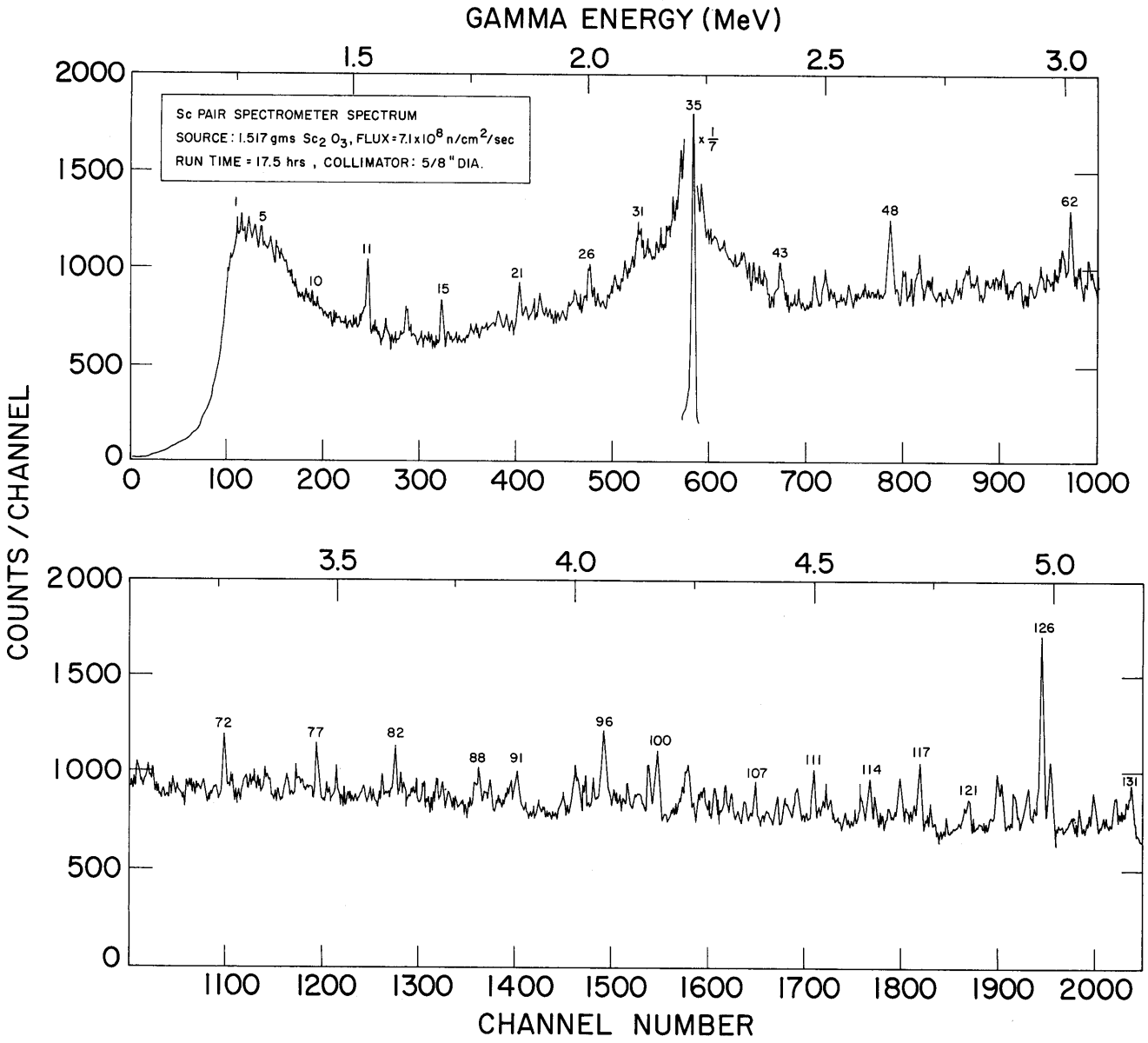
GAMMA ENERGY (MeV)
1.5
2.0
2.5
3.0
Sc PAIR SPECTROMETER SPECTRUM
SOURCE : 1.517 gms Sc2 O3, FLUX = 7.1 x 10^8 n/cm^2/sec
RUN TIME = 17.5 hrs , COLLIMATOR: 5/8" DIA.
x 1/7
1
5
10
11
15
21
26
31
35
43
48
62
2000
1500
1000
500
0
0
100
200
300
400
500
600
700
800
900
1000
3.5
4.0
4.5
5.0
72
77
82
88
91
96
100
107
111
114
117
121
126
131
1100
1200
1300
1400
1500
1600
1700
1800
1900
2000
COUNTS / CHANNEL
CHANNEL NUMBER

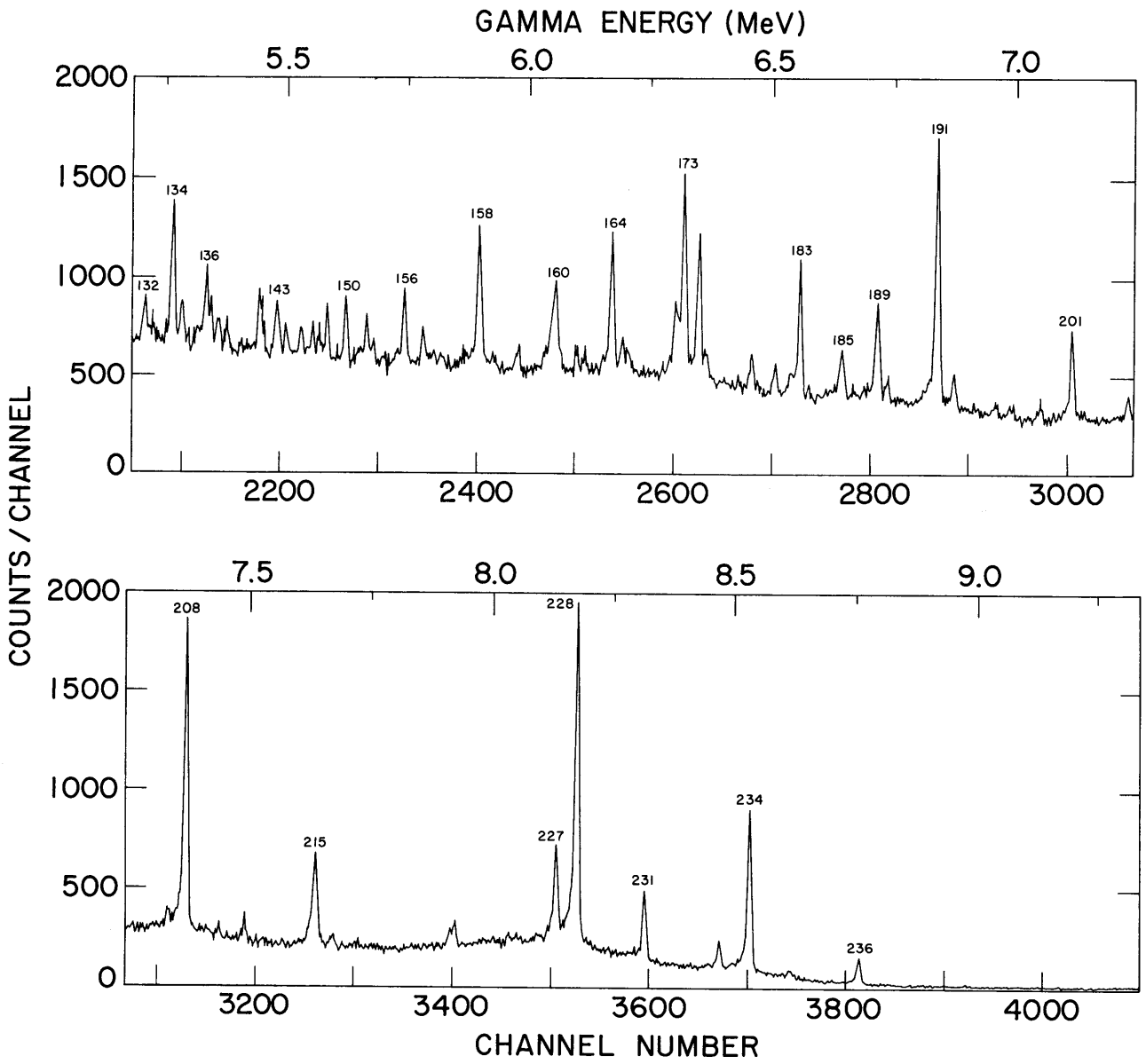

FIGURE 55 SCANDIUM PAIR SPECTROMETER SPECTRUM

TABLE 14

ENERGIES AND INTENSITIES OF GAMMA RAYS IN SCANDIUM COMPTON SUPPRESSION SPECTRUM

	THIS WORK			VAN ASSCHE (V1)	
LINE	E (KEV)	I (NO./100 CAPTS)	NOTES	E (KEV)	I (NO./100 CAPTS)
				52.011	2.4
				61.771	0.10
				89.140	0.006
				142.528	11.4
1	145.2(X)	28.1990(Y)	D	147.010	13.7
2	157.9	.1818	B	157.349	0.03
				159.295	0.07
				185.930	0.01
				202.930	0.05
3	174.6	.3285	B		
4	180.1	.0559	B		
5	191.3	.3142	B		
6	197.2	.3858	B		
7	215.9	8.6100		216.368	8.3
8	227.7	45.1088	D	227.769	22.3
				228.710	10.7
9	243.0	.1242	B		
				278.280	0.04
				279.946	0.05
10	279.4	.7727		280.725	0.70
11	295.2	17.1266		295.243	13.7
				301.750	0.01
				314.624	0.20
				350.545	0.06
				357.003	0.13
12	359.9	.2891	B		
				372.120	0.03
				377.200	0.06
				392.290	0.05
13	400.0	1.0876	D	399.745	0.77
				402.710	0.39
				421.650	0.02
				437.480	0.09
				442.410	0.33
				477.530	0.05
14	485.4	1.2962		485.999	2.3
				492.180	0.07
				496.780	0.22
				507.214	0.33
15	511.0	14.8976	B		
				518.180	0.12
				527.130	0.09
				533.620	0.07
16	539.2	1.9312		539.400	2.8
				547.110	1.2
17	554.6	4.8005		554.530	6.6
18	585.1	5.6916		584.800	7.0
19	601.9	.2489		600.180	0.12
20	627.5	6.9360		627.500	8.4
21	643.6	.7590		643.120	0.84
-	686.9	.4958		685.660	0.56
23	689.7	.5472	B		

CONTINUATION OF TABLE 14

LINE	THIS WORK E (KEV)	THIS WORK I (NO./100 CAPTS)	NOTES	VAN ASSCHE (V1) E (KEV)	VAN ASSCHE (V1) I (NO./100 CAPTS)
24	696.7	.5537	B		
				711.020	0.49
25	722.2	1.6630		721.890	1.6
26	750.4	.4113	B		
27	773.6	2.3322		773.970	1.6
28	789.1	.1835	B		
29	807.6	2.1493		807.690	1.6
30	825.6	.2135	B		
31	835.3	.7712		835.110	0.5
32	842.3	.3169		843.750	0.5
33	860.5	1.2716		860.810	1.5
34	888.6	1.6234	C		
35	899.3	.8327		898.780	4.3
36	1014.2	.9898			
37	1057.0	1.8015		1058.040	0.4
38	1085.6	1.7751			
39	1121.9	2.8172	C		
40	1134.2	.5058	Q		
41	1165.1	1.5145			
42	1200.9	2.6418			
43	1225.9	1.5545			
44	1270.5	1.1445			
45	1285.7	1.4083			
46	1293.8	1.5185			
47	1322.5	1.1755			
48	1334.5	1.5671			
49	1604.8	1.3442			
50	1617.8	1.6948			
51	1693.3	1.2993			
52	1712.3	1.1854	B		
53	1858.5	2.0402			
54	1898.8	.4973	Q		
55	1927.6	.7900	Q		
56	2223.3	38.4402	B		

(X) ACCURACY OF ENERGIES IS ABOUT 1 KEV
(Y) ONLY TWO SIGNIFICANT FIGURES, INTENSITIES OF STRONG PEAKS ACCURATE TO ABOUT 20 PERCENT

NOTES
B --- BACKGROUND GAMMA RAY
C --- RADIOACTIVE DECAY GAMMA RAY
D --- DOUBLET PEAK
Q --- MARGINAL PEAK

TABLE 15

ENERGIES AND INTENSITIES FOR GAMMA RAYS IN SCANDIUM PAIR SPECTROMETER SPECTRUM

	THIS WORK			GROSHEV (G2)		BARTHOLOMEW (B4)	
LINE	E (KEV)	I (NO./100 CAPTS.)	NOTES	E (MEV)	I (NO./100 C) (Z)	E (MEV)	I (NO./100 C)
1	1249.4(X)	3.8859(Y)		1.24(2)	1.0		
2	1259.1	3.3029					
3	1273.1	6.5948					
4	1285.8	6.8545					
5	1298.9	5.7474					
6	1318.9	4.9810					
7	1332.0	3.9043		1.33(2)	2.0		
8	1342.9	1.5750					
9	1398.0	.9959					
10	1413.2	1.3589					
11	1533.2	5.2944	B				
12	1573.9	3.6604					
13	1618.3	1.9355	B				
14	1650.0	1.1373					
15	1692.5	3.1921					
16	1707.3	.7103					
17	1755.4	.7197					
18	1811.1	1.1832	D	1.79(2)	1.0		
19	1836.6	.3090					
20	1841.9	.5496					
21	1857.9	1.5979		1.86(2)	1.2		
22	1871.6	.5695					
23	1890.1	.8028					
24	1900.6	1.1265					
25	1976.4	.6167					
26	2006.7	1.2157					
27	2024.3	.3351					
28	2060.9	.6428					
29	2080.8	.4630					
30	2096.5	.3327					
31	2109.5	2.0611	GR	2.12(3)	1.5		
32	2154.2	.2981					
33	2181.1	.1042					
34	2198.6	.2375					
35	2223.3	68.2603	B,H-2				
36	2241.7	.6182					
37	2270.3	.4226					
38	2330.7	.7035					
39	2341.6	.1981					
40	2351.0	.3563					
41	2365.2	.2436					
42	2373.6	.1466					
43	2406.4	.9516					
44	2445.5	.2584					
45	2477.7	.7294					
46	2501.5	.2541					
47	2551.1	.4192					

CONTINUATION OF TABLE 15

LINE	THIS WORK E (KEV)	THIS WORK I (NO./100 CAPTS.)	NOTES	GROSHEV (G2) E (MEV)	GROSHEV (G2) I (NO./100 C)	BARTHOLOMEW (B4) E (MEV)	BARTHOLOMEW (B4) I (NO./100 C)
48	2636.1	2.0353					
49	2665.6	.7033					
50	2680.2	.1386					
51	2696.6	1.1789					
52	2717.1	.6093					
53	2774.6	.1357					
54	2795.5	.6556					
55	2817.4	.1436					
56	2869.5	.2573					
57	2905.9	.7511		2.90(2)	1.2		
58	2927.0	.3246					
59	2950.9	.4921					
60	2963.4	.1850					
61	2995.0	.5920					
62	3011.6	.9054					
63	3029.1	.2150					
64	3033.2	.2324					
65	3051.1	.2305					
66	3082.0	.1746					
67	3106.8	.3485					
68	3117.3	.3417					
69	3159.4	.1359					
70	3222.5	.2000					
71	3247.6	.2134					
72	3266.3	.6801					
73	3310.2	.2981					
74	3351.8	.4873					
75	3397.2	.2818					
76	3416.0	.3473					
77	3458.7	.5661					
78	3477.5	.2045					
79	3500.0	.4015					
80	3556.1	.1344					
81	3597.6	.1815					
82	3622.9	.5070		3.60(3)	1.0		
83	3635.9	.1425					
84	3684.7	.2276					
85	3709.3	.1725					
86	3722.7	.1914					
87	3735.4	.2056					
88	3799.5	.4056	D				
89	3812.6	.0862					
90	3822.3	.2211					
91	3879.2	.4595					
92	3975.2	.3190					
93	4001.2	.7635		4.00(3)	1.0		
94	4023.6	.3100					
95	4039.6	.1380					
96	4062.1	1.1273					

CONTINUATION OF TABLE 15

LINE	THIS WORK E (KEV)	THIS WORK I (NO./100 CAPTS.)	NOTES	GROSHEV (G2) E (MEV)	GROSHEV (G2) I (NO./100 C)	BARTHOLOMEW (B4) E (MEV)	BARTHOLOMEW (B4) I (NO./100 C)
97	4111.1	.1748					
98	4134.2	.3250	GR				
99	4153.9	.3977					
100	4172.5	.8618					
101	4236.3	.4560	GR				
102	4264.2	.4817	GR				
103	4294.4	.2761					
104	4311.6	.2184					
105	4326.8	.1823					
106	4357.0	.2025					
107	4377.9	.3325					
108	4425.6	.2363					
109	4439.9	.3822					
110	4466.0	.2062					
111	4500.3	.4702					
112	4526.4	.5200	GR				
113	4598.0	.3132					
114	4617.1	.3941					
115	4627.8	.1989					
116	4680.2	.4332					
117	4721.3	.5663					
118	4744.9	.1138					
119	4777.2	.0909					
120	4815.8	.2265					
121	4823.6	.2961					
122	4882.5	.4062					
123	4892.6	.3531					
124	4916.9	.2592		4.90(3)	1.0		
125	4949.1	.4987					
126	4975.1	1.8057					
127	4993.6	.5958					
128	5056.2	.1801					
129	5084.7	.3237					
130	5130.8	.2701		5.13(3)	0.5		
131	5163.1	.6079					
132	5211.8	.1217					
133	5225.7	.1368					
134	5267.3	.9917		5.25(3)	0.7		
135	5285.7	.4107					
136	5335.8	.6048					
137	5345.9	.2933					
138	5359.6	.2890					
139	5378.3	.3824					
140	5408.0	.1008					
141	5446.3	.4497					
142	5452.2	.3676					
143	5482.1	.7058					
144	5498.1	.2348					

CONTINUATION OF TABLE 15

LINE	THIS WORK E (KEV)	THIS WORK I (NO./100 CAPTS.)	NOTES	GROSHEV (G2) E (MEV)	GROSHEV (G2) I (NO./100 C)	BARTHOLOMEW (B4) E (MEV)	BARTHOLOMEW (B4) I (NO./100 C)
145	5531.3	.2735					
146	5555.6	.2091					
147	5569.3	.2097					
148	5584.4	.3983					
149	5606.1	.0421					
150	5623.0	.7330					
151	5638.2	.0909					
152	5648.7	.1570					
153	5654.8	.1801					
154	5666.7	.4950					
155	5681.0	.2470					
156	5743.6	.7309					
157	5780.8	.2585					
158	5897.3	1.5825		5.85(2)	0.6		
159	5980.6	.2804		5.95(3)	0.6		
160	6055.1	1.8476	D	6.00(3)	0.6		
161	6096.1	.1509					
162	6100.2	.1400					
163	6115.1	.2211					
164	6170.3	1.5633					
165	6193.1	.2638					
166	6201.5	.1754					
167	6235.9	.0566					
168	6246.2	.0621					
169	6258.3	.0464					
170	6276.7	.0948					
171	6290.7	.0707					
172	6299.6	.7413					
173	6318.1	2.1544		6.33(2)	3.0	6.35(1)	2.3
174	6350.2	1.4813					
175	6361.6	.1213					
176	6367.7	.1108					
177	6418.4	.0431					
178	6430.2	.1409					
179	6456.2	.4442					
180	6468.8	.0716					
181	6506.4	.3468					
182	6536.8	.2967					
183	6556.5	1.7457					
184	6576.2	.1053					
185	6644.4	.7063					
186	6667.5	.0401					
187	6691.5	.1208					
188	6697.7	.0496					
189	6716.5	1.2965		6.71(3)	1.5		
190	6738.7	.3164					
191	6839.6	3.8758		6.83(2)	3.5	6.84(2)	2.3
192	6874.0	.4334					
193	6916.4	.0638					
194	6924.8	.0494					

CONTINUATION OF TABLE 15

LINE	THIS WORK E (KEV)	THIS WORK I (NO./100 CAPTS.)	NOTES	GROSHEV (G2) E (MEV)	GROSHEV (G2) I (NO./100 C)	BARTHOLOMEW (B4) E (MEV)	BARTHOLOMEW (B4) I (NO./100 C)
195	6961.3	.0810					
196	6965.7	.0919					
197	6988.3	.0819					
198	6997.4	.0771					
199	7052.2	.1795					
200	7081.2	.0802					
201	7117.1	1.1763		7.12(4)	0.8	7.15(4)	0.6
202	7232.6	.3225					
203	7261.6	.0678					
204	7271.6	.0418					
205	7279.6	.0443					
206	7321.0	.0614					
207	7331.1	.2303					
208	7367.7	4.8673	B,PB-208				
209	7437.7	.1030					
210	7482.6	.0492					
211	7490.3	.3114					
212	7514.8	.1010					
213	7527.8	.1421					
214	7568.2	.0997					
215	7635.8	1.5659		7.63(3)	1.2	7.65(3)	0.9
216	7672.6	.3581					
217	7691.5	.0908					
218	7717.4	.0700					
219	7725.4	.0541	B				
220	7914.7	.2608	B				
221	7924.5	.3811					
222	8019.0	.0712					
223	8023.5	.0702					
224	8034.2	.1856					
225	8052.8	.0980					
226	8092.4	.0498					
227	8132.3	1.5368					
228	8174.7	6.0538		8.18(2)	8.0	8.175(11)	3.7
229	8242.1	.1335					
230	8294.5	.0604					
231	8315.2	1.4046		8.30(3)	1.3	8.31(2)	0.8
232	8411.2	.0533					
233	8470.0	.5262					
234	8531.5	3.0721		8.54(2)	3.7	8.539(10)	1.9
235	8613.1	.2208					
236	8759.5	.5431		8.82(5)	0.7	8.85(8)	0.3

(X) ACCURACY OF ENERGIES IS ABOUT 1 KEV
(Y) ONLY TWO SIGNIFICANT FIGURES, INTENSITIES OF STRONG LINES ACCURATE TO ABOUT 20 PERCENT
(Z) NUMBERS IN PARENTHESES INDICATE ERROR IN LAST DIGIT

NOTES
B --- BACKGROUND GAMMA RAY
D --- PARTIALLY RESOLVED DOUBLET
GR --- GROUP OF SEVERAL PEAKS

identified compared to 24 reported by Groshev (G2). In most cases, the energies of the present work agree with those of the previous works within their error limits. However, the energy of the capturing state to ground state γ ray , 8.760 MeV, is somewhat lower than the previous values, 8.82 $\pm$ .05 MeV (G2), 8.85 $\pm$ .08 MeV (B7). Nevertheless, as is seen in Table 16, this value leads to a binding energy for Sc^{46} of 8760.5 $\pm$ 1.0 keV which is in excellent agreement with two values of the binding energy determined from (d,p) studies, 8759 $\pm$ 8 keV (M9) and 8766 $\pm$ 8 (R1).

No attempt was made to construct a complete level scheme for Sc^{46}. Instead, various well known low energy levels (less than about 1 MeV) determined by (d,p) studies (R2) and (n,γ) studies (V1) were calculated from the scandium high energy data. Since these levels have been determined to an accuracy of better than 0.1 keV from low energy bent-crystal data, the agreement of level values obtained using the high energy data serves as a good check on the accuracy of this data. Figure 56 shows the levels obtained by subtracting various high energy γ-ray transitions from the binding energy of Sc^{46} (taken equal to the γ-ray transition energy from the capturing state to the ground state). In the two-step transition to the 142.5 keV level, the order of the cascade has not been determined -- the largest γ ray is assumed to cascade first in Fig. 56. The agreement between the levels obtained in this work and those from the bent-crystal study is excellent. The mean difference of the levels compared is 0.4 keV.

This partial level scheme is in good agreement with one proposed by Neill (N3) with the following differences: (1) no 7.99-MeV γ-ray transition to the 775-keV level was observed in this work, (2) new single-step transitions were observed to the 1124-keV and 1270-keV levels, and (3) a new double-step transition to the 143-keV level was found (in agreement with the level scheme of Groshev (G2)).

TABLE 16

SOME TWO-STEP CASCADES IN Sc^{46} FROM THE CAPTURING STATE TO THE GROUND STATE

Cascade Number	γ_1(keV)	γ_2(keV)	$\gamma_1 \gamma_2$(keV)
1	8760.4	--	8760.4
2	8532.4	227.7*	8760.1
3	8175.5	585.1	8760.6
4	8133.1	627.5	8760.6
5	7925.2	835.3	8760.6
6	7673.3	1085.6	8758.9
7	7491.0	1270.5	8761.5
8	7438.4	1322.5	8760.9
9	7052.8	1707.3	8760.1
10	6917.0	1841.9	8758.9
11	6698.2	2061.0	8759.2
12	6430.7	2330.8	8761.5
13	6418.9	2341.7	8760.6
14	6258.8	2501.6	8760.3
15	5408.3	3351.9	8760.3
16	5163.4	3597.8	8761.2
17	4721.6	4039.8	8761.4
18	4466.2	4294.6	8760.9
		Mean =	8760.45 keV
		Standard deviation of individual cascade sum =	0.79 keV

*Ground state transitions which agree with Sc^{46} levels determined by (d,p) studies (R2), within the experimental error of these levels, $\pm$ 10 keV.

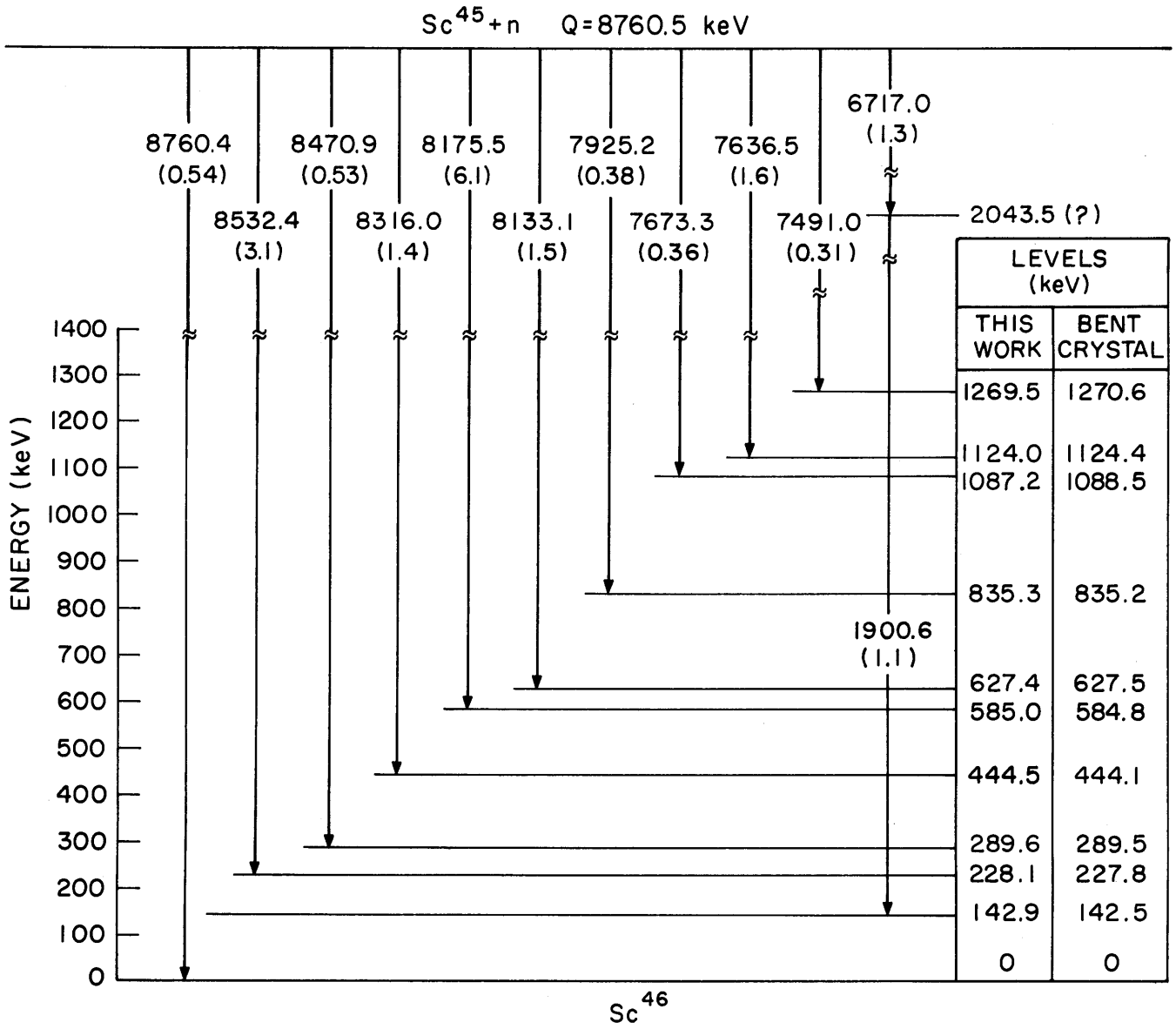

FIGURE 56 PARTIAL Sc^{46} LEVEL DIAGRAM

Table 16, in addition to giving a mean value for the binding energy of Sc^{46}, gives values for several Sc^{46} high energy levels, accurate to about 1 keV. Ground state transitions which agree with levels from (d,p) work (R2), are underlined in Table 16. Seven levels, not shown in Fig. 56, are present in this table. The standard deviation of an individual cascade is 0.79 keV for the 18 cascades listed.

5.4 Germanium

An 8.015 gm germanium crystal (about 1.5 mm thick) was used to obtain the Compton suppression spectrum shown in Fig. 57. The use of this thin source minimized the error in the low energy γ-ray intensities caused by neglecting source self-absorption. A 44.76 gm germanium crystal was used as the source to obtain the pair spectrometer spectrum shown in Fig. 58. Both germanium sources were $\geq$ 99.99% pure. Germanium has 4 stable isotopes, which contribute significantly to its thermal neutron capture cross section. Consequently, it is not surprising that the thermal neutron capture spectrum of natural germanium is quite complex. Note the appearance in the pair spectrum of a hump similar to the one present in the scandium spectrum.

The energies and intensities calculated from the spectrum of Fig. 57 are listed in Table 17. Also listed are the energies of germanium capture γ rays measured with NaI and reported by Greenwood (G8). The agreement between energy values is within the error of the NaI data. Note that some 47 germanium capture γ rays have been identified in the low energy region compared to 13 observed with NaI.

Table 18 lists the high energy data for thermal capture in natural germanium obtained from the pair spectrum of Fig. 58. Nearly 190 peaks have been identified in the capture spectrum of germanium in the energy

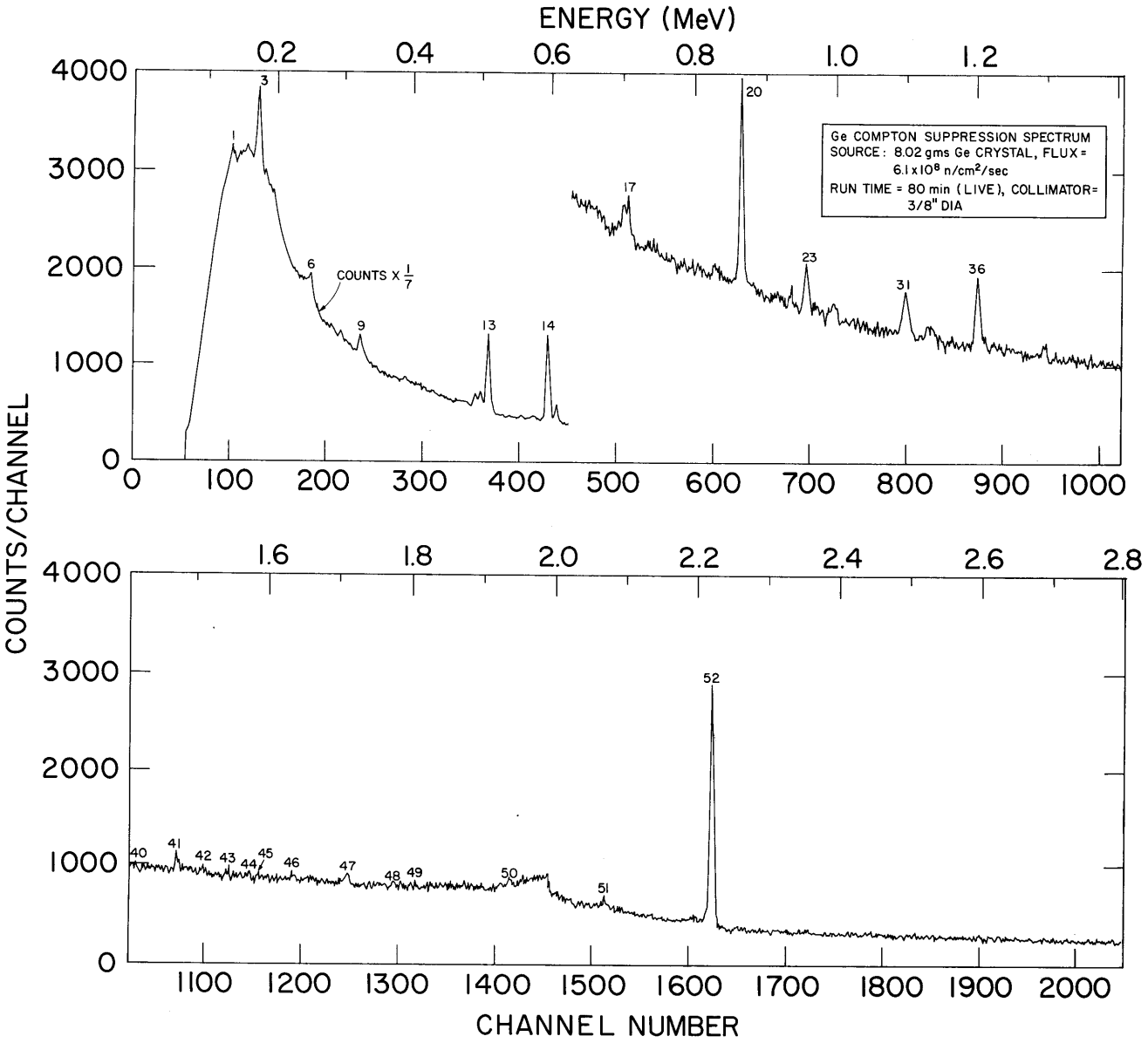

FIGURE 57 GERMANIUM COMPTON SUPPRESSION SPECTRUM

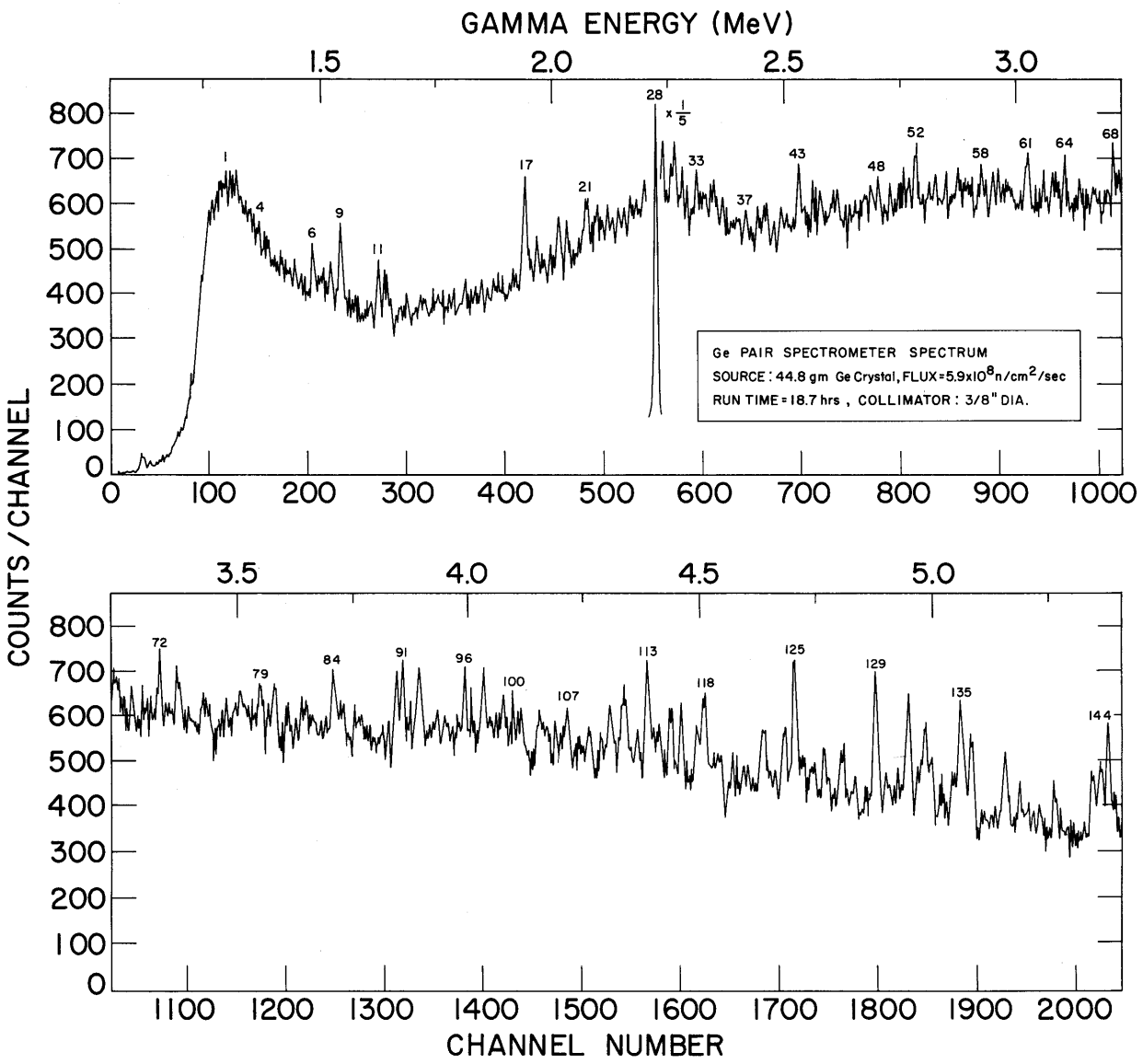
GAMMA ENERGY (MeV)
1.5
2.0
2.5
3.0
3.5
4.0
4.5
5.0
COUNTS / CHANNEL
CHANNEL NUMBER
Ge PAIR SPECTROMETER SPECTRUM
SOURCE : 44.8 gm Ge Crystal, FLUX = 5.9x10^8 n/cm^2/sec
RUN TIME = 18.7 hrs , COLLIMATOR : 3/8" DIA.
x 1/5

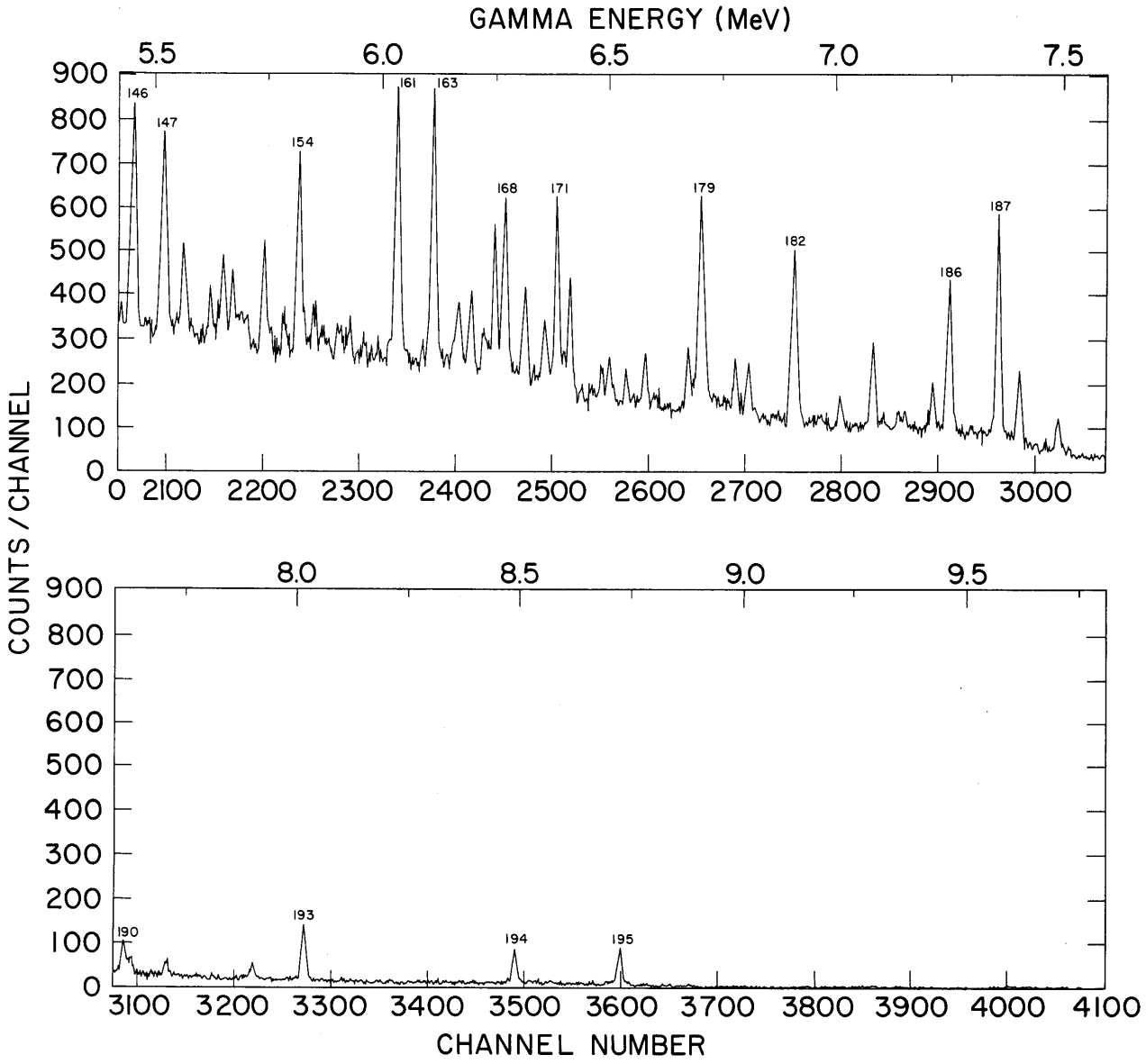

FIGURE 58 GERMANIUM PAIR SPECTROMETER SPECTRUM

TABLE 17

ENERGIES AND INTENSITIES FOR GAMMA RAYS
IN GERMANIUM COMPTON SUPPRESSION SPECTRUM

	THIS WORK			GREENWOOD (G8)	
LINE	E (KEV)	I (NO./100 CAPTS.)	NOTES	E (KEV)	NOTES
1	138.3(X)	1.1730(Y)		139	Q
2	160.5	.5389	B		
3	174.7	8.4878		176	
4	185.4	.5233			
5	196.7	.7066	B		
6	252.8	5.3285		252	
7	283.4	1.4400			
8	297.4	1.9449			
9	326.2	4.8574		322	
10	391.3	1.2513		388	Q
11	492.7	3.5792			
12	500.4	4.9689		507	Q
13	511.0	32.3566	B		
14	595.9	44.1631		599	
15	608.1	9.3319			
16	703.2	5.4438		705	
17	708.7	5.4822			
18	806.7	1.4594			
19	831.8	2.4349			
20	868.2	20.2520		867	
21	897.3	.7936			
22	940.3	1.8375			
23	961.0	7.3753		962	
24	984.3	2.0487			
25	999.0	5.9243	GR		
26	1027.4	1.0261			
27	1033.6	.9646			
28	1041.8	.9013			
29	1045.9	.5916			
30	1061.1	.8713			
31	1100.7	10.9929		1105	
32	1132.2	2.8003			
33	1137.6	2.9885			
34	1149.5	1.9869			

CONTINUATION OF TABLE 17

LINE	THIS WORK E (KEV)	THIS WORK I (NO./100 CAPTS.)	THIS WORK NOTES	GREENWOOD (G8) E (KEV)	GREENWOOD (G8) NOTES
35	1167.3	1.0585			
36	1202.6	10.5900	A	1200	
37	1299.0	3.0029	D	1275	
38	1313.8	1.2221			
39	1360.8	1.2224			
40	1413.6	1.0001			
41	1471.1	3.5367			
42	1508.7	1.5410			
43	1545.4	2.6733	D		
44	1573.9	1.9223	D		
45	1587.9	1.3456			
46	1633.9	2.0115			
47	1714.0	2.7725	B		
48	1776.5	2.9374			
49	1806.8	1.4905			
50	1940.4	2.5789			
51	2072.3	3.2985			
52	2223.3	78.5840	B,H-2		

(X) ACCURACY OF ENERGIES IS ABOUT 1 KEV
(Y) ONLY TWO SIGNIFICANT FIGURES, INTENSITIES OF STRONG PEAKS ACCURATE TO ABOUT 20 PERCENT

NOTES
A --- CONTRIBUTION OF DOUBLE ESCAPE PEAK OF HYDROGEN GAMMA HAS BEEN SUBTRACTED FROM THE INTENSITY
B --- BACKGROUND GAMMA RAY
D --- PARTIALLY RESOLVED DOUBLET
GR --- GROUP OF SEVERAL PEAKS
Q --- QUESTIONABLE LINE

TABLE 18

ENERGIES AND INTENSITIES OF GAMMA RAYS IN GERMANIUM PAIR SPECTROMETER SPECTRUM

LINE	E (KEV)	I (NO./100 CAPTS)	NOTES	LINE	E (KEV)	I (NO./100 CAPTS)	NOTES
1	1274.9(X)	6.5242(Y)	QI	55	2853.0	.2857	
2	1283.6	2.9395		56	2878.1	.3392	
3	1298.6	3.2991		57	2900.4	.7329	GR
4	1347.7	5.0389	QI	58	2928.6	.9051	GR
5	1429.0	1.6712		59	2953.7	.3720	
6	1469.5	4.8661		60	2964.5	.2798	
7	1494.4	3.4201		61	3028.2	.7621	
8	1510.5	3.6142		62	3061.9	.2873	
9	1532.6	7.4079	B	63	3081.1	.2934	GR
10	1602.2	1.3180		64	3109.6	.5004	D
11	1619.3	3.2315	B	65	3139.6	.1857	
12	1634.5	1.1087		66	3169.4	.3149	
13	1638.6	1.0580		67	3200.3	.3676	
14	1682.4	1.0193		68	3211.9	.3159	
15	1815.3	1.2873		69	3237.8	.5210	
16	1845.4	.8631		70	3276.9	.4003	
17	1940.6	4.3105		71	3299.6	.4660	GR
18	1965.3	.9817		72	3334.9	.6160	
19	2013.9	2.0594		73	3374.9	.7293	
20	2031.8	1.5396		74	3432.0	.4569	GR
21	2073.4	1.6668		75	3469.8	.1539	
22	2101.8	.9972		76	3479.0	.3168	
23	2120.7	.4691		77	3503.6	.0677	
24	2144.2	.5655		78	3509.2	.1427	
25	2154.5	.3898		79	3552.7	.7672	
26	2169.2	.3324		80	3583.0	.4231	
27	2198.9	.5634		81	3613.0	.6006	D
28	2223.3	32.0651	B	82	3628.0	.1645	
29	2238.3	.3444		83	3642.9	.5496	
30	2263.7	1.3132	D	84	3710.0	.6030	
31	2282.7	.5673		85	3725.0	.2588	
32	2292.5	.4544		86	3731.9	.3307	
33	2311.7	.6023		87	3766.8	.5718	
34	2344.0	.3871		88	3817.3	.3154	
35	2351.1	.5988		89	3830.8	.3129	
36	2370.4	.5931		90	3849.2	.6389	
37	2420.0	.6810		91	3862.7	.8012	
38	2460.0	.3490		92	3879.5	.1196	
39	2465.3	.5261		93	3896.0	.9766	
40	2480.5	.4029		94	3934.7	.0922	
41	2496.9	.5614		95	3952.4	.2897	
42	2509.7	.5013		96	3996.4	.2775	
43	2531.5	1.1463	D	97	4010.1	.2600	
44	2564.4	.3833		98	4036.7	.4493	
45	2580.0	.7524		99	4078.3	.2069	
46	2616.5	.4417	D	100	4099.5	.1485	
47	2689.4	.5369		101	4110.2	.1813	
48	2705.0	.3334		102	4117.0	.2011	
49	2730.1	.3090		103	4157.5	.3914	
50	2760.1	.3520		104	4165.2	.3227	
51	2772.2	.2841		105	4172.9	.2930	
52	2782.6	.7501		106	4190.3	.5134	
53	2814.4	.3891		107	4217.4	.6518	
54	2828.7	.5399		108	4265.9	.4127	

CONTINUATION OF TABLE 18

LINE	E (KEV)	I (NO./100 CAPTS)	NOTES
109	4289.7	.3834	
110	4308.6	.6985	
111	4337.6	1.1069	
112	4366.5	.2896	
113	4390.3	1.2596	
114	4415.7	.5999	
115	4442.2	.5407	
116	4464.3	.4604	
117	4496.9	.4383	
118	4513.7	.6059	
119	4574.2	.3993	
120	4583.7	.0651	
121	4597.8	.1671	
122	4607.5	.1085	
123	4645.7	.7563	
124	4687.3	.4670	
125	4708.4	1.0382	
126	4771.2	.2700	
127	4812.8	.5567	
128	4838.7	.3297	
129	4882.1	1.2677	
130	4906.2	.3696	
131	4930.2	.1490	
132	4952.5	.9489	
133	4989.0	1.7819	GR
134	5026.5	.2265	
135	5064.5	.9611	
136	5089.1	.6662	
137	5161.9	.7463	
138	5191.8	.2708	
139	5222.8	.1116	
140	5237.4	.1869	
141	5267.4	.4010	
142	5349.6	.5595	
143	5368.5	.6429	
144	5383.8	1.1017	
145	5422.8	.0656	
146	5450.0	1.9430	
147	5518.4	2.2322	
148	5560.9	.8983	
149	5620.5	.4468	
150	5650.0	.7445	
151	5669.7	.2879	
152	5740.2	1.1664	
153	5785.3	.4668	
154	5816.9	1.7671	
155	5850.5	.3998	
156	5873.6	.1776	
157	5900.8	.3962	
158	5931.0	.3491	
159	5960.7	.2613	
160	5993.6	.0961	
161	6036.3	3.1308	
162	6093.0	.1748	
163	6115.4	2.8994	
164	6171.9	.9150	
165	6199.9	.7204	
166	6228.2	.3813	
167	6251.2	1.4500	
168	6273.8	1.7259	
169	6319.3	.9105	
170	6360.0	.4605	
171	6389.3	1.4912	
172	6418.1	.7085	
173	6445.8	.2700	
174	6489.3	.2206	
175	6505.6	.3060	
176	6543.1	.2024	
177	6585.1	.5457	
178	6680.8	.7861	
179	6707.7	2.8907	
180	6785.6	.4897	
181	6814.0	.4767	
182	6915.2	2.2877	
183	7018.5	.3062	
184	7090.3	.9279	
185	7223.8	.4476	
186	7259.5	1.7383	
187	7367.7	2.9846	B
188	7415.2	.8962	
189	7499.9	.4915	
190	7628.3	.6172	
191	7727.5	.1923	B
192	7916.3	.1999	B
193	8030.0	.7978	
194	8498.0	.5481	
195	8732.2	.6840	
196	9602.0	.1700	*
197	10202.0	.0900	*

(X) ACCURACY OF ENERGIES IS ABOUT 1 KEV, UNLESS NOTED OTHERWISE
(Y) ONLY TWO SIGNIFICANT FIGURES, INTENSITIES OF STRONG PEAKS ACCURATE TO ABOUT 20 PERCENT

NOTES
B --- BACKGROUND GAMMA RAY
D --- PARTIALLY RESOLVED DOUBLET PEAK
GR --- GROUP OF SEVERAL PEAKS
QI --- QUESTIONABLE INTENSITY VALUE DUE TO POOR STATISTICS
* --- OBSERVED IN A SEPARATE, LOWER GAIN RUN --ENERGY ACCURATE TO ABOUT 3 KEV

TABLE 19

SOME POSSIBLE 2-STEP CASCADES IN Ge^{71}

Cascade	γ_1 (keV)	γ_2 (keV)	$\gamma_1 + \gamma_2$ (keV)
1	7259.9	--	7259.9
2	6200.2	1061.1	7261.3
3	6093.3	1167.3	7260.6
4	5961.0	1299.0	7260.0
5	5620.7	1638.6	7259.4
6	4838.9	2420.0	7258.9
			Mean = 7260.2

Standard deviation of individual cascade = 1.04 keV

TABLE 20

SOME POSSIBLE 2-STEP CASCADES IN Ge^{74}

Cascade	γ_1 (keV)	γ_2 (keV)	$\gamma_1 + \gamma_2$ (keV)
1	8732.8	1469.5	10202.3
2	8030.5	2169.2	10199.7
3	7090.7	3109.7	10200.3
4	6489.6	3710.1	10199.7
5	6036.6	4165.3	10201.9
6	5785.5	4415.8	10201.4
			Mean = 10,200.9

Standard deviation of individual cascade = 1.09 keV

range 1.2 to 10.2 MeV. The fraction of germanium γ-ray intensity observed is about .86.

The binding energies of several germanium isotopes may be obtained by summing two-step cascades from the capturing state to the ground state of each of these nuclides. As shown in Table 19, the binding energy of Ge^{71} is

$$7260.2 \pm 2.0 \text{ keV}.$$

This is in agreement with a previously measured value of $7.30 \pm .08$ MeV (N4). The binding energy of Ge^{74}, computed in Table 20 from 6 cascade sums, is

$$10{,}200.9 \pm 2.0 \text{ keV},$$

which agrees with the earlier value of $10.16 \pm .11$ MeV (N4). Note that the standard deviation of an individual cascade in these two tables is about 1 keV. The 6489.6-keV γ ray is close to the binding energy of Ge^{73}, $6.46 \pm .08$ MeV (N4), while the 6446.1-keV γ ray agrees with the binding energy of Ge^{74}, $6.43 \pm .03$ MeV (N4).

5.5 Zirconium

A 189.2 gm sample of zirconium metal (99.9% purity) was used to obtain the Compton suppression spectrum and the pair spectrometer spectrum, shown in Figs. 59 and 60, respectively. Since zirconium has a small capture cross section ($\sigma \approx .18$ b), particular care must be taken to insure that impurities, with high cross sections, do not contaminate the capture spectrum. A check of a list of impurities supplied with the zirconium sample revealed that cadmium (with a listed impurity of $< .3$ ppm), because of its high cross section, could introduce contamination. Indeed, the energies of about 7 lines in the zirconium Compton suppression spectrum agreed with the energies of the stronger low energy Cd capture γ rays within their ex-

perimental error (from 2 to 5 keV) (M10). A rough calculation using the intensity values of Motz (M10) indicates that the cadmium impurity level is perhaps 10 times as great as the listed value.

Table 21 lists the energies and intensities for the γ rays shown in Fig. 59. The capture γ-ray spectrum of cadmium was obtained to facilitate selection of its contamination lines in the zirconium spectrum. The lines thought to originate from capture in cadmium are so indicated in Table 21. Note that over 60 zirconium low energy capture γ rays have been identified.

The energies and intensities of the γ rays in the zirconium pair spectrometer spectrum are listed in Table 22. Contamination of this spectrum by cadmium lines is not as great as for the low energy spectrum since the intensity of cadmium high energy γ rays is lower. Over 100 zirconium high energy capture γ rays have been identified compared to 4 previously reported γ rays (K5). These 4 lines are also listed in Table 22. The energies and intensities agree quite well within the experimental errors.

A proposed level scheme for Zr^{92}, which contributes 60% of the capture cross section, is given in Fig. 61. It should be noted that this level scheme, containing 37 γ-ray transitions, is only a partial one. A more extensive analysis of the data would probably result in many more of the observed capture γ rays being fitted into the level scheme of Zr^{92}. Zr^{90}, Zr^{92}, and Zr^{94}, which contribute 18%, 15%, and 6% to the cross section, respectively, probably account for many of the capture γ rays. The fraction of the total γ-ray intensity observed is about 0.90.

The binding energy of Zr^{92}, obtained from cascade sums, as shown in Table 23, is

$$8635.5 \pm 1.0 \text{ keV}.$$

This value is in good agreement with the value of $8.65 \pm .05$ MeV, obtained by Kinsey (K5). The standard deviation of an individual cascade is 0.67 keV.

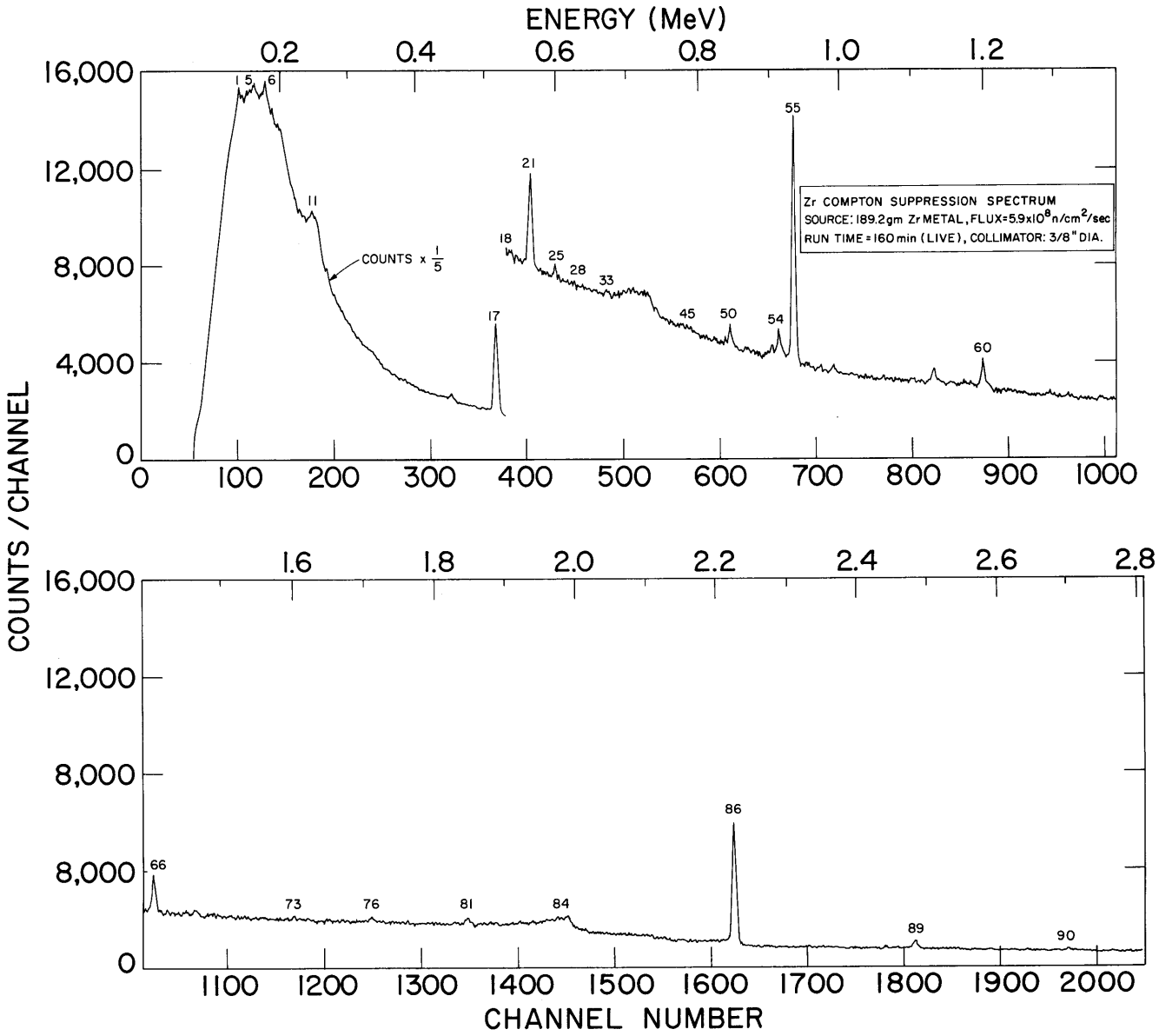

FIGURE 59 ZIRCONIUM COMPTON SUPPRESSION SPECTRUM

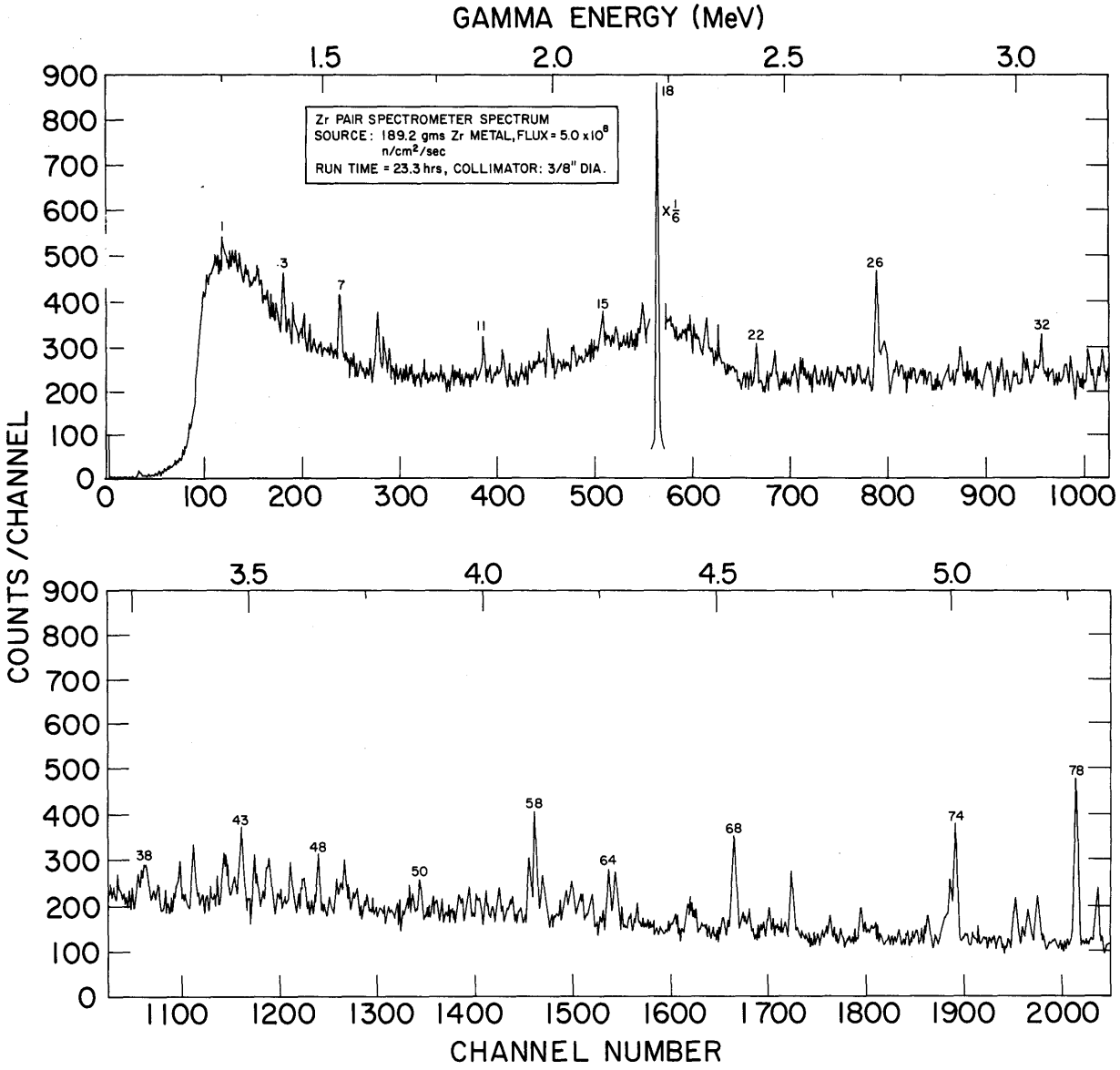
GAMMA ENERGY (MeV)
1.5
2.0
2.5
3.0
Zr PAIR SPECTROMETER SPECTRUM
SOURCE: 189.2 gms Zr METAL, FLUX = 5.0 x 10^8 n/cm²/sec
RUN TIME = 23.3 hrs, COLLIMATOR: 3/8" DIA.
X 1/6
COUNTS / CHANNEL
CHANNEL NUMBER
3.5
4.0
4.5
5.0

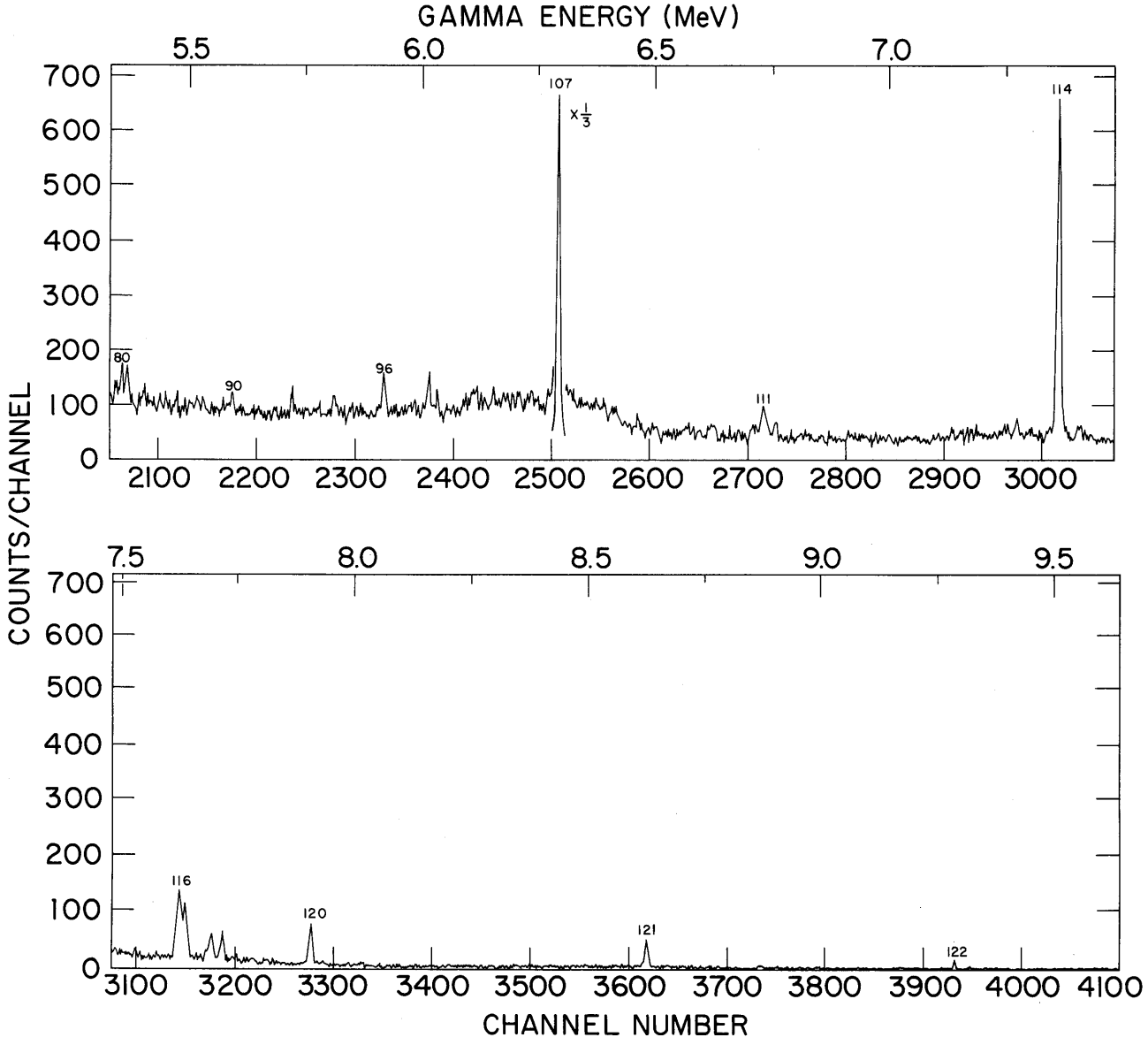

FIGURE 60 ZIRCONIUM PAIR SPECTROMETER SPECTRUM

TABLE 21

ENERGIES AND INTENSITIES OF GAMMA RAYS IN ZIRCONIUM COMPTON SUPPRESSION SPECTRUM

LINE	E (KEV)	I (NO./100 CAPTS)	NOTES
1	139.4(X)	2.0800(Y)	
2	143.0	1.1640	
3	149.2	.8578	Q
4	153.1	.5111	Q
5	159.9	2.8165	B
6	175.0	2.2232	B
7	184.8	.7304	B
8	193.3	.5768	Q
9	225.1	1.4376	Q
10	230.9	1.5594	Q
11	243.5	1.8762	
12	265.5	1.1522	
13	311.9	.5053	
14	379.7	1.2221	
15	447.6	2.4818	
16	491.8	1.6719	
17	511.0	81.0154	B
18	530.4	1.6261	
19	534.6	.1442	
20	540.3	1.8891	
21	561.0	19.8685	F
22	576.4	.5089	E
23	581.9	.3734	
24	585.9	.3220	
25	595.7	2.0794	B
26	602.1	.4944	
27	614.6	.3682	
28	623.4	.8438	
29	628.6	.8638	
30	635.5	.5185	
31	644.2	.4360	
32	653.3	.8223	E
33	669.5	1.8702	
34	680.2	.4032	
35	694.1	.5359	
36	701.1	.5490	
37	708.1	.6471	
38	719.0	.6104	
39	723.1	.3077	
40	727.2	.2523	E
41	738.1	.4986	
42	754.4	.5331	E
43	759.8	.6186	
44	773.7	1.1091	
45	783.3	.4417	
46	788.8	.4638	
47	821.5	.3762	
48	831.1	.6799	
49	838.0	.6232	
50	843.7	4.3905	
51	866.8	1.4186	
52	885.7	.7068	
53	904.8	1.4836	
54	913.1	7.3189	
55	934.3	67.2705	
56	972.8	2.0343	
57	991.7	3.0179	
58	1060.6	.7681	
59	1131.5	5.8435	
60	1201.4	11.6056	B
61	1297.2	.4216	
62	1310.9	.5748	
63	1323.1	.4685	
64	1350.9	.5786	
65	1368.0	1.7574	E
66	1403.8	13.7381	F
67	1425.0	1.3804	
68	1452.4	1.3581	
69	1463.0	3.2115	
70	1490.4	1.2947	
71	1495.9	.2522	E
72	1524.9	.7392	
73	1604.0	1.3913	
74	1653.5	2.8766	
75	1670.0	1.2486	
76	1712.0	2.6380	B
77	1756.2	1.2580	
78	1760.5	.8329	
79	1797.7	.9105	
80	1801.8	.9236	
81	1849.7	5.4584	
82	1921.4	.5930	
83	1940.6	2.3363	
84	1975.7	.8582	
85	2102.5	1.3083	
86	2223.3	76.1631	B
87	2328.5	.9030	
88	2435.8	1.7241	
89	2478.4	6.6477	
90	2696.1	1.9846	

(X) ACCURACY OF ENERGIES IS ABOUT 1 KEV
(Y) ONLY TWO SIGNIFICANT FIGURES, INTENSITIES OF STRONG PEAKS ACCURATE TO ABOUT 20 PERCENT

NOTES
B --- BACKGROUND GAMMA RAY
E --- GAMMA RAY FROM CAPTURE IN CADMIUM IMPURITY
F --- PORTION OF INTENSITY FROM CAPTURE IN CADMIUM IMPURITY
Q --- MARGINAL PEAK

TABLE 22

ENERGIES AND INTENSITIES FOR GAMMA RAYS IN ZIRCONIUM PAIR SPECTROMETER SPECTRUM

	THIS WORK			BARTHOLOMEW (B4)	
LINE	E (KEV)	I (NO./100 CAPTS.)	NOTES	E (MEV)	I (NO./100 CAPTS)
1	1268.9(X)	11.0479(Y)	QI		
2	1344.9	6.7469	QI		
3	1404.7	20.7642			
4	1427.2	9.5917	QI		
5	1452.0	6.0114	QI		
6	1466.8	4.7637			
7	1532.9	15.6106	B		
8	1617.1	10.1400	B		
9	1631.5	2.5203			
10	1642.3	2.5880			
11	1847.3	3.2475			
12	1890.0	1.9204			
13	1987.7	3.0537			
14	2044.3	1.5966			
15	2106.2	2.2280			
16	2134.8	1.2428			
17	2191.3	1.8215			
18	2223.3	114.8315	B		
19	2294.8	1.5319			
20	2329.1	.9194			
21	2355.9	.7293			
22	2437.4	1.5350			
23	2478.1	1.2584			
24	2518.3	.7428			
25	2532.7	1.1660			
26	2693.6	5.5510			
27	2708.0	2.7670			
28	2874.1	.6758			
29	2938.9	2.1482			
30	2962.5	.4608			
31	3008.4	.3895	GR		
32	3045.7	.6191			
33	3098.8	.6477			
34	3109.2	.5746			
35	3147.5	.7474			
36	3177.4	.6272			
37	3211.4	.4035			
38	3270.6	1.0872	GR		
39	3342.9	.5127			
40	3372.2	1.2818			
41	3438.5	1.3740			
42	3461.4	.4188			
43	3475.1	1.7787			

CONTINUATION OF TABLE 22

	THIS WORK			BARTHOLOMEW (B4)	
LINE	E (KEV)	I (NO./100 CAPTS.)	NOTES	E (MEV)	I (NO./100 CAPTS)
44	3503.7	1.7081			
45	3535.0	1.0440			
46	3580.1	.9073			
47	3610.2	1.2071			
48	3638.2	1.1733			
49	3696.5	2.2778	GR		
50	3858.2	.6608			
51	3941.0	.8519			
52	3962.5	.5142			
53	3979.9	.7189			
54	4000.7	.5129			
55	4028.2	.5503			
56	4056.4	.7142			
57	4092.2	1.1081			
58	4104.9	1.7775			
59	4121.2	.6924			
60	4170.8	.6033			
61	4183.6	.6968			
62	4203.0	.5974			
63	4228.5	.5542			
64	4262.5	1.2564			
65	4278.1	1.1674			
66	4406.6	.4452			
67	4438.0	1.1718	GR		
68	4530.6	2.0394			
69	4654.7	1.1765			
70	4738.1	.3173			
71	4804.8	.4849			
72	4947.8	.6297	B		
73	4996.2	1.2105			
74	5007.1	2.2523			
75	5136.2	1.0572			
76	5163.4	.9160			
77	5182.3	.7515			
78	5263.8	3.3613			
79	5310.1	1.1863			
80	5362.6	.2364			
81	5371.6	.3351			
82	5411.2	.1657			
83	5444.3	.2084			
84	5455.8	.1426			
85	5479.6	.2099			
86	5497.4	.2282			
87	5508.0	.1792			
88	5522.9	.2178			
89	5535.7	.2126			

CONTINUATION OF TABLE 22

LINE	THIS WORK E (KEV)	THIS WORK I (NO./100 CAPTS.)	NOTES	BARTHOLOMEW (B4) E (MEV)	BARTHOLOMEW (B4) I (NO./100 CAPTS)
90	5596.7	.4987			
91	5692.3	.2570			
92	5728.0	.4591			
93	5786.9	.1415			
94	5818.4	.4354			
95	5855.6	.1161			
96	5919.1	.5931	B		
97	5990.7	.1712			
98	6019.5	.4497	B		
99	6037.0	.2058			
100	6098.0	.2178			
101	6123.2	.6412			
102	6158.9	.2688			
103	6180.5	.2571			
104	6196.8	.1833			
105	6209.2	.3351			
106	6238.8	.2283			
107	6295.2	18.2448		6.30(3)(Z)	16
108	6415.4	.2682			
109	6465.9	.1508			
110	6623.6	.5598			
111	6735.3	.6918	B		
112	6761.1	.3546			
113	7279.4	.4121			
114	7367.7	7.4679	B		
115	7409.8	.4171		7.38(6)	0.5
116	7626.9	2.1128	B		
117	7645.3	1.4460	B		
118	7701.8	.4965		7.71(4)	1
119	7725.5	.5573	B		
120	7915.4	.8373	B		
121	8635.1	.9155		8.66(4)	1
122	9299.8	.2189	B		

(X) ACCURACY OF ENERGIES IS ABOUT 1 KEV
(Y) ONLY TWO SIGNIFICANT FIGURES, INTENSITIES OF STRONG PEAKS ACCURATE TO ABOUT 20 PERCENT
(Z) NUMBERS IN PARENTHESES INDICATE ERROR IN LAST DIGIT

NOTES
B --- BACKGROUND GAMMA RAY
QI --- QUESTIONABLE INTENSITY DUE TO POOR STATISTICS
GR --- GROUP OF SEVERAL PEAKS

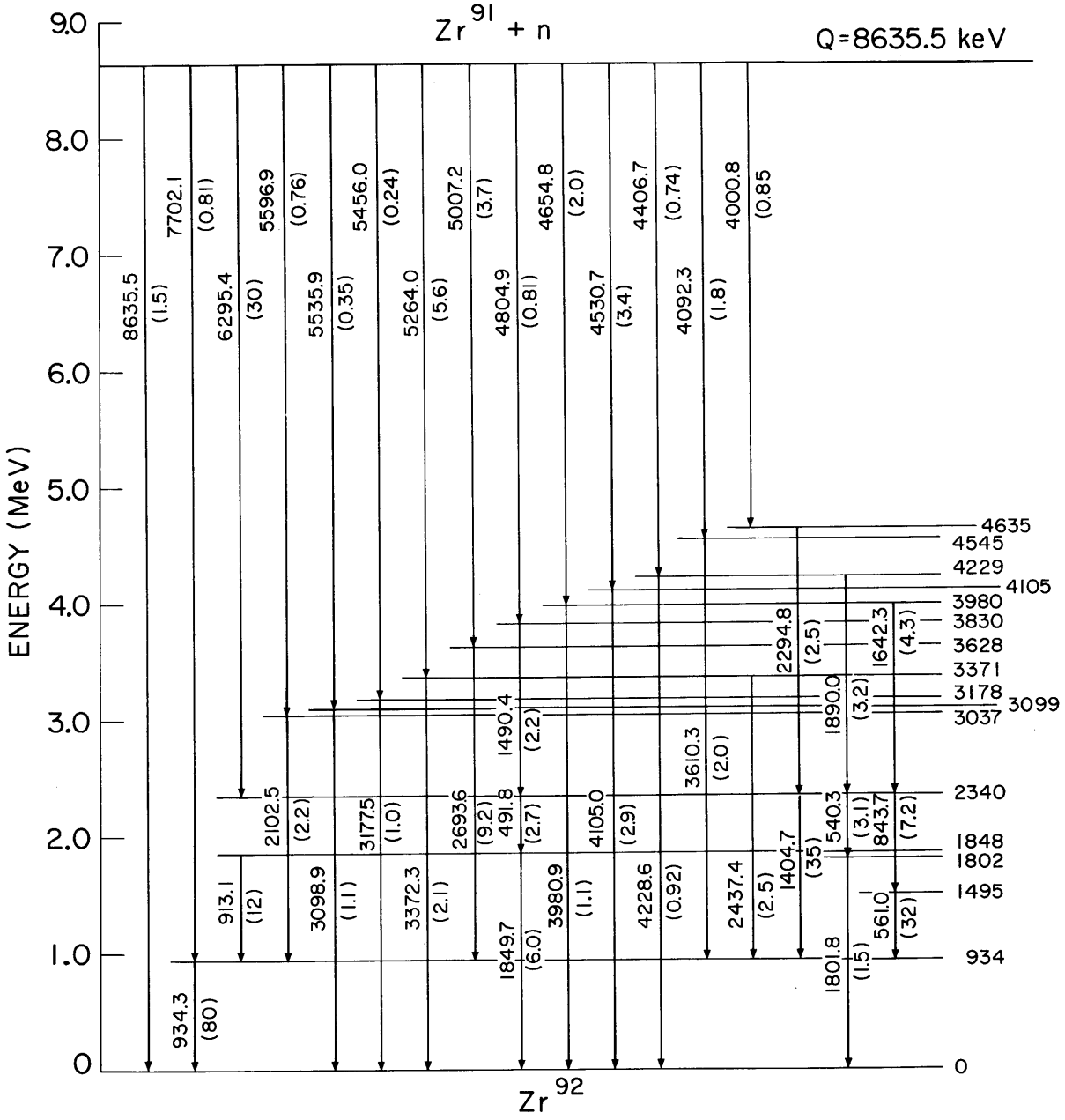

FIGURE 61 PROPOSED LEVEL DIAGRAM FOR Zr^{92}

TABLE 23

SOME 2-STEP CASCADES IN Zr^{92} FROM THE CAPTURING STATE TO THE GROUND STATE

Cascade	γ_1 (keV)	γ_2 (keV)	$\gamma_1 + \gamma_2$ (keV)
1	8635.5	--	8635.5
2	7702.1	934.3	8636.5
3	5535.9	3098.9	8634.7
4	5264.0	3372.3	8636.2
5	4654.8	3980.0	8634.8
6	4530.7	4105.0	8635.7
7	4406.7	4228.6	8635.3

Mean = 8635.53

Standard deviation of an individual cascade = 0.67 keV

The 6415.6-keV γ ray agrees with the binding energy of Zr^{95}, 6.42 $\pm$ .05 MeV (W3), and the 7279.7-keV γ ray agrees with the binding energy of Zr^{91}, 7.2 $\pm$ .1 MeV (L2).

5.6 Accuracy of Energy Values

One means of checking the precision of capture gamma energies is to compare the sum of the energies of different cascade transitions between the same two energy levels. The results presented in Tables 9, 12, 13, 16, 19, 20 and 23 indicate that the precision of well-defined capture γ rays is about 0.5 keV. The accuracy of the energies of these γ rays is limited by the accuracy of the Pb calibration line to about 1 keV.

The degree of agreement between cascade sums in Fe^{55}, (see Table 13), 0.96 keV, indicates that even weak intensity γ rays may be determined

to an accuracy of about 1 keV. Except for the 9298-keV γ ray, the intensities of all the γ rays in Table 13 are less than 0.5 γ's per 100 captures in natural iron.

5.7 Accuracy of Intensity Values

Verification that the absolute intensity of strong capture γ rays may be determined to an accuracy of about 10 to 20% is afforded by beryllium, which has a well-established decay scheme (see Fig. 49). Intensity values may be checked by determining whether the intensity of γ rays feeding a level is equal to those originating from that level. When this is done, using the values given in Table 8, it is found that at the 5959-keV level the outgoing intensity is about 8% greater than the incoming intensity, while at the 3368-keV level the incoming intensity is about 8% greater than the outgoing intensity. Furthermore, the intensity of γ rays originating from the capturing state agrees with that directly feeding the ground state within less than 1%. This agreement verifies the correctness of the spectrometer's relative efficiency curves over the energy range of the transitions, about 0.8 to 7 MeV.

The accuracy of the absolute efficiency curves can be verified by comparing intensity values with those obtained on a different instrument -- as was done in Tables 8, 11, 14, 15 and 23. Also, one can calculate the fraction of the total γ-ray intensity observed. For the simple beryllium capture γ-ray spectrum, in which all γ rays are resolved, this fraction should be unity and its deviation from unity is a measure of inaccuracies in the absolute intensities. The value of 0.98 for this fraction provides an independent verification of the accuracy of the absolute intensity values. Calculation of the fraction of γ-ray intensity observed in the case of iron, scandium, germanium and zirconium provides further verification of

intensity values. 98% of the iron capture γ-ray intensity was observed. For elements in which considerably less than 100% of the intensity was observed, there was a corresponding indication of unresolved γ rays in the capture spectra of these elements, which accounted for the fact that a portion of the γ-ray intensity was not observed.

CHAPTER VI

CONCLUSIONS AND RECOMMENDATIONS FOR FUTURE WORK

6.1 Conclusions

A large coaxial Ge(Li) detector, when used in a pair spectrometer and in a Compton suppression system, provides an effective means for obtaining thermal neutron capture gamma spectra over practically the entire capture gamma energy range. The energy resolution of such a spectrometer is comparable or better than the magnetic high resolution gamma spectrometers (about 0.5% at 1 MeV and 0.1% at 7 MeV). Furthermore, the greater efficiency of the Ge(Li) spectrometer (about 0.1% intrinsic pair peak efficiency at 5 MeV) allows the use of an external neutron beam geometry. This arrangement simplifies sample changing and allows many different elements to be studied in a short period of time (approximately 1 day per element).

The pair spectrometer, effective in the energy range of 1.2 to 12 MeV, affords a signficant improvement in the peak to background ratio, eliminates single escape and full energy peaks, and yields considerably more uniform backgrounds than a Ge(Li) detector operated directly. These features help reduce errors in capture gamma intensities caused by large uncertainties in the value of the background to be subtracted when determining peak areas. Use of the Ge(Li) spectrometer in the Compton suppression mode allows the study of capture gamma spectra in the energy range from 100 keV to 3000 keV. This mode of operation enhances full energy peaks and diminishes the other spectral features -- double escape peaks, single escape peaks, and Compton background. The Ge(Li) spectrometer is capable of determining the energies of capture γ rays (with well-defined spectral peaks) to an

accuracy of about 1 keV. Furthermore, the capture gamma spectra of elements with cross sections of a few tenths of a barn and many weak intensity γ rays may be studied.

The capture γ-ray data obtained may be analyzed to obtain more accurate (about $\pm$ 1 keV) binding energies and level energies. The ability of the Ge(Li) spectrometer to resolve a larger fraction of the γ-ray intensity (for example, 98% in the case of iron) enables the determination of more complete level diagrams.

6.2 Recommendations For Future Work

6.2.1 Ge(Li) Detector Development

The following are recommended for future improvements in the fabrication of Ge(Li) detectors:

(1) Establishment of a low temperature (-20°C to -50°C) "clean up" facility capable of operating without attention for a minimum of 8 hrs. This could be done most simply by placing a fluorocarbon drift bath and magnetic stirrer in a refrigerator freezer.

(2) Construction of "double open ended" coaxial detectors to improve timing characteristics.

(3) Investigation of drifting at lower temperatures (20°C to 40°C) and higher voltages (500 to 2000 volts). Drifting at these lower temperatures might eliminate the need for lengthy low-temperature "clean up" drifts.

(4) Development of a low capacitance, large volume detector by using the A-C method of drift (J2), the U-shaped junction detector configuration (A2), or some new concept.

6.2.2 Study of Capture γ-Rays

Recommendations for future work and improvements which can be

made in the study of capture γ rays are as follows:

(1) Replacement of the polyethylene section of the γ-ray collimator with one made of bismuth in order to reduce the strong hydrogen capture γ-ray background.

(2) Construction of a permanent fixture to hold and position the liquid nitrogen dewar. This would eliminate the possibility of a change in spectrometer efficiency caused by misalignment of the Ge(Li) detector with respect to the collimator.

(3) Establishment of a coincidence setup. The present external beam facility and Ge(Li) pair spectrometer could be used by adding a directly operated large Ge(Li) detector at 180° to the present γ-ray collimator. It might prove advisable to use a more finely collimated neutron beam and to decrease the source to detector distance.

(4) Study separated isotopes. Although the present set up would probably be adequate for high cross section nuclides, use of an internal target would probably be necessary for low cross section nuclides. The Ge(Li) spectrometer could be set up at the currently used through-port, 9CH2, looking at an internal source, which would be positioned from the other side of the through-port, 9CH1.

(5) Improvement of the spectrometer resolution through the use of a cooled FET preamp and a lower capacitance large Ge(Li) detector.

(6) Improvement of the pair spectrometer efficiency by using a large planar Ge(Li) detector in the shape of a flat parallelepiped and by using an aluminum detector mount in place of the copper one presently used. The flat detector will allow a greater percentage of 511-keV γ rays to escape to the NaI detectors and should offer a lower capacitance.

APPENDIX A

CALCULATION OF PAIR SPECTROMETER EFFICIENCY

The absolute pair spectrometer efficiency as a function of γ energy, $\eta_{pair}(E)$, is expressed as,

$$\eta_{pair}(E) = T_{LiF}(E)\, \eta_1(E)\, \eta_2(E)\, \eta_3(E)\, \eta_4$$

where:

T_{LiF} is the transmission factor for γ rays of energy, E, through the 1.6-cm thick slab of LiF,

$\eta_1(E)$ is the probability of a pair production interaction occuring in the Ge(Li) detector,

$\eta_2(E)$ is the probability that the electron and positron pair formed will <u>not</u> escape from the Ge(Li) detector,

$\eta_3(E)$ is the probability that the energetic electron and positron will <u>not</u> lose any energy by bremsstrahlung which escapes the Ge(Li) detector,

η_4 is the probability that both 511-keV gammas, resulting from annihilation of the positron in the Ge(Li) detector will escape from the Ge(Li) detector and be totally absorbed by the NaI crystals. Every event occuring in the photopeak is assumed to fall within the 511-keV window.

T_{LiF} was determined experimentally for low energies (< 3 MeV) using several radioactive sources and was calculated at high energies using a density value for the LiF slab inferred from the low energy values. It was found that over the energy range, 1-10 MeV, T_{LiF} could be approximated by the following quadratic function,

$$T_{LiF} \approx - 0.00285\, E^2 + 0.0443\, E + 0.784,$$

whose accuracy was consistent with other approximations made.

TABLE A.1

LINEAR ATTENUATION COEFFICIENTS FOR GERMANIUM*

Energy (MeV)	$\mu_{Compton}(cm^{-1})$	$\mu_{pair}(cm^{-1})$	$\mu_{total}(cm^{-1})$
1	.33	0	.330
2	.21	.008	.218
3	.17	.021	.191
4	.14	.034	.169
5	.12	.043	.163
6	.10	.054	.154
7	.094	.062	.156
8	.084	.073	.157
9	.079	.084	.161
10	.074	.090	.164

*From reference (S1)

T_{LiF} varied from 83% at 1 MeV to 94% at 10 MeV.

$\eta_1(E)$ was expressed as,

$$\eta_1(E) = (1 - e^{-\mu_T \bar{x}}) \frac{\mu p}{\mu T}$$

where μ_T = total linear attenuation coefficient for gamma rays in germanium (cm^{-1}),

μ_p = pair production attenuation coefficient for gamma rays in germanium (cm^{-1})

$\bar{x}$ = "effective" average thickness of the Ge(Li) detector perpendicular to the incident γ beam.

Table A.1 gives a listing of germanium attenuation coefficients used in this calculation. Because of the coaxial geometry of the Ge(Li) detector it was difficult to determine $\bar{x}$; consequently, a semi-empirical approach was used. Making the reasonable assumption that $\eta_1(E)$ constituted the principal contribution to the variation of η_{pair} in the range of 1-3 MeV, a value of $\bar{x}$ was found for which $\eta_1(E)$ best agreed with the experimental variation of efficiency in the low energy range. The value obtained for $\bar{x}$, 1.45 cm, is quite consistent with the physical dimensions of the active volume of the Ge(Li) detector.

$\eta_2(E)$ was approximated by the following expression,

$$\eta_2(E) \approx (EVR)_f \, w_f + (EVR)_b \, w_b \, .$$

EVR, the effective volume ratio, is defined as the ratio of that volume effective in stopping energetic electrons and positrons to the total active volume. "f" and "b" denote respectively the front or "closed end" region of the detector and the back portion (region containing the p-type core). The w's are weighting factors which account for the fact that more electrons and positrons are produced in the front region as a result of γ attenuation in the detector. For the purposes of this calculation, the trapezoidal cross sectional area of the detector was replaced by an equivalent circular cross sectional area. Figure A.1 shows a cross sectional sketch of the cylindrical detector. The effective volume is calculated by summing the volume represented by the unshaded region and the volumes represented by the shaded regions, each multiplied by the fraction of electrons which do not escape from the active volume of the detector. The fractions used for

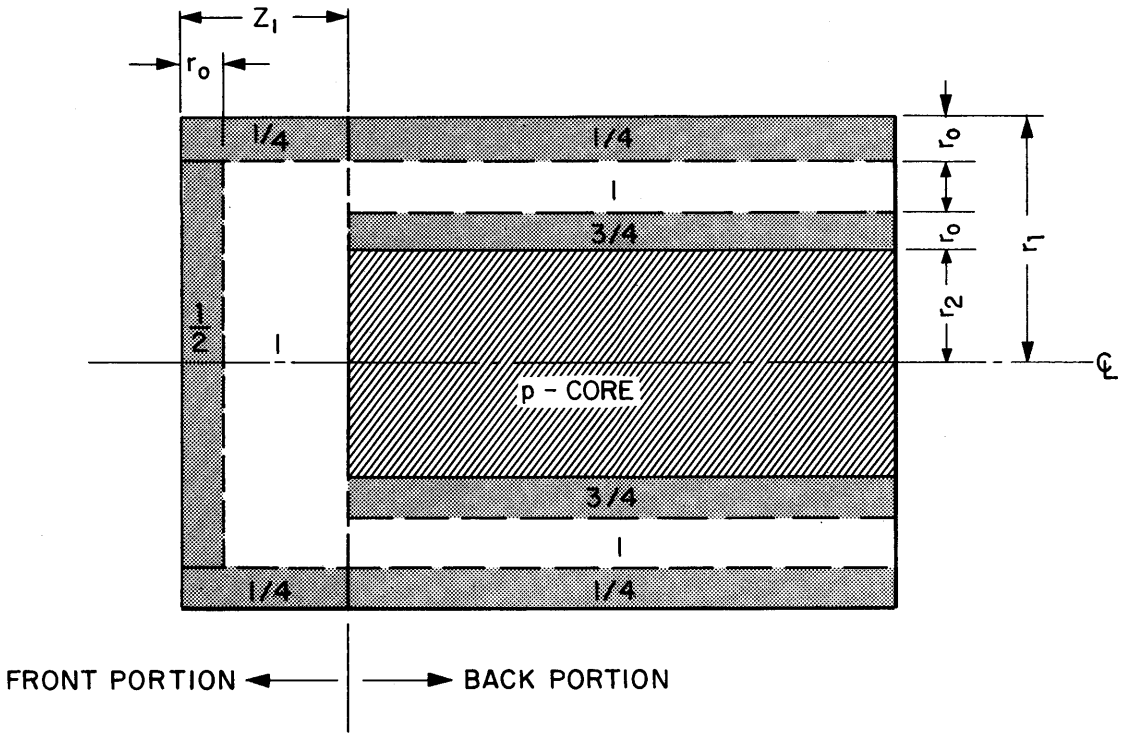

$r_1 = 1.5$ cm

$r_2 = 0.7$ cm

$Z_1 = 1.0$ cm

$r_o(\text{cm}) = \frac{533\,E_e - 106}{5330}$

E_e = ELECTRON ENERGY (MeV)

FIGURE A.1 CROSS SECTIONAL SKETCH OF IDEALIZED CYLINDRICAL DETECTOR

each region are shown in the sketch. The relative sizes of the shaded and unshaded regions depend on r_o, the electron range, and hence on the electron energy. The expressions for $(EVR)_f$, $(EVR)_b$, w_f and w_b are as follows:

$$(EVR)_f = \frac{(r_1 - r_o)^2(z_1 - r_o) + \frac{1}{2}(r_1 - r_o)^2 r_o + \frac{1}{4} z_1 r_o (2r_1 - r_o)}{z_1 r_1^2}$$

$$(EVR)_b = \frac{\left[(r_1 - r_o)^2 - (r_o + r_2)^2\right] + \frac{1}{4}\left[r_1^2 - (r_1 - r_o)^2\right] + \frac{3}{4}\left[(r_o + r_2)^2 - r_2^2\right]}{r_1^2 - r_2^2}$$

for $|r_1 - r_o| > |r_o + r_2|$

$$(EVR)_b = \frac{\frac{1}{4}\left[r_1^2 - \left(\frac{r_1 + r_2}{2}\right)^2\right] + \frac{3}{4}\left[\left(\frac{r_1 + r_2}{2}\right)^2 - r_2^2\right]}{r_1^2 - r_2^2}$$

for $|r_1 - r_o| \leq |r_o + r_2|$

$$w_f = \frac{1}{2 - e^{-\mu_T z_1}}$$

$$w_b = \frac{1 - e^{-\mu_T z_1}}{2 - e^{-\mu_T z_1}}$$

Values used for r_1, r_2, and z_1 are given in Fig. A.1.

The electron and positron formed by a pair production interaction of a gamma ray of energy E, have a continuous distribution of energies (E2). The simplifying assumption was made in the electron range calculation that the electrons and positrons resulting from pair production have an average energy, $E_e = \frac{3}{4}(E - 1.022)$. Then, the electron range, r_o, was determined using a semiempirical formula (E2),

$$r_o = \frac{533\,E_e - 106}{5330}.$$

η_3, which is quite difficult to calculate in even an approximate manner, was determined using a semiempirical approach. The fraction of the electron energy radiated as bremsstrahlung varies approximately as E_e (E2); consequently, η_3 was assumed to be a linear function of E. Assuming that bremsstrahlung loss was negligible for $E_\gamma < 4$ MeV and requiring that the calculated efficiency agree with the experimental, the following expression for η_3 was obtained:

$$\eta_3(E) = 0 \qquad E < 4 \text{ MeV}$$

$$\eta_3(E) = 1.1 - .15(E - 4.0) \qquad 4 \text{ MeV} \leqq E \leqq 10 \text{ MeV}$$

η_4 was calculated using the following expression:

$$\eta_4 = g\,\epsilon_1^2\,\epsilon_2^2$$

where,

g is a geometric factor,

ϵ_1 is the probability that a 511-keV photon will escape from the active volume of the Ge(Li) detector,

ϵ_2 is the probability that a 511-keV γ will escape through the Ge(Li) detector "dead layer" and the snout dewar Al wall and be totally absorbed by a NaI crystal.

The surrounding NaI crystals offer approximately a 3π - geometry. Hence, $g \approx 0.75$. ϵ_1 and ϵ_2 were squared in the expression for η_4 since there are two 511-keV photons involved. ϵ_1 was expressed as $e^{-\mu_{Ge} t}$ where t is the average thickness of germanium which a 511-keV photon must traverse in order to escape. Taking t = 1.6 cm gave $\epsilon_1 = .452$. The probability of a 511-keV gamma being totally absorbed in a NaI

crystal can be expressed as $(P)(1 - e^{-\mu x})$ where μ is the linear absorption coefficient for 511-keV γ's in NaI, P is the photofraction for the NaI crystal (about .75 (M11)), and x is the average thickness of the NaI (about 3 inches.) Assuming a germanium dead layer of 2 mm and an aluminum wall thickness of 3 mm, a transmission factor, T, of 0.848 was determined. ϵ_2, which is $TP(1 - e^{-\mu x})$ was found to be 0.445. Note that $g\epsilon_2^2 = .148$, which is the ratio of the efficiency of the detector operated in the pair spectrometer mode to the efficiency in the direct mode, agrees with the experimental value of $\sim$.14 (see Section 3.3.1). Finally, η_4 was calculated to be 0.302. It is noted that η_4 is independent of the incident γ energy.

Since some portions of the above calculation required "trial and error" to obtain the most suitable semiempirical parameters, a computer program was written to carry out the efficiency calculation from 1 to 10 MeV in intervals of 1 MeV. A listing of the FORTRAN II program is given in Table A.3.

Table A.2 presents results of the efficiency calculation and shows the contributions of the individual efficiency factors. This calculation provided a consistent efficiency curve, which is in good agreement with experimental data, for use in determining capture gamma intensities.

TABLE A.2

RESULTS OF EFFICIENCY CALCULATION FOR PAIR SPECTROMETER

Energy (MeV)	η_1	η_2	η_3	η_4	$\eta_{pair} \times 10^4$
1	0	1.00	1.00	.0302	0
2	.010	.923	1.00		2.39
3	.027	.823	1.00		5.89
4	.044	.733	1.00		8.86
5	.056	.651	.950		9.69
6	.070	.578	.809		9.28
7	.080	.512	.650		7.72
8	.095	.454	.500		6.20
9	.100	.409	.350		4.39
10	.116	.357	.200		2.36

TABLE A.3

FORTRAN LISTING OF EFFCY CODE

```
      COMMON XMUC,XMUT,XMUP,H1,H2,R1,R0,R4,Z1,IE,BETA,XAV,H3,T
      DIMENSION XMUC(10),XMUT(10),XMUP(10),H1(10),H2(10),A(10),
     1B(10),R0(10),ATCOF(10),EVRF(10),EVRB(10),H3(10),T(10)
      READ  10,(XMUC(I), I=1,10)
      READ 10,(XMUP(I), I=1,10)
      READ 21,N1,H4
21    FORMAT (I6,F6.4)
      J = 0
50    J = J+1
 10   FORMAT (10F6.3)
      READ 20,XAV,BETA,R1,R4,Z1
20    FORMAT (5F6.3)
      IE = 0
 30   IE = IE + 1
      CALL ETAI
      CALL ETA2
      CALL ETA3T
      EFF = H1(IE)*H2(IE)*H3(IE)*T(IE)*H4
      PRINT 70,IE,EFF
70    FORMAT (I6,F12.6)
      IF (IE-10) 30,40,40
 40   PRINT 10,(H1(I), I=1,10)
      PRINT 10,(H2(I), I =1,10)
      PRINT 10,(H3(I), I=1,10)
      IF(J-N1) 50,60,60
60    END
```

ETA1 SUBROUTINE

```
      SUBROUTINE ETAI
      COMMON XMUC,XMUT,XMUP,H1,H2,R1,R0,R4,Z1,IE,BETA,XAV
      DIMENSION XMUC(10),XMUT(10),XMUP(10),H1(10),H2(10),A(10),
     1B(10),R0(10),ATCOF(10),EVRF(10),EVRB(10)
      XMUT(IE) = XMUC(IE) +XMUP(IE)
      A(IE) = 1.0 - EXPF(-XMUT(IE)*XAV)
      B(IE) = (XMUP(IE) + BETA*XMUP(IE)*XMUC(IE))/(XMUT(IE))
      H1(IE) = A(IE) * B(IE)
      RETURN
      END
```

ETA2 SUBROUTINE

```
      SUBROUTINE ETA2
      COMMON XMUC,XMUT,XMUP,H1,H2,R1,R0,R4,Z1,IE,BETA,XAV,H3,T
      DIMENSION XMUC(10),XMUT(10),XMUP(10),H1(10),H2(10),A(10),
     1B(10),R0(10),ATCOF(10),EVRF(10),EVRB(10),H3(10),T(10)
      EGAM = IE
      E = .75*(EGAM-1.022)
      R0(IE) = (530.*E-106.)/5330.
      ATCOF(IE) = 1.0-EXPF(-(XMUT(IE)*Z1))
      X = (R1-R0(IE))**2
      EVRF(IE) = (X*Z1 -.5*X*R0(IE) + (.25*R0(IE))*(2.*R1-R0(IE
     1))*Z1)/(R1**2*Z1)
      Y1 = R1**2 -R4**2
```

```
      COND = R1-2.*R0(IE) -R4
      IF (COND) 100,100,200
  100 Y2 = ((R1+R4)**2)/4.
      EVRB(IE) = (.25*(R1**2-Y2) + .75*(Y2-R4**2))/Y1
  200 Y3= (R0(IE) +R4)**2
      EVRB(IE) = ((X-Y3) + .25*(R1**2-X) +.75*(Y3-R4**2))/Y1
      H2(IE)= (EVRF(IE) + ATCOF(IE)*EVRB(IE))/(1.0+ATCOF(IE))
      RETURN
      END
```

ETA3T SUBROUTINE

```
      SUBROUTINE ETA3T
      COMMON XMUC,XMUT,XMUP,H1,H2,R1,R0,R4,Z1,IE,BETA,XAV,H3,T
      DIMENSION XMUC(10),XMUT(10),XMUP(10),H1(10),H2(10),A(10),
     1B(10),R0(10),ATCOF(10),EVRF(10), EVRB(10),H3(10),T(10)
      IF (IE-5)1,2,2
1     H3(IE) = 1.0
      GO TO 3
2     E = IE
      H3(IE) = 1.1 -.150*(E-4.0)
 3    E = IE
      T(IE) = -.00285*E**2 + .04425*E + .784
      RETURN
      END
```

APPENDIX B

DESCRIPTION OF "PLOTS" COMPUTER CODE

A computer code, PLOTS, was written to plot the spectral data using a CALCOMP plotter at the MIT Computation Center. PLOTS performs the following functions: (1) it reads the data cards (up to 4095 channels), (2) it performs a scaling of any desired region of the spectrum, and (3) it calls plotting subroutines (available at the MIT Computation Center) whose arguments are specified so as to determine such things as graph size, axis designation, headings, etc. A FORTRAN listing of PLOTS is given in Table B.1. The plotting subroutines have been described elsewhere (C1), therefore, no description is given here.

TABLE B.1

FORTRAN LISTING OF PLOTS CODE

```
C   GAMMA RAY SPECTRA PLOTTING PROGRAM WITH SCALING PROVISION
      DIMENSION X(4095),Y1(4095),B(800)
      J = 0
   50 J = J + 1
C  GIVE BUFFER AREA TO CALCOMP ROUTINES
      CALL PLOTS1(B,800)
C   PUT ID NUMBER ON GRAPH
      CALL SYMBL5 (4.0,9.0,.2,20H ID NO. = M4179-2844,0.,20)
      READ 20, NUM
      PRINT 20 , NUM
   20 FORMAT (I6)
C   PUT RUN NUMBER ON GRAPH
      CALL NUMBR1 (8.5,8.2,.2,NUM,0.,-1)
C   READ IN AND SET UP DATA
      READ 2,N1,N6,NL,NU,FACTOR
    2 FORMAT (4I6,F6.1)
      X(1) = 1.0
      DO 1I = 2,N1
    1 X(I) = X(I-1) + 1.0
      READ 3, (Y1(I), I=1,N1)
    3 FORMAT (7X, 7(F6.0,1X)/(8(F6.0,1X)))
C     LABEL PICTURE
      CALL SYMBL5 (4.0,8.2,.2,16H LINEAR PLOT NO.,0.,16)
      DO 400I = NL,NU
      Y1(I)=Y1(I)/FACTOR
  400 CONTINUE
C     DO PLOTTING
      CALL PICTUR  (40.95,8.,15H CHANNEL NUMBER,15,17H NUMBER OF COUNTS,
     1  17,X,Y1, N1,0.,0)
      DO 30I = 1, N1
      Y1(I) = 0.0
   30 CONTINUE
      IF (N6 - J)51,51,50
   51 END FILE 10
      CALL EXIT
      END
```

APPENDIX C

DESCRIPTION OF "EANDI" COMPUTER CODE

"EANDI" calculates the energy and intensity of each spectral peak using the methods discussed in Chapter 4. This code performs the following general functions: (1) reads in the data and necessary control parameters, (2) calls seven subroutines, each of which performs a step in the calculation, and (3) outputs the results.

The input parameters are identified in Table C.1, which lists them in the order in which they are read by the code. The card format may be obtained from the FORTRAN listing of EANDI (Table C.4). Table C.2 shows the typical input format for the pair spectrometer run of beryllium, run 517.

TABLE C.1

INPUT DATA FOR "EANDI"

Parameter Number	Designation	Description
1	N1	Number of data channels (e.g., 4095)
2	N2	Number of the pulser peak (in linearity check) to be used as lower reference point (linearity correction defined to be zero at this point).
3	N3	Number of the pulser peak to be used as upper reference point.
4	N4	Number of peaks to be analyzed.
5	N5	Number of the spectral peak which will serve as the low energy calibration point.
6	N6	Number of the spectral peak which will serve as the high energy calibration point.

TABLE C.1 (Continued)

Parameter Number	Designation	Description
7	IRUN	Run identification number.
8	NP	Number of multiple partially resolved peaks to be analyzed.
9	NR	Number of experimental runs to be analyzed.
10	XNMP(I)	Channel number location of the maximum counts/channel for the highest energy peak in the i^{th} multiple peak group.
11	XNOP(I)	Multiplicity of the i^{th} multiple peak group (must be $\leq$ 4).
12	J1	Control number: J1 = 0 for Compton suppression runs, J2 = 2 for pair spectrometer runs.
13	J2	Number of spectrometer efficiency points to be used.
14	FDGE	$\mathcal{F}$ factor in Eq. 4-10.
15	SANGL	Solid angle, defined in Eq. 4-11.
16	FWGT	Weight (in mg) of Au monitor foil.
17	AUCNT 1	GM tube count rate (cpm) of one side of monitor foil.
18	AUCNT 2	GM tube count rate (cpm) of other side of monitor foil.
19	FLXCST	Constant in equation relating flux to count rate of monitor foil.
20	TIME 1	Time (in hrs) after irradiation that AUCNT 1 was determined.
21	TIME 2	Time (in hrs) after irradiation that AUCNT 2 was determined.
22	SIGMA	Thermal capture cross section of source (cm^2).
23	ATOMS	Total number of atoms of source material.

TABLE C.1 (Continued)

Parameter Number	Designation	Description
24	EFFCY(I)	The efficiency of the spectrometer at the i^{th} energy interval. (For Compton suppression runs the energy interval = 0.1 MeV and I = 1 corresponds to 0.1 MeV, while for pair spectrometer operation the interval = 0.5 MeV and I = 1 corresponds to 1 MeV.
25	COUNT(I)	Number of counts in the i^{th} channel of the: (a) linearity check run (first time read), (b) spectral data (second time read).
26	KPO	Channel number containing maximum counts (one for each peak).
27	KP1	Control parameter designating number of channels, about KPO, to be used for fit. KP1 = 1, 3 channels used KP1 = 2, 5 channels used
28	KP2	KP0 - LC (LC defined in Fig. 46).
29	KP3	UC - KP0 (UC defined in Fig. 46).
30	KEYB	Control parameter designating if average is to be taken to determine background limits KEYB = 1, no average KEYB = 3, average taken.
31	N40	Control parameter for LINFT, determines minimum number of counts/channel required in order that a channel be considered part of a pulser peak.
32	EGAM1	Low calibration energy.
33	EGAM2	High calibration energy.

TABLE C.2

INPUT FORMAT FOR EANDI, RUN 517

```
  4095     20     80     17      4     15    517      1      1
  0.00
  0.00
 219.85    E 00 1.6  E-051.905 E 001.491 E 02 1.451E 029.20  E 05
5.717 E 00 6.917E 00 1.195E 01 1.0  E-26 7.24 E 24
.00   E-04.66   E-04 2.2  E-04 4.0  E-04 5.8  E-04 7.6  E-048.9   E-04
9.7   E-04 9.7  E-04 9.6  E-04 9.2  E-04 8.5  E-04 7.7  E-04 6.9  E-04
6.1   E-04 5.3  E-04 4.4  E-04 3.3  E-04 2.2  E-04
000000 000000 000000 000000 000000 000000 000000 000000 000007
000000 000000 000000 000000 000000 000000 000000 000000 000015
000000 000000 000000 000000 000000 000001 000000 000000 000023
                                  .
                                  .
                                  .

 10
000000 000000 000000 000000 000000 000000 000000 000000 000007
000011 000011 000006 000006 000014 000003 000005 000012 000015
000010 000009 000010 000007 000011 000015 000018 000016 000023
                                  .
                                  .
                                  .

   124      2      2      4      1
   419      2      2      2      1
   566      2      2      2      1
   584      2     12      8      1
   765      2      5      7      1
  1150      2      8      8      1
  1188      2      7      8      1
  2431      2      5      4      1
  2462      2      4      4      1
  2510      2      4      3      1
  2611      2      2      4      1
  2660      2      3      3      1
  2701      2      2      3      1
  2813      2      4      7      1
  2852      2     12      8      1
  3096      2      4      3      1
  3127      2     12      8      1
 2223.30 6809.40
```

LINEARITY DATA

SPECTRAL DATA

The functions of each individual subroutine are as follows:

(1) LINFT - Automatically identifies and determines the peak center of all pulser peaks in the linearity check data. Peak centers are taken as the centroid of the pulser peak area above a prescribed base line. Then, at each peak center channel location it computes a linearity correction (in channels) of the type shown plotted in Fig. 29.

(2) AREA - Subtracts the background under each peak and determines the number of counts in the peak using the method outlined in Section 4.3.2.

(3) LSTSQ - Performs a least squares fit of a Gaussian function to the upper portion of each peak as discussed in Section 4.3.2. Determines the peak center and the full width at half maximum (fwhm) for each peak.

(4) RESIDL - Calculates E_{RMS} and O_{RMS} as described in Section 4.3.2.

(5) ADJUST - Determines the true peak center (as defined in Section 4.3.2) for each peak. Second order interpolation is used to determine the linearity correction factor for a particular channel number.

(6) ENERGY - Calculates the energy of each peak, having established an energy scale by using EGAM1 and EGAM2.

(7) INTSTY - Calculates the flux and the number of captures. Uses second order interpolation to determine the spectrometer efficiency at each peak energy. Then, the intensity of each peak is calculated from Eq. 4-10.

The output format is illustrated in Table C.3, which shows the output for run 517. Most of the output parameters are self-explanatory. P/B ratio is the ratio of the peak area to the background area under the peak; it gives an indication of the relative statistical error in different peak area determinations. RESID(OBSV) and RESID(FIT) are O_{RMS} (see Eq. 4-5) and E_{RMS} (see Eq. 4-4), respectively. In addition to this printed

TABLE C.3

OUTPUT FORMAT FOR EANDI, RUN 517

ANALYSIS OF CAPTURE GAMMA SPECTRUM, RUN NUMBER 517

LINE	ENERGY(KEV)	INTENSITY	PEAK WIDTH(KEV)	B/P RATIO	RESID(FIT)	RESID(OBSV)	T.P. CENTER	PEAK AREA
1	1274.37	37.4725	6.71	13.82	.01594	.03647	115.3587	254.50
2	1888.23	3.6404	5.17	7.88	.03778	.04455	418.6189	179.00
3	2187.20	2.6075	5.58	10.93	.02455	.03604	566.3153	201.00
4	2223.30	501.1778	7.66	.37	.02383	.01221	584.1488	40380.50
5	2589.42	24.8137	8.68	1.28	.11470	.03557	765.0184	2876.50
6	3366.95	34.9015	8.28	.77	.14094	.02733	1149.1343	6712.00
7	3443.46	12.5237	7.94	1.77	.01982	.03836	1186.9301	2493.00
8	5957.95	1.1775	5.22	4.88	.27110	.06688	2429.1329	292.00
9	6020.55	.6930	5.61	6.84	.16069	.07143	2460.0583	170.50
10	6117.18	.2185	6.25	20.60	.03531	.07153	2507.7956	53.00
11	6321.93	.6383	9.85	5.47	.08148	.07259	2508.9438	150.00
12	6420.16	.6943	9.44	5.59	.05364	.06884	2657.4738	160.50
13	6502.80	.7109	9.36	4.20	.20984	.07126	2698.2955	162.00
14	6732.82	2.6835	9.63	4.07	.07811	.05762	2811.9312	585.00
15	6809.40	61.4521	9.01	.42	.03270	.02139	2849.7635	13194.50
16	7306.20	.9721	6.02	4.18	.22918	.07773	3095.1937	188.00
17	7367.72	40.7075	9.53	.35	.02888	.02832	3125.5856	7765.00

output, the line number, its energy and its intensity is punched out on cards, which are used to prepare tables, such as those presented in Chapter 5. A FORTRAN listing of "EANDI" and its subroutines is given in Table C.4.

TABLE C.4

FORTRAN LISTING OF EANDI CODE

```
      COMMON COUNT,CENTR,CORR,F,AREAP,RAREA,A,C,D,AA,PCENR,
     1RES,RESOB,TPC,EGAM,AIGAM,EFFCY,FWHM,N1,N2,N3,N4,N5,N6,K,L,LW,ILC,I
     2UC,INDEX,EGAM1,EGAM2,J1,J2,SANGL,FWGT,AUCNT1,AUCNT2,TIME1,TIME2,
     3TIME3,FLXCST,BACKM,KEYB,SIGMA,ATOMS,PEAKH
      DIMENSION COUNT(4095),CENTR(200),CORR(200),F(20),AREAP(300),
     1RAREA(300),A(3,4),C(20,4),D(20,4),AA(3,3),PCENR(300),
     2RES(300),RESOB(300),TPC(300),EGAM(300),AIGAM(300),EFFCY(40),FWHM(3
     300),PEAKH(300),XNMP(30),XNOFP(30)
      NRI =0
 1000 NRI = NRI + 1
      READ INPUT TAPE 4,1,N1,N2,N3,N4,N5,N6,IRUN,NP,NR
    1 FORMAT (9I6)
      READ INPUT TAPE 4,700,(XNMP(I),I=1,NP)
      READ INPUT TAPE 4,700,(XNOFP(I),I=1,NP)
  700 FORMAT (12F6.2)
      INCRE = 1
      READ INPUT TAPE 4, 40, J1,J2,FDGE,SANGL,FWGT,AUCNT1,AUCNT2,FLXCST
   40 FORMAT (2I2,6E10.3)
      PRINT 40,J1,J2,FDGE,SANGL,FWGT,AUCNT1,AUCNT2,FLXCST
      READ INPUT TAPE 4, 41, TIME1,TIME2,TIME3,SIGMA,ATOMS
   41 FORMAT (5E10.3)
      PRINT 41, TIME1,TIME2,TIME3,SIGMA,ATOMS
      READ INPUT TAPE 4, 50, (EFFCY(I), I = 1,J2)
   50 FORMAT (7E10.3)
      PRINT 50, (EFFCY(I), I = 1,J2)
      DO 60I = 1,J2
   60 EFFCY(I) = EFFCY(I)*FDGE
      READ INPUT TAPE 4, 2, (COUNT(I), I = 1,N1)
   2  FORMAT (7X,7(F6.0,1X)/(8(F6.0,1X)))
      CALL LINFT
      PRINT 80, (CENTR(I),CORR(I),I=1,L)
   80 FORMAT (2F18.3)
      DO 4I = 1,N1
   4  COUNT(I)= 0.0
      READ INPUT TAPE 4, 2, (COUNT(I) , I = 1,N1)
      INDEX = 0
   5  INDEX = INDEX + 1
      READ INPUT TAPE 4,6,KP0,KP1,KP2,KP3,KEYB
    6 FORMAT (5I6)
      K = KP0-KP1
      LW = 2*KP1
      ILC = KP0-KP2
      IUC = KP0+KP3
      CALL AREA
      CALL LSTSQ
      CALL RESIDL
      CALL ADJUST
      NMP   = XNMP(INCRE)
      NOFP = XNOFP(INCRE)
      IF (INDEX-NMP)600,601,600
  601 INCRE = INCRE + 1
      IF (NOFP - 3) 602,603,604
  604 TOTAL = PEAKH(INDEX)+PEAKH(INDEX-1)+PEAKH(INDEX-2)+PEAKH(INDEX-3)
      DO 620 I = 1,4
      JIN1 = (INDEX-4)+I
      AREAP(JIN1) = AREAP(JIN1)*(PEAKH(JIN1)/TOTAL)
  620 CONTINUE
      GO TO 600
```

```
  603 TOTAL = PEAKH(INDEX)+PEAKH(INDEX-1)+PEAKH(INDEX-2)
      DO 621 I = 1,3
      JIN2 = (INDEX - 3)+ I
      AREAP(JIN2) = AREAP(JIN2)*(PEAKH(JIN2)/TOTAL)
  621 CONTINUE
      GO TO 600
  602 TOTAL = PEAKH(INDEX)+PEAKH(INDEX-1)
      DO 622 I = 1,2
      JIN3 = (INDEX-2) + I
      AREAP(JIN3) = AREAP(JIN3)*(PEAKH(JIN3)/TOTAL)
  622 CONTINUE
  600 IF (INDEX-N4) 5,7,7
    7 READ INPUT TAPE 4,8,EGAM1,EGAM2
    8 FORMAT (2F8.2)
      CALL ENERGY
      CALL INTSTY
      PRINT 9, IRUN
    9 FORMAT(1H1,47H ANALYSIS OF CAPTURE GAMMA SPECTRUM, RUN NUMBER
     1, I6)
      PRINT 10
   10 FORMAT (3X,5H LINE,2X,12H ENERGY(KEV),5X,12H INTENSITY  ,
     12X,16H PEAK WIDTH(KEV),2X,10H B/P RATIO,2X,12H  RESID(FIT), 2X,
     212H RESID(OBSV),2X,12H T.P. CENTER,2X,12H PEAK  AREA )
      DO 11I = 1,N4
      PRINT 12, I,EGAM(I),AIGAM(I),FWHM(I),RAREA(I),RES(I),RESOB(I),
     1TPC(I),AREAP(I)
   12 FORMAT (2X,I6,4X,F10.2,4X,F10.4,5X,F10.2,5X,F10.2,
     12(7X,F7.5),4X,F10.4,2X,F12.2)
      PUNCH 99,I,EGAM(I),AIGAM(I)
   99 FORMAT (4X,I3,4X,F7.1,4X,F8.4)
   11 CONTINUE
      IF (NRI -NR)1000,2000,2000
 2000 CALL EXIT
      END
```

LINFT SUBROUTINE

```
      SUBROUTINE LINFT
      COMMON COUNT,CENTR,CORR,F,AREAP,RAREA,A,C,D,AA,PCENR,
     1RES,RESOB,TPC,EGAM,AIGAM,EFFCY,FWHM,N1,N2,N3,N4,N5,N6,K,L,LW,ILC,I
     2UC, INDEX,EGAM1,EGAM2,J1,J2,SANGL,FWGT,AUCNT1,AUCNT2,TIME1,TIME2,
     3TIME3,FLXCST,BACKM,KEYB,SIGMA,ATOMS,PEAKH
      DIMENSION COUNT(4095),CENTR(200),CORR(200),F(20),AREAP(300),
     1RAREA(300),A(3,4),C(20,4),D(20,4),AA(3,3),PCENR(300),
     2RES(300),RESOB(300),TPC(300),EGAM(300),AIGAM(300),EFFCY(40),FWHM(3
     300),PEAKH(300),SUM(20),XMOM(20)
      READ INPUT TAPE 4, 41, N40
   41 FORMAT (I3)
      XN4 = N40
      J = 0
      L = 0
      I = 0
    3 I = I + J + 1
      IF (I-N1) 31,7,7
   31 J = 0
      IF (COUNT(I)-XN4) 3,3,4
    4 J = J+1
      IPLJ = I+J
      IF (COUNT(IPLJ) -XN4) 5,5,4
```

```
    5  SUM(1) = 0.0
       XMOM(1) = 0.0
       DO 6 K2 = 1,J
       K1 = I+K2-1
       XK =K2
       SUM(K2+1) = SUM(K2) + COUNT(K1)
       XMOM(K2+1) = XMOM(K2) + (XK-0.5)*COUNT(K1)
    6  CONTINUE
       L = L+1
       XI = I
       XII = XI-0.5
       CENTR(L) = (XMOM(J+1)/SUM(J+1)) +XII
       IF (I-N1) 3,7,7
    7  XN = N3-N2
       SLOPE = (CENTR(N3)-CENTR(N2))/XN
       DO 8 M=1,L
       XM = M
       XN2 = N2
       CORR(M) = (CENTR(N2) + (XM-XN2)*SLOPE) - CENTR(M)
    8  CONTINUE
       RETURN
       END
```

AREA SUBROUTINE

```
       SUBROUTINE AREA
       COMMON COUNT,CENTR,CORR,F,AREAP,RAREA,A,C,D,AA,PCENR,
      1RES,RESOB,TPC,EGAM,AIGAM,EFFCY,FWHM,N1,N2,N3,N4,N5,N6,K,L,LW,ILC,I
      2UC,INDEX,EGAM1,EGAM2,J1,J2,SANGL,FWGT,AUCNT1,AUCNT2,TIME1,TIME2,
      3TIME3,FLXCST,BACKM,KEYB,SIGMA,ATOMS,PEAKH
       DIMENSION COUNT(4095),CENTR(200),CORR(200),F(20),AREAP(300),
      1RAREA(300),A(3,4),C(20,4),D(20,4),AA(3,3),PCENR(300),
      2RES(300),RESOB(300),TPC(300),EGAM(300),AIGAM(300),EFFCY(40),FWHM(3
      300),PEAKH(300),BACK(50),TOT1(50),TOT2(50),G(50)
       IF (KEYB-2)5,20,20
    5  BACK1 = COUNT(ILC)
       BACK2 = COUNT(IUC)
       GO TO 30
   20  BACK1 = (COUNT(ILC) +COUNT(ILC-1) +COUNT(ILC+1))/3.0
       BACK2 = (COUNT(IUC) + COUNT(IUC-1) + COUNT(IUC+1))/3.0
   30  IDELT = IUC-ILC
       DELT = IDELT
       THETA = (BACK2-BACK1)/DELT
       BACKM = (BACK1 +BACK2)/2.0
       IDM1= IDELT-1
       TOT1(1) = 0.0
       TOT2(1) = 0.0
       DO 1I = 1,IDM1
       XI = I
       BACK(I) = BACK1 + THETA*XI
       J = I + ILC
       G(I) = COUNT(J) -BACK(I)
       TOT1(I+1) = TOT1(I) + G(I)
       TOT2(I+1) = TOT2(I) + BACK(I)
    1  CONTINUE
       AREAP(INDEX) = TOT1(IDELT)
       RAREA(INDEX) = TOT2(IDELT)/TOT1(IDELT)
       RETURN
       END
```

LSTSQ SUBROUTINE

```
      SUBROUTINE LSTSQ
      COMMON COUNT,CENTR,CORR,F,AREAP,RAREA,A,C,D,AA,PCENR,
     1RES,RESOB,TPC,EGAM,AIGAM,EFFCY,FWHM,N1,N2,N3,N4,N5,N6,K,L,LW,ILC,I
     2UC,INDEX,EGAM1,EGAM2,J1,J2,SANGL,FWGT,AUCNT1,AUCNT2,TIME1,TIME2,
     3TIME3,FLXCST,BACKM,KEYB,SIGMA,ATOMS,PEAKH
      DIMENSION COUNT(4095),CENTR(200),CORR(200),F(20),AREAP(300),
     1RAREA(300),A(3,4),C(20,4),D(20,4),AA(3,3),PCENR(300),
     2RES(300),RESOB(300),TPC(300),EGAM(300),AIGAM(300),EFFCY(40),FWHM(3
     300),PEAKH(300),BB(3,2),E(3)
      LPL1 = LW+1
      DO 400I = 1,LPL1
      KK = K+I-1
      F(I) = LOGF(COUNT(KK))
400   CONTINUE
      DO 10I = 1,LPL1
      C(I,1) = 1.0
      C(I,2) =I-1
      C(I,3) = ((I-1)**2)
      C(I,4) = F(I)
 10   CONTINUE
      DO 30 K1 = 1,3
      DO 30 J = 1,4
      D(I,J) = C(I,J)*C(1,K1)
      DO 20 I=2,LPL1
 20   D(I,J) = D(I-1,J) +C(I,J)*C(I,K1)
 30   A(K1,J) = D(LPL1,J)
      DO 40I = 1,3
      DO 40J = 1,3
 40   AA(I,J) = A(I,J)
      DO 50I = 1,3
 50   BB(I,1) = A(I,4)
      DD = 1.0
      M=XSIMEQF(3,3,1,AA,BB,DD,E)
      GO TO (60,70,80), M
 60   XK = K
      XMAX = XK + (-(AA(2,1))/(2.0*AA(3,1)))
      PCENR(INDEX) = XMAX
      X0 = (-(AA(2,1))/(2.0*AA(3,1)))
      FMAX = AA(3,1)*X0**2 + AA(2,1)*X0 + AA(1,1)
      CNTMAX = EXPF(FMAX)
      PKHGT = CNTMAX - BACKM
      PEAKH(INDEX) = PKHGT
      HOVR2 = PKHGT/2.0
      FOVR2 = CNTMAX -HOVR2
      IF (FOVR2) 200,200,201
201   YOVR2 = LOGF(FOVR2)
      ZZ = AA(1,1) - YOVR2
      VZ = AA(2,1)**2-4.0*AA(3,1)*ZZ
      IF (VZ) 200,200,202
202   VV = SQRTF(VZ)
      FWHM(INDEX) = ABSF(VV/AA(3,1))
      GO TO 204
200   FWHM(INDEX) = 0.0
      PRINT 203,INDEX
203   FORMAT(27H ARGUMENT NEG. FOR LINE NO., I6)
204   RETURN
```

```
70 PRINT 71
71 FORMAT (9H OVERFLOW)
   RETURN
80 PRINT 81
81 FORMAT (15H AA IS SINGULAR)
   RETURN
   END
```

RESIDL SUBROUTINE

```
   SUBROUTINE RESIDL
   COMMON COUNT,CENTR,CORR,F,AREAP,RAREA,A,C,D,AA,PCENR,
  1RES,RESOB,TPC,EGAM,AIGAM,EFFCY,FWHM,N1,N2,N3,N4,N5,N6,K,L,LW,ILC,I
  2UC,INDEX,EGAM1,EGAM2,J1,J2,SANGL,FWGT,AUCNT1,AUCNT2,TIME1,TIME2,
  3TIME3,FLXCST,BACKM,KEYB,SIGMA,ATOMS,PEAKH
   DIMENSION COUNT(4095),CENTR(200),CORR(200),F(20),AREAP(300),
  1RAREA(300),A(3,4),C(20,4),D(20,4),AA(3,3),PCENR(300),
  2RES(300),RESOB(300),TPC(300),EGAM(300),AIGAM(300),EFFCY(40),FWHM(3
  300),PEAKH(300),BB(3,2),E(3),FPRIM(20),R(20),ROB(20)
   LPL1 = LW + 1
   DO 10I = 1,LPL1
10 FPRIM(I) = AA(1,1) + AA(2,1)*C(I,2) + AA(3,1)*
  1(C(I,2)**2)
   R(1) = (FPRIM(1) -F(1))**2
   DO 20I = 2,LPL1
20 R(I) = R(I-1) + ((FPRIM(I) -F(I))**2)
   X = LW - 2
   RES(INDEX) = SQRTF(R(LPL1)/X)
   ROB(1) = 1.0/COUNT(K)
   DO 40I = 2,LPL1
   KK = K+I - 1
40 ROB(I) = ROB(I-1) + (1.0/COUNT(KK))
   Y =LPL1
   RESOB(INDEX) = SQRTF(ROB(LPL1)/Y)
   RETURN
   END
```

ADJUST SUBROUTINE

```
   SUBROUTINE ADJUST
   COMMON COUNT,CENTR,CORR,F,AREAP,RAREA,A,C,D,AA,PCENR,
  1RES,RESOB,TPC,EGAM,AIGAM,EFFCY,FWHM,N1,N2,N3,N4,N5,N6,K,L,LW,ILC,I
  2UC,INDEX,EGAM1,EGAM2,J1,J2,SANGL,FWGT,AUCNT1,AUCNT2,TIME1,TIME2,
  3TIME3,FLXCST,BACKM,KEYB,SIGMA,ATOMS,PEAKH
   DIMENSION COUNT(4095),CENTR(200),CORR(200),F(20),AREAP(300),
  1RAREA(300),A(3,4),C(20,4),D(20,4),AA(3,3),PCENR(300),
  2RES(300),RESOB(300),TPC(300),EGAM(300),AIGAM(300),EFFCY(40),FWHM(3
  300),PEAKH(300)
   IOTA = 0
10 IOTA = IOTA + 1
   IF (CENTR(IOTA) - PCENR(INDEX)) 10,10,20
20 G1 = CORR(IOTA - 1)
   G2 = CORR(IOTA)
   G3 = CORR(IOTA + 1)
```

```
      C1 = CENTR(IOTA -1)
      C2 = CENTR(IOTA)
      C3 = CENTR(IOTA +1)
      CX = PCENR(INDEX)
      D12 = (G2-G1)/(C2-C1)
      D23 = (G3-G2)/(C3-C2)
      D123 = (D23-D12)/(C3-C1)
      GX = G1 + (CX-C1)*D12 + ((CX-C1)*(CX-C2)*D123)
      TPC(INDEX) = PCENR(INDEX) + GX
      RETURN
      END
```

ENERGY SUBROUTINE

```
      SUBROUTINE ENERGY
      COMMON COUNT,CENTR,CORR,F,AREAP,RAREA,A,C,D,AA,PCENR,
     1RES,RESOB,TPC,EGAM,AIGAM,EFFCY,FWHM,N1,N2,N3,N4,N5,N6,K,L,LW,ILC,I
     2UC,INDEX,EGAM1,EGAM2,J1,J2,SANGL,FWGT,AUCNT1,AUCNT2,TIME1,TIME2,
     3TIME3,FLXCST,BACKM,KEYB,SIGMA,ATOMS,PEAKH
      DIMENSION COUNT(4095),CENTR(200),CORR(200),F(20),AREAP(300),
     1RAREA(300),A(3,4),C(20,4),D(20,4),AA(3,3),PCENR(300),
     2RES(300),RESOB(300),TPC(300),EGAM(300),AIGAM(300),EFFCY(40),FWHM(3
     300),PEAKH(300)
      SLP = (EGAM2-EGAM1)/(TPC(N6)-TPC(N5))
      DO 10I = 1,N4
      EGAM(I) = EGAM1 + SLP*(TPC(I)-TPC(N5))
      FWHM(I) = FWHM(I)*SLP
   10 CONTINUE
      RETURN
      END
```

INTSTY SUBROUTINE

```
      SUBROUTINE INTSTY
      COMMON COUNT,CENTR,CORR,F,AREAP,RAREA,A,C,D,AA,PCENR,
     1RES,RESOB,TPC,EGAM,AIGAM,EFFCY,FWHM,N1,N2,N3,N4,N5,N6,K,L,LW,ILC,I
     2UC,INDEX,EGAM1,EGAM2,J1,J2,SANGL,FWGT,AUCNT1,AUCNT2,TIME1,TIME2,
     3TIME3,FLXCST,BACKM,KEYB,SIGMA,ATOMS,PEAKH
      DIMENSION COUNT(4095),CENTR(200),CORR(200),F(20),AREAP(300),
     1RAREA(300),A(3,4),C(20,4),D(20,4),AA(3,3),PCENR(300),
     2RES(300),RESOB(300),TPC(300),EGAM(300),AIGAM(300),EFFCY(40),FWHM(3
     300),PEAKH(300),GAMOUT(300)
      AUCNT0 =(AUCNT1*EXPF((.0107)*TIME1)+AUCNT2*EXPF((.0107)*TIME2))
     1/2.0
      DECAY = (1.0-EXPF(-(.0107)*TIME3))
      FLUX = (FLXCST*AUCNT0)/(DECAY*FWGT)
      CAPTRS = (36.  )*SIGMA*FLUX*ATOMS*TIME3
      IF (J1-1) 10,20,20
   10 I = 0
   15 I = I+1
      XEGAM = 0.0
   16 XEGAM = XEGAM + 100.0
      IF (XEGAM-EGAM(I)) 16,17,17
   17 IEGAM = XEGAM*(.010) + 0.00001
```

```
      E1 =XEGAM - 100.
      E2 = XEGAM
      E3 = XEGAM + 100.
      EX = EGAM(I)
      GO TO 35
   20 I = 0
   25 I = I+1
      XEGAM = 1000.
   26 XEGAM = XEGAM + 500.
      IF (XEGAM - EGAM(I)) 26,27,27
27    IEGAM = ((.002)*XEGAM)-.999999
      E1 = XEGAM - 500.
      E2 = XEGAM
      E3 = XEGAM+ 500.
      EX = EGAM(I)
   35 G1 = EFFCY(IEGAM-1)
      G2 = EFFCY(IEGAM)
      G3 = EFFCY(IEGAM+1)
      D12 = (G2-G1)/(E2-E1)
      D23 = (G3-G2)/(E3-E2)
      D123=(D23-D12)/(E3-E1)
      GX=G1 + (EX-E1)*D12 + (EX-E2)*(EX-E1)*D123
      GAMOUT(I) = AREAP(I)/(GX*SANGL)
      AIGAM(I) = GAMOUT(I)/CAPTRS
      IF (J1-1) 40,50,50
   40 IF(I-N4) 15,60,60
   50 IF(I-N4) 25,60,60
   60 PRINT 70, FLUX,CAPTRS
   70 FORMAT (5X,7H FLUX =,E12.3,5X,9H CAPTRS =, E12.3)
      RETURN
      END
```

APPENDIX D

DESCRIPTION OF "CHKBE AND CASFND" CODE

"CHKBE and CASFND" calculates the fraction of total γ-ray intensity observed and searches for all one- and two-step transitions between any two specified energy levels.

The γ-ray energies, EGAM, and intensities, AIGAM, are inputed to the code from cards, outputed by the "EANDI" code. Cards containing the energies and intensities of background lines are removed before the card deck is inputed to this code. Additional input parameters are the following:

NI -- number of energies and intensities to be considered,

NRUNA -- number of different runs to be executed,

NUM -- run number for identification purposes,

BE -- "average" binding energy for element,

ALDIFF -- allowed tolerance on cascade sums (about 1.5 keV)

N2 -- number of energy level differences to be inputed,

XM -- atomic weight of element,

XLEVEL -- energy level difference.

The code outputs the fraction of the γ-ray intensity observed, a listing of recoil corrected energies, and a list of all one- and two-step transitions between each energy level difference, XLEVEL, specified. The input and output formats may be determined from the FORTRAN listing of the code in Table D.1.

TABLE D.1

FORTRAN LISTING OF CHKBE AND CASFND CODE

```
C CHKBE  AND CASFND PROGRAMS
C CHECKS SUM TO BINDING ENERGY AND FINDS CASCADES
      DIMENSION SUM(500),EGAM(500),AIGAM(500),XLEVEL(100)
      NRUN = 0
  500 READ 5,N1,NRUNA,NUM,BE,ALDIFF,N2,XM
    5 FORMAT (3I6,2F7.1,I6,F7.1)
      READ 100,(XLEVEL(I),I = 1,N2)
  100 FORMAT (10F7.1)
      NRUN =NRUN+1
      PRINT 1,NUM
    1 FORMAT (1H1,11H RUN NUMBER,I6)
      READ 10,(EGAM(I),AIGAM(I),I=1,N1)
   10 FORMAT (11X,F7.1,4X,F8.4)
      DO 9I = 1,N1
      EGAM(I) = EGAM(I) + ((EGAM(I)**2)/((1.87E 06)*XM))
      PRINT 11,I,EGAM(I),AIGAM(I)
   11 FORMAT (10X,I6,16X,F7.1,15X,F8.4)
    9 CONTINUE
      SUM(1) = 0.
      DO 30I = 1,N1
      SUM(I+1) = SUM(I) + EGAM(I)*AIGAM(I)*(.01)
   30 CONTINUE
      SBE = SUM(N1+1)
      FRAC = SBE/BE
      PRINT 41,SBE,BE,FRAC
   41 FORMAT (9H SUM BE =,F18.4,17H BINDING ENERGY =,F18.4,
     1 26H FRACTION OF GAMMAS SEEN =,F18.4)
      DO 105 I = 1,N2
      J = 0
  102 J = J +1
      DIFF1 = ABSF(EGAM(J) -XLEVEL(I))
      IF (DIFF1 - ALDIFF) 103,103,110
  110 IF (EGAM(J)-XLEVEL(I))102,103,104
  103 PRINT 203,XLEVEL(I),EGAM(J)
  203 FORMAT (8H LEVEL =,F7.1,8H GAMMA =,F7.1)
  104 JM1 = J-1
      DO 105 K1 = 1,JM1
      DO 105 K2 = 1,JM1
      GAMMA2 = EGAM(K1) + EGAM(K2)
      DIFF2 = ABSF(GAMMA2-XLEVEL(I))
      IF (DIFF2-ALDIFF) 106,106,105
  106 PRINT 206,EGAM(K1),EGAM(K2),GAMMA2
  206 FORMAT (10X,F7.1,2H +,F7.1,2H =,F7.1)
  105 CONTINUE
      IF (NRUN - NRUNA)500,600,600
  600 CALL EXIT
      END
```

REFERENCES

A1 G. Armantrout, IEEE Trans. on Nucl. Science, NS-12, Feb., 1966.

A2 G. Armantrout, "U-Junction Ge(Li) Drift Detectors," IEEE Trans. on Nucl. Science, NS-13, (to be published).

B1 G. A. Bartholomew, Nuclear Spectroscopy, Part A (ed. Ajzenberg-Selove) Academic Press, New York, 1960, p. 304.

B2 G. A. Bartholomew, et al, Proceedings International Conference on the Neutron Interactions with the Nucleus, Columbia Univ., New York, TID-7547, 1957, p. 252.

B3 G. A. Bartholomew, Annual Review of Nuclear Science, 11 (ed. E. Segre), Annual Reviews, Palo Alto, 1961, p. 259.

B4 G. A. Bartholomew and L. A. Higgs, Compilation of Thermal Neutron Capture Gamma Rays, AECL-669, July 1958.

B5 G. A. Bartholomew and M. R. Gunye, Can. J. Physics, 43, (1965), 1128.

B6 G. A. Bartholomew, et al, Can. J. Physics, 44, (1966), 2111.

B7 G. A. Bartholomew and B. B. Kinsey, Phys. Rev., 89, 386, (1953).

C1 Computation Center Memo Number CC-243, MIT, Jan. 1965.

E1 G. T. Ewan and A. J. Tavendale, Can. J. Physics, 42, (1964) p. 2286.

E2 R. D. Evans, The Atomic Nucleus, McGraw-Hill Co., 1955.

F1 H. J. Fiedler, et al, Nucl. Inst. and Methods, 40, 229-234, (1966).

F2 U. Fano, Phys. Rev., 72, 26 (1947).

F3 N. F. Fiebiger, et al, Phys. Rev., 125, 6, 2031 (1962).

G1 R. C. Greenwood, et al, Scintillation Spectrometer Measurements of Thermal Neutron Capture Gamma Rays from Natural Elements, Report No. ARF-1193-23.

G2 L. V. Groshev, et al, Atlas of Gamma-Ray Spectra from Radiative Capture of Thermal Neutrons, (English translation by J. B. Sykes, Pergamon Press, London, 1959).

G3 R. C. Greenwood, Atlas of Neutron Capture Gamma Spectra from Some 74 elements measured using NaI(Tl) Scintillation Detectors, Report No. IITRI-1193-53. (to be published).

G4 L. V. Groshev, et al, Nucl. Phys., 58, (1964), 465.

G5 F. S. Goulding and W. L. Hansen, Automatic Lithium Drifting Apparatus for Silicon and Germanium Detectors, Report No. UCRL-11261.

G6 F. S. Goulding, Semiconductor Detectors for Nuclear Spectrometry Report No. UCRL-16231 (July, 1965).

G7 R. C. Greenwood, "Precise Measurement of Primary Capture Gamma-Ray Energies Using a 'Bootstrap' Method," Proceedings of Slow Neutron Conference, ANL, Nov., 1966, (to be published).

G8 R. C. Greenwood, et at, Scintillation Spectrometer Measurements of Thermal Neutron Capture Gamma Rays from Natural Elements Report ARF-1193-17, p. 14, Dec. 1962.

H1 L. B. Hughes, et al, Nucl. Phys., 80 (1966) 131-144.

H2 L. B. Hughes, et al, Can. J. Physics, 44 (1966) 2041-2051.

H3 W. L. Hansen and B. V. Jarrett, Techniques for the Fabrication of Lithium Drifted Germanium Detectors, UCRL-11589, (Aug. 1964).

H4 W. L. Hansen and B. V. Jarrett, Nucl. Instr. and Methods, 31, (1964) p. 301-306.

H5 R. Heath, et al., IEEE Trans. on Nucl. Science, NS-13, 3, (June, 1966) 445-456.

H6 J. N. Hanson, S.M. Thesis, Dept. of Nuclear Engineering, MIT, 1965.

H7 F. B. Hildebrand, Introduction to Numerical Analysis, McGraw-Hill, Inc., 1956, p. 262.

I1 T. L. Isenhour and G. H. Morrison, Analytical Chemistry, 38, 2, (Feb. 1966), p. 162-7.

I2 T. L. Isenhour and G. H. Morrison, Analytical Chemistry, 38, 2, (Feb. 1966), p. 167-9.

I3 T. Inouye, private communication.

J1 H. E. Jackson, A. I. Namenson, and G. E. Thomas, Physics Letters, 17, 3.

J2 M.A. Jamini, "Production of Lithium Drifted Germanium Detectors by A.C. Drift," IEEE Trans. on Nucl. Science, NS-13, (to be published).

K1 A. H. Kazi, N. C. Rasmussen, and Hans Mark, Rev. of Sci. Instr. 31, 9, 983-987.

K2 H. W. Kraner, J. A. Sovka, and R. W. Breckenridge, Jr., Nucl. Instr. and Methods, 36, 328, 1965.

K3 J. Kantele and P. Suominen, Nucl. Instr. and Methods, 41 (1966) 41-44.

K4 J. W. Knowles, Can. J. Physics, 40 (1962) 257.

K5 B. B. Kinsey and G. A. Bartholomew, Can. J. Physics, 31, 1051, 1953.

L1 W. G. Lussie and J. L. Brownlee, "The Measurement and Utilization of Neutron Capture Gamma Radiation," Modern Trends in Activation Analysis, Proceedings 1965 International Conference, p. 194-199.

L2 Landolt-Bornstein, Energy Levels of Nuclei: A = 5 to A = 257, editor, K. H. Hellwege, Springer-Verlag, Berlin, 1961.

M1 H. Motz and G. Backstrom, Neutron Capture Radiation Spectroscopy Chapter XIII, Alpha-, Beta-, and Gamma-Ray Spectroscopy, (ed. Kai Siegbalm), North-Holland Publishing Co., Amsterdam, 1965.

M2 H. L. Malm, A. J. Tavendale, and I. L. Fowler, Can. J. Physics, 43, 7, (July, 1965).

M3 G. L. Miller, et al, IEEE Trans. on Nucl. Science, NS-10, 220, (Jan. 1963).

M4 H. L. Malm and I. L. Fowler, IEEE Trans. on Nucl. Science, NS-12, (Feb, 1966).

M5 J. W. Mayer, IRE Trans. on Nucl. Science, NS-9 (3), 129 (1962).

M6 F. Mahoney, private communication.

M7 H. Mann, et al, IEEE Trans. on Nucl. Science, NS-13, 3, (June, 1966).

M8 H. T. Motz, et al, Pile Neutron Research in Physics, IAEA, Vienna, 1962, p. 225

M9 M. Mazari, Mass. Inst. of Tech., Laboratory for Nucl. Science, Progress Report, p. 44, Nov., 1957.

M10 H. J. Motz, Phys. Rev., 104, 1353, 1956.

M11 W. F. Miller, et al, Review of Scientific Instr., 28, 717, (1957).

N1 A. Namenson, H. E. Jackson, and R. K. Smither, Phys. Rev., 146, 3, 844-852.

N2 R. G. Nisle, Nucleonics Handbook of Nuclear Research and Technology, McGraw-Hill, New York, p. 204.

N3 J. M. Neill, N. C. Rasmussen, and T. J. Thompson, Measurement of Gamma-Ray Spectra for Thermal Neutron Capture, AFCRL-63-341.

N4 Nuclear Data Sheets, 1959.

O1 V. J. Orphan and N. C. Rasmussen, "A Pair Spectrometer Using a Large Coaxial Lithium Drifted Germanium Detector," IEEE Trans. on Nucl. Science, Oct., 1966 (to be published).

O2 V. J. Orphan and N. C. Rasmussen, "A Ge(Li) Spectrometer for Studying Neutron Capture Gamma Rays," Nucl. Instr. and Methods, (to be published).

P1 W. V. Prestwich, private communication.

P2 W. V. Prestwich, et al, Can. J. Phys., 43, (1965) 2086-2087.

P3 M. S. Popa and M. I. Cristu, Nucl. Instr. and Methods, 34, (1965) 192-196.

R1 J. Rapaport, MIT Thesis, unpublished.
J. Rapaport, A. Sperduto, and W. W. Buechner, Bull. Am. Phys. Soc., 8, (1963) 48.

R2 J. Rapaport, A. Sperduto, and W. W. Buechner, Phys. Rev., 151, 3, (1966).

S1 J. A. Sovka and N. C. Rasmussen, Nondestructive Analysis of Irradiated MITR Fuel by Gamma-Ray Spectroscopy, MITNE-64, AFCRL-65-787 (Oct., 1965).

S2 K. F. Smith and J. E. Cline, IEEE Trans. on Nucl. Science, NS-13, 3, (June, 1966).

S3 A. Sperduto and W. W. Buechner, Phys. Rev., 134, 1B, B142-B163, April, 1964.

T1 A. J. Tavendale and G. T. Ewan, Nucl. Instr. and Methods, 26, (1963).

T2 A. J. Tavendale, IEEE Trans. on Nucl. Science, NS-13, 3, June, 1966.

T3 A. J. Tavendale, IEEE Trans. on Nucl. Science, NS-12, 1, 255 (1965).

V1 P. Van Assche, et al, Nucl. Phys. 84, (1966) 661-672.

W1 O. A. Wasson, et al, Phys. Rev., 136, 6B, B1640.

W2 C. H. Westcott, et al, Effective Cross Section Values for Well-

Moderated Thermal Reactor Spectra, AECL-1101, Nov. 1, 1960.

W3 N. S. Wall, Phys. Rev., 96, 664 (1954).

Unclassified

Security Classification

DOCUMENT CONTROL DATA - R&D

(Security classification of title, body of abstract and indexing annotation must be entered when the overall report is classified)

1. ORIGINATING ACTIVITY *(Corporate author)*
Massachusetts Institute of Technology
77 Massachusetts Avenue
Cambridge, Massachusetts

2a. REPORT SECURITY CLASSIFICATION
unclassified

2b. GROUP

3. REPORT TITLE
Study of Thermal Neutron Capture Gamma Rays Using a Lithium Drifted Germanium Spectrometer

4. DESCRIPTIVE NOTES *(Type of report and inclusive dates)*
Scientific Report Interim

5. AUTHOR(S) *(Last name, first name, initial)*
Orphan, Victor J.
Rasmussen, Norman C.

6. REPORT DATE
January 1967

7a. TOTAL NO. OF PAGES
203

7b. NO. OF REFS
74

8a. CONTRACT OR GRANT NO.
AF19(628)5551

b. PROJECT ~~NO.~~ and Task No. 5620-03

c. ~~TASK~~ DoD Element No. 61445014

d. DoD Subelement No. 681301

9a. ORIGINATOR'S REPORT NUMBER(S)
MITNE-80
Scientific Report No. 1

9b. OTHER REPORT NO(S) *(Any other numbers that may be assigned this report)*
AFCRL-67-0104

10. AVAILABILITY/LIMITATION NOTICES
Distribution of this document is unlimited.

11. SUPPLEMENTARY NOTES

12. SPONSORING MILITARY ACTIVITY
Hq. AFCRL, OAR (CRW)
United States Air Force
L.G. Hanscom Field, Bedford, Mass.

13. ABSTRACT

A gamma-ray spectrometer, using a 30 cc coaxial Ge(Li) detector, which can be operated as a pair spectrometer at high energies and in the Compton suppression mode at low energies provides an effective means of obtaining thermal neutron capture gamma spectra over nearly the entire capture gamma energy range. The energy resolution (fwhm) of the spectrometer is approximately 0.5% at 1 MeV and 0.1% at 7 MeV. Capture gamma-ray energies can be determined to an accuracy of about 1 keV. The relatively high efficiency of this spectrometer allows the use of an external neutron beam geometry, which simplifies sample changing. Using a 4096 channel pulse height analyzer, the capture gamma spectrum of an element may be obtained in about one day. Low cross section (order of 0.1 b) elements with many weak intensity gammas may be studied. Over 100 gamma rays have been identified in the spectrum of one such element, Zr. The spectra of Be, Sc, Fe, Ge, and Zr are presented.

DD FORM 1 JAN 64 1473

Unclassified

Security Classification

Unclassified

Security Classification

14. KEY WORDS	LINK A		LINK B		LINK C	
	ROLE	WT	ROLE	WT	ROLE	WT
Gamma-ray spectroscopy Capture γ rays Ge(Li) γ-ray detectors Pair spectrometer						

INSTRUCTIONS

1. ORIGINATING ACTIVITY: Enter the name and address of the contractor, subcontractor, grantee, Department of Defense activity or other organization *(corporate author)* issuing the report.

2*a*. REPORT SECURITY CLASSIFICATION: Enter the overall security classification of the report. Indicate whether "Restricted Data" is included. Marking is to be in accordance with appropriate security regulations.

2*b*. GROUP: Automatic downgrading is specified in DoD Directive 5200.10 and Armed Forces Industrial Manual. Enter the group number. Also, when applicable, show that optional markings have been used for Group 3 and Group 4 as authorized.

3. REPORT TITLE: Enter the complete report title in all capital letters. Titles in all cases should be unclassified. If a meaningful title cannot be selected without classification, show title classification in all capitals in parenthesis immediately following the title.

4. DESCRIPTIVE NOTES: If appropriate, enter the type of report, e.g., interim, progress, summary, annual, or final. Give the inclusive dates when a specific reporting period is covered.

5. AUTHOR(S): Enter the name(s) of author(s) as shown on or in the report. Enter last name, first name, middle initial. If military, show rank and branch of service. The name of the principal author is an absolute minimum requirement.

6. REPORT DATE: Enter the date of the report as day, month, year, or month, year. If more than one date appears on the report, use date of publication.

7*a*. TOTAL NUMBER OF PAGES: The total page count should follow normal pagination procedures, i.e., enter the number of pages containing information.

7*b*. NUMBER OF REFERENCES: Enter the total number of references cited in the report.

8*a*. CONTRACT OR GRANT NUMBER: If appropriate, enter the applicable number of the contract or grant under which the report was written.

8*b*, 8*c*, & 8*d*. PROJECT NUMBER: Enter the appropriate military department identification, such as project number, subproject number, system numbers, task number, etc.

9*a*. ORIGINATOR'S REPORT NUMBER(S): Enter the official report number by which the document will be identified and controlled by the originating activity. This number must be unique to this report.

9*b*. OTHER REPORT NUMBER(S): If the report has been assigned any other report numbers *(either by the originator or by the sponsor)*, also enter this number(s).

10. AVAILABILITY/LIMITATION NOTICES: Enter any limitations on further dissemination of the report, other than those imposed by security classification, using standard statements such as:

(1) "Qualified requesters may obtain copies of this report from DDC."

(2) "Foreign announcement and dissemination of this report by DDC is not authorized."

(3) "U. S. Government agencies may obtain copies of this report directly from DDC. Other qualified DDC users shall request through

_____."

(4) "U. S. military agencies may obtain copies of this report directly from DDC. Other qualified users shall request through

_____."

(5) "All distribution of this report is controlled. Qualified DDC users shall request through

_____."

If the report has been furnished to the Office of Technical Services, Department of Commerce, for sale to the public, indicate this fact and enter the price, if known.

11. SUPPLEMENTARY NOTES: Use for additional explanatory notes.

12. SPONSORING MILITARY ACTIVITY: Enter the name of the departmental project office or laboratory sponsoring *(paying for)* the research and development. Include address.

13. ABSTRACT: Enter an abstract giving a brief and factual summary of the document indicative of the report, even though it may also appear elsewhere in the body of the technical report. If additional space is required, a continuation sheet shall be attached.

It is highly desirable that the abstract of classified reports be unclassified. Each paragraph of the abstract shall end with an indication of the military security classification of the information in the paragraph, represented as *(TS), (S), (C), or (U).*

There is no limitation on the length of the abstract. However, the suggested length is from 150 to 225 words.

14. KEY WORDS: Key words are technically meaningful terms or short phrases that characterize a report and may be used as index entries for cataloging the report. Key words must be selected so that no security classification is required. Identifiers, such as equipment model designation, trade name, military project code name, geographic location, may be used as key words but will be followed by an indication of technical context. The assignment of links, rules, and weights is optional.

Unclassified

Security Classification